

Stony Brook University



OFFICIAL COPY

The official electronic file of this thesis or dissertation is maintained by the University Libraries on behalf of The Graduate School at Stony Brook University.

© All Rights Reserved by Author.

**The Roles of the IFT & BBS proteins
in *Drosophila*
Mechanosensory and Chemosensory Cilia**

A Dissertation Presented

by

Eugene Lee

to

The Graduate School

in Partial Fulfillment of the

Requirements

for the Degree of

Doctor of Philosophy

in

Neuroscience

Stony Brook University

December 2007

Stony Brook University

The Graduate School

Eugene Lee

We, the dissertation committee for the above candidate for the
Doctor of Philosophy degree, hereby recommend
acceptance of this dissertation.

Maurice J. Kernan, Ph.D. -Dissertation Advisor
Associate Professor
Department of Neurobiology and Behavior

Michael Frohman, M.D., Ph.D. -Chairperson of Defense
Professor
Department of Pharmacology

Simon Halegoua, Ph.D.
Professor
Department of Neurobiology and Behavior

Howard Sirotkin, Ph.D.
Assistant Professor
Department of Neurobiology and Behavior

Aaron Neiman, Ph.D.
Associate Professor
Department of Biochemistry and Cell Biology

This dissertation is accepted by the Graduate School

Lawrence Martin
Dean of the Graduate School

Abstract of the Dissertation

The Roles of the IFT & BBS proteins

in *Drosophila* Mechanosensory and Chemosensory Cilia

by

Eugene Lee

Doctor of Philosophy

In

Neuroscience

Stony Brook University

2007

In *Drosophila*, mechanosensory and chemosensory transduction takes place in cilia, and mutants lacking cilia have sensory defects. Intraflagellar transport (IFT) machinery is required for cilia assembly and maintenance. Comparative genomics combined with domain analysis identified many cilia-related genes, including IFT and Bardet-Biedl syndrome (BBS) proteins.

The mutant, *reduced mechanoreceptor potential A* (*rempA*) has truncated cilia and no sound-evoked response. Here, we report that *rempA* encodes IFT140, one of the IFT-A proteins. IFT-B protein accumulates at the tips of *rempA* cilia, suggesting that REMPA is involved in retrograde transport. A functional YFP-REMPA fusion protein localizes specifically on the connecting cilium in es organs. In chordotonal organs, REMPA is distributed along the cilia during differentiation, and then concentrates on the ciliary dilation, a structure whose composition and function are unknown. In a *kinesin-II* hypomorph mutant, REMPA localizes on reduced ciliary dilations which distally position

inside dendritic caps. REMPA is undetected in another IFT-A mutant, *oseg1*, implying that REMPA composes ciliary dilations together with OSEG1. In a retrograde motor mutant, *btv*, NOMPB and REMPA are dispersed along the cilia and accumulate at the tip of the distal cilia suggesting BTV might be involved in retrograde transport. Moreover, IAV, an auditory ion channel which normally localizes proximal to ciliary dilations, leaks into the distal zone, suggesting that IFT-A proteins organize ciliary dilations, which partition the chordotonal cilia into two functionally distinct compartments.

BBS 1, 3, and 8 functions are limited to chemosensory transduction. The behavior and electrophysiological responses to auditory stimuli of *BBS* mutants are normal. The localization of REMPA protein was not affected in *BBS* mutants. A larval chemotaxis assay revealed that *BBS1* has a severe chemosensory defect and *BBS3* has high sensitivity to lower concentrations of an odor. A proboscis extension reflex test found that fly *BBS* mutants have a lower frequency to 1M sugar solution. BBS1 localized specifically on chemosensory cilia in an adult labellum and on the dorsal organs in a larva, suggesting that BBS function is not correlated to a general IFT-based transport mechanism, but might be related to chemosensory receptor trafficking in *Drosophila*.

To
My Beloved Family,

Bong Sub Lee
and
Jae Sim Choi

Table of contents

List of Illustrations	vii
Acknowledgement	ix
Chapter 1 : Introduction	1
1.1. Eukaryotic cilia and flagella	3
1.2. IFT	9
1.3. BBS	14
1.4. The current model for IFT and BBS	25
1.5. Sensory cilia in <i>Drosophila</i>	27
Chapter 2 : <i>rempA</i> encodes IFT140.	43
2.1. Phenotype of <i>rempA</i>	48
2.2. Positional cloning of <i>rempA</i>	51
2.3. The property of REMPA protein	54
Chapter 3 : Expression and localization of REMPA.	73
3.1. In chordotonal organs	78
3.2. In external sensory organs	83
3.3. Mislocalization of EMPA in other mutants	87
Chapter 4 : Chemosensory defects in <i>BBS</i> mutants.	130
4.1. Generation of BBS1 and 8 deletion mutants	137
4.2. Chemosensory phenotype	142
4.3. Localization of BBS1	148
Chapter 5 : Discussion	178
5.1. IFT-A in mechanosensory cilia in fly	180
5.2. Type I mechanosensory organs	187
5.3. BBS proteins in chemosensory cilia	191
5.4. The Model for IFT-based transport in fly cilia	193
References	203

List of Illustrations

Chapter 1

Figure 1-1. Schematic of a ciliary structure	36
Table 1-1. The components of Intraflagellar transport (IFT)	38
Figure 1-2. Schematic of transporting mechanism on nematode cilia	40
Figure 1-3. Schematic of <i>Drosophila</i> ciliated sensory organs	42

Chapter 2

Figure 2-1. An electrophysiological defect of REMPA and rescue phenotype	58
Figure 2-2. The ciliary morphology of <i>rempA</i> mutants by RFP expression	60
Figure 2-3. The ultrastructure of <i>rempA</i> mutant cilia	62
Figure 2-4. NOMP B localization in IFT-A mutants, <i>oseg1</i> and <i>rempA</i>	65
Figure 2-5. Mapping and sequence analysis of <i>rempA</i>	67
Figure 2-6. Sequence analysis of REMPA protein with its orthologs	69
Figure 2-7. Domain comparison of IFT-A, COP, and CHC	72

Chapter 3

Figure 3-1. REMPA localization on chordotonal neurons	100
Figure 3-2. REMPA localization on larval and embryonic ciliary dilations	102
Figure 3-3. REMPA and Eys localization in mechanosensory mutants	105
Figure 3-4. NOMP B localization on developing cilia	107
Figure 3-5. REMPA localization in es neuronal cilia	109
Figure 3-6. REMPA localization on a connecting cilium of es neurons	111
Figure 3-7. REMPA localization on a connecting cilium of campaniform sensilla	113
Figure 3-8. REMPA localization in <i>oseg1</i> mutant	115
Figure 3-9. REMPA delocalization in <i>btv</i> es and chordotonal cilia	117
Figure 3-10. NOMP B delocalization in <i>btv</i> chordotonal cilia	119
Figure 3-11. The ciliary morphology of <i>btv</i> mutant	121
Figure 3-12. REMPA localization in <i>kinesinII</i> mutants	123
Figure 3-13. REMPA and NOMP B localization in <i>dyf-1</i> mutant	125
Figure 3-14. REMPA and NOMP B localization in <i>BBS8</i> mutant	127
Figure 3-15. IAV localization in <i>btv</i> and <i>rempA</i> mutants	129

Chapter 4

Figure 4-1. <i>Drosophila</i> <i>BBS</i> homologs and structures	151
Figure 4-2. The cytogenetic map and the deletion scheme of <i>BBS1</i>	153
Figure 4-3. The cytogenetic map and the amino acid sequence alignment of <i>BBS3</i>	155
Figure 4-4. The cytogenetic map and the deletion scheme of <i>BBS8</i>	157
Figure 4-5. The schematic of larval chemotaxis assay and the scoring method	159
Figure 4-6. The sound-evoked response of <i>BBS</i> mutants	161
Figure 4-7. Larval chemotaxis assay of <i>BBS1</i> and <i>BBS3</i>	164
Figure 4-8. The exponential gradient assay for larval chemotaxis of <i>BBS1</i> and <i>BBS3</i>	166
Figure 4-9. The single droplet assay for <i>BBS1</i> and <i>BBS3</i>	168
Figure 4-10. The steep linear gradient assay for <i>BBS3</i>	171
Figure 4-11. PER test for <i>BBS</i> mutants	173

Figure 4-12. The morphology of chemosensory cilia in <i>BBS</i> mutants	175
Figure 4-13. The localization of BBS1 protein on chemosensory ciliated neurons	177
Chapter 5	
Figure 5-1. The summary of protein localization in mutants	198
Figure 5-2. The functional relationship between ES and CHO	200
Figure 5-3. The IFT-based transporting mechanism in chordotonal cilia	202

Acknowledgement

The end is the beginning of a next step. Through last six years, I have realized that a goal is not accomplished without patience, together with a commitment and passion. This is the most fruitful learning from my dissertation work.

I thank my advisor, Dr. Maurice Kernan, who motivated me with unexhausted curiosity and a creative idea on science. His help, patience, and support enabled me to keep doing my project. He is so warm, gentle, and open-minded. Sometimes, he showed culturally Korean behavior, so I got Irish Maurice mixed with Korean Maurice. His serious attitude on science makes me want to be a female Maurice.

I am very lucky to have nice committee members. I thank Drs. Michael Frohman who is my chair, Simon Halegoua, Howard Sirotkin, and Aaron Neiman for their guidance and help. Their critical mind and suggestion on my research impressed me and made me to see my research in a different view. I don't doubt they will always be there even after I leave stony brook because I believe once my committee forever my committee.

I love to express my thankful heart to two former lab members, Dr. Yun Doo Chung and Dr. James Baker, for their friendship, help, and critical comments. I show my appreciation to the members of Frohman lab and Gergen lab for helping me. It was enjoyable to talk with them. Also, I can't skip mentioning my thank to my former advisors and professors in former colleges where I have obtained diplomas. They have been always there for me and haven't hesitated to give me an invaluable advice. I thank them to share their wisdom and personal experience with me.

I thank my friends including Suk-Kyung Lee for their comfort and friendship.

Without them, my life would have been more terrible and lonelier in Stony Brook. Also, I would like to thank many church friends in Korea who never forget to pray for me.

Every midnight when I came back home after work, I always watched the moon in a dark sky, missing my family. I guess they also missed me so much. I truly thank my family, Ki-Ho, Bo-Eun, Mi-Jeong, Seung-Hee, aunts, and uncles, and their families for support, endless love, and prayer. Especially, chatting with Yoo Min and Joon Hyuk through Internet animated and energized me. Most importantly, I thank my Mom and Dad for their sacrifice, love, encouragement, and prayer. I can't thank them enough for their love and trust.

Lastly, I would like to give thanks and honor to my God who does not break a bruised reed and not snuff out a smoldering wick, and thank him for being with me and showing me the way of my life all the time.

Chapter 1: Introduction

1. Eukaryotic cilia and flagella
2. IFT
3. BBS
4. The current model for IFT and BBS
5. Sensory cilia in *Drosophila*

Primary cilia play an important role in development, physiology, and sensory perception. Cilia are assembled and maintained by intraflagellar transport (IFT), a bidirectional transport pathway composed of two subcomplexes: anterograde IFT-B and retrograde IFT-A complexes depending on different motors. An alteration in IFT particles results in a functional defect of cilia which consequently results in many disorders. In Drosophila, mechanosensory and chemosensory transduction takes place in cilia, and ciliary dysfunction leads to mechanosensory and chemosensory deficits. A combination of comparative genomics and mutant analyses has discovered many ciliary proteins.

Bardet-Biedl syndrome (BBS) proteins have been recently cloned and identified to be involved in ciliary function. The broad spectrum of BBS symptoms raises an interest of their functional involvement in cilia. Related to IFT, BBS7 and BBS8 have been reported to couple two IFT subcomplexes in nematode, and BBS1 and BBS4 knockout mice are anosmic. However, the role of BBS proteins in the sensory cilia of Drosophila is not clear. In this chapter, I will describe cilia, IFT particles, and BBS proteins. A current model for IFT transport and fly ciliary structure where mechanosensory and chemosensory stimuli are transduced will also be discussed.

1. Eukaryotic cilia and flagella

Cilia (flagella) are evolutionarily well-conserved in eukaryotes. Cilia and flagella have the same internal structure and are only different in length. Cilia generally are grouped on the surface of a cell and are 5-10 μ m long. Flagella are long and slender projections of about 50 μ m. Cilia found in protozoans are for either locomotion or simple movement of liquid over the surface. Some eukaryotic cilia and flagella are also motile. They move the cell by beating in a whip-like motion in a coordinated wave.

1.1. Structure and Components

Cilia (or flagella) are hair-like organelles projected from a basal body at a cell surface. Basal bodies are structurally composed of 9 microtubular triplets, located at the base of the cilium or flagellum and serve as a microtubule organization center anchoring cilia. Cilia have a 9+2 axonemal structure, a cytoskeletal unit having a ring of nine doublet microtubules, around a central pair of singlet microtubules. How doublet microtubules come out of triplets in basal body is unknown. Microtubules are cylindrical structures composed of 13 parallel protofilaments, each of which is tightly packed with α and β -tubulin heterodimers. These 13 protofilaments are in same polarity field, so each microtubule has a plus (+)-directed end and a minus (-)-directed end. The doublet microtubule is made up of one complete microtubule (A tubule) and one incomplete microtubule (B tubule).

An axonemal structure of a cilium contains many accessory proteins required for proper function. Axonemal dyneins, inner and outer dynein arms, are attached to doublet microtubules and link them to each other to produce a sliding force for motility by

hydrolyzing ATP using their ATPase activity. Therefore, in the presence of ATP, dynein arms enable microtubule doublets to slide against each other, leading to the bending of cilia and flagella as a whole. The nexin and radial spoke is thought to regulate the motility. They hold the doublets in plane to keep the sliding in limited lengthwise. The cooperation of these proteins yields a beating of cilia. On the other hand, cilia of 9+0 axonemal structure missing a central pair of singlet microtubules are called primary cilia. This type of cilia is widely distributed in almost every mammalian cell (<http://memberjs.global2000.net/bowser/cilialist.html>). Usually, primary cilia are immotile due to the lack of motility-related components, except embryonic nodal cilia which are motile by bearing dynein arms (Nonaka et al., 1998).

1.2. Distribution and Function

The primary function of cilia and flagella is motility. Since the axonemal structure is well conserved through organisms, the molecular mechanism of motility is also well conserved. With cilia or flagella, a single cell organism is able to move and a multicellular organism moves fluids or particles over a surface. In eukaryotic cells, motile cilia are found in epithelial cells of the trachea, on the ependymal cells of the brain subventricular region, in fallopian tubes of the female reproductive organ, and on sperm. The flagellum in a sperm tail is used to propel the cell forward, and the beating cilia in the oviduct carry an ovum along the reproductive tract. The motile cilia in trachea clear mucus and dirt out of the lung.

Unlike motile cilia, non-motile primary cilia are known to be involved in sensory perception. In human, primary cilia are primarily found in photoreceptor cells and

olfactory neurons. The outer segment of the photoreceptor cell is a highly modified primary cilium connected to an inner segment by a connecting cilium. The outer segment where the photoreceptors reside is responsible for transducing visual stimuli. Cilia on the dendritic knob of olfactory neurons have the olfactory receptors to contact odorants. A kinocilium in cochlea is involved in mechanosensory perception. Primary cilia other than in peripheral sensory organs serve as mechanosensors, measuring flow rate in the lumen of the collecting duct tubule of kidneys (Nauli et al., 2003). Besides, primary cilia in a liver and a pancreas seem to carry out an important physiological and pathological role by either sensing extracellular fluid flow or regulating ion transport (Sanzen et al., 2001; Zhang et al., 2005).

Recent studies on the role of cilia on embryonic development have found that nodal cilia in early embryos are involved in determining left-right asymmetry (Nonaka et al., 2002; Nonaka et al., 1998), and for tissue patterning like limb bud formation in the late developmental stage (Huangfu et al., 2003). Cilia are also involved in significant signaling pathways of sonic hedgehog signaling (Huangfu and Anderson, 2005; Huangfu et al., 2003) as well as planar cell polarity (PCP) signaling (Park et al., 2006) on development. In vertebrate, primary cilia not only function as a sensor of the extracellular environment for physiological regulation but also contribute to developmental regulation.

In nematodes and insects, cilia are well modified as the dendritic appendage of a bipolar sensory neuron where mechanosensory and chemosensory stimuli are transduced. In insects, two type I sensory organs, external sensory (ES) organ and internal chordotonal organ (CHO), harbor dendritic cilia which explains ciliary dysfunction leads to mechanosensory and chemosensory defects.

1.3. Cilia-related diseases

The symptoms are likely to be caused by ciliary failure can be inferred from the distribution and the function of cilia. The phenotype of ciliary impairments appears heterogeneous, depending on which functional component of ciliary structure is affected. For example, vertebrate have both motile and non-motile primary cilia. If there is a defect on dynein arms responsible for the cilia motility, the symptom reflects the distribution of motile cilia. There are many diverse diseases that have been discovered related to ciliary deficit such as primary cilia dyskinesia (PCD), polycystic kidney disease (PKD), retinal degeneration, respiratory disease, Bardet-Biedl syndrome (BBS), *situs inversus* (Bisgrove and Yost, 2006; Davenport and Yoder, 2005; Pazour and Rosenbaum, 2002).

PCD comes from the disorder of motile cilia in human beings, so a PCD patient suffers from chronic respiratory infection, male infertility, and hydrocephalus (Eley et al., 2005). An alternation of nodal ciliary flow causes an aberrant left-right development (Ferrante et al., 2006), indicating that ciliary motility plays an important role in early development. Both findings that normal left-right determination occurred when nonmotile nodal cilia were exposed to the leftward extracellular fluid and that rightward flow reversed the left-right axis in wild type embryos demonstrate that the asymmetric flow per se is sufficient for the left-right specification as well as that cilia are involved in physiological function (Nonaka et al., 2002; Nonaka et al., 1998). There are proposed two models as to how fluid flow is related to left-right asymmetry : morphogen flow model and two cilia model (McGrath et al., 2003; Nonaka et al., 1998). Morphogen flow model proposes that signaling molecules are transported to the left side by ciliary flow, but virtually no asymmetric distribution of proteins are detected (Tanaka et al., 2005). Two cilia model in which two populations of primary cilia exist in the embryonic node

suggests that peripheral non-motile cilia detect the fluid flow generated by central motile cilia, which in turn triggers the following signaling pathway (Sarmah et al., 2005). A defect in primary cilia reveals that primary cilia are associated with many cell types. The most well-known impairment is hereditary renal dysfunction known as autosomal dominant PKD (ADPKD), autosomal recessive PKD (ARPKD), and nephronophthisis (NPHP). Polycystin 1 and polycystin 2 are transmembrane proteins that heterodimerize to form non-selective calcium ion channels, whose loss results in PKD. Polycystic kidney disease proteins including Polycystin-1, Polycystin-2, Polaris (IFT88), and Cystin are all colocalized in renal cilia (Yoder et al., 2002). The disruption of cilia or abrogated Polycystin1 and 2 blocks the Ca^{2+} influx which is required for the regulation of cell proliferation, apoptosis, and nephron function, suggesting that cilia serve to detect mechanical flow (Boletta and Germino, 2003; Nauli et al., 2003; Praetorius and Spring, 2001; Praetorius and Spring, 2003). However, how primary cilia are connected to the cyst formation is not clearly understood. NPHP also shows cystic formation in kidney, pancreas, and liver, and *situs inversus*, retinal degeneration, brainstem malformation, and mental retardation. Six genes have been identified for NPHP and those proteins are likely to function in primary cilia (Olbrich et al., 2003; Olbrich et al., 2002; Otto et al., 2002; Otto et al., 2003).

Several lines of evidence strongly support that the disruption of cilia-dependent signaling gives rise to developmental abnormalities. Ciliary defect in Shh-dependent pattern formation of a neural tube and a limb bud formation displays a neural tube defect and polydactyly (Huangfu et al., 2003; Liu et al., 2005; May et al., 2005). With ciliary loss, the downstream target gene expression of Shh signaling is decreased (Huangfu and Anderson, 2005). The Shh activation looks to be correlated to the localization of Smo on

cilia which is required for the activation and the transport to nucleus of Gli transcription factor, but underlying mechanism is not determined and how cilia are involved in this process is elusive (Corbit et al., 2005). Similarly, cilia are involved in switching between canonical Wnt signaling and the non-canonical Wnt/planar cell polarity pathway, through which two different end points were reached. Increased Inversin on primary cilia by fluid flow inhibits canonical Wnt pathway and activates PCP pathway by interacting with Disheveled (Dvl1) and PCP proteins, leading to the normal regulation on several processes including mitotic reorientation of proliferating cells (Okada et al., 2005; Simons et al., 2005). Therefore, ciliary defect results in increased β -catenin expression and Wnt signaling transcription factor, eventually disturbing tubulogenesis (Fischer et al., 2006; Simons et al., 2005).

Bardet-Biedl syndrome has been recently reported to be related to ciliary function (Ansley et al., 2003). It clinically shows kidney dysfunction, retinal degeneration, polydactyly, situs inversus, obesity, mental retardation, and diabetes (Beales et al., 1999). One topic of my thesis study is BBS proteins in *Drosophila*, so I will discuss more detail on BBS in a following subchapter.

As primary cilia play an important role in sensory perception, vision, olfaction, and hearing are all affected by ciliary defect as well. The loss of cilia leads to an aberrant accumulation of opsin and arrestin in the inner segment, which results in photoreceptor degeneration (Marszalek et al., 2000). This retinitis pigmentosa brings about night blindness and progressive visual loss. X-linked RP (XLRP), the most severe form of Retinitis pigmentosa (RP), has been reported to have a systemic phenotype, e.g. hearing loss, sinusitis and primary ciliary dyskinesia, indicating that XLRP is an instance of ciliary dysfunction related to the retinal degeneration (Zito et al., 2003). In hair cells of

the inner ear, the loss of the order of kinocilium and stereocilia incurs deafness (Holme and Steel, 2002). Olfaction is affected by the ciliary defect as well. BBS1 and BBS4 null mice have an impaired sense of smell and disrupted dendritic microtubule organization in olfactory epithelium (Kulaga et al., 2004).

In addition, Alstrom syndrome (ALMS), oral-facial-digital type I syndrome (OFD1), and Meckel-Gruber syndrome (MGS) are related to ciliary defect (Ferrante et al., 2006; Hearn et al., 2002; Keller et al., 2005). ALMS includes similar symptoms to BBS, and ALMS1 protein and *Odf1* protein of OFD1 are all identified to localize on centrosomes and the base of cilia (Ferrante et al., 2006; Hearn et al., 2002). MGS is characterized by symptoms found in ciliary dysfunction and its *Chlamydomonas* ortholog is listed on the flagella/basal body proteomes (Keller et al., 2005).

2. IFT (Intraflagellar transport)

As cilia are very tiny protruding structures of a cell without machinery for protein synthesis, they require a specialized pathway termed intraflagellar transport (IFT) to move structural and signaling proteins synthesized in the cytoplasm to a ciliary compartment. IFT is bidirectional transporting machinery for development and maintenance of cilia. (reviewed in (Rosenbaum and Witman, 2002)). IFT is composed of at least 16 polypeptides which are grouped into two subcomplexes: retrograde complex A

and anterograde complex B. Reportedly, IFT depends on kinesin-II and *osm-3* for an anterograde movement from the base to the tip and on cytoplasmic dynein for coming back to the base of cilia from the tip (Cole et al., 1993; Hou et al., 2004; Ou et al., 2005; Signor et al., 1999; Snow et al., 2004). Because IFT proteins are the essential component to construct cilia, the defect of IFT particles directly leads to failure of the function which cilia are implicated in. In this subchapter, I will explain IFT subparticles and motors, and list defects incurred by IFT disruption.

2.1. Motors

There are three classes of motors involved in a variety of biological movements such as mitosis, axoplasmic transport and secretion: kinesins, dyneins, and myosins (Karcher et al., 2002). Kinesin is composed of $\alpha_2\beta_2$ tetrameric complex, moving toward the microtubule-plus end at speeds of 0.6-0.8 $\mu\text{m/s}$. It contains motor domain at N-terminal and α helical coiled coil stalk domain formed by the homodimerization of two heavy chains. At C-terminal, it is connected to two globular β light chains (de Cuevas et al., 1992; Hirokawa et al., 1989). Many kinds of kinesin proteins have homology on motor domain and rest of the domain is diverse, implying the interaction with different cargos (Moore and Endow, 1996). Here, I will explain Kinesin-II, one family of kinesin motor found in cilia and flagella, and cytoplasmic dynein.

The anterograde motor

Typical heterotrimeric anterograde Kinesin-II motor is composed of three parts: two motor subunits of KIF3A (85kDa) and KIF3B (95kDa) and non-motor subunit of kinesin-associated protein (KAP, 115kDa) (Scholey, 1996; Yamazaki et al., 1995;

Yamazaki et al., 1996). Two motor subunits of Kinesin-II belong to Kif3 family whose sequence structural property has globular domains of both N- and C-termini linked by α -helical stalk (Cole et al., 1993). By the study of the temperature-sensitive mutant of *Chlamydomonas*, *fla10*, Kinesin II has been suggested to function as an anterograde motor. *fla10* mutant flagella was not elongated and rather got shorten in nonpermissive temperature (Cole et al., 1998; Huang et al., 1977; Kozminski et al., 1995). Subsequently, in mouse, nodal cilia was absent by the knockout of Kinesin motor protein (Nonaka et al., 1998) and sea urchin blastulae have short cilia with the injection of antibody against kinesin-II motor (Morris and Scholey, 1997). Mammalian photoreceptors, opsin and arrestin, are also transported by Kinesin-II protein from inner segmental cilium to outer compartment (Marszalek et al., 2000). *Drosophila* KLP68D is extensively expressed in CNS and in a subset of PNS at a late embryonic stage (Pesavento et al., 1994). Mutations in *Drosophila* KLP64D and KAP lead to absent ciliary axonemal structure and eliminated auditory response (Sarpal et al., 2003). These findings strongly supported that Kinesin II holoenzyme plays a role of anterograde motor for the cilia/flagella assembly and maintenance.

The retrograde motor

Cytoplasmic dynein has been suggested as a retrograde motor by studies with *Chlamydomonas* mutants of cytoplasmic dynein light chain and Heavy Chain 1b (Pazour et al., 1998; Porter et al., 1999). A defect in cytoplasmic dynein light chain 8 (LC8) results in short flagella. There is no defect of KinesinII movement in these mutants, but all accumulate IFT particles at the tip of cilia (Pazour et al., 1998). Dhc1b (Dynein heavy chain isoform) was upregulated in sea urchin after deciliation (Gibbons et al., 1994) and

accumulates IFT particles at the tip of a very short flagella as well, suggesting that DHC1b is a subunit of retrograde cytoplasmic dynein motor (Pazour et al., 1999). Che3, *C. elegans* mutant homolog for DHCb1, also has short sensory cilia and filled with IFT particles (Signor et al., 1999; Wicks et al., 2000). *Drosophila* cytoplasmic dynein mutant, *btv* (unpublished data), has a defect in both the behavioral response to courtship pulse song and sound-evoked response (Eberl et al., 2000). Interestingly, EM analysis shows that *btv* deletion leads to an enlarged ciliary dilation filled with vacuoles without parachrySTALLINE inclusions.

2.2. IFT particles

Most IFT proteins are well conserved through ciliated organisms as shown in Table 1-1 (Avidor-Reiss et al., 2004; Ostrowski et al., 2002; Pazour, 2004; Rosenbaum and Witman, 2002). IFT particles are first identified in *Chlamydomonas reinhardtii* by a biochemical approach, being found at ~16S in sucrose gradients (Kozminski et al., 1993; Piperno and Mead, 1997). Many cilia related genes in *C. elegans* and *Drosophila* have X-box promoter motif regulated by RFX-type transcription factor for ciliary differentiation (Dubruille et al., 2002; Efimenko et al., 2005). Also, ciliary proteins including IFT molecules contain protein-protein interacting motifs like WD40 or TPR (Avidor-Reiss et al., 2004; Cole, 2003; Li et al., 2004). Thus, comparative genomic search combined with domain analysis has been used for identifying novel cilia-related genes (Avidor-Reiss et al., 2004; Blacque et al., 2005) The IFT function has been explored by extensive studies on IFT mutants in *Chlamydomonas* and *C. elegans*. All IFT-A mutants have morphologically truncated or stumpy cilia and IFT-B mutants commonly have completely missing cilia. Recently, it has been discovered that IFT is directly involved in

signal transduction by reorganizing signaling molecules during mating in *Chlamydomonas* (Wang et al., 2006).

In *C. elegans*, sensory ciliary mutants defective in chemotaxis, osmotic avoidance, dauer larva formation, and dye filling have uncovered several IFT subunit genes including *osm-5* (Cole et al., 1998; Fujiwara et al., 1999; Haycraft et al., 2003; Haycraft et al., 2001; Perkins et al., 1986). The IFT-A complex includes IFT144, IFT140, IFT139, and IFT122, of which the IFT140 and IFT122 proteins are conserved in *C. elegans* and *Drosophila*. These proteins are known to be involved in retrograde transport in *Chlamydomonas* and *C. elegans* (Blacque et al., 2006; Qin et al., 2001).

The IFT-B complex is composed of more proteins than IFT-A. IFT172 which was identified as a LIM homeodomain transcription factor binding protein is discovered to be involved in Hedgehog signaling in mouse embryos through the study of *wimple*, the IFT172 mouse homolog (Huangfu and Anderson, 2005; Huangfu et al., 2003). IFT27, Rab-like small G protein, is required for the stability of IFT-A and IFT-B subcomplexes as well as cytokinesis and cell cycle (Qin et al., 2007). NGD5, whose *Chlamydomonas* homolog IFT52 locates around a transitional fiber, is downregulated by opioid treatment and expressed in rat brains (Deane et al., 2001; Wick et al., 1995). Also, the human IFT57 homolog, hippo, was reported to interact with Huntingtin-interacting protein (HIP) and to contribute to the pathogenesis of Huntington disease (Gervais et al., 2002).

Especially, mutation in *Osm-5*, *IFT88* and *polaris* homolog, provides a lucid evidence that cilia are involved in many physiological and developmental processes. Tg737 encodes Polaris which is a mouse homolog of IFT88, an anterograde IFT component (Pazour et al., 2002). Tg737 insertional allele causes ARPKD where primary cilia were discovered to fail to assemble. This defect was observed in *Chlamydomonas*

IFT88 mutant as well (Pazour et al., 2000), suggesting that the malfunction of primary cilia in kidney is related to kidney disease. Mutant mice have disorganization in the retinal outer segment and mislocalization of opsin into inner segment (Pazour et al., 2000; Yoder et al., 2002), leading to the complete loss of rod cells (Marszalek et al., 2000). The degeneration of rod cell by IFT defect is similar to that observed in retinitis pigmentosa and other progressive blindness. This is similar to *C. elegans*, where an abnormal ciliary construction and maintenance results in defective sensory perception and development. The *Tg737* mice are embryonic lethal and the embryos lack nodal cilia, ultimately leading to defective in left-right determination (Murcia et al., 2000). In addition, *nompB*, *IFT88* fly homolog only affects the differentiation of sensory cilia but not sperm tail formation (Han et al., 2003).

3. BBS (Bardet-Biedl syndrome)

Biedl and Bardet first described Bardet-Biedl Syndrome (BBS; OMIM209900) as a genetically heterogeneous autosomal recessive disorder in human. Its primary symptoms include obesity, pigmentary retinopathy, polydactyly, mental retardation, and renal dysfunction (Beales et al., 1999). Additionally, BBS patients show speech disorder, developmental delay, ataxia, poor coordination, diabetes mellitus, dental crowding, and congenital heart disease (Katsanis et al., 2001b). BBS prevalence is relatively low in

north America and Europe, at the rate of 1:140000 to 160000, while the rate is 1:13500 or 1:17500 respectively in Kuwait and Newfoundland (Farag and Teebi, 1989; Klein and Ammann, 1969). Genetic heritage of BBS is not explained by Mendelian inheritance completely. Moreover, recent reports propose that BBS is related to ciliary function (Ansley et al., 2003). However, how various phenotypes of BBS are functionally connected to cilia and cilia-related function is entirely concealed.

3.1. The phenotypes of BBS

The most distinctively common phenotypes between BBS and ciliary disorder are rod-cone dystrophy and renal dysfunction, which are all progressive. The blindness in BBS patients rapidly progresses. In *Bbs2*-null mice, mislocalization of rhodopsin leads to apoptosis of photoreceptors, the primary ciliated cell of the retina (Nishimura et al., 2004). This is similar to the IFT mutants, *Kif3a* conditional mutant and *Tg737* hypomorphic mouse where disrupted IFT result in the accumulation of opsin on the inner segment, followed by degeneration of the outer segment (Marszalek et al., 2000; Pazour et al., 2002). Renal dysfunction can be caused by ciliary malfunction through the homozygous mouse of *Tg737* hypomorphic allele (Pazour et al., 2000). These common phenotypes strongly suggest that the BBS symptoms are also related to ciliary dysfunction.

BBS is unlikely to have phenotypes usually observed in primary ciliary dyskinesia (PCD), which has defects in axonemal structure of motile cilia. PCD includes bronchiectasis, sinusitis, dextrocardia and infertility. Especially, BBS doesn't seem to show *situs inversus* found in Kartagener Syndrome (KS) patients. *Situs inversus* displays randomized left-right asymmetry due to a ciliary defects in the embryonic node (Beales et al., 1999; Ibanez-Tallon et al., 2003). *Tg737* allele is also required for left-right axis

determination (Murcia et al., 2000). Recently, it was reported that the disruption of *inversin*, the gene mutated in infantile nephronophthisis (NPHP2), give rise to renal cystic formation, *situs inversus*, and pancreatic islet cell dysplasia (Mochizuki et al., 1998; Morgan et al., 1998; Otto et al., 2003). *Situs inversus* and pancreatic dysplasia are associated with Hedgehog signaling as well (diIorio et al., 2002; Huangfu et al., 2003), suggesting that cilia play an important role in left-right symmetrical development.

However, of BBS patients, only one case was reported to have manifesting a randomization of left-right asymmetry (Ansley et al., 2003). Therefore, the question as to whether or not the left-right symmetry is also affected by BBS proteins remains to be answered. Besides, whereas the infertility frequently found in PCD and KS is mainly caused by sperm immotility, the primary gonadal failure is the main reason for infertility in BBS (Beales et al., 1999).

Obesity, one of the most prominent phenotypes of BBS, is quite interesting but a difficult issue to link to ciliary function. Almost nothing is known about how BBS causes obesity. If BBS plays a role in cilia, what is the mechanism of ciliary disorder underlying the obesity? Is it related to the core reason causing obesity? Or, the obesity is indirectly caused by BBS? Then, how do BBS patients obtain obesity? It might be related to energy metabolism, unregulated adipose cell proliferation, and signaling pathway or satiety control in CNS. No difference in energy metabolism has been reported when comparing BBS patients and general obese patients, indicating that BBS is not associated with energy metabolism (Grace et al., 2003). Mutation analysis on BBS6 showed no link between specific mutations and obesity (Andersen et al., 2005). The observation on BBS-4 null mice illustrated that increased food intake leads to the obesity, suggesting that Bbs4 deficiency alters the function of hypothalamic neurons (Mykytyn et al., 2004).

Interestingly, abnormalities of both the pituitary and hypothalamus were postulated in BBS patients (Burn, 1950). However, possible defects in glucose regulation cannot be ruled out because glucose tolerance tests have yet to be examined on BBS null mice. BBS patients have other secondary phenotypes like diabetes, hypertension, and congenital heart defect. Intriguingly, a recent report show that Tg737 is expressed in the islets of pancreas and Tg737 mutant mice have a problem in glucose regulation (Zhang et al., 2005). This suggests a possible link between ciliary function and secondary phenotype of BBS. On the other hand, *tubby* mutants demonstrate different possibilities. *tubby* mutant mice exhibit late onset obesity, neurosensory defects, and photoreceptor cell defects which are not dissimilar to those observed in BBS (Carroll et al., 2004). The loss of function mutant and the localization of *tub* gene in hippocampus and hypothalamus firmly speculate that the phenotype of BBS including obesity, hypertension, and diabetes might be originated from the defect in hypothalamus, not related to ciliary dysfunction. A recent study of BBS gene expression in adipose tissue by quantitative real-time PCR demonstrated that BBS genes showed differentially increasing expression throughout adipogenesis, suggesting that BBS proteins might have a significant role for the obesity etiology (Forti et al., 2007). However, it is not sufficient to determine the relationship for ciliary function of BBS proteins and obesity. Many questions should be answered regarding this issue: how hypothalamic regulation affects the obesity, why particularly the defect of hypothalamus is yielded by these genes, whether the ciliary components are related to the hypothalamic development or function, how many pathways are involved in developing obesity, and to what extent diverse factors affect the obesity.

3.2. The molecular aspect of BBS

Twelve genes encoding BBS proteins have been so far identified in human (Ansley et al., 2003; Badano et al., 2003a; Chiang et al., 2006; Chiang et al., 2004; Li et al., 2004; Mykytyn et al., 2001; Mykytyn et al., 2002; Nishimura et al., 2001; Slavotinek et al., 2000; Stoetzel et al., 2006; Stoetzel et al., 2007). As shown in Table 4-1, for BBS1, 2, and 7, there is no shared common domain, and only partial homology is recognized among some of them. BBS2 and BBS7 share the SCOP (structural classification of proteins) domain which is predicted to encode six-bladed β -propeller structure. BBS 1 and BBS7 partly overlap in a SCOP region, suggesting the possibility that abnormal function of this domain could be a reason for the common phenotype of each locus mutation (Badano et al., 2003a). The domain structure analysis predicts that BBS4 and BBS8 contain TPR (tetratricopeptide repeat) domain, indicating these could be involved in protein-protein interaction. BBS4 also has homology with the O-linked acetylglucosamine transferase family, implying that BBS4 might interact with other proteins on the glycosylate specific residue (Mykytyn et al., 2001). BBS8 contains prokaryotic *pilF* domain which is implicated in the assembly of type IV pili, which mediate bacterial twitching motility (Merz et al., 2000). Analysis of independent human BBS3 families uncovered the mutation on *ARL (ADP ribosylation factor-like) 6*. ARL6 is a member of RAB-SAR-ARF-ARL family of a small GTP binding protein superfamily (Fan et al., 2004). BBS6 isolated for McKusick-Kaufman syndrome (MKKS) has been found to be evolved from an eukaryotic chaperonin, CCT subunits, and to be diverged to a functionally distinct chaperonin-like protein locating around centrosome (Kim et al., 2005).

Unlike other BBS genes revealed by genetic linkage mapping, BBS9, BBS10,

BBS11, and BBS12 have been identified by single nucleotide polymorphism (SNP) based microarray mapping (Chiang et al., 2006; Stoetzel et al., 2006; Stoetzel et al., 2007). BBS9 has been discovered as a parathyroid hormone-responsive gene B1 (Nishimura et al., 2005). BBS10 and BBS12 are vertebrate-specific protein and form a novel branch of type II chaperonin superfamily together with BBS6. The simultaneous suppression of these proteins in zebrafish early development produced more severe BBS phenotype than when one protein was suppressed, suggesting the functional redundancy by genetic interaction might be the case (Stoetzel et al., 2006; Stoetzel et al., 2007). BBS11 has been identified to be a *TRIM32* encoding an E3 ubiquitin ligase which functional analysis using knock down and expression pattern in zebrafish illustrated that it is involved in BBS phenotype (Chiang et al., 2006). TRMP32 contains ring finger for E3 ubiquitin-protein ligase activity, B-box, NHL domain of a catalytic activity in peptidyl-glycine alpha-amidating monooxygenase, and WD40 domain. Interestingly, different mutant phenotype came out depending on which domain it has mutation, suggesting that different domain of TRIM32 is likely to serve for different processes (Chiang et al., 2006).

The most striking evidence supporting the involvement of BBS in ciliary function is the localization of BBS8. Mouse BBS8 was found in ciliated structure including maturing spermatids, connecting cilia of the retina, columnal epithelial cells in the lung, olfactory epithelia and the telencephalon (Ansley et al., 2003). Especially, BBS is localized near the centrosomes and basal bodies in mammalian cells, interacting with pericentriolar material 1 protein (PCM1), which is known to be involved in ciliogenesis (Ansley et al., 2003). BBS4 localizes to the centriolar satellites of centrosomes and basal bodies of primary cilia, and interacts with PCM1, suggesting BBS4 is a player in

targeting and anchoring of pericentriolar proteins and microtubule organization (Kim et al., 2004). BBS4 also colocalizes with BBS8 near the centrosome, interacting with PCM1 (Ansley et al., 2003). Remarkably, promoter regions of BBS proteins predict the localization by sharing the x-box sequence which is regulated by a transcription factor specifically found in cilia. It addresses that BBS genes must be highly conserved in ciliated organisms, but not in nonciliated ones, which is later proved by comparative genomics (Avidor-Reiss et al., 2004; Li et al., 2004). BBS3 and BBS5 were found to be uniquely expressed in the mechanosensory and chemosensory organs in both *C. elegans* and *D. melanogaster* (Fan et al., 2004; Li et al., 2004). The disorganization of olfactory organ by the loss of either BBS1 or BBS4 causes anosmia (Kulaga et al., 2004), supporting the role of BBS in the microtubule organization of cilia. All these results strongly suggest that ciliary function seems to be responsible for the BBS phenotypes.

3.3. Triallelic inheritance

Perplexingly, BBS is genetically complex for the penetrance and the expressivity. Genetic diseases are classified into two types: Mendelian and complex traits. In classical Mendelian inheritance, the phenotype appears as a consequence of mutations in one (dominant) or both (recessive) copies of a gene. On the contrary, complex traits result from more than one gene and their interaction with environmental factors. Though BBS has been regarded as an autosomal recessive disease, this does not explain the broad spectrum of BBS phenotypes. Katsanis *et al.* proposed the triallelic inheritance: two homozygous mutation at one locus and a third mutation at another locus are required for the penetrance and expressivity of the phenotype (Katsanis et al., 2001a).

All the phenotypes presented by BBS patients do not contain overlapped or

common characteristics with respect to specific expression and localization on the body. The diverse severity of phenotype caused by identical mutations on loci suggests genetic heterogeneity. Complex inheritance is also supported by sequencing analysis of BBS patients. In one BBS pedigree, unaffected and affected siblings were noted with the same mutation on one locus, but subsequent sequencing data exhibited that the only affected sibling contained the mutation in both copies of another locus. In addition, one affected individual carried two nonsense mutations on one locus and a single nonsense mutation on another locus, whereas the unaffected one had no other mutation on different locus despite having two nonsense mutations identical as affected one (Katsanis et al., 2001a). Moreover, 47% with BBS2 and 37% with BBS6 of investigated family showed the involvement of another locus. The more cases of triallelic inheritance have been reported in different loci as shown in Table 1-3. However, Mykytyn *et al.* questioned the relevance of the triallelic inheritance in BBS, claiming that the common BBS1 missense mutation is not involved in triallelic inheritance. They presented the case of no M390R mutation in the patients having two mutations on other loci and found affected individuals who have only homozygous mutations on *BBS1* without any alteration on another loci (Mykytyn et al., 2002). BBS1 is a major causal component in BBS, accounting for one third of BBS, and *BBS1* is very well conserved from *Drosophila* to Mammalia. The most prevalent mutation in BBS1 is M390R, which is extensively found in European families, signifying that *BBS1* is transmitted from a common ancient source (Beales et al., 2003; Mykytyn et al., 2003).

However, Beales *et al.* presented that mutant alleles in *BBS1* participated in complex inheritance upon analyzing hundreds of independent families having BBS symptoms. The patients having two mutations on M390R and another mutation on BBS2

or BBS6 showed more severe phenotype than those having only two M390R mutations on BBS1. This implies that the most common mutation in BBS1, M390R, is involved in oligogenic inheritance and that the third mutation might act as a modifier in the expressivity and be pathogenic (Badano et al., 2003b). Although BBS had been suggested to follow the recessive transmission, the subsequent mapping of new BBS loci and the sequencing analysis of larger number of families from diverse ethnic background have weighed on the complexity of BBS inheritance. *in vitro* studies using BBS6 point mutation of T325P in HeLa cells displayed that the variant imparts severe consequences to the protein function (Badano et al., 2003b). Given these findings, they might participate in a multiprotein complex or sequentially affect the same cellular process, but most of them remain elusive.

There is only one example of a triallelic requirement for a Mendelian trait, Charcot-Marie-Tooth neuropathy type 1A. But this is a dominant trait requiring three copies (alleles) of normal gene to manifest diseases (Lupski et al., 1991). Although the Mendelian inheritance has been accepted as a basic heritage principle, uncovered are more and more diseases which cannot be accounted for by Mendelian inheritance such as phenylketonuria (PKU), hypophenylketouria, cystic fibrosis (CF) and *etc.* (Badano and Katsanis, 2002). There are many examples of recessive inheritance with a modifier of penetrance. *Drosophila* cell adhesion protein, *fasciclin* I gene, requires the mutation on both copies and additional mutation of the tyrosine kinase *Abl* for the manifestation (Elkins et al., 1990). The effect of modifier genes varies from the penetrance to the suppression. In mice, the mutant gene causing the disorganization (Ds) phenotype displays various penetrances in different strains. The dominant modifier of nonsyndromic deafness gene *DFNB26* in humans suppresses the deafness (Nadeau, 2001). For BBS, it is

not clear whether mutations in two genes are always required for the expression of the phenotype or only one gene acts as a modifier. Because each mutation on BBS do not exactly correlate with its phenotype and penetrance, to address how these variants of each locus contribute to the phenotype through what kind of genetic interaction is instrumental in furthering the understanding of the underlying mechanism of BBS.

Interestingly, the identification of MGC1203 by yeast two hybrid and computational genomics for ciliary proteins exemplifies an involvement of an interactor or a modifier in BBS penetrance and oligogenic inheritance (Badano et al., 2006; Li et al., 2004). The epistatic contribution of MGC1203 encoding a pericentriolar protein to BBS has been addressed by BBS patient cases that though father and progenies all have a homozygous M390R mutation (BBS1), but only progenies are affected who retain heterozygous MGC1203 (C430T) mutation. This protein also localizes on where BBS symptoms are found and was immunoprecipitated with BBS proteins (Badano et al., 2006). This finding suggests that multiple traits of BBS might be able to be epistatically modulated by diverse molecular components.

3.4. Animal Model systems of BBS

Challengingly, the phenotype of human BBS is hard to explain with corresponding genotype or the combination of the genotype. We do not know which feature directly comes from the causal gene, what kind of consequence results from the interaction with other factors, or which phenotype is shared with other disorder. Contrary to the limited genetic manipulation and numerous factors considered in human model, we are able to study the relationship of genes and the phenotype under the same genetic background with animal model systems.

In mouse, loss of *Bbs1*, *bbs2* and *bbs4* resulted in partial or complete anosmia. Histological findings range from severe reduction of the ciliated border and disorganization of the dendritic microtubule network to trapping of olfactory ciliary proteins in dendrites and cell bodies (Kulaga et al., 2004; Nishimura et al., 2004). *bbs2* and *bbs4* knock-out mice also display obesity and apoptotic retinal degeneration, and fail to form spermatozoa flagella, rather than altering the global development of both motile and primary cilia (Mykytyn et al., 2004; Nishimura et al., 2004). The immunostaining of the mouse with anti-BBS5 and anti-gamma tubulin, centrosomal and basal body marker revealed the localization of BBS5 on the apical surface of the multiciliated ependymal cells lining the ventricles of the brain, exclusively around the basal body (Li et al., 2004). Consequently, these findings raise a question why BBS genes are not involved in every ciliary function in general. Besides, the phenotype caused by mutations of proteins involved in PCP pathway was shared by the deletion of BBS6 protein in both mouse and zebrafish. The genetic interaction of *BBS6* gene and PCP genes such as *vangl2* was observed, directly indicating that BBS protein is involved in PCP pathway (Ross et al., 2005).

The localization of *bbs* genes around basal bodies suggests that their roles might be related to the ciliogenesis or ciliary function. Particularly, a genetic manipulation of *C. elegans* allows to dissect the localization of BBS protein *in vivo*: all known BBS proteins are specifically localized to ciliary neurons (Blacque et al., 2004; Fan et al., 2004; Li et al., 2004). *C. elegans* BBS3 homolog resides in the ciliated sensory neuron and moves back and forth along the cilia, which is reminiscent of IFT, implying that BBS3 can be a cargo or interacting with IFT components (Chiang et al., 2004; Fan et al., 2004). The disruption of both *Bbs7* and *8* in *C. elegans* results in structural and functional defects of

shortened cilia and chemosensory abnormalities. Mislocalization and diminished intensity of IFT components stemming from BBS 7 and 8 dysfunction implicates that BBS7 and 8 might be interacting with IFT proteins at the base of the cilia (Blacque et al., 2004). *C. elegans* homologs of *Bbs1, 2, 7, and 8* were expressed only in ciliated cells (Ansley et al., 2003). The localization and expression of BBS-5 on *C. elegans* is restricted to the base of cilia in amphids, labial neurons, phasmids, and the sensory rays of the male tail. Furthermore, RNA interference of BBS5 inhibited the formation of flagella in *Chlamydomonas* supporting the role of BBS protein in flagella and basal body function (Li et al., 2004). However, much still remains unknown as to the potential role of BBS in ciliogenesis and maintenance. Another puzzle in the BBS research is whether all *Bbs* genes share a functional redundancy or are in charge of different roles consequentially resulting in broad spectrum of phenotypes.

4. The Current Model for IFT and BBS

Recently, it was reported that heterotrimeric kinesin II and homodimeric osm-3 cooperate for an anterograde movement in nematode sensory cilia (Ou et al., 2005; Snow et al., 2004). *C. elegans* sensory cilia differentiate into two domains, 4 μm long ‘middle segment’ of 9 doublet microtubules and 2.5 μm long ‘distal segment’ of 9 singlet microtubules. Osmotic avoidance defective (OSM-3) kinesin was first reported in *C.*

elegans, which contains all functional domains having homology with kinesin heavy chain and extensively expresses in chemosensory neurons of *C. elegans* (Tabish et al., 1995). Mutation in *osm-3* causes defective chemotaxis behavior as well as missing distal segment of sensory dendrites (Perkins et al., 1986; Shakir et al., 1993). Scholey *et al.* investigated the transporting mechanism on *C. elegans* sensory cilia by measuring the velocity of transporting proteins tagged by GFP in different mutant backgrounds (Ou et al., 2005; Snow et al., 2004). The motility measurement by spinning disc confocal microscopy found that IFT particles move in different velocities, at 0.7 $\mu\text{m/s}$ in the middle segment and at 1.3 $\mu\text{m/s}$ in the distal segment and mostly constant speed in retrograde movement (Snow et al., 2004). Unlike *Drosophila* KAP mutant where cilia are absent (Sarpal et al., 2003), *C. elegans* KAP-1 mutant retains a full length of cilia and displays no defect for osmotic avoidance and dye-filling behavior (Snow et al., 2004). Instead, *osm-3* mutation leads to truncation of cilia retaining a middle segment only and double mutant of *KAP-1* and *osm-3* has completely disrupted cilia (Snow et al., 2004), suggesting that two kinesin motors cooperate for a middle segment assembly while only *osm-3* is responsible for the distal segment. Coherently, IFT particles were moved at 1.2-1.3 $\mu\text{m/s}$ rate in a KAP-1 mutant which is as same as the velocity by OSM-3 kinesin motor, while deficit in OSM-3 kinesin resulted in a 0.5 $\mu\text{m/s}$ movement only in a middle segment. This confirms that two kinesin-II motors cooperate for transporting IFT particles in a middle segment, but only OSM-3 kinesin motor works for the distal segment (Snow et al., 2004). Mutant analysis by measuring the velocity of IFT particles identified more proteins involved in the transporting of complexes. In either BBS7 or BBS8 mutants, subcomplexes A and B moved at different speeds. Subcomplex A moved at 0.5 $\mu\text{m/s}$ in a middle segment, and subcomplex B was at 1.3 $\mu\text{m/s}$, subsequently

accumulated on the middle or distal segment tips (Ou et al., 2005). This finding implies that IFT-A components are attached to kinesin II and IFT-B components are connected to OSM-3, and two subcomplexes are coupled by BBS7 and BBS8 (Ou et al., 2005). Besides, *dyf-1*, one of dye-filling mutants missed a distal segment, led to the inactivation of OSM-3, and limited the movement of IFT particles to a middle segment at 0.5 $\mu\text{m/s}$, suggesting that OSM-3 is connected to IFT complex through DYF-1 (Ou et al., 2005). Taken together, it suggests an interesting mechanism that two kinesin-II motors work together for transporting IFT particles along the cilia compartment in nematode. It will be interesting to test whether this functional coordination of two anterograde motors is also adopted in *Drosophila* mechanosensory or chemosensory cilia.

5. Sensory cilia in *Drosophila*

Mechanosensory transduction in Drosophila

Drosophila has two types of sensory organs. Type I sensory organs contain ciliated neurons surrounded by three accessory cells. In contrast, type II sensory organs contain numerous multiple dendritic (md) neurons which are not ciliated.

Mechanosensory and chemosensory stimuli are transduced through modified ciliary endings of the dendritic processes in type I ciliated neurons. Type I mechanosensory organs are categorized into two groups: external sensory (ES) organs like a bristle and

campaniform sensilla are external; chordotonal organs (CHO) are internal (Fig. 1-3). The sensory processes of type I neurons are divided into an outer segment and an inner segment (Keil, 1997). The outer segment of the cilium is where the transducing apparatus resides (Chung et al., 2001; Gong et al., 2004; Kim et al., 2003). A sensory neuron and three supporting cells comprising type I sensory organ all originate from a single sensory precursor cell (Bodmer et al., 1989).

The short mechanosensory cilium in ES organs is attached to a bristle base (Fig. 1-3). The ciliary outer segment in mechanosensory bristles is modified into a tubular body, a tight complex of microtubules embedded in electron-dense substance (Avidor-Reiss et al., 2004; Chung et al., 2001; Keil, 1997). Three supporting cells, tormogen, trichogen, and thecogen complete the mechanically functional ES organ (Hartenstein and Posakony, 1989). The thecogen cell, which is the innermost supporting cell ensheathing a sensory process of a ciliated neuron, is thought to produce dendritic cap protein (Keil, 1997). Tormogen and trichogen cells contribute to form the constitutional barrier for polarized distribution of ions by shaping cuticular bristle socket and shaft (Chung et al., 2001; Keil, 1997). As ES organs are exposed to the external environment, it is easier to gain the access to the physiological measurement of receptor potential. In a rest stage, the K⁺ enriched receptor lymph generated by two supporting cells always displays the positive to the reference potential, generating the voltage difference, transepithelial potential (TEP), between the apical and basal sides of the epithelium. (Keil, 1997). Upon deflections of bristles, the influx of K⁺ from the receptor lymph into the neurons elicits depolarization, whose resulting current gives rise to mechanoreceptor potential (MRP) (Eberl et al., 2000; Kernan et al., 1994).

Chordotonal ciliated neurons located on the second antennal segment (antennal

chordotonal organ) and legs (femoral chordotonal organ) are involved in hearing and proprioception. An antenna, fly hearing center, has 3 compartments: a1 antennal segment or scape, a2 or pedicel, and a3 or funiculus. The rotation of a3 and arista around the stalk of a3 upon sound stimuli stretches Johnston's Organ (JO), which is a chordotonal organ in antennae, in a2. This gates the mechanosensory transducing channels and activates the signaling cascade for auditory response by unknown mechanism. The species-specific courtship song eliciting the acoustic response is composed of the trains of 5-10ms pulses having 30-45ms interpulse intervals and a 160 Hz sinusoidal wave (Caldwell and Eberl, 2002). Near field sound suitable for particle velocity detection has 80-95 dB amplitude. JO is composed of 150-200 scolopidia, chordotonal sensory units. One scolopidium consists of a monodendritic neuron, a scolopale cell, a cap cell and a ligament cell. Usually, two or three ciliated neurons in chordotonal organs are innervated in a scolopale cell which is thought to be an equivalent of a thecogen cell in ES organs (Fig. 1-3). The scolopale rods assembled by scolopale cells ensheath the extracellular receptor lymph space for the ionic reservoir to drive receptor potentials (Carlson et al., 1997), but the main ion component for the receptor lymph in chordotonal organs and underlying mechanism of hearing in JO are not known. Nevertheless, the extracellular recording from nerves between the first and second antennal segments evoked by sound stimuli has been used as a significant means of hearing test for a fly. This measurement together with MRP recording isolated mechanosensory defective fly mutants like *nomp* and *remp* (Kernan et al., 1994).

Channels in CHO cilia are activated by stretch stimulation, and ES cilia locating on the body surface are stimulated by bristle deflection or deformation. This is why ciliary dysfunction causes hearing loss and uncoordinated behavior in fly (Baker et al.,

2004; Chung et al., 2001; Han et al., 2003). Interestingly, a chordotonal cilium has a modified axonemal structure at $\frac{3}{4}$ from the base termed as a ciliary dilation. It is a distinguished bulky structure having paracrystalline inclusion and a tubular array of unknown composition and function. Particularly, two independent TRPV channel subunits of IAV and NAN localize on the proximal cilia limited by a ciliary dilation. This is different from the previous speculation that mechanical stimulation would be delivered by a direct physical contact of dendritic cap and the channel proteins. Instead, it leaves a possibility that another channel might exist for the chordotonal activation to transduce the mechanosensory stimuli (Gong et al., 2004).

Chemosensory transduction in *Drosophila*

Flies obtain information related to the food, oviposition, and habitat to survive through chemosensory organs, which requires a specialized structure such as antenna and maxillary palp for adult and antenno-maxillary complex at the anterior tip for larvae (Carlson, 1996). For chemosensory transduction, cilium is also an essential structure in *Drosophila*. Cilia extended from olfactory receptor neurons (ORN) are bathed in the lymph surrounded by multiporous sensory bristles, which are called sensilla (Stocker, 1994). *Drosophila* olfactory organs are constituted by antenna and maxillary palp in adult (Riesgo-Escovar et al., 1994) and by antenno-maxillary complex in larva. *Drosophila* has three types of sensillum: trichoid, coeloconic, and basiconic sensilla (Fig. 1-3). Each sensillum has differential morphological shapes: club-shaped basiconia, spine-shaped trichoid, cone-shaped coeloconia. All three types of sensilla are located on the 3rd antenna segment, whereas only basiconic sensilla are found on maxillary palp (Carlson, 1996; de Bruyne et al., 1999; Stocker, 1994). Sensilla possess one or more bipolar neurons. Over

1000 receptor neurons are located in the third segment of the antenna (Stocker et al., 1990). The fly has an antennal lobe, which is the equivalent of the olfactory bulb in mammals. The antennal lobe has 43 glomeruli where the axons projected from peripheral neuron meet the higher neuron processing (Stocker, 1994).

DOR (Drosophila Olfactory Receptor) genes were initially discovered by differential display (Vosshall et al., 1999) and genomic sequence analysis (Clyne et al., 1999), which was long after vertebrate and nematode receptors were identified. This is because *DORs* have non-conserved primary sequence. *DOR* genes encode a novel gene family of G-protein coupled receptors with seven transmembrane domains. Ultimately, about 60 *DOR* genes were revealed by the completion of the *Drosophila* genome project (Adams et al., 2000). Expressed are 35 genes of these in antenna, 7 in maxillary palp, while 17 genes are not detected in an adult fly. Each *DOR* is expressed in distinct, non-overlapped subset of neurons in olfactory organs, and a given olfactory neuron expresses only a single *DOR* gene except *Or83b*. For other species, each murine olfactory neuron seems to be functionally distinct, expressing a single receptor only, while one nematode chemosensory neuron expresses up to 20 odorant receptors (Malnic et al., 1999; Troemel et al., 1995; Troemel et al., 1997). *Or83b* is ubiquitously coexpressed with other receptors in olfactory neurons. The deletion of *Or83b* mislocalizes other receptors and disrupts electrical responses to odors (Larsson et al., 2004; Vosshall, 2000; Vosshall et al., 1999; Vosshall et al., 2000). Another interesting issue in an olfactory system is a small soluble odorant binding protein (OBP). OBP is found intensely around the dendrite in the sensilla. They are thought to be involved in assisting odorants to bind to receptors or terminating their interaction (Hekmat-Scafe et al., 1997; Park et al., 2000). However, function is not clearly identified yet.

Gustatory organ is a contact chemosensory system where non-volatile compounds are detected by the contact through the tip pore of a long and bent bristle. Whether it has a pore or not on the surface is the main morphological difference between olfactory and mechanosensory bristles. One mechanosensory neuron and three chemosensory neurons are innervated in a taste sensillum (Stocker, 1994). While the fly olfactory system is predominantly placed on the antenna and maxillary palp, gustatory organs are dispersed through all the body including labellum (proboscis), wing margin, and leg tarsi (Stocker, 1994). Insect taste system is different from mammalian in three points. First, a ligand binds to the primary sensory neuron directly projecting to the brain, while mammalian sensory epithelial cells on the epithelium of the tongue stimulated by a ligand activates the primary neuron (Stocker, 1994). Second, insects have multiple taste organs as mentioned above. Third, there is no sequence similarity between insect gustatory receptor gene (Gr) and mammalian genes.

In mammals, the detection occurs in the taste buds, in which 50-120 taste cells are located. Taste cells are expressing G-protein coupled receptors (GPCR) and channels that detect different types of taste: bitter, sweet, umami, sour, and salty (Lindemann, 1996). Distinct combination of three T1 receptor (T1R) family members are functionally responsible for sweet and umami perception (Li et al., 2002; Nelson et al., 2002; Nelson et al., 2001). The T2R family detects bitter-tasting and is composed of more genes (40 in mouse, 28 in human) but there is no sequence similarity between T1R and T2R (Montmayeur and Matsunami, 2002). In *Drosophila* gustatory receptors (Gr) are encoded by about 70 genes (Clyne et al., 2000; Dunipace et al., 2001; Scott et al., 2001). *Drosophila* taste receptors are also G protein-coupled seven transmembrane domain protein (Scott et al., 2001). The expression study of gustatory receptors has been achieved

by Gal4-UAS system and RT-PCR.

I explained *Drosophila* sensory system where ciliary function is involved. Because dissecting the ciliary function is directly connected to revealing the mechanism underlying the mechanosensory transduction in *Drosophila*, our lab has made an effort to identify mechanosensory mutants screened by Dr. Kernan and to draw a whole picture. It had not been known what kind of proteins are involved in ciliary function except structural proteins like IFT particles until the comparative genomic analysis accomplished by the completion of genomic mapping isolated plenty of genes presumably involved in ciliated cells. As a result of screening and identifying genes involved in mechanosensory transduction, two classes of genes were discovered. One is for the differentiation of sensory cilia like IFT proteins and the other is the transduction apparatus like channel subunits. NOMPA is a component of the dendritic cap (Chung et al., 2001), and *nompB* belongs to anterograde IFT-B subparticles (Han et al., 2003). *osegl* is one of retrograde IFT-A proteins (Avidor-Reiss et al., 2004). *nompC*, *iav*, and *nan* were reported to encode mechanosensory transduction channel subunits (Gong et al., 2004; Kim et al., 2003; Walker et al., 2000). For my thesis research, I have examined and compared two sets of ciliary proteins, IFT-A molecules and BBS proteins. The first project for my thesis research was to identify which gene causes the phenotype of *rempA* and where REMPA protein localizes in sensory neurons, and the second was about BBS proteins in *Drosophila* sensory organs. When I almost finished the mapping for *rempA*, I found that candidates for *rempA* were the *Drosophila* homologs for *BBS8* and IFT140. Concomitantly, BBS8 protein was reported to localize on ciliary neuron in *C. elegans*, and BBS has been suggested to be implicated in very diverse pathology in humans

(Ansley et al., 2003). Subsequently, BBS proteins are proposed to be involved in IFT-based transporting in *C. elegans* and zebrafish (Blacque et al., 2004; Snow et al., 2004). Because we have a few mechanosensory mutants which defective phenotype came from mutations in IFT proteins, I wanted to know how BBS proteins are involved in and how differently BBS contribute to mechanosensory transduction as well as to determine whether both IFT and BBS proteins are involved in ciliogenesis of *Drosophila* sensory cilia as suggested in *C. elegans*. Interestingly, it turned out that IFT-A and BBS function is unique in *Drosophila* different from in *C. elegans*. Therefore, in following chapters, I will present many interesting findings I have obtained from REMPA and BBS study in *Drosophila* sensory cilia and discuss how selectively ciliary proteins are involved in respective sensory organs. In chapter 2, I will define the phenotypes of *rempA* mutants including behavioral, electrophysiological, the morphology of sensory cilia, and the localization of other mechanosensory-related molecules. Besides, I will demonstrate that *rempA* is the *Drosophila* homolog of the retrograde IFT component, IFT140. In chapter 3, I will present the subcellular localization of REMPA protein fused with YFP in CHO and ES organs. In addition, I will delineate how IFT molecules work together and how IFT is related to the structure of the mechanosensory cilia by demonstrating the localization of REMPA in several different mechanosensory mutants. In chapter 4, I will show that BBS mutants have chemosensory specific defect and that BBS1 localizes on chemosensory neurons. In Chapter 5, I will conclude the result that I presented in chapter 2-4 and discuss the different roles of IFT-A and BBS proteins in sensory cilia in fly. Besides, I will discuss the functional relationship between ES and chordotonal cilia by comparing the localization of molecules involved in mechanosensory transduction, and compare the transporting system on sensory cilia of *Drosophila* and *C. elegans*.

[Figure 1-1] Schematic of a ciliary structure

(A) Illustration of a cilium projected from a cell surface. It has 9+2 axonemal structure where nine doublet microtubules surround one pair of single microtubule (B). On the base, there is a basal body containing nine triplet microtubules (D). Cross sections of a basal body (a) and a cilium (b) reveal a conspicuous structure of each. A cilium has components like dynein arms and radial spokes required for cilia motility and beat regulation. (C) presents the 9+0 axonemal structure of a primary cilium, which doesn't have motility function due to the lack of dynein arms.

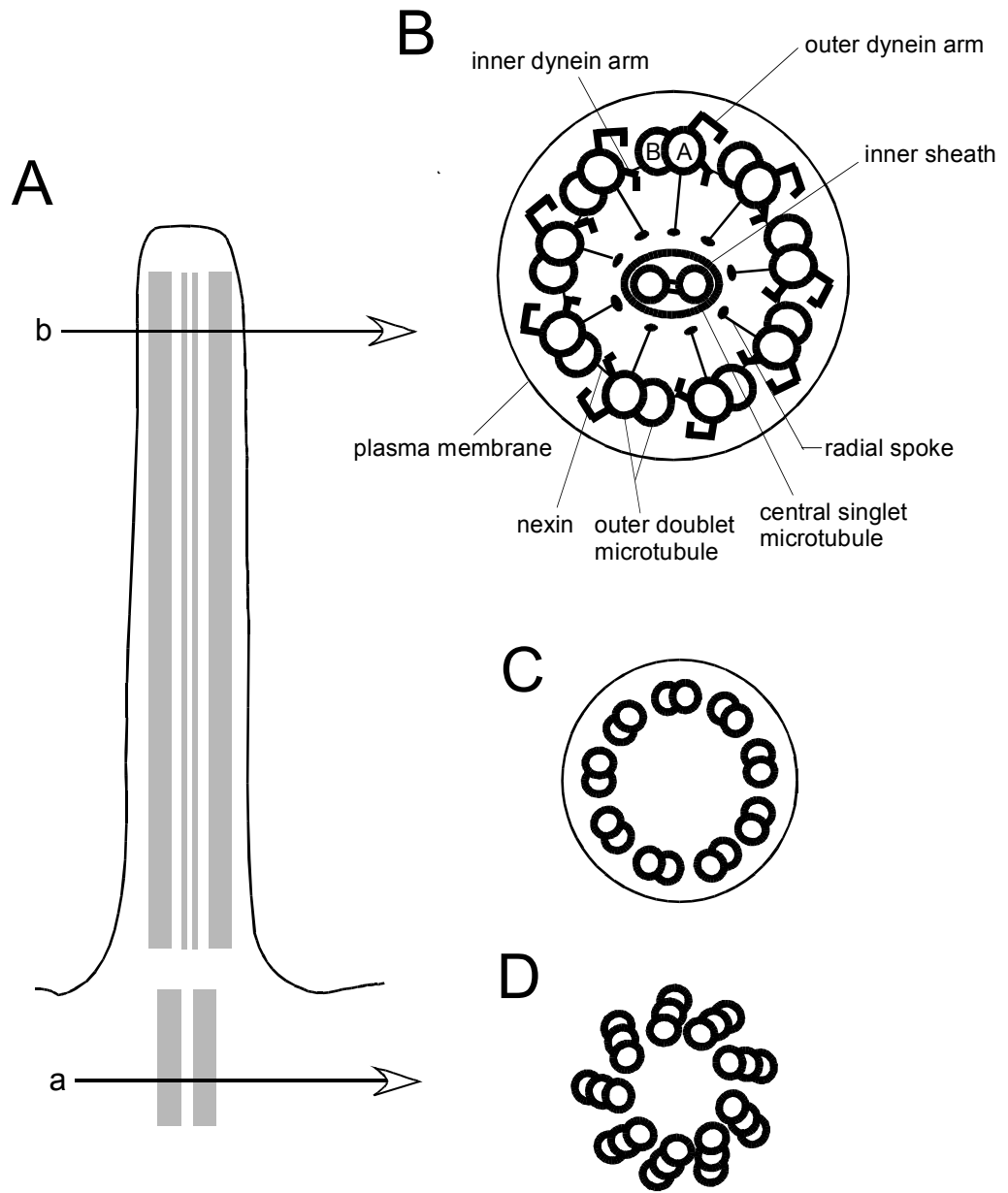


[Table 1-1] The components of Intraflagellar transport (IFT)

IFT particles were first isolated and identified from diflagellated green algae, *Chlamydomonas*. IFT particles are well conserved through eukaryotic organisms. IFT components are composed of two subparticles, anterograde IFT-B and retrograde IFT-A. IFT-B proteins are involved in transporting from the base to the tip of a cilium depending on a kinesin II motor. Kinesin II motor is heterotrimeric proteins composed of two motor subunits and one non motor component. Notably, another kinesin II motor, *osm-3*, which motor function was presented in *C. elegans*, is conserved in *Drosophila* and mammals. Due to the property of anterograde transporting, mutations in IFT-B and kinesinII motors end up with missing cilia or flagella. The IFT-A molecules in charge of the retrograde movement from the tip of a cilium back to the base are dependent on cytoplasmic dynein motor. With the lesion of these proteins, cilia are truncated retaining a short length of cilia. IFT genes are transcriptionally regulated by DAF-19 in *C. elegans* and RFX in *Drosophila*. CG combined number in *Drosophila* orthologs represents the predicted gene signified by the Berkeley Drosophila genome project.

Intraflagellar transport components

	<i>Chlamydomonas reinhardtii</i>	<i>C. elegans</i>	<i>Drosophila melanogaster</i>	<i>Mammal</i>	<i>Domain structure</i>
IFT-A	IFT144 IFT140 IFT139 IFT122	Che-11 DAF-10	REMPA OSEG1		TPR, WD40 WD40
IFT-B	IFT172 IFT88 IFT81 IFT80 IFT72/74 IFT57/55 IFT52 IFT46 IFT27 IFT20	OSM-1 OSM-5 CHE-13 OSM-6	OSEG2 NOMPB CG8853 CG9595 CG30441	Wimple Polaris Hippi NGD5 AL99202	WD40, LIM TPR PxxP Ras-like GTPase
		CHE-2	CG9333		WD40
Kinesin II	FLA10 FLA8	KLP85 KLP95	KLP64D KLP68D	KIF3A KIF3B	
	FLA3	CeKAP	DmKAP	KAP3A/B	
		OSM-3	CG17461	KIF17	
Adaptor		DYF-1	CG5142	FLJ13946	TPR
Cytoplasmic Dynein	DHC1b LIC3 LC8	CHE-3 XBX-1	BTV(DHC36D)) CG3769	DHC2 D2LIC	
regulator		DAF-19	dRFX	RFX1-5	

[Figure 1-2] Schematic of transporting mechanism on nematode cilia

The IFT transporting mechanism based on the two anterograde motors in two separate compartments of sensory cilia was suggested in *C. elegans*. The anterograde transporting is carried out by the coordination of two motors, heterotrimeric kinesinII and homodimeric kinesinII (*osm-3*). The IFT complex is able to be back to the base by cytoplasmic dynein (A). Interestingly, only *osm-3* motor works for the distal segment of sensory cilia (B), which was confirmed by the different velocity of the complex in each compartment. Two subcomplexes are coupled by BBS7 and BBS8. Thus, malfunction of BBS7 and BBS8 renders the IFT-B complex to step into the distal segment and IFT-B complex shows the higher speed by *osm-3* in the middle segment (D). The *osm-3* is conjugated to IFT-B particles by Dyf-1, which mutations leads to the release of OSM-3 and the truncated form retaining only middle segment (C).

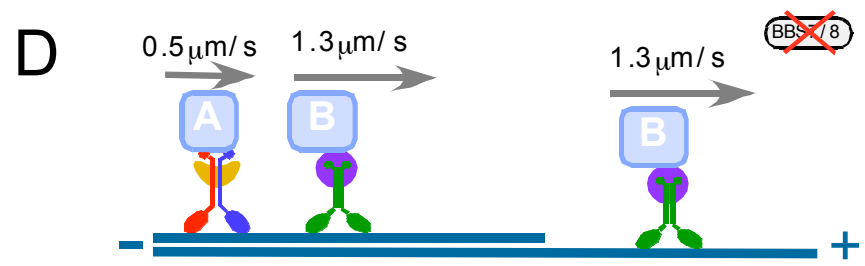
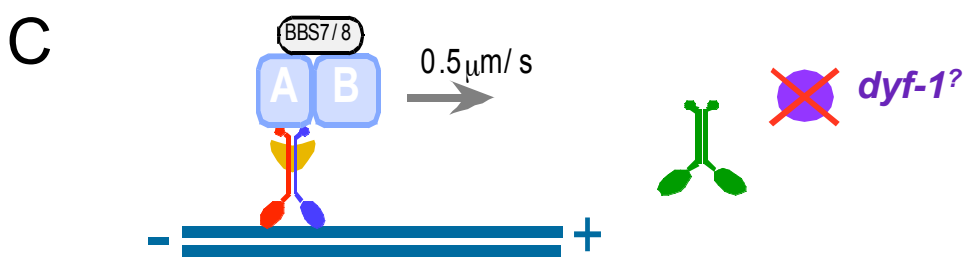
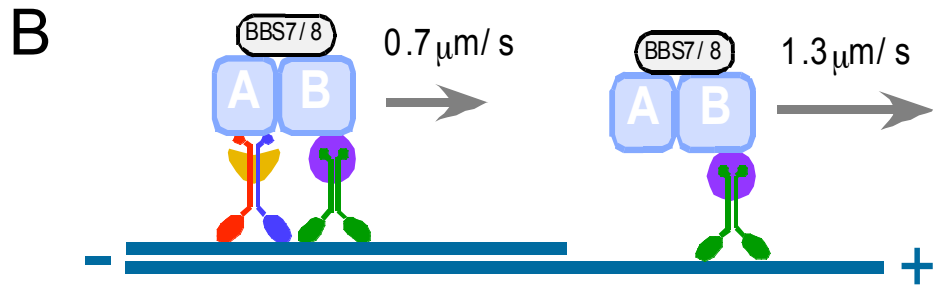
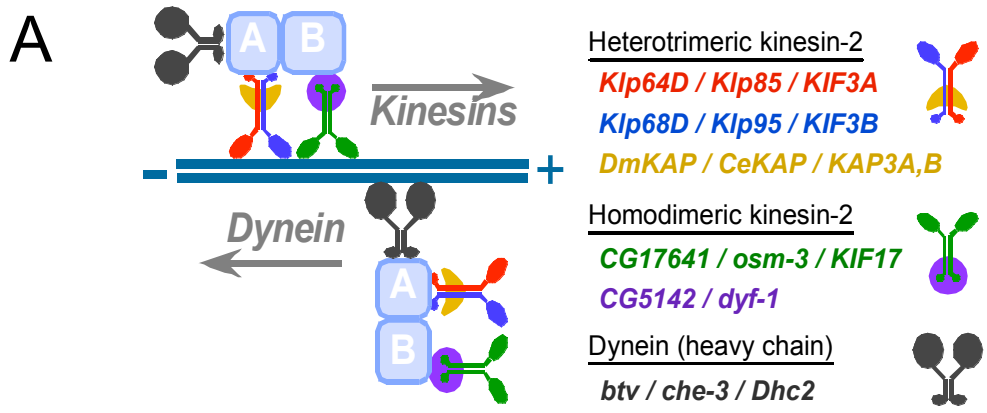
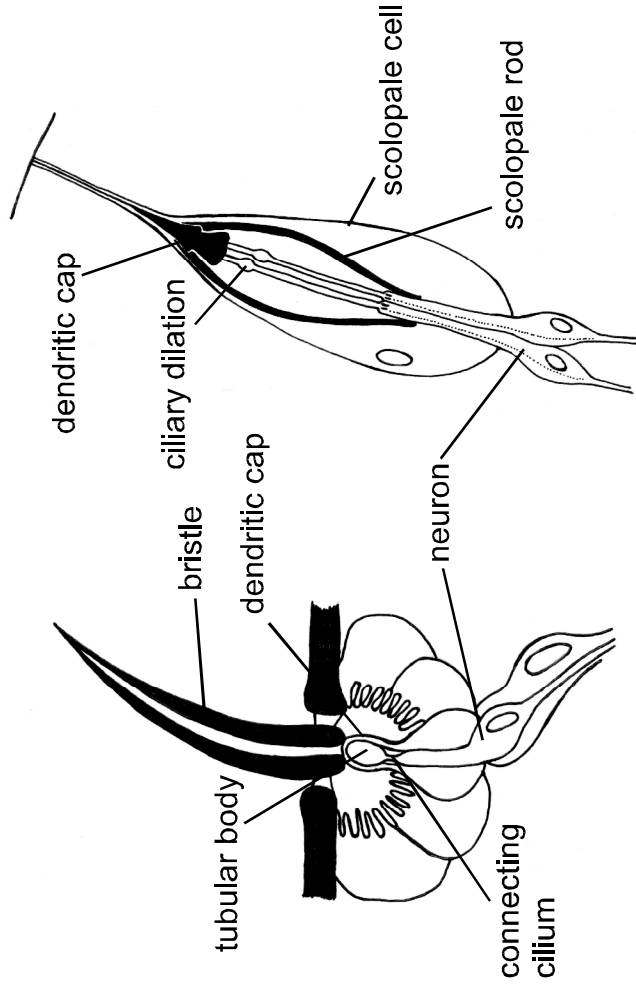


[Figure 1-3] Schematic of Drosophila ciliated sensory organs

Type I sensory organ is composed of External Sensory (ES) organ and chordotonal organ which all contain a ciliated neuron surrounded by supporting cells. Chordotonal cilia are surrounded by a scolopale cell. On the other hand, chemosensory sensilla are also external organ which possesses long cilium reaching out into the long bristle compared to the short cilium of an es organ contacting the base of bristle through a dendritic cap. Olfactory sensilla have a pore on the bristles, while gustatory sensilla have a pore at the tip of a bristle.

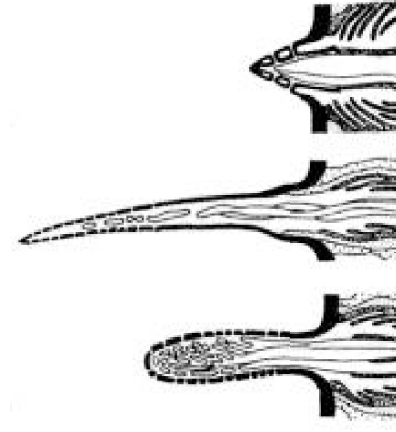
Type I MECHANOSENSORY organ



External Sensory (ES) organ

Chordotonal organ (CHO)

CHEMOSENSORY sensilla



basiconic sensillum
trichoid sensillum
coeloconic sensillum

Chapter 2:

rempA encodes IFT140

1. Phenotypes of *rempA*
2. Positional cloning of *rempA*
3. The property of REMPA protein

rempA (reduced mechanoreceptor potential A) is a severely mechanosensory-defective mutant, showing uncoordinated behavior, no auditory response, and severely reduced mechanoreceptor potentials in bristle recording. The first aim of my dissertation research was to identify what protein is encoded by rempA and to characterize the role of the protein in mechanosensory transduction. The expression of cytoplasmic RFP (red fluorescent protein) revealed that rempA mutants have truncated cilia. This was confirmed by electron microscopy, which also found that the ciliary dilation, in particular, appeared disorganized and disrupted. An anterograde IFT protein, GFP-NOMP B, accumulated at the tip of shortened cilia in rempA, and in oseg1, another retrograde transporter mutant, supporting the idea that REMPA is involved in retrograde transport together with IFT122/OSEG1.

rempA was found to encode IFT140, one of the IFT-A proteins. Sequencing genomic DNA from three rempA alleles found a large deletion and two nonsense mutations. The rescued sound evoked response of ift140- transformed flies verified that the defective mechanosensory phenotype of rempA alleles is caused by the mutations in IFT140. IFT 140 has WD40 β -propeller motifs at the N-terminus and tetratricopeptide repeat (TPR) motifs at the C-terminus, implying that IFT140 might be involved in protein-protein interactions. Interestingly, this motif arrangement is similar to that of some COP proteins which are responsible for vesicular trafficking between endoplasmic reticulum (ER) and Golgi.

Materials and methods

Stocks

rempA has three alleles: *rempA¹* was obtained by mutagenizing with EMS (Kernan et al., 1994); *y¹ w^{67c23}*; *P{w^{+mC}=lacW}ex^{k12913}/CyO* has been obtained from bloomington stock center; *l(2)21Ci¹/CyO* were kindly given by Dr. Heitzler. Flies carrying *elav::GAL4*, *UAS::RFP/FM7* and deficiencies (*Df(2L)al*, *Df(2L)L124*, and *Df(2L)BSC16*) for complementation tests were obtained from Drosophila stock center at Bloomington, IN. *GFP::NOMPB* and *NOMPA::GFP* transgenic flies were generated by Dr. Young-Goo Han, a previous graduate student, and Dr. Yun Doo Chung, a previous postdoctoral fellow, in the laboratory. Flies were kept on standard medium at 21-25°C.

Visualization of ciliated neuron and antibody staining

To examine the ciliary morphology of *rempA* flies, larvae of *elav::GAL4*, *UAS::RFP/FM7;rempA¹/CyO* and of *elav::GAL4*, *UAS::RFP/FM7; rempA¹/rempA¹* were examined. Live specimens were prepared by flattening 1st instar larvae under cover slip onto the cover glass without fixation, and immediately were observed under confocal microscope. To make sure the localization and the length of cilia labeled by RFP, differential interference contrast images were also taken on the same field of RFP images. To examine *NOMPA::GFP* localization in *rempA* background, femoral chordotonal organs in *rempA¹/CyO;NOMPA::GFP* and *rempA¹/rempA¹;NOMPA::GFP* were observed.

Pupal antenna and legs were isolated in PBT (0.2% Triton-X in PBS) and fixed in

4% formaldehyde in PBT. After wash with PBT for 3 times of 10 minutes, samples were mounted with mounting media, Vectashield (Vectorlabs, CA) on slide glass. A confocal microscope (Leica, DMIRE2) was used for analyses.

For the GFP::*NOMPB* localization in *rempA* background, early and late pupae of *rempA¹/CyO, P{GAL4-Kr.C}DC3, P{UAS-GFP.S65T}DC7;GFP::*NOMPB* and *rempA¹/rempA¹;GFP::*NOMPB* were selected and dissected out. After fixation and washing in PBT, samples were incubated in blocking solution (PBT with 5% normal goat serum) for 1 hour at room temperature. Overnight incubation in primary antibody solution of mAb 22C10 (1:100 dilution, Developmental Studies Hybridoma Bank, Iowa City, IA) at 4°C was followed by treatment of Alexafluor 546-conjugated goat anti-mouse antibody (1:500 dilution, Molecular Probes, Eugene, OR) in blocking solution for two hours at room temperature. Mounting and observation with confocal microscopy was performed as described above.**

Electrophysiological recording of mechanosensory responses

Auditory responses on the second segment antenna were recorded as described in Eberl et al (Eberl et al., 2000). Flies briefly anesthetized on ice are placed at the trimmed tip of yellow pipette tips, positioning head including antennae outward from the tips to make it possible to access the antennae. For extracellular recording for auditory response, tungsten electrodes are inserted into the head and antenna. Upon the pulse sound stimulation, the response is recorded.

Primers and sequencing

To sequence candidate genes in the mutant flies, I designed primers for two

candidate genes: 8 pairs of primer set for CG11838 and 6 pairs for CG13691.

For CG11838, primer sets are as follow:

Set A sense : GTGCGATCAAGTGGTGAATG
antisense : GAAGCAGATCAGCAGCAACA

set B sense : ATCGTCCTGCTGCAGTTCA
antisense : GGACGTTCCCTGCACACAGA

set C sense : TGTAAAATGAGCGGACGTG
antisense : CTCCACTGTCTGCAGGATCTC

set D sense : TGAGCTTGGTGATGAGTAATGG
antisense : TCTTCAGCCGGATCACGTT

set E sense : CTCCTTGCAACCCAGTCATT
antisense :CTCCGCCTTGTGGTAGACAG

set F sense : AAGCGCTACATCCAGACCAC
antisense : ACTGTGATAGTCGCCCTGCT

set G sense : GGAGGAACTATCCGAGATGCT
antisense : GCATTCCAGATGAGATCGAA

set H sense : GCGGATGTAAAGGCAATTCT
antisense : AAAATTCCAAATGGCCCAAG

For CG13691, primer sets are as follow:

set A sense : TGTGGAATTCTCAACATCTGTG
antisense : AGTTTCGAAGTGGCATCACC

set B sense : CGAAGAGCGGAGCCTTTT
antisense : TTGGTCTTATAGCTTGTAATGCACA

set C sense : AGGACGATGGAGGGAATGAG

antisense : GTA AAGCTGCAGTGCGTCCT

set D sense : GCCGGCGTTCTTTTCTATTC

antisense : TTGTAGATTCCTCCGCTGCT

set E sense : GTGTCCCAACAGGGTGAATC

antisense : CAGGAGTGCGTTGCACAG

set F sense : GTCTATATGGCGGGCAAATC

antisense : GCCAGAAGCAACCTTTTCAG

The genomic DNA of *rempA*¹ homozygote was isolated by incubating a mashed single fly in 50 µl of squishing buffer (10mM Tris-HCL, 8.2 pH, 1mM EDTA, 25mM NaCl and 200 µg/ml proteinase K) at 37°C for 1 hour, followed by inactivation at 95°C for 5 min. Each amplified PCR fragment was purified by gel extraction and sequenced using BigDye Terminator Cycle Sequencing Ready Reaction Kit (PE Applied Biosystems, Foster City, CA). The sequencing results were analyzed by sequence analyzing program, Sequencher™ version 4.2.2, Gene Codes Corporation, Ann Arbor, MI).

2.1. Phenotypes of *rempA*

rempA has uncoordinated behavior like other mechanosensory mutants. *rempA* larvae are touch-insensitive. By electrophysiological recording, *rempA* showed no auditory response and severely reduced mechanoreceptor potential in bristles. The

expression of cytoplasmic RFP transcribed by specific neuronal promoter, *elav*, on ciliated neuron revealed that *rempA* cilia are still present, but truncated. Ultrastructural analysis revealed the truncation of chordotonal cilia by showing intact axonemal structure in the proximal part of chordotonal cilia but not in the distal, and especially a ciliary dilation is disorganized in *rempA*. NOMPA::GFP, a dendritic cap protein, was also disorganized, and GFP-NOMPB accumulated on the short ciliary tip.

rempA has uncoordinated behavior.

rempA is one of mechanosensory mutant flies isolated by impaired sound-evoked response in auditory recording at antennae (Kernan et al., 1994). *rempA* adult flies exhibit severe uncoordination: being unable to stand or walk. Pupae hardly eclose and young adult flies are often found stuck in the food media. Deafness and uncoordinated behavior compellingly suggest that the structure or a transduction apparatus involved in sensing mechanical stimuli may be defective.

rempA mutant has impaired electrophysiological response in sensory organs.

The severely reduced mechanoreceptor potential from bristle recordings in *rempA* flies explains the defect in proprioception (Fig. 2-1). As fly hearing takes place in antenna which has a Johnston organ (JO) composed of scolopidium, a chordotonal ciliary unit, it is speculated that *rempA* flies would have a defect related to cilia. The auditory recording measured in antenna shows that there is no response to a sound in *rempA* flies (Fig. 2-1). Three *rempA* alleles consistently show no sound-evoked response (Fig. 2-1)

rempA mutant has truncated cilia.

To determine if the behavioral and electrophysiological defect of *rempA* is associated with ciliary morphology or with sensory transduction, neuronal morphology was examined by the expression of *elav-GAL4, UAS-CD8::RFP* system. The expression of RFP on neuronal cilia in *rempA* larval chordotonal organ shows that cilia are present, but are truncated compared to wild type (Fig. 2-2A-D). Most larval chordotonal *cilia* of *rempA* were truncated at the level of a position where a ciliary dilation is supposed to be present. Also, the organized localization pattern of NOMPA, the dendritic cap protein, in a wild type femoral chordotonal organ is disrupted in *rempA* (Fig. 2-2).

Ultrastructure of rempA cilia

For the precise axonemal architecture in cilia, the ultrastructure of *rempA* cilia by electron microscopy (EM) was examined by collaborators, Dr. Elena Loukianova and Dr. Daniel Eberl (University of Iowa, Iowa city, IA) (Fig. 2-3A-D). EM study illustrates that *rempA* cilia are defective in axonemal ultrastructure. Ciliary dilation is disrupted and disorganized, and the distal part beyond the ciliary dilation is missing (2-3B). The longitudinal section of chordotonal organ in *rempA* antenna, though the section was not perfectly perpendicular, roughly displayed the missing distal part and a missing ciliary dilation (Fig. 2-3C-D). 9+2 axonemal structures are often incompletely formed (Fig. 2-3B, arrow). Other structures like basal body, dendritic tip, and scolopale rods look normal (Fig. 2-3B). Around the truncated region of cilia, many vacuoles are found, and sometimes, microtubular subunits are absent (Fig. 2-3B).

GFP-NOMP B accumulates in cilia of IFT-A mutants, rempA and oseg1.

Structural defects of cilia were observed in *nompB* mechanosensory mutant in a

previous study (Han et al., 2003). NompB/IFT88, one of the anterograde IFT-B proteins, localizes along the cilia, suggesting that NOMPA is implicated in the transporting process for cilia differentiation (Han et al., 2003). We rationalize that *rempA* might affect the localization pattern of NOMPB, if both proteins are all involved in ciliary anatomy. To test this, GFP-NOMPB localization in *rempA* antennae was assayed. As shown in Fig. 2-4, GFP-NOMPB distributed along the cilia in wild type where at the distal cilia the denser localization was displayed, but it accumulates on the tip of *rempA* chordotonal cilia (Fig. 2-4D-F). Interestingly, this localization pattern of NOMPB in *rempA* was consistent with that in *oseg1*, one of mechanosensory mutants (Fig. 2-4A-B). The GFP::NOMPB was stacked up at the tip of *oseg1* cilia as well (Fig. 2-3B, D). OSEG1 is one of retrograde transporters involved in cilia assembly and maintenance, in which the defect leads to truncated cilia and deafness (Avidor-Reiss et al., 2004). This finding strongly suggests that REMPA might be involved in IFT transporting and especially in retrograde function in fly mechanosensory cilia.

2.2. Positional cloning of *rempA*

rempA complementation test ended up with two candidate genes.

Previous recombination mapping located *rempA* at the end of the left arm of the

second chromosome. The key criterion for the complementation test for mapping of *rempA* was the uncoordinated behavior phenotype. Because homozygote mutant flies uncoordinated upon eclosion can't walk or fly, they were found on the bottom of a fly vial. To find the region where *rempA* fails to complement, I used four deficiency chromosomes (*Df(2L)BSC16*, *Df(2L)al*, *Df(2L)BSC4*, and *Df(2L)L124*). *Df(2L)BSC4* and *Df(2L)BSC16* were generated by P-element recombination respectively, so end points of each deficiency are defined.

However, one original P element, $y^1 w^{67c23}; P\{w^{+mC}=lacW\}ex^{k12913}/CyO (ex^{k12913})$ used to produce *Df(2L)BSC16* failed to complement and ex^{k12913} is homozygote lethal. *Df(2L)BSC16* failed to complemented *rempA¹*. Though ex^{k12913} places on the upstream of *ex* according to the cytogenetic map, the possibility of a regulatory effect on the neighbor gene, *CG13691* which is *BBS8* fly homolog could not be ruled out because *BBS8* is a basal body protein identified in *C. elegans* and mammal, and its failure causes ciliary dysfunction linked to BBS syndrome (Ansley et al., 2003). Another candidate gene was *CG11838* which encodes IFT140, one of retrograde transport components previously cloned in *Chlamydomonas*, and it is required for the construction of cilia. Therefore, I choose two candidates for *rempA*: *BBS8* (*CG13691*) and *IFT140* (*CG11838*).

***rempA* encodes IFT140.**

Whether *rempA* encodes *BBS8* or *IFT140* fly homolog was determined by sequencing of *rempA* genomic DNA with primers designed for each gene. I designed 6 sets of primers for *CG13691* and 8 sets for *CG11838* and sequenced *rempA* homozygote genome. Consequently, *rempA* turns out to be an *IFT 140* fly homolog.

Three alleles of *rempA* have all lesions on *IFT140* (Fig 6). *rempA¹* contains one

nonsense mutation where one base change of G to A leads to a stop codon instead of Tryptophan (W) at the amino acid position 404. A nonsense mutation was also found in *l(2)21Ci^l* where G was altered to A which causes a change of Tryptophan (W) to a stop codon at amino acid 616. *ex^{k12913}* turned out to have a second site mutation for CG11838. It contains a big deletion including most of exon 4 and the first part of exon 5. This causes a frameshift resulting in the early termination, keeping 34 amino acids from the deletion start position. Sequencing disclosed that *rempA* has three alleles: *rempA^l*, *ex^{k12913}*, and *l(2)21Ci^l*.

Though all three alleles failed to complement each other and the deficiency chromosome, *Df(2L)BSC16*, the outcome behavioral phenotype displayed slightly different in terms of the severity. When each allele was crossed with the deficiency chromosome to rule out the homozygosity of detrimental missense mutation possibly caused by an EMS treatment, the transheterozygous mutant phenotype revealed that *l(2)21Ci^l/Df(2L)BSC16* had less severe uncoordination than other two transheterozygous mutants, *rempA^l/Df(2L)BSC16* and *ex[k12913]/Df(2L)BSC16*. Flies of *l(2)21Ci^l/Df(2L)BSC16* look inactive and are able to stand, walk, and mate, suggesting that *l(2)21Ci^l* might be a hypomorphic allele for *rempA* presumably due to the readthrough at a stop codon. The nonsense mutation is strongly suppressed by a following cytosine and weakly suppressed by a following guanine (Chao et al., 2003) (Fig. 2-5C). Nevertheless, *l(2)21Ci^l/Df(2L)BSC16* displays as complete loss to auditory stimuli as other *rempA* alleles, and the nonsense mutation in *rempA^l* is also followed by a guanine in the context, arguing that the truncated protein form of *l(2)21Ci^l* might be stable enough to behave partially functional. But, to explain this differential severity, truncated protein or mRNA stability should be examined.

To verify that the mutant phenotype originated from the injury on *IFT140* and not from the second site mutation, a germ line transformation with the genomic DNA fragment isolated from a BAC clone was performed. I will give a detailed explanation on the germ line transformation in the next chapter. Briefly speaking, the mutant phenotype of *rempA* was fully rescued by the germ line transformation of the transgene, *p{rempA-YFP}*+ (Fig 2-1).

2.3. The Property of REMPA

rempA is 4,826 bp long, and REMPA amino acid sequence holds 50% similarity and 28% identity with *C.elegans* homolog, *che-11*. It is 23% identical with a mammalian homolog which is a selective LIM binding factor. The amino acid sequence alignment with other species shows a well conserved amino acid sequence (Fig. 2-6A). The functional domain prediction by REP (<http://www.embl-heidelberg.de/~andrade/papers/rep/search.html>) and SMART (<http://smart.embl-heidelberg.de>) predicts that REMPA has 5 WD40 repeats at the N-terminus and 7-8 TPR motifs at the C-terminus (Fig. 2-7A). WD 40 repeats contain a Trp-Asp (WD) dipeptide at the end of about 40 amino acids, and TPRs are degenerate ~34 amino acid long motifs. TPR motifs have conserved hydrophobic residues (D'Andrea and Regan, 2003). I examined TRP motifs of REMPA predicted by REP, showing that TPR motifs are perfectly matched to the conventional domain search criteria (data not shown) (Das et al., 1998). These domain

structures imply that REMPA might function by interacting with other IFT molecules or signaling molecules transported on cilia, because these motifs are proposed to involve a protein-protein interaction, but the mechanism and function remains to be identified. The native promoter region contains an x-box (GCAACCATGACAAC) motif recognized by the RFX transcription factor at -81 bp upstream from the translation start site.

REMPA has similar protein structure with COP

It is suggested that IFT transporters are evolved from coated vesicle transporters based on the structural similarity and sequence homology (Jekely and Arendt, 2006). Strikingly, the domain structure of REMPA resembles COP and clathrin vesicle coats in having WD40 repeats at the N terminus and TPR motifs at the C-terminus (Avidor-Reiss et al., 2004). There are three kinds of coated vesicle transporters: clathrin, COPI, COPII (Kirchhausen, 2000). These vesicles are involved in intracellular trafficking between internal membranes and the plasma membrane (Fig. 2-7B): Clathrin serves for endocytosis and movement from Golgi to endosomes; COPI traffics intra-Golgi and from the Golgi to the ER; COPII from the ER to the Golgi (Kirchhausen, 2000). WD40 repeats are folded into a β -propeller structure which is highly symmetrical and anti-parallel (Smith et al., 1999). TPR motifs are usually present in 3-16 tandem repeats and arranged as helix-loop-helix structures. One motif has a pair of antiparallel α -helices of an equivalent length, and neighbor motifs are packed to a parallel arrangement. The characteristic N-terminal WD40 and C-terminal TPR motifs of REMPA suggests the combinational structure of an N-terminal β -propeller with a C-terminal α -superhelix. Interestingly, this structural feature is found in components of the nuclear pore complex and vesicle coated complexes like COPI, COPII, and clathrin coats. Moreover, the

secondary structure predicted by consensus approach at http://npsa-pbil.ibcp.fr/cgi-bin/npsa_automat.pl?page=/NPSA/npsa_secons.html supports the similar domain composition of IFT molecules and vesicle complex components (Fig. 2-7A) (Jekely and Arendt, 2006). Hidden Markow Model homology search also showed the distant sequence similarity of IFT with coated vesicle components (Avidor-Reiss et al., 2004). Notably, REMPA by psi-blast search at http://npsa-pbil.ibcp.fr/cgi-bin/npsa_automat.pl?page=/NPSA/npsa_psiblast.html retrieved coatomers and clathrin chains. These provide positive evidence suggesting that IFT proteins might be evolved from coatomers.

More interestingly, the polymerization of the triskelion (three legged) shape of clathrin heavy chains displays a lattice form (Edeling et al., 2006; Ybe et al., 1999). The clathrin heavy chain (chc) motif is also similar with the TPR motif with two exceptions that chc has a shorter length and no hydrophobic residues. Clathrin N termini have β -propeller structures, indicating that it has a similar structural property with the WD40 repeat. (Eberl et al., 2000; Edeling et al., 2006). The structural organization of COPII cage appears similar to ciliary dilations (Gurkan et al., 2006). Taken together, the sequence similarity, the combination of a domain structure, the second structure prediction, and the morphological architecture of a ciliary dilation and a COP vesicle all unambiguously support that IFT particles are an evolutionary descendent of the coated vesicle.

[Figure 2-1] The uncoordinated behavior and electrophysiology

The measurement of extracellular potential in *rempA* alleles shows no sound-evoked response to pulse stimuli. *rempA¹*, *l(2)21Ci¹*, *k12913*, and *l(2)21Ci¹/k12913* having transheterozygotic genotype showed no auditory response, but wild type containing these mutant genotypes on one chromosome showed normal auditory response. Genomic rescue flies in mutant background shows that auditory response is fully restored.

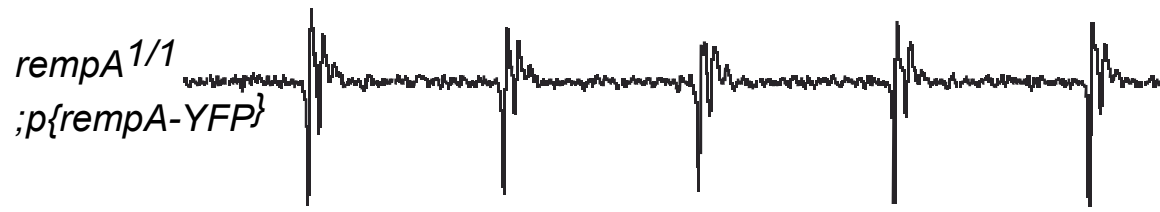
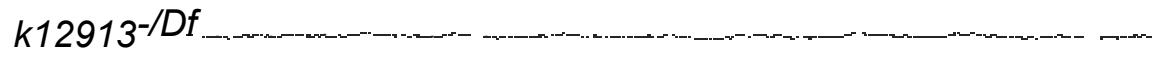
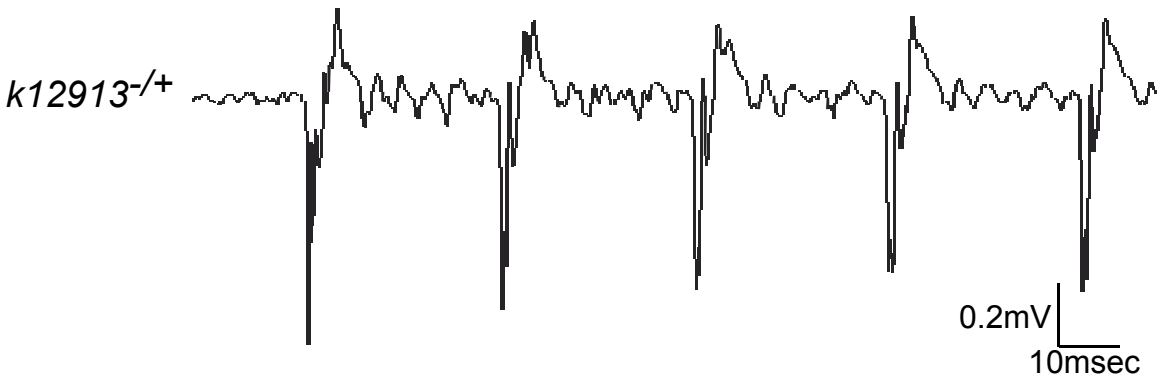
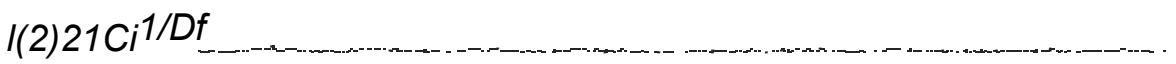
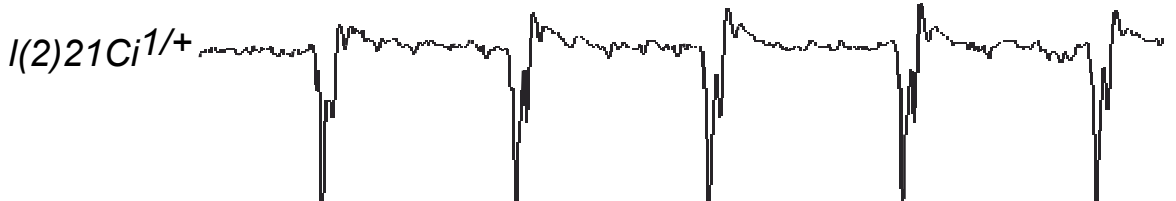
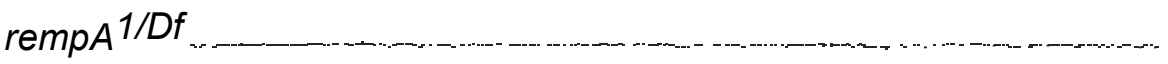


[Figure 2-2] The ciliary morphology of *rempA* by RFP expression

The ciliary morphology of lateral chordotonal organ in *rempA* larvae and femoral and antennal chordotonal organs in pupae was examined by RFP expression. Scale bar: 8 μ m.

(A-C) *rempA*/+ has displays long cilia which have a bulky structure on the middle, the ciliary dilation (A). An arrow indicates a ciliary dilation (A, arrow). Cap cells and scolopale cells are observed through DIC image (B). A ciliary dilation appears bulky (B, arrow). The cilia visualized by RFP locate in the scolopale cells and the tips of cilia are extended into the cap cells (C, merged).

(D-F) *rempA* chordotonal cilia in a larva were truncated (D, arrow). The cilia retain proximal part of a whole length of cilia. Compared to *rempA*/+ cilia, distal parts were missed at the level of a ciliary dilation. Also, the bulky structure was not detected in *rempA*. However, other external structures like a scolopale cell and a cap cell appear normal (E, DIC). In a merged picture (F), the cilia end around the proximal ends of cap cells (F, arrows).

(G-J) In *rempA*/+ pupal antennal (G) and femoral (H) chordotonal cilia have long extending outer segments. However, *rempA* has truncated chordotonal cilia around the position where a ciliary dilation locates in pupal stage (I and J, arrows).

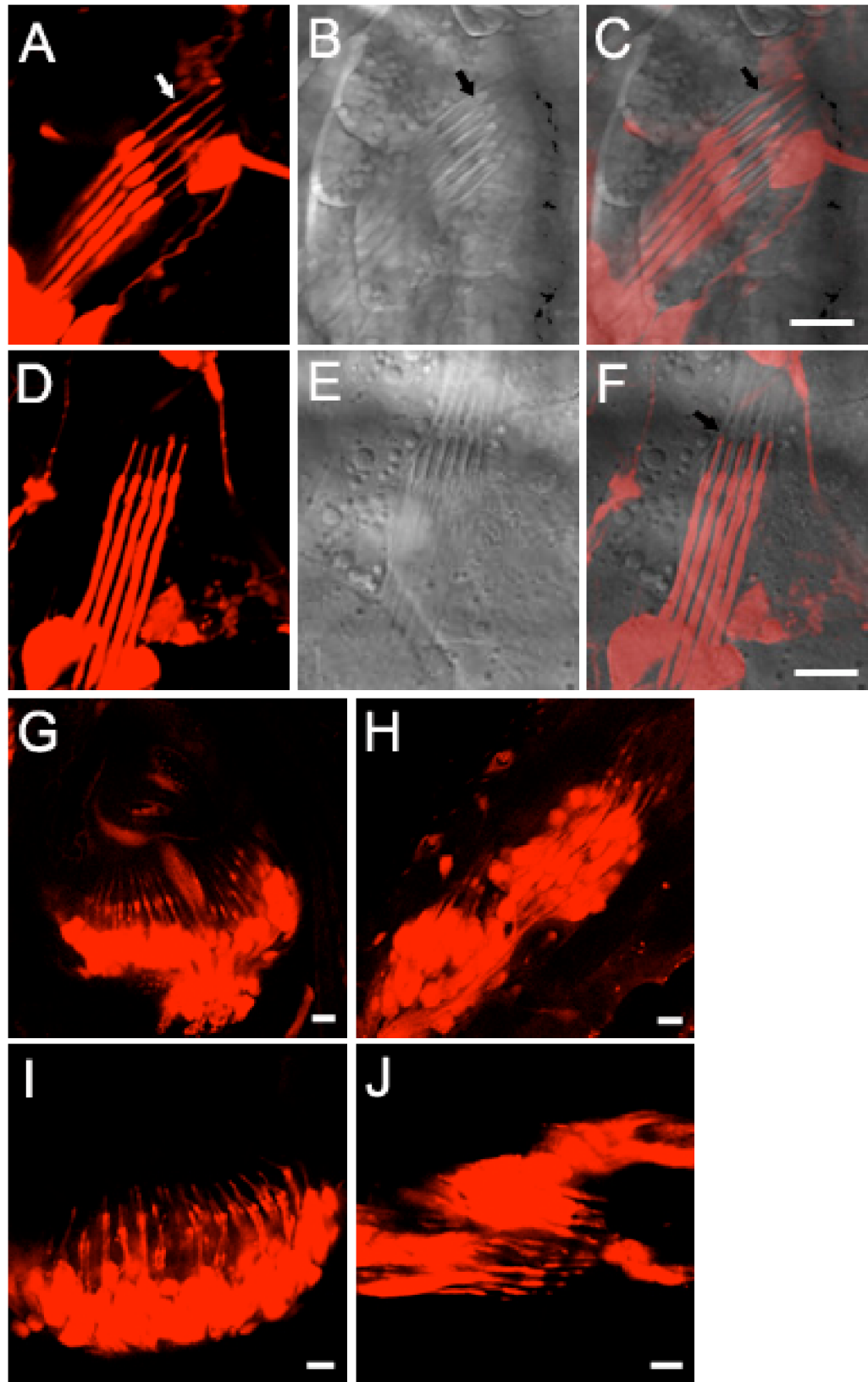


[Figure 2-3] Ultrastructure obtained by EM verified the truncation of a ciliary outer segment and presented the disrupted ciliary dilation.

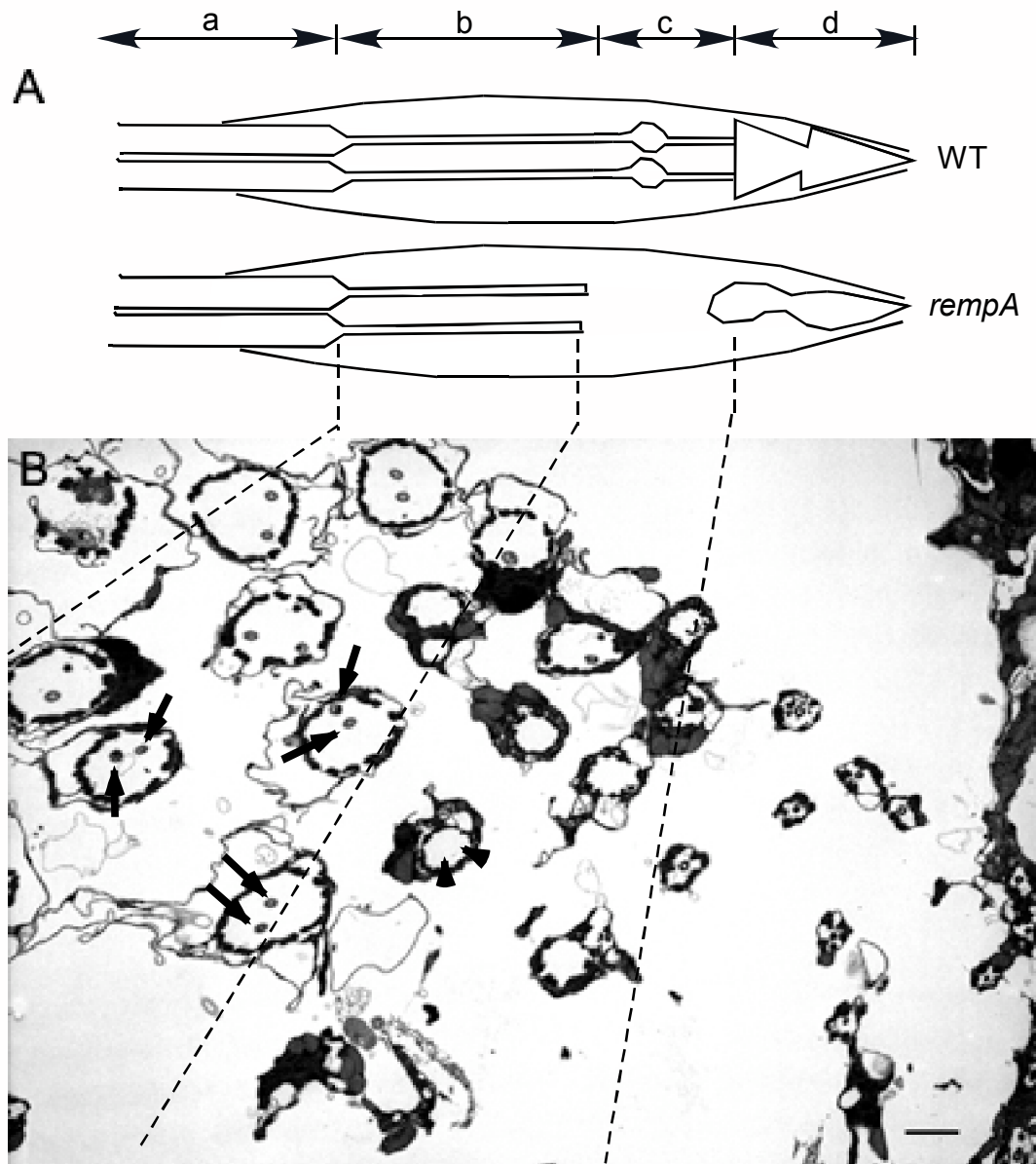
(A-B) A slightly slanted section of *rempA* antennal chordotonal organs presents 4 different parts of ciliary dendrites. (a) indicates the inner segment of ciliary neurons. A ciliary outer segment is illustrated from (b) to (d). In (b), every scolopale cell exhibits two ciliary axomenal structures (B, arrows), indicating that proximal region of *rempA* cilia is retained. *rempA* has missing cilia at (c) and (d), which is shown by EM (B, arrowheads).

The dendritic cap appears in (d), implying that dendritic cap is present. Scale bar: 1 μm

(C-D) The longitudinal section of *rempA* chordotonal organ illustrates disrupted and disorganized ciliary dilations (arrows). Though it is not perfectly perpendicular, the approximate location of a ciliary dilation displays an abnormal ciliary dilation (C and D, arrows) below the dendritic cap. Scale bar: 1 μm

(E) The schematic cartoon for a ciliary dilation innervated in a scolopale cell. Two ciliary neurons were innervated into one scolopale cell. The dendritic cap surround the distal part of cilia and ciliary dilations locate on 2/3 region from the ciliary base.

(F-H) The longitudinal section of wild type chordotonal organs shows that two cilia are innervated in one scolopale cell and ciliary dilations locate below the dendritic cap (F, Scale bar: 1 μm). The cross section of ciliary dilation indicates that 9 doublet microtubules surround the ciliary dilation in the center. The similar pattern of electron dense structure of a ciliary dilation is observed both in cross section and in longitudinal section (G and H, short arrows, scale bar: 0.25 μm). The different plane shows a different pattern of electron dense structures (H, short arrows).



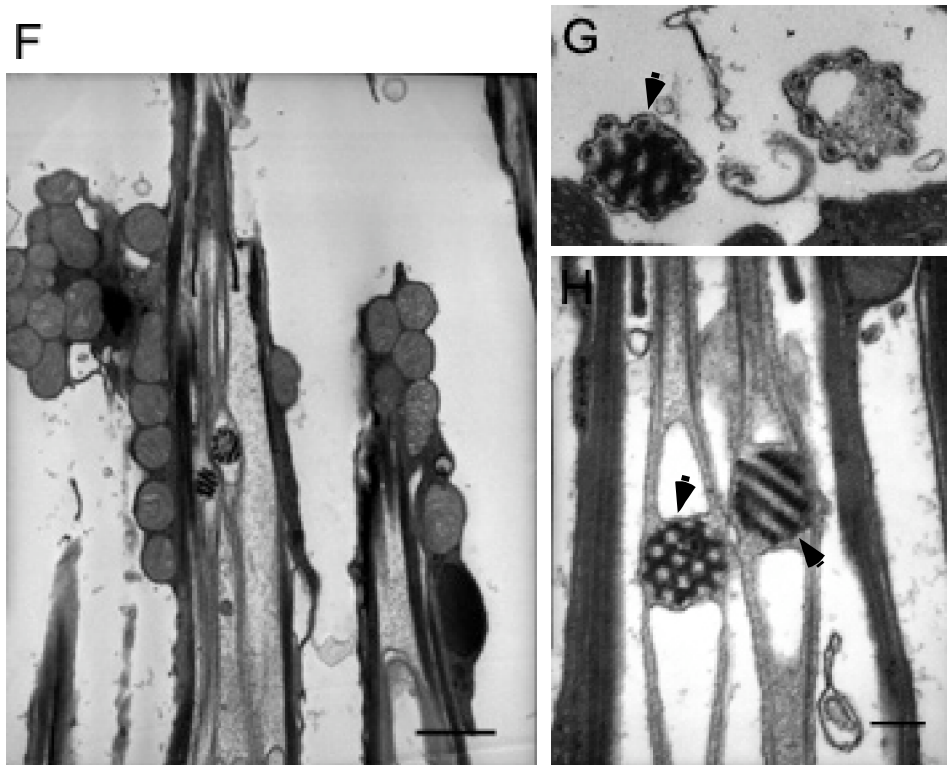
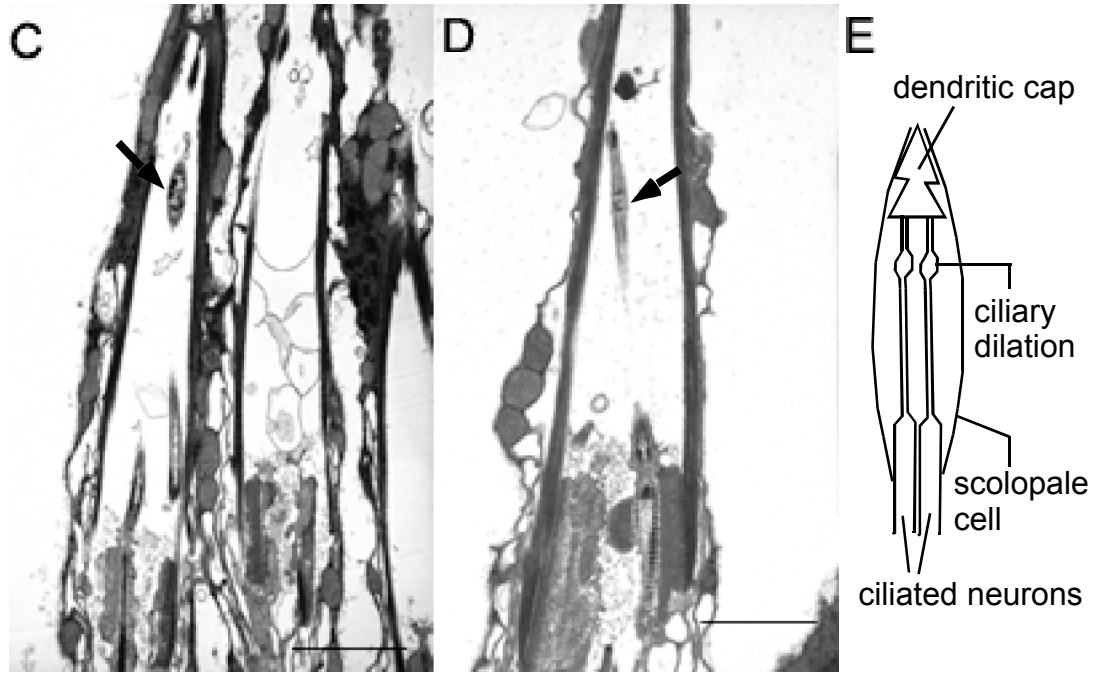


[Figure 2-4] NOMP B accumulations in IFT-A mutants

NOMP B accumulates on the tips of *rempA*, *oseg1* shortened chordotonal cilia. All pictures were counterstained with the monoclonal antibody 22C10 (red), which labels the inner segment of mechanosensory neurons in chordotonal organ. Scale bar: 8 μ m.

(A and B) The wild type antennal chordotonal organ (A) has a normal length of cilia and NOMP B stains along the whole cilia and looks to accumulate around the ciliary dilation (arrows). However, *oseg1* (B) has very short cilia compared to *rempA* (D) and NOMP B accumulated on tips of very short *oseg1* cilia (arrows).

(C and D) NOMP B accumulated on tips of the truncated *rempA* cilia (D, arrow). The NOMP B distribution in a heterozygote (C) was not different from that in an *oseg1* heterozygote. It was localizing along the cilia and the signal looks dense around a ciliary dilation (arrow).

(E and F) The larval chordotonal organ of *rempA* shows consistently accumulation of NOMP B on the tip of truncated cilia (F, arrows). Wild type has a normal distribution of NOMP B along the cilia (E, arrows).

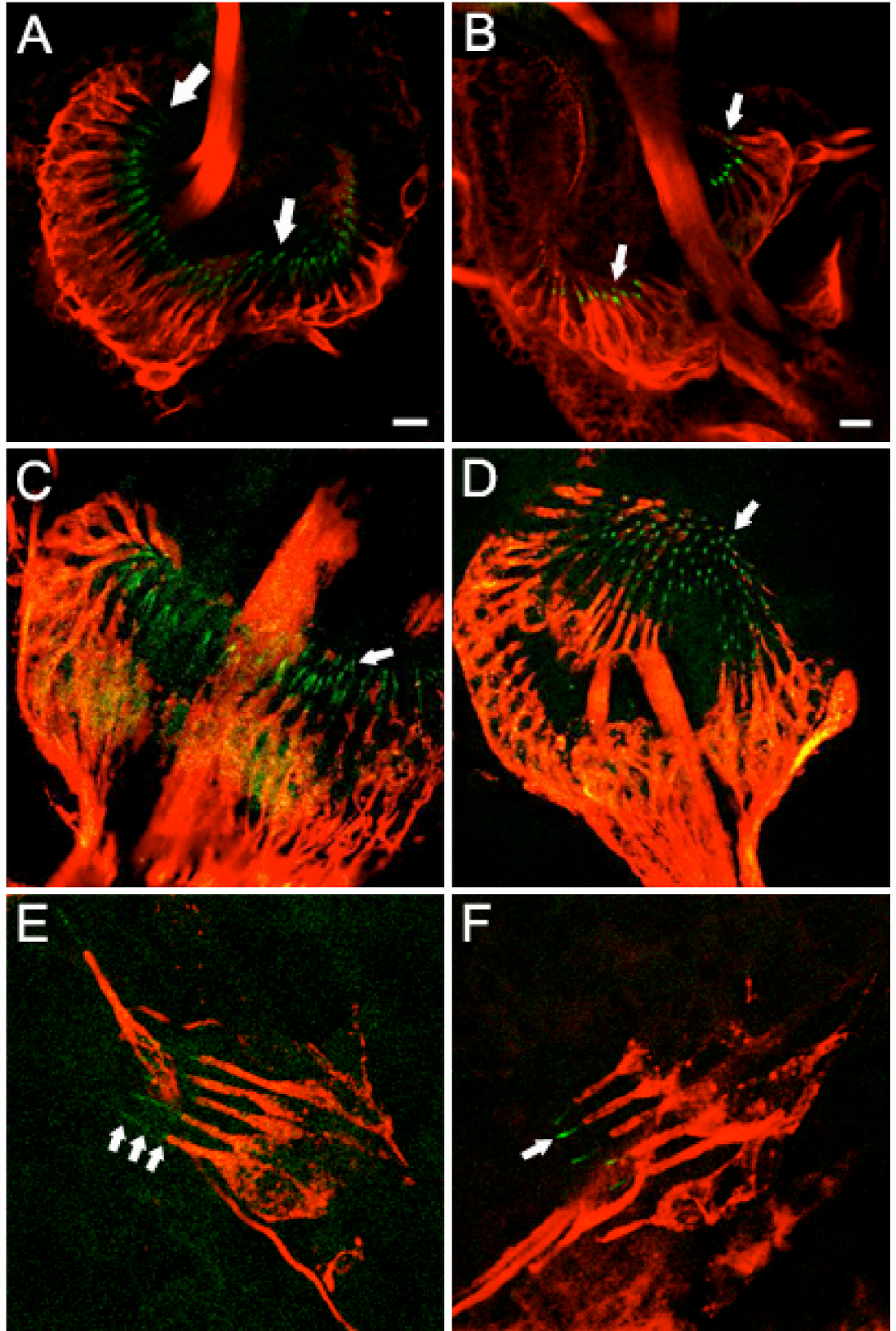


[Figure 2-5] Positional cloning shows that *rempA* encodes IFT140

(A) The complementation test uncovered the *rempA* region to 21C4 to 21D1. The region includes 21 candidate genes including BBS8 and IFT140. BBS8 and IFT140 are known to be involved in ciliary function in other organisms.

(B) Sequencing for *BBS8* and *IFT140* showed that three *rempA* alleles have a mutation or a deletion in the *IFT140* coding sequence. No significant missense mutation was found in *BBS8*. This indicates that *rempA* encodes the *IFT140* fly homolog. In addition, *IFT140* contains x-box, a regulatory motif known to be contained in ciliary genes on 81pb upstream from the translation start codon of *IFT140*.

(C) *rempA¹* has a nonsense mutation that G is replaced by A, which leads to a stop codon instead of W at 465. The single base pair change of G to A in *l(2)21Ci¹* causes a stop codon at 676 instead of W. In k12913, a big deletion caused by the same sequence ‘GCAA’ in exon 4 and exon 5 leads a frameshift to end with a stop codon after 34aa. One possible mechanism to take account of the sedentary behavioral phenotype of *l(2)21Ci¹* might be the readthrough where a termination is weakly suppressed at a stop codon followed by guanidine(G), thus leading to a hypomorph. Though *rempA¹* allele has also a stop codon followed by G, *rempA* shows severe uncoordination, indicating that *rempA¹* is not affected by readthrough.

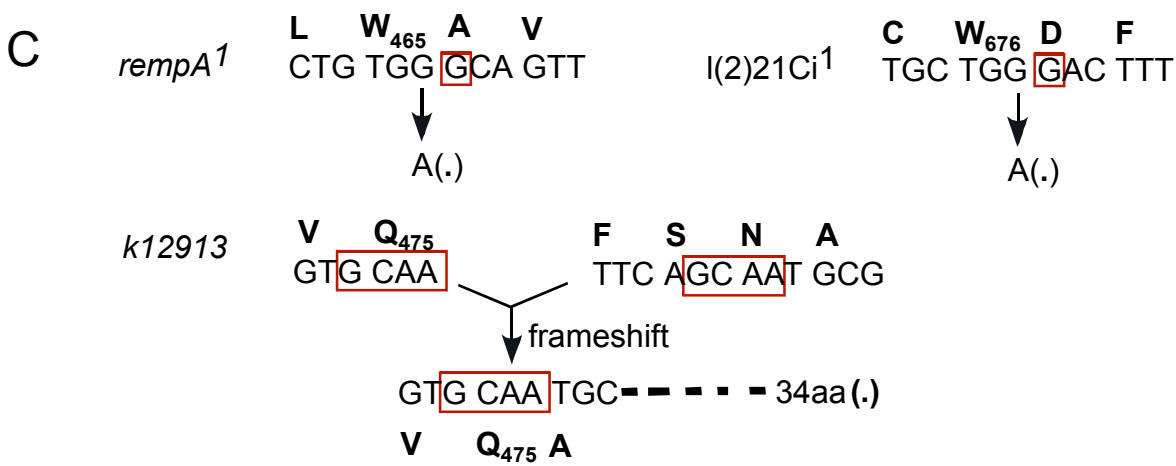
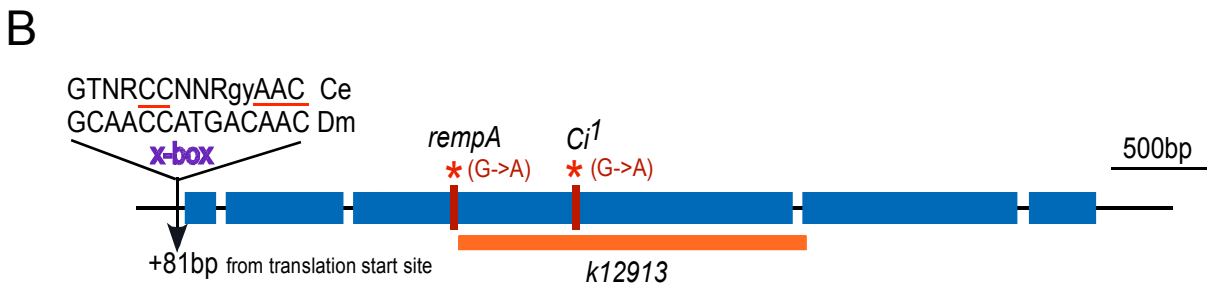
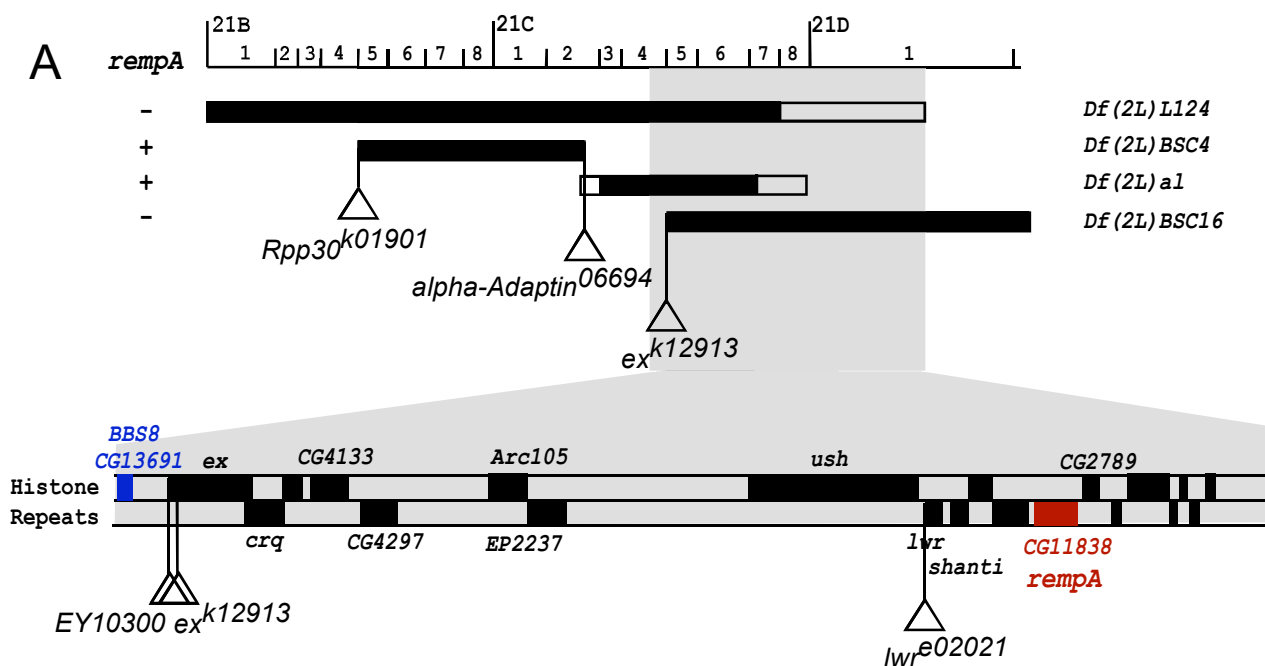


[Figure 2-6] REMPA amino acid sequence is well conserved.

(A) The thin line indicates 5 WD40 motifs and 8 TPR motifs are outlined by thick lines.

Notably, TPR motifs of REMPA are well conserved compared to WD40 motifs.

Interestingly, 4th WD40 motif includes the part of a sequence specifically inserted to *remA*. The first TPR motif includes a non-conserved sequence.

(B) Schematic shows the domain structure of REMPA. WD40 motifs are on N terminus, and TPR motifs are mostly on C terminus.

(C) The phylogenetic tree for IFT140 homologs indicates that vertebrate homologs are close to each other and the arthropod homologs are in the same subbranch.


```

Dm_REMPA-PB gaMkr...pkLLKwMGQYL...ESSGDwDA...vKhKae...WFSQV...I...CYI...lki...s...Kra...Da...Ar...q
Ag_I FT140 gaLk...CYM...catt...D...peLLR...WVA...QYVES...GDMEGA...ki...YqR...sg...DWFS...QVRI...I...CFI...Gq...Va...RA...De...l...Ar...a
Hs_I FT140 psLeI...YV...Kmk...D...ktLw...RWA...QYVES...GDMDAA...hy...el...ar...Dh...FSL...VRI...h...CF...Gn...Vq...KA...aq...l...Ane
Cr_I FT140 teLq...NYI...cands...ReLI...I...WVG...YLES...GEYa...kAl...dc...Yr...KAg...Ds...I...VVR...I...h...CF...G...dwk...a...Ede...vt...n
che-11 kqte...QYV...r...kr...Eer...vyski...l...kni...nsqf...R...s...Lys...WVG...YLES...VE...LEGA...r...sf...Yss...Ak...D...Y...C...VVR...V...K...G...Q...kt...de...A...ar...L...me

Dm_REMPA-PB SGRRAACTHLARHYENVYKFKQEAImFETTRACTFSNATRI...CKENDF...qEE...wt...Vas...ssr...qr...k...al...AA...V...FEE...c...Nf...khr...ve
Ag_I FT140 SGRRAACYHLGRVYENS...GKLG...EAL...qFY...TRACT...Yg...NA...VRI...CKE...HE...ppd...Lwt...VAct...ar...ar...Dkas...AA...Y...EE...s...edyr...RA...V...m
Hs_I FT140 IGHIAASYHLARQYES...qee...Vg...qAV...hFY...TRACa...Fk...NA...I...RL...CKE...ng...Ld...Dq...L...m...N...AL...I...Sspe...DM...I...e...AA...R...Y...EE...k...g...Q...md...RA...V...m
Cr_I FT140 SApnAAs...HLARQY...Eas...GR...I...pe...A...r...Y...TI...AK...r...Y...S...ng...VRL...AK...h...EL...ds...D...L...m...NL...AL...k...St...pa...VM...I...d...Ad...Y...T...ra...k...Q...he...KA...at
che-11 SKDKAAC...Y...I...GR...NY...E...ng...D...V...V...K...AV...K...F...I...TK...Ar...al...S...s...AT...RL...A...KE...HD...M...k...p...r...La...NL...CL...m...a...gg...s...EL...V...s...AA...R...Y...E...DI...p...g...v...ah...KA...V...m

Dm_REMPA-PB LYHRAGMLNKAWEAF...S...e...p...Ei...e...l...e...s...D...l...a...p...d...S...D...a...e...I...n...RC...AD...FF...c...s...i...e...q...F...q...k...w...h...L...a...k...t...k...h...l...e...k...a...l...g...l...u...s...e...k...g...p
Ag_I FT140 LYHRAGMLNKAWEAF...S...e...p...E...L...V...I...A...s...E...L...u...s...S...D...p...L...V...g...R...C...AD...FF...V...g...i...e...q...y...K...A...V...g...L...L...a...n...a...q...l...a...R...A...L...a...V...c...a...E...h...r...V...p
Hs_I FT140 LYHRAGMLNKAWEAF...S...e...p...E...L...V...I...A...s...E...L...u...s...S...D...p...L...V...g...R...C...AD...FF...V...g...i...e...q...y...K...A...V...g...L...L...a...n...a...q...l...a...R...A...L...a...V...c...a...E...h...r...V...p
Cr_I FT140 LYHRAGMLNKAWEAF...S...e...p...E...L...V...I...A...s...E...L...u...s...S...D...p...L...V...g...R...C...AD...FF...V...g...i...e...q...y...K...A...V...g...L...L...a...n...a...q...l...a...R...A...L...a...V...c...a...E...h...r...V...p
che-11 LYHRAGMLNKAWEAF...S...e...p...E...L...V...I...A...s...E...L...u...s...S...D...p...L...V...g...R...C...AD...FF...V...g...i...e...q...y...K...A...V...g...L...L...a...n...a...q...l...a...R...A...L...a...V...c...a...E...h...r...V...p

Dm_REMPA-PB VTEELsleMLTpe...g...-...E...f...e...a...t...r...v...h...l...v...q...L...G...E...F...I...q...q...e...s...d...M...h...s...A...T...K...K...F...T...Q...A...G...D...K...L...S...G...D...I...D...K...I...F...F...A...n...M...S...K...R...E
Ag_I FT140 VTEELsleMLTpe...g...-...D...L...a...E...g...e...r...t...a...L...I...r...L...G...D...I...q...e...Q...G...d...Y...H...a...T...K...K...F...T...Q...A...G...D...K...L...S...G...D...I...D...K...I...F...F...A...n...M...S...K...R...E
Hs_I FT140 VTEELsleMLTpe...g...-...D...L...a...E...g...e...r...t...a...L...I...r...L...G...D...I...q...e...Q...G...d...Y...H...a...T...K...K...F...T...Q...A...G...D...K...L...S...G...D...I...D...K...I...F...F...A...n...M...S...K...R...E
Cr_I FT140 VTEELsleMLTpe...g...-...D...L...a...E...g...e...r...t...a...L...I...r...L...G...D...I...q...e...Q...G...d...Y...H...a...T...K...K...F...T...Q...A...G...D...K...L...S...G...D...I...D...K...I...F...F...A...n...M...S...K...R...E
che-11 VTEELsleMLTpe...g...-...D...L...a...E...g...e...r...t...a...L...I...r...L...G...D...I...q...e...Q...G...d...Y...H...a...T...K...K...F...T...Q...A...G...D...K...L...S...G...D...I...D...K...I...F...F...A...n...M...S...K...R...E

Dm_REMPA-PB YVYMAANYLCA...L...W...C...S...D...P...Q...V...L...K...h...I...V...I...F...Y...T...K...G...Q...A...F...D...s...L...A...N...F...y...a...l...C...A...G...I...E...E...F...q...u...g...k...A...L...t...a...M...q...e...a...s...K...C...E...k...l...s...-...-...-...-...h
Ag_I FT140 YVYMAANYLCA...L...W...C...S...D...P...Q...V...L...K...h...I...V...I...F...Y...T...K...G...Q...A...F...D...s...L...A...N...F...y...a...l...C...A...G...I...E...E...F...q...u...g...k...A...L...t...a...M...q...e...a...s...K...C...E...k...l...s...-...-...-...-...h
Hs_I FT140 YVYMAANYLCA...L...W...C...S...D...P...Q...V...L...K...h...I...V...I...F...Y...T...K...G...Q...A...F...D...s...L...A...N...F...y...a...l...C...A...G...I...E...E...F...q...u...g...k...A...L...t...a...M...q...e...a...s...K...C...E...k...l...s...-...-...-...-...h
Cr_I FT140 YVYMAANYLCA...L...W...C...S...D...P...Q...V...L...K...h...I...V...I...F...Y...T...K...G...Q...A...F...D...s...L...A...N...F...y...a...l...C...A...G...I...E...E...F...q...u...g...k...A...L...t...a...M...q...e...a...s...K...C...E...k...l...s...-...-...-...-...h
che-11 YVYMAANYLCA...L...W...C...S...D...P...Q...V...L...K...h...I...V...I...F...Y...T...K...G...Q...A...F...D...s...L...A...N...F...y...a...l...C...A...G...I...E...E...F...q...u...g...k...A...L...t...a...M...q...e...a...s...K...C...E...k...l...s...-...-...-...-...h

Dm_REMPA-PB aqhvynn...r...t...V...nd...V...Kai...L...e...l...q...a...l...r...e...g...h...q...l...v...g...s...c...R...M...i...k...p...-...e...l...p...p...h...A...h...I...I...M...L...r...a...l...v...v...K...d...Y...s...e...a...g...k...L...k...E
Ag_I FT140 aqhvynn...r...t...V...nd...V...Kai...L...e...l...q...a...l...r...e...g...h...q...l...v...g...s...c...R...M...i...k...p...-...e...l...p...p...h...A...h...I...I...M...L...r...a...l...v...v...K...d...Y...s...e...a...g...k...L...k...E
Hs_I FT140 aqhvynn...r...t...V...nd...V...Kai...L...e...l...q...a...l...r...e...g...h...q...l...v...g...s...c...R...M...i...k...p...-...e...l...p...p...h...A...h...I...I...M...L...r...a...l...v...v...K...d...Y...s...e...a...g...k...L...k...E
Cr_I FT140 aqhvynn...r...t...V...nd...V...Kai...L...e...l...q...a...l...r...e...g...h...q...l...v...g...s...c...R...M...i...k...p...-...e...l...p...p...h...A...h...I...I...M...L...r...a...l...v...v...K...d...Y...s...e...a...g...k...L...k...E
che-11 aqhvynn...r...t...V...nd...V...Kai...L...e...l...q...a...l...r...e...g...h...q...l...v...g...s...c...R...M...i...k...p...-...e...l...p...p...h...A...h...I...I...M...L...r...a...l...v...v...K...d...Y...s...e...a...g...k...L...k...E

Dm_REMPA-PB tvKdst...w...a...s...g...l...e...r...s...i...v...h...K...I...a...q...c...h...L...e...f...d...l...I...w...n...a...g...r...q...v...t...a...s...t...s...g...t...a...a...t...g...M...s...t...s...g...M...t...t...d...d...D...p...D...E...e...l...t...e...e...h
Ag_I FT140 tvKdst...w...a...s...g...l...e...r...s...i...v...h...K...I...a...q...c...h...L...e...f...d...l...I...w...n...a...g...r...q...v...t...a...s...t...s...g...t...a...a...t...g...M...s...t...s...g...M...t...t...d...d...D...p...D...E...e...l...t...e...e...h
Hs_I FT140 tvKdst...w...a...s...g...l...e...r...s...i...v...h...K...I...a...q...c...h...L...e...f...d...l...I...w...n...a...g...r...q...v...t...a...s...t...s...g...t...a...a...t...g...M...s...t...s...g...M...t...t...d...d...D...p...D...E...e...l...t...e...e...h
Cr_I FT140 tvKdst...w...a...s...g...l...e...r...s...i...v...h...K...I...a...q...c...h...L...e...f...d...l...I...w...n...a...g...r...q...v...t...a...s...t...s...g...t...a...a...t...g...M...s...t...s...g...M...t...t...d...d...D...p...D...E...e...l...t...e...e...h
che-11 tvKdst...w...a...s...g...l...e...r...s...i...v...h...K...I...a...q...c...h...L...e...f...d...l...I...w...n...a...g...r...q...v...t...a...s...t...s...g...t...a...a...t...g...M...s...t...s...g...M...t...t...d...d...D...p...D...E...e...l...t...e...e...h

```

B putative domain of REMPA



C

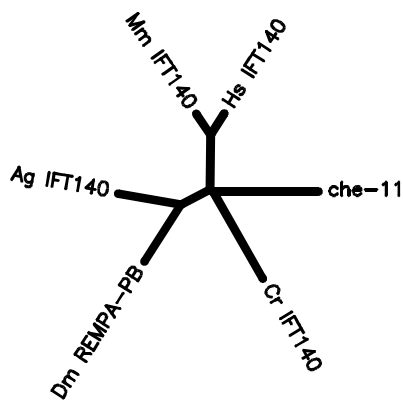
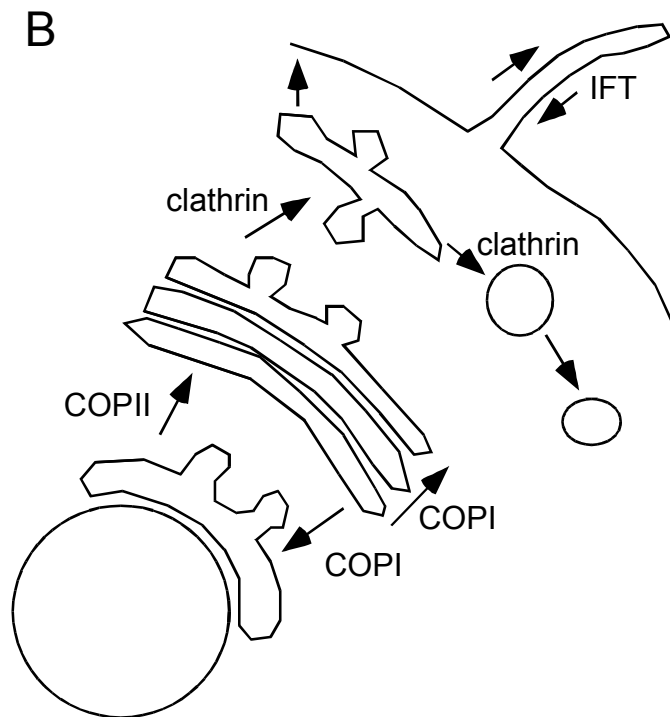
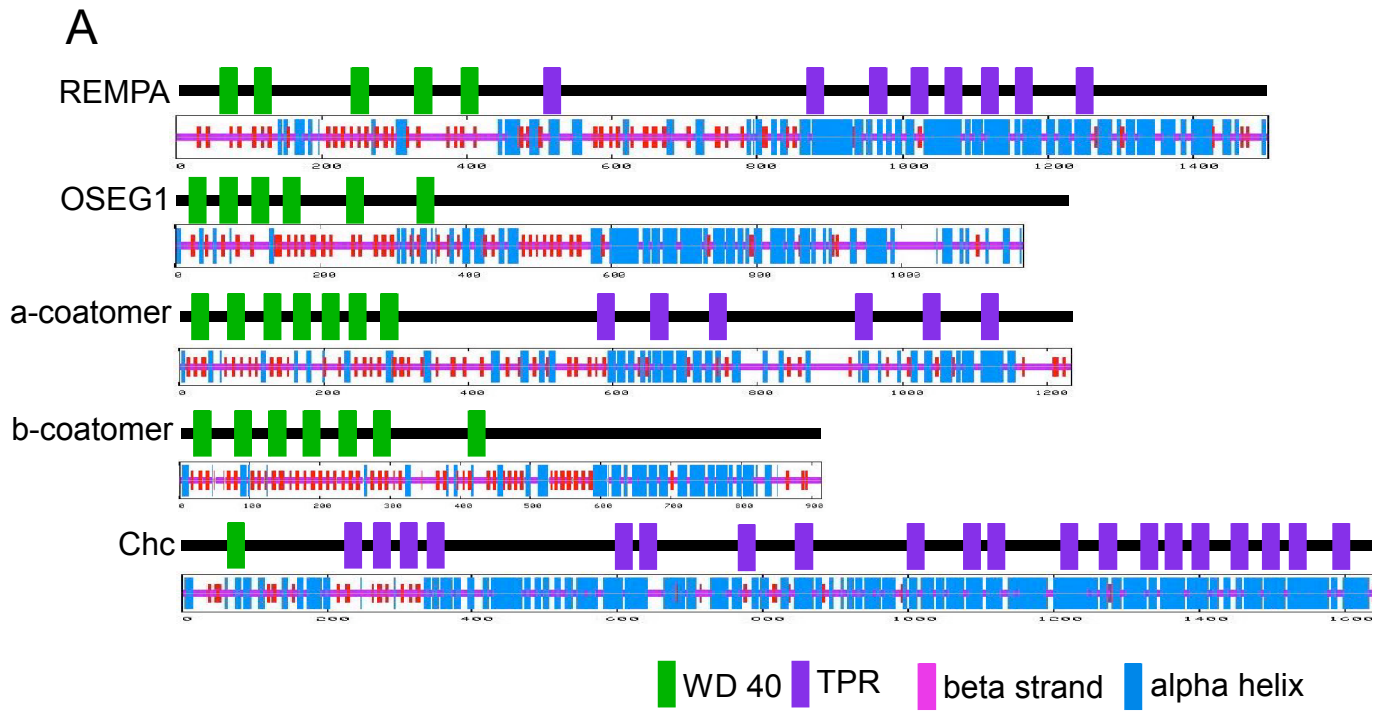


[Figure 2-7] The domain composition analysis of IFT-A, COP molecules and clathrin heavy chain displays the similar architecture.

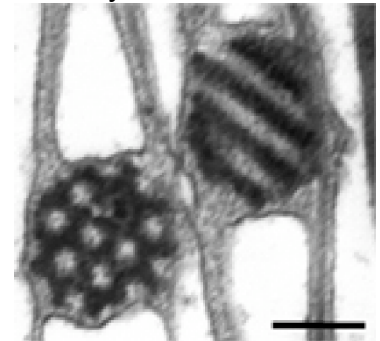
(A) All have N-terminal WD40 motifs and C-terminal TPR motifs. Consistently, the second structure analysis predicts that all have β -propeller and α -helices.

(B) The schematic illustrates the intracellular trafficking: COP II is involved in transporting from the ER to the Golgi; COPI is shuffling between Golgi cisternae and from the Golgi to the ER; Clathrin is moving from the Golgi to endosome or lysosome and related to endocytosis; IFT is responsible for the intraciliary trafficking.

(C) The EM analysis shows a ciliary dilation of an electron dense structure. The electron dense repeat of a ciliary dilation is about 56nm. The whole shape of a ciliary dilation is similar to that of COP vesicles. This EM was generated by Dr. Elena Loukianova in Dr. Daniel Eberl's lab (U of Iowa). Scale bar: 0.25 μ m



C ciliary dilation



Chapter 3:

Expression & localization of *REMPA*

1. In chordotonal organs
2. In external sensory organs
3. Mislocalizations in IFT-related mutants

To investigate the function of REMPA in mechanosensory transduction, A YFP-tagged REMPA was expressed using its native promoter. In chordotonal organs of transgenic flies, REMPA localizes specifically on the ciliary dilation. Ciliary dilations are electron-dense structures in the cilia whose molecular composition and function are unknown. REMPA locates along the cilia when cilia differentiate and is concentrated on the ciliary dilation as ciliary differentiation is completed. To confirm that REMPA is a molecular component of the ciliary dilation, REMPA-YFP localization was examined in a kinesin-II hypomorph, in which the ciliary dilation is reduced and shifted distally into the dendritic cap. REMPA-YFP shows a similar shift in a kinesin-II hypomorph, indicating that REMPA is indeed a component of ciliary dilation. This is consistent with the ultrastructural defect found in EM analysis.

*To ask if another IFT-A protein is also a component of the ciliary dilation, REMPA localization in an *oseg1/IFT122* mutant was examined. REMPA was not detected in *oseg1*, suggesting that *OSEG1* and REMPA are required together for the stability of an IFT-A subcomplex and its localization. In the dynein mutant, *btv*, where the ciliary dilation is missing but has the full-length chordotonal cilia, REMPA dispersed along the cilia, accumulating on their apical ends, indicating that BTV is not necessary for the stability of IFT-A proteins.*

*Two TRPV ion channel subunits, NAN and IAV, are localized in chordotonal cilia, proximal to the ciliary dilation. In *iav* mutants, REMPA localization is normal, showing that REMPA localization is activity-independent. IAV is not detected in *rempA* mutants and leaked to the distal part from the proximal region of a ciliary dilation in *btv* mutants. Taken together, a ciliary dilation might be an IFT-A supercomplex partitioning the chordotonal cilia into functionally distinct compartments in a *btv*-dependent manner.*

*In es organs, REMPA labels the connecting cilium. This REMPA labeling zone was distinguished from NOMPA staining region, and overlapped with the area stained by Eyes shut (Eys). REMPA was also apically delocalized in a connecting cilium in *btv* mutant es organs, suggesting the function of BTV as a retrograde motor in both chordotonal and es organs.*

**dyf-1* is completely missing cilia, and neither REMPA nor NOMPB were detected in *dyf-1*, suggesting that *DYF-1* is a component of IFT-A and is required for the stable maintenance of IFT complex. *BBS8* and *BBS1* appear to retain the full-length of cilia, unlike in *C. elegans*. REMPA and NOMPB normally localized in *BBS8* and *BBS1* mutants, indicating that BBS proteins are not required for mechanosensory transduction.*

Materials and methods

stocks

Two other alleles for *rempA*, $y^1 w^{67c23}; P\{w^{+mC}=lacW\}ex^{k12913}/CyO$ and $l(2L)Ci^1/CyO$ were obtained from Bloomington stock center and Dr. Heitzler respectively. IFT120 fly homolog (CG7161), $w^{1118}; P\{w^{+mC}=EP\}CG7161^{EP3616}/TM6B$, Tb^1 , $klp64D^{k1}$, and $klp64D^{n124}$ were obtained from Bloomington stock center. Flies were kept on standard medium at 21-25 °C. Transgenic flies for GFP-NOMPA and GFP-NOMP B fusion proteins were generated by Dr. Chung and Dr. Han (Chung et al., 2001; Han et al., 2003). Flies for elav-Gal4, CD8::GFP and deficiency chromosomes ($Df(2L)al$, $Df(2L)L124$, and $Df(2L)BSC16$) for the positional cloning are from *Drosophila* stock center at Bloomington. Cytoplasmic dynein motor mutant, *btv*, and two *kinesinII* hypomorphic allele, $klp64D^{L4}$ and $klp64D^{K5}$, were offered by Dr. Daniel Eberl. $klp64D^{n123}$ and $klp64D^{K1}$ for *kinesinII*-null mutants are from *Drosophila* stock center at Bloomington.

To test the genetic interaction among IFT proteins, NompB-GFP localization was examined in different IFT mutant backgrounds. $rempA/CyOGFP;NompB-GFP$, $btv/CyO;NompB-GFP$, CG7161 recombined with NompB-GFP were generated by genetic crosses and chordotonal organs of second antennal segment of each stock were manipulated for detecting the NompB-GFP localization.

Cloning of rempA-Venus construct and Transformation

For the rescue construct $P\{rempA+\}$, EcoRI-EcoRI fragment of 8339bp was isolated from BAC clone, BACR48E08 (DGRC, Bloomington, IN), subcloned into

pBluescript KSII+, and transferred into pCaSpeR4 vector by SpeI and KpnI. This includes about plus 2.9kb upstream region from the translation start site and 3.5 kb of the 3'UTR region. In order to generate the *rempA-Venus* fusion construct, tagging on C-terminal region was designed. XmaI-NotI fragment of about 3kb was removed from pBS-rempA plasmid where one XmaI site is on exon 6 and NotI is on the vector. 90 oligo dimers without stop codon were synthesized and inserted for the missing region of exon 6 using XmaI and NotI. Amplified Venus (DRGC, Bloomington, ID) fragment was inserted by NotI and SacII, which was followed by a stop codon. AAG sequence was placed as a spacer between exon 6 and venus. 3' UTR fragment of 1.8kb was amplified from pBS-rempA by PCR and added by SacII and XbaI on 3' region after *rempA-Venus* plasmid was subcloned into pCaSpeR4 vector with EcoRI and SacII. The mixture of final fusion construct and helper plasmid was injected into eggs of *yw* fly stock for germ line transformation as described by Rubin and Spradling (Rubin and Spradling, 1982).

Embryos collection and fixation

Embryos were collected after a 13-15 hours incubation of adult flies in 25C incubator. After dechorinating with 50% chloride solution followed by washing with flowing tap water completely, embryos were fixed with equal volumes of 37% formaldehyde and n-heptane in a scintillation vial by vigorous shaking for 5 minutes. Fixed embryos were washed with PBS 3-4 times and transferred to a petridish. The vitelline membrane was mechanically removed by a pointy needle. The procedure for the label with specific markers is the same as described in a previous chapter.

Antibody staining and confocal microscopy

For the expression in an external sensory organ, pupal abdomen and halteres were dissected from either pupae or pharate adults. For chordotonal organ, pupal antennae and legs were dissected in PBT at 24-48 hours after pupation. The procedure for antibody staining is the same as described in a previous chapter. 21A6 (Developmental Studies Hybridoma Bank, Iowa City, IA), the monoclonal antibody against Eyes shut, was diluted to 1:250 and 546- or 647-conjugated goat anti-mouse antibodies (1:1000 dilution, Molecular Probes, Eugene, OR) were used as a secondary antibody. For actin filament staining, Alexa fluor 568-conjugated phalloidin (1:1000) was added in secondary antibody incubation.

3.1. In chordotonal organs

The fact that *rempA* encodes IFT140 has been proved by the complete rescue of the electrophysiological response to the auditory stimuli and by indistinguishable behavior of $P\{rempA\}^+$ transgene flies as shown in (Fig. 2-1). The fully rescued mechanosensory response also implies that the transformed $P\{rempA\}^+$ contains normal protein activity of IFT140. Previous studies in *Chlamydomonas reinhardtii* and *Caenorhabditis elegans* found that IFT particles are involved in ciliogenesis and in signaling transduction. To determine what function IFT-A subcomponents do in mechanosensory cilia of *Drosophila*, the subcellular localization of REMPA on ciliary

neurons was explored. *Drosophila* has two kinds of type I sensory organs where ciliated endings are involved in mechanosensory transduction. To specify the subcellular localization of REMPA, a few antibodies denoting particular structures in a ciliary organ were utilized: for example, anti-NOMPA for dendritic cap, phalloidin for scolopale cells, and 22C10 for an inner segment of ciliary neurons.

REMPA localizes on a ciliary dilation.

The most striking finding in this study is that REMPA specifically labels the ciliary dilation, suggesting that REMPA is a component of a ciliary dilation. The previous study identified that NOMPB localizes along the chordotonal cilia (Han et al., 2003). Initially, REMPA localization was expected to be detected in a similar pattern as NOMPB because they are classified into IFT particles so they might cooperate in ciliary assembly together. Surprisingly, the localization of REMPA specified only one spot on a cilium in antennal and femoral chordotonal organs (Fig. 3-1C and J). REMPA visualization by a counter staining with Alexa568-conjugated phalloidin, which specifically detect F-actin on the scolopale cells, illustrates two foci at 3/4 from the proximal base of cilia inside a scolopale cell (Fig. 3-1 C and J). Considering that two or three neurons innervate into one scolopale in Johnston's organ (Eberl, 1999), REMPA in a specific location indicates a certain position on two cilia in one scolopale. To determine if REMPA localizes on the ciliary tip, the chordotonal organ was examined by counterstaining with anti-NOMPA. Since the ciliary tip extends into a dendritic cap, REMPA might be inside of a dendritic cap. The staining with anti-NOMPA on $p\{remPA\}^+$ chordotonal cilia results in no colocalization at a tip, rather, a little small gap

between NOMPA and REMPA labeling spots (Fig. 3-1L, arrowheads).

To identify where REMPA localizes on chordotonal cilia, the larval chordotonal organ was explored, because DIC microscopy easily discriminates the overall structure of a larval chordotonal organ. Intriguingly, DIC image of larval CHO shows that REMPA localizes explicitly on a ciliary dilation (Fig. 3-2A-C, arrowheads). As mentioned in the introductory chapter, the ciliary dilation is a unique structure only found in arthropod chordotonal organ, and its molecular component and function are hitherto undetermined. A bulky structure near the cap cell in DIC image is the ciliary dilation (Fig. 3-2A, arrowheads). This structure is perfectly overlapped with YFP location in a merged picture (Fig. 3-2C, arrowheads). This strongly supports that REMPA localizes on ciliary dilation and REMPA might be one of the components comprising the ciliary dilation. This finding is consistently observed in embryos (Fig. 3-2D-F, arrowheads). At embryonic stage 17, the unambiguous labeling of REMPA is precisely locating on the round structure of cilia in a merged picture (Fig. 3-2F). This is separate from the dendritic cap of an arrow shape (Fig. 3-2D and F, arrows).

Localization of REMPA during development

More interestingly, REMPA presented discernable localization pattern as cilia differentiate. REMPA locates along the cilia in an early stage, but concentrates on a ciliary dilation as ciliary differentiation completes (Fig. 3-1A-C). This differential expression pattern was also observed during embryonic development (Fig. 3-1D-F). In stage 15, REMPA appears on the cytoplasm and along the cilia, gradually moves to cilia, and finally congregates on a ciliary dilation at stage 17 when ciliary differentiation is complete (Fig. 3-1D-F).

REMPA and 21A6 mark discrete fractions on chordotonal cilia.

A recent study reported that 21A6, the Agrin/Perlecan-related protein, is required for epithelial lumen formation of fly eyes and localizes on ciliary dilation of embryonic CHO (Husain et al., 2006). This would provide a good insight into the function of a ciliary dilation with REMPA if 21A6 colocalizes with REMPA on a ciliary dilation. To see two proteins localize on identical cilia, I stained $p\{remPA-YFP\}^+$ chordotonal organ with 21A6 antibody. However, their localization is distinctively separate on adult cilia (Fig. 3-1H and I, arrows and arrowhead) as well as on embryonic chordotonal cilia (Fig. 3-1D-F). Noticeably, 21A6 positions at a near proximal region to a ciliary dilation as if it forms a belt around the cilia. This strip-like pattern of 21A6 staining parallels the cilium, and it looks to locate on a scolopale cell not on a cilium. Additionally, 21A6 is partly detected around the base of cilia (Fig. 3-1H-I, arrows). In an early stage, 21A6 appears to surround growing cilia, and 21A6 places mainly on the proximal area to the ciliary dilation and minorly situates around the ciliary base (Fig. 3-1D-F, H, and I). Figure 3-1G delicately shows that 21A6 encircles each cilium on the proximal region in differentiating cilia. The RFP-filled femoral chordotonal neurons stained with 21A6 evidently display that 21A6 localizes around the ciliary base and on the proximal compartment around the cilia (Fig. 3-1K). However, it still needs further analysis in order to define the subcellular localization of 21A6.

Moreover, the interesting point is that the limited district of cilia specified by 21A6 is where TRP hearing channel subunits of NAN and IAV were discovered to localize (Gong et al., 2004). To test that the loss of TRPV channel activity affect the localization of 21A6, 21A6 staining was performed in iav^1 chordotonal organ. 21A6 localization properly distributes in iav^1 mutant and is unable to be distinguished from

wild type, indicating that 21A6 localization is independent of the localization or the activity of TRPV channels (Fig 3-3B and C). On the contrary, 21A6 is delocalized to the basal area of chordotonal cilia in IFT mutant backgrounds in which ciliary structure is found to have a morphological defect like either missing or shortened cilia (Fig. 3-3 D-I). *oseg1* has missing cilia (Avidor-Reiss et al., 2004), and *rempA* has truncated cilia (Fig. 2-2). *btv* has disrupted ciliary dilation (Eberl et al., 2000). Repeated staining with 21A6 of these IFT mutants revealed the altered localization of 21A6, suggesting that 21A6 on scolopale cells might be tightly connected with molecular components on cilia. To determine the functional contribution of 21A6 for the formation of the chordotonal cilia, it might be interesting to examine the localization of REMPA, NOMP B, and BTV in *21A6* mutant. Considering that IFT mutants have defective ciliary structure while *iav* mutant appears to have normal ciliary morphology (Gong et al., 2004), it is very likely that 21A6 is functionally related to the morphological structure of cilia.

The similar but differential pattern of REMPA and NOMP B localization

The dispersed REMPA along the differentiating cilia concentrates on a ciliary dilation, but NOMP B has been found to localize along the cilia (Han et al., 2003). To clearly define the localization of anterograde and retrograde IFT molecules, REMPA and NOMP B chordotonal cilia were meticulously explored during development. Interestingly, NOMP B has similar localization pattern to REMPA throughout ciliary development (Fig. 3-4A-C). The consecutive observations on different pupae stages from very early to after cuticle secretion result in differential localization pattern of NOMP B in different pupal stages. NOMP B is expressed along the cilia in an early to middle stage but not evenly (Fig. 3-4A and B), which was followed by the concentration on the distal part of the cilia.

In this stage, they were also scattered on the proximal part of the cilia, labeling the base of the cilia, but mostly they concentrated on the distal cilia (Fig. 3-4C).

To spatially define the area occupied by NOMP/B on differentiated cilia, colabeling with 21A6 was carried out. A comparative localization of 21A6 and REMPA on identical cilia manifested that 21A6 localizes on a ciliary compartment proximal to the ciliary dilation. This relative position of NOMP/B to 21A6 on cilia would seem to provide a key underlying the transporting operation on cilia. NOMP/B colabeled with 21A6 outlines itself from the distal boundary of the 21A6 labeling region to the distal tip. However, it doesn't signify two specific foci, unlike REMPA, rather it localizes around the ciliary dilation (Fig. 3-4D and E, arrows). Furthermore, NOMP/B was detected on the microtubule structure in a very thin line distal to the ciliary tip (Fig. 3-4E). In summary, REMPA and NOMP/B, both locate along the cilia during ciliary differentiation, and after which concentrate on a specific region. However, REMPA specifically moves onto a ciliary dilation, whereas NOMP/B is broadly concentrated on the distal area including ciliary dilation.

3.2. In external sensory organs

The other type I sensory organ containing a ciliary structure is ES organs. In contrast to chordotonal organs aggregated on the antennae and legs containing long cilia

ensheathed by scolopale cells, ES organs disseminate all over the body surface and have very short cilia. While chordotonal cilia are activated by stretch stimuli, the response in ES organ is evoked by the deflection of bristle shaft or the distortion of the cuticular dome (reviewed in Eberl, 1999 and Keil, 1997). The outer segment of cilium in ES organs is mostly occupied by a big microtubule-rich tubular body at the most distal part and a tiny connecting cilium (Fig1-3). The tubular body is connected to a bristle base through dendritic cap proteins. The structural component and function of the tubular body is currently unknown and it is speculated as an anchoring site of mechanosensory transduction channels (Avidor-Reiss et al., 2004). *rempA* mutant flies show proprioceptive deficit and severely reduced mechanoreceptor potential on bristles. This behavioral phenotype reflects that *rempA* has a certain function on ES cilia.

To determine which compartment in ES organs is the functional equivalent to a ciliary dilation, I examined whether the function of REMPA is conserved in both ciliated sensory organs. This would not only provide a fundamental key for how two sensory organs are evolutionally related to each other but furthermore would allow us to designate the functional identity of structural components of *Drosophila* ciliary organs. With this rationale, I attempted to examine the localization of REMPA in ES organs.

RempA localizes on a connecting cilium in abdominal bristle cilia.

To define the localization of REMPA in ES organs, pupal abdomen and campaniform sensillae of pupal halteres were dissected and examined. The preliminary observation of REMPA in ES organs informed us that it does not place close enough to the bristle base, entailing that it is unlikely to locate on the tubular body (Fig. 3-5A-F). DIC microscopy (Fig. 3-5A-D) and confocal microscopy (Fig. 3-5E and F) consistently

visualize that of REMPA localizes apart from a bristle base.

To analyze the localization of REMPA more precisely, I counterstained the $P\{rempA\}^+$ -transformed pupal abdomen with the antibody raised against NOMPA, which specifically labels the most distal part of the outer segment of cilia (Chung et al., 2001). The NOMPA antibody did not colocalize with REMPA, instead REMPA proximally localized next to the NOMPA staining region, implying that it might localize on a connecting cilium (Fig. 3-6A-F). The relative localization of NOMPA and REMPA resembles the labeling pattern of NOMPA and 21A6 on identical abdominal bristle cilia (Chung et al., 2001).

21A6 antigen is distinctively proximal to the GFP-NOMPA localizing place (Chung et al., 2001). I considered if the REMPA localizes proximally right next to NOMPA, REMPA must colocalize with 21A6. Indeed, the staining of REMPA abdomen with 21A6 antibody resulted in the colocalization of REMPA and 21A6, strongly supporting that REMPA might localize on a connecting cilium (Fig. 3-6G-J, arrows). Moreover, the 21A6 staining seems to cover around the REMPA region because the size of staining area occupied by 21A6 looks a little bigger (Fig. 3-6H and J, arrows), suggesting that 21A6 might possibly localize on surrounding lumen inside a thecogen cell which would be homologous to a scolopale in a chordotonal organ (Merritt, 1997).

RempA localizes on a connecting cilium in a campaniform sensilla.

Though the identified localization pattern of REMPA by NOMPA and 21A6 firmly suggest that REMPA might place on a connecting cilium, it is not conclusive until it is analyzed by immuno-EM or section staining. Moreover, the cuticular autofluorescence and multi-planed configuration of a bristle make it limited to access the

corresponding structure with DIC microscopy. However, the outer segment of cilia in campaniform sensilla which have a different morphological shape at each level from proximal to distal successfully substantiates the labeling area of REMPA in ES organs. The outer segment of campaniform sensilla of haltere has a round shape at the proximal level and has a flattened rod shape at the most distal level where a tubular body is present.

To validate the localization of REMPA on a connecting cilium in ES organs, I examined the shape labeled by REMPA in campaniform sensilla. Undoubtedly, NOMPA labeling pattern showed a rod form because it stained the extracellular matrix protein, the outermost region of a tubular body (Fig. 3-7F). If REMPA does not localize on tubular body of campaniform cilia as found in the abdominal bristle, it would display a round form labeling on campaniform sensilla. As hypothesized, the localization of REMPA shows a round form not a rod form (Fig. 3-7A) unlike NOMPA, implying that REMPA localization is present on the lower level of the outer sensilla while NOMPA localizes on the most distal part of a campaniform sensilla. The observation from the side view clearly displays that REMPA does not place on the most distal end of a campaniform sensilla by showing the gap to the apical surface (Fig. 3-7B, arrowheads). This solid finding indicates that REMPA localizes on a connecting cilium and not on the tubular body of the cilia in ES organs.

The colabeling with 21A6 and REMPA shows an identical pattern as detected in abdominal bristles. They overlap and the 21A6 labeling region seems to surround the REMPA area (Fig. 3-7C, arrows). Similarly, NOMPB localizes on a connecting cilium in ES organs (Fig. 3-7D, arrowheads). The round shape of NOMPB labeling and its position from the side view shows that NOMPB limitedly localizes on a connecting cilium (Fig. 3-7D and E, arrowheads). These results suggest that IFT-A and IFT-B might be involved

in a ciliary transporting process together especially on a connecting cilium in ES organs and a connecting cilium might be an important compartment for ciliary maintenance. One question raised from the monitoring on the NOMPB- and REMPA-labeled campaniform sensilla is that NOMPB labeling region looks slightly longer than REMPA occupancy (Fig. 3-7B and E). However, it is currently unable to determine if this is a resolutional artifact or if it connotes their differential function for ES cilia. The comparative localization of REMPA and NOMPB on identical cilia at the same time is to present their differential occupancy on a connecting cilium.

3.3. Mislocalization of REMPA in other mutants

To illuminate the intracellular interaction or genetic regulation of REMPA, REMPA localization was examined in IFT component- related mutants. Though the interaction within an IFT subcomplex can be inferred from a biochemical fractionation and from a domain analysis (Baker et al., 2003), the detailed function of each IFT molecule on transporting and loading/unloading of cargoes still remains to be answered. So far, very little information was revealed about this issue. For example, in nematode, the IFT-A complex was conjugated to kinesin-II motor for the movement to the distal tip (Ou et al., 2005). Mammalian IFT20 serves as a bridge between KIF3B and IFT-B subcomplex (Baker et al., 2003). Since REMPA specifically localizes on a ciliary dilation

which is a very interesting structure whose function is not known until now, the localization of REMPA in diverse IFT-related mutants possessing different morphological characteristics will provide valuable information on the regulation of the molecular movement as well as provide insight on the function of a ciliary dilation for chordotonal cilia. Therefore, I examined REMPA localization in diverse mutant backgrounds in order to know what effect the lack of each protein of IFT components makes on REMPA behavior.

REMPA is not stable in the absence of OSEG1

Two retrograde IFT-A orthologs are conserved in *Drosophila*: IFT140/REMPA and IFT122/OSEG1. Previously, NOMPB, one of the IFT-B particles, accumulated on the tip of truncated IFT-A cilia, suggesting that IFT-A proteins are involved in retrograde transport (Fig. 2-4). To know whether one retrograde protein also accumulates on the tip of the truncated cilia with the lack of the other IFT-A particle, REMPA localization was examined in *oseg1* chordotonal cilia. Different from our expectations, no REMPA signal was detected (Fig. 3-8B and D).

To explore whether this is due to the loss of ciliary dilation in *oseg1*, the target place for REMPA, which in turn leads to the instability of REMPA, or due to the early degradation of IFT-A subcomplex without OSEG1, I examined the REMPA localization in *oseg1* antennal chordotonal cilia in an early stage when ciliary differentiation is progressing. It results that REMPA is not detected in *oseg1* chordotonal cilia both at early and late stages, suggesting that particles composed of an IFT-A subcomplex are indispensable for the stability or the formation each other. Notably, this is dissimilar from the accumulated NOMPB. Therefore, the absence of REMPA in an early stage of *oseg1*

chordotonal cilia weights on the speculation that each IFT-A protein might be required for the formation of IFT-A subcomplex rather than for complex stability.

BTV is required for the localization of NOMP B and REMPA on sensory cilia.

Btv, the *Drosophila* homolog for cytoplasmic dynein, has long been suggested as a retrograde motor involved in moving back to the base of cilia from the tip. I have presented that IFT formation might not be able to be accomplished without the presence of each IFT-A protein by showing the lack of REMPA signal in *oseg1* cilia. NOMP B accumulated on the tips of truncated cilia both in *rempA* and *oseg1* (Fig. 2-4), and REMPA and OSEG1 require each other for complex formation (Fig. 3-8). If BTV possesses a retrograde motor function, NOMP B will accumulate on the tips of *btv* cilia, like NOMP B in IFT-A mutants. To test this, I examined NOMP B localization in *btv* chordotonal cilia. Unexpectedly, NOMP B was dispersed along the cilia with small accumulation at the most apical tips of *btv* cilia (Fig. 3-10). To determine whether this dispersed pattern stems from the difference in IFT-A and IFT-B molecules, I examined the REMPA localization in *btv* mutant cilia. Similarly, REMPA was also dispersed along the cilia in an unspecified pattern and slightly accumulated at the most apical tip near the cuticle (Fig. 3-9I and J).

These findings provide 3 points to discuss. First, the dispersed delocalization pattern of IFT-A and IFT-B particles reflects that *btv* mutants might have a full length of cilia, while IFT-A mutants have shortened cilia and IFT-B mutants are missing cilia. To define the length of cilia in *btv* mutant flies, I observed the morphology of chordotonal cilia by filling with RFP and by detecting NOMP A localization. The *btv* cilia filled with RFP promoted by *elav* appear to keep the whole cilia, but it looks thicker than a normal

width found in wild type (Fig. 3-11E and F). From previous studies, the disorganized dendritic cap has been always discovered in the IFT mutants that keep shortened or missing cilia, but it is not clear whether it is due to the defective axonemal structure or simply due to the short cilia which do not make a contact to the dendritic cap.

To see the contour of dendritic cap in *btv*, I utilized DIC microscopy and a genetic manipulation with NOMPA tagged by GFP. The DIC image illustrates that the dendritic cap in *btv* is not disordered, being indiscernible from the wild type (Fig. 3-11A and B). In *btv*, the normal double arrow shape of a dendritic cap, scolopale cells, and the full length of cilia are still present without ciliary dilations (Fig. 3-11A and B). The DIC image of *btv* presents missing ciliary dilation (Fig. 3-11B). Besides, the 21A6 delocalized in *btv* antennal chordotonal cilia, supporting that 21A6 might be related to ciliary structure (Fig. 3-11D). Figure 3-11D displays the untruncated cilia of *btv*. The well organized NOMPA localization pattern proves that *btv* doesn't have a defect in the formation of dendritic caps (Fig. 3-11G and H). These data strongly suggest that *btv* has full length cilia though it has a structural defect of cilia and is missing ciliary dilation. Also, this implies that the dendritic cap formation might be related to the length of cilia not to the axonemal structure of cilia. Taken together with delocalization of REMP in *btv*, BTV might function as a retrograde motor as well as contain an unknown regulatory function for the proper localization of functional molecules on mechanosensory cilia.

Second, the newly visualized part of cilia by NOMPB and REMPA in *btv* requires further exploration to determine if it is involved in the mechanosensory transduction or what molecules it reside in. The IFT particles accumulated on the tips of *btv* cilia near the cuticle which suggest a necessity to reconsider the functional anatomy of cilia. Conventionally, the outer segment of a cilium has been referred to from the base

to the tip which is the end of the microtubule doublet. This tip has been thought to be physically connected to a dendritic cap, through which the mechanical stimulus is delivered to activate channels by stretching a cilium. The distal portion of the microtubule doublet is made of a singlet microtubule which is connected to the cuticle. The distal part to the dendritic cap visualized by the delocalized IFT particles is unable to be envisioned by tagged IFT molecules in wild type. In *btv* mutants, however, this region is revealed and raises a couple of questions: do IFT particles move to reach this district, and are any other channel subunits localizing here? How functionally different the singlet microtubule is from the doublet and how differently they contribute to the *Drosophila* mechanosensory transduction?

Third, the accumulation of IFT molecules on *btv* ciliary tips suggests that BTV functions as a retrograde motor. If BTV acts as a retrograde motor in *Drosophila* cilia, not only IFT-A particles but also IFT-B particles would be transported by BTV from tip to base. The similar delocalization pattern of NOMP-B and REMPA in *btv* chordotonal cilia confirms that BTV might be implicated in the transporting of the IFT complex from the tip back to the base of cilia, suggesting that BTV is not necessary for the stability of the IFT complex nor the formation. It has been reported that a ciliary dilation is disrupted in *btv* chordotonal organ (Eberl et al., 2000). The findings of disrupted ciliary dilation and dispersed REMPA localization generate an interesting hypothesis that the retrograde motor might be involved in the formation of a ciliary dilation by the regulatory contribution to REMPA localization. The different pattern of REMPA in *oseg1* and *btv* mutants strongly supports that IFT-A particles behave quite differently from the conventional consideration on the retrograde motor: IFT-A molecules might be dispensable for the stability of each other, supposedly functionally form a ciliary dilation,

while *btv* does influence the motility or positioning of IFT molecules but not the stability of IFT-A particles for performance.

More interestingly, the failure of BTV affects REMPA localization in ES organs as well. *btv* flies have a sedentary behavior, which is different from an uncoordinated IFT-A mutant behavior, *rempA* and *oseg1*, suggesting that they might have a defect only on chordotonal cilia but not on ES cilia. This leads to a hypothesis that BTV is functioning in a chordotonal organ not in an ES organ, and this is able to be accessed by an examination of REMPA localization in ES cilia. For this, abdominal bristle cilia and campaniform sensilla of *btv* flies were investigated. Surprisingly, REMPA which originally positioned on the lower level of outer segment of sensilla was found to reach up to the outmost end where usually NOMPA is found (Fig. 3-9A-F). This was confirmed by a rod form labeled by REMPA, like NOMPA staining (Fig. 3-9A). It displays the straightforward delocalization of REMPA to the apical surface in *btv* campaniform sensilla (Fig. 3-9B). In an abdominal bristle, REMPA also extended to the NOMPA staining region of tubular body (Fig. 3-9C-F), which is different from the differential occupancy of REMPA and NOMPA found in wild type (Fig. 3-6C and F).

The delocalization pattern of REMPA in *btv* CHO and ES organs is similar in that the REMPA scattered along the cilia escaping out of the original localization spot. The delocalization and accumulation of REMPA in *btv* suggests that BTV might be involved in retrograde transporting in ES organs as well. However, this should be confirmed by the electrophysiological measurement like the bristle recording. The function of BTV in ES organs should not be limited to the retrograde motor. The altered labeling of REMPA in *btv* ES cilia raises a few questions like how the delocalized REMPA can account for the sedentary behavior (Eberl et al., 2000), where is the turnover

point of the axonemal structure on ES cilia, and other than a retrograde motor, are there additional functions of BTV in ES cilia. Besides, a subtle defect of *bTV* MRP unable to be detected in current technology or an indiscernible behavior should not be ruled out.

REMPA localization in kinesin mutants

Kinesin II has been identified to be an anterograde motor for IFT by the study of *Chlamydomonas* temperature sensitive mutant, *fla10* (Cole et al., 1998). *Drosophila* Kinesin II is composed of three subunits, Klp64D, Klp68D and DmKap. A *klp64D* mutant fly has missing cilia and Klp64D is required for the sound evoked response (Sarpal et al., 2003). NOMP-B, one of IFT-B molecules accumulates on the base of cilia in *Klp64D*^{*kl/n123*} null mutant (Han et al., 2003). Interestingly, *klp64D*^{*k5/14*}, the weakest hypomorph, contains a complete length of cilia and responds to pulse sound in slightly reduced fashion than severe alleles. Moreover, it keeps the deformed ciliary dilation positioning further toward the dendritic cap (Sarpal et al., 2003). Though a ciliary dilation in *Klp64D*^{*k5/14*} allele is deformed and out of the original position, EM still shows bulky silhouette which is reminiscent of a ciliary dilation (Sarpal et al., 2003). I asked whether REMPA accumulates on the ciliary base in the null mutant, like NOMP-B and where REMPA localize in the *Klp64D*^{*k5/14*} hypomorph which has a reduced ciliary dilation.

To determine this, I examined localization of REMPA in *Klp64D*^{*k5/14*} and *Klp64D*^{*kl/n123*} by double staining with phalloidin (Fig. 3-12E-H). Interestingly, REMPA localizes on a deformed and mislocalized ciliary dilation inside a dendritic cap of *Klp64D*^{*k5/14*}. Phalloidin staining, which marks the whole shape of a scolopale cell, clearly revealed REMPA localization on the tip of cilia (Fig. 3-12F). The DIC image describes a narrow and elongated dendritic cap shape of *Klp64D*^{*k5/14*} compared to the wild type and

REMPA locates on the bulky structure near the ciliary tip often inside the dendritic cap (Fig. 3-12A-D). It was hard to find the bulky structure in DIC images of *Klp64D^{k5/14}*, because it seemed to be embedded inside the dendritic cap. This is strong evidence that REMPA is a structural component of a ciliary dilation, considering that REMPA signal was not detected in *oseg1* chordotonal cilia (Fig. 3-8) and delocalized in *btv* where ciliary dilations are disrupted (Fig. 3-9). This finding in hypomorphic *kinesin II* also highlights the Kinesin II protein as an anterograde motor as well as BTV as a retrograde motor in that the less transported BTV due to the less amount of KinesinII proteins allows a ciliary dilation to apically misplace inside a dendritic cap. It is not known how, but it is clear that kinesinII and BTV might be involved in the regulation of the positioning and organized formation of a ciliary dilation. In a *kinesinII* null mutant, REMPA accumulated on the base of cilia, but this was very dim compared to NOMP B accumulation (Han et al., 2003). This implicates that REMPA might be unstable on an inappropriate position.

REMPA and NOMP B were not detected in dyf-1

As previously explained in Chapter 1, nematode cilia have two kinesin motors, kinesin II and *osm-3*, which work together for anterograde transporting from base to tip of cilia (Fig. 1-2). *Osm-3* has been proposed to be connected to IFT-A subcomplex through DYF-1 protein (Ou et al., 2005). Thus, *C. elegans dyf-1* has the distal segment missed, because it loses OSM-3 with the lack of DYF-1. As the functional involvement of DYF-1 in the distal segment of nematode cilia provides a good marker to compare two ciliary modulation systems of a nematode and a fly, I examined localization of REMPA and NOMP B as well as a ciliary morphology in *dyf-1*. A *dyf-1* deletion fly has been generated using the FLP-FRT recombination technique (Parks et al., 2004) by Nan Wang

and Dr. Kernan in the lab (unpublished data). *dyf-1* flies are uncoordinated and have no auditory response (unpublished data). Interestingly, RFP expression in sensory neurons shows that *dyf-1* has completely missing cilia like *nompB* or *kinesin II* null mutants (Fig. 3-13A and B). Scolopale cells looks normal but dendritic caps are severely disorganized (Fig. 3-13 C and D). More interestingly, REMPA and NOMPB were not detected in *dyf-1* (Fig. 3-13 E-H). The absence of NOMPB is dissimilar from accumulated NOMPB at the tip of an inner segment in *kinesin II* mutant (Han et al., 2003), suggesting that DYF-1 contributes to the stability of IFT complex as a member of IFT-A components. Similarly, 21A6 also delocalized to the basal part as found in other mechanosensory mutants which have a morphological defect on cilia (Fig. 3-13E and F), supporting the hypothesis that 21A6 might be interconnected to the ciliary structure.

BBS-8 might not be involved in mechanosensory function in Drosophila.

BBS8 and BBS7 have been suggested to be involved in the coupling of IFT-A and IFT-B subcomplex in *C. elegans* (Snow et al., 2004). BBS7 is not conserved in *Drosophila*. To examine whether the transporting mechanism including BBS proteins proposed in nematode also fits in *Drosophila* mechanosensory cilia, I generated *BBS8* deletion mutant. I will explain how I generated the *BBS8* deletion mutant in the following chapter.

As a result, BBS mutation in fly mechanosensory cilia shows quite different phenotype than in nematode in several aspects. First, a *BBS8* fly mutant looks to normally behave. If the function of BBS8 proteins is involved in mechanosensory cilia, mutant flies should show either uncoordinated or sedentary behavior, like mechanosensory mutants of *Drosophila*.

Second, BBS8 ciliary morphology is normal (Fig. 3-14A and B). *C. elegans* *BBS8* mutants have truncated cilia, but the expression of RFP in *BBS8* flies delineates the complete set of cilia including an outer segment and an inner segment. This different morphology in flies and nematodes is compatible with each behavior profile. Moreover, the whole structure of *BBS8* chordotonal organ including a ciliary dilation, ciliary compartments, cap cells, and scolopale cells appears normal with DIC image (Fig. 3-14C and D).

Ciliary configuration and behavior pattern of *BBS8* flies do not give any indications for its involvement in mechanosensory function. If BBS8 functions to couple two subcomplexes in *Drosophila* mechanosensory cilia like in nematodes, REMPA might be either mislocalized or be destabilized to degrade on the base of cilia whereas NOMP B might be localizing along the cilia and accumulating on the tip of cilia. To test this, REMPA localization was examined in *BBS8* (Fig. 3-14E-F). It resulted in the normal localization both of REMPA on a ciliary dilation in *BBS8* mutants as in wild type (Fig. 3-14E-F). Third, the sound-evoked response in *BBS8* antennae is not distinguished from wild type, which I will present in the chapter 4.2. Taken together, the coupling function of BBS8 protein proposed in nematode is not conserved in *Drosophila*. It is, rather, not selectively involved in mechanosensory function in *Drosophila* sensory cilia.

IAV is delocalized in *btv* and absent in *rempA*

The auditory transduction is mediated by two TRPV channel subunits, IAV and NAN, in Johnston's organs of a *Drosophila* antenna (Gong et al., 2004). Interestingly, NAN and IAV colocalize on the cilia proximal to the ciliary dilation (Gong et al., 2004). I found that REMPA specifically localizes on ciliary dilation in my dissertation study,

and proposed that a ciliary dilation might be a supercomplex of IFT-A components based on the finding, the abnormal delocalization of REMPA in *oseg1* and *btv*. To know the function of a ciliary dilation for localizing of TRPV channel subunits on the proximal cilia, IAV localization was examined in *rempA* which has shortened cilia and *btv* which lacks the ciliary dilation. Interestingly, IAV was not detected in *rempA* mutants (Fig. 3-15A and B), which is different from the accumulation of NOMP-B at the tip of *rempA* truncated cilia (Fig. 2-4C-F). It suggests that REMPA serves to stabilize the IFT subcomplex including cargo or the ciliary dilation does an important function for the stable localization of TRPV channel subunits. In a *btv* mutant, IAV delocalizes along the cilia, leaking beyond the ciliary dilation with scattered accumulation at the base of cilia. This suggests that the ciliary dilation do functionally partition the ciliary outer segment into two distinct compartments, the proximal and the distal. Taken together, the ciliary dilation is required for the proper localization of TRPV proteins and it might be a sorting station for functional compartment of chordotonal cilia. However, to investigate the function of REMPA on the ciliary dilation, I need to analyze the protein domain of REMPA as well as an interacting mechanism between IFT and cargos, which all remain to be answered.

[Figure 3-1] The localization of REMPA is developmentally differential on chordotonal cilia.

(A-C) REMPA shows developmentally differential localization pattern on antennal chordotonal cilia. In early stage when cilia are differentiating, REMPA localizes on cilia as well as cytoplasm (A, arrows). In the middle of ciliary differentiation, REMPA in cytoplasm moves to ciliary region (B, arrow), and finally concentrates on ciliary dilation after cilia are completely formed (C, arrow). (yellow, REMPA; red, phalloidin-Alexa568)

(D-F) The differential localization pattern of REMPA on ciliary development is also observed in an embryonic development. At the 15 stage, cilia are short, and REMPA is found on the cytoplasm and along the short cilia (D, arrows). At stage 16, most REMPA signal is found on growing cilia (E, arrows), and eventually converged into the ciliary dilation at stage 17 (F, arrows). 21A6 stains distinguished region from REMPA marking spot. Eys appears to embrace the cilia at the proximal level of cilia not beyond the ciliary dilation. Based on the REMPA localization on ciliary dilation in embryos, ciliary differentiation is most likely completed at stage 17. (yellow, REMPA; blue, 21A6)

(G-H) In adult chordotonal cilia, REMPA labeling is distinguished from 21A6 staining. In the early stage of antennal chordotonal cilia, REMPA also localizes along the cilia and on the cytoplasm (G) and Eys looks to cover each cilium in a scolopale cell (G, arrows). Eys locates on the proximal region of the ciliary dilation in differentiated cilia, particularly not on cilia, but in scolopale cells (H, arrowheads). In femoral chordotonal cilia, the regional discrepancy occupied by REMPA and Eys is evident that Eys localizes proximally apart from REMPA labeling spot (arrow) and the scolopale rod shape is detected by 21A6 staining (I, arrowhead). (yellow, REMPA; red, phalloidin; blue, 21A6)

(J) Two foci (circle) labeled by REMPA are found in one scolopale cell stained by

phalloidin in femoral chordotonal organ. (yellow, REMPA; red, phalloidin-Alexa568)

(K) Ciliary neurons were visualized by filling with RFP driven by *elav* promoter.

Costaining with 21A6 illustrates that Eys does not localize on the cilia. Eys seems to position inside a scolopale cell, wrapping a proximal region of cilia (arrows). It also locates around the base of cilia.

(L) REMPA does not overlap with NOMPA on antennal chordotonal cilia. (yellow, REMPA; red NOMPA) An arrowhead indicates gaps between NOMPA labeling region and REMPA localizing area (arrows).

Scale bar: 8 μm .

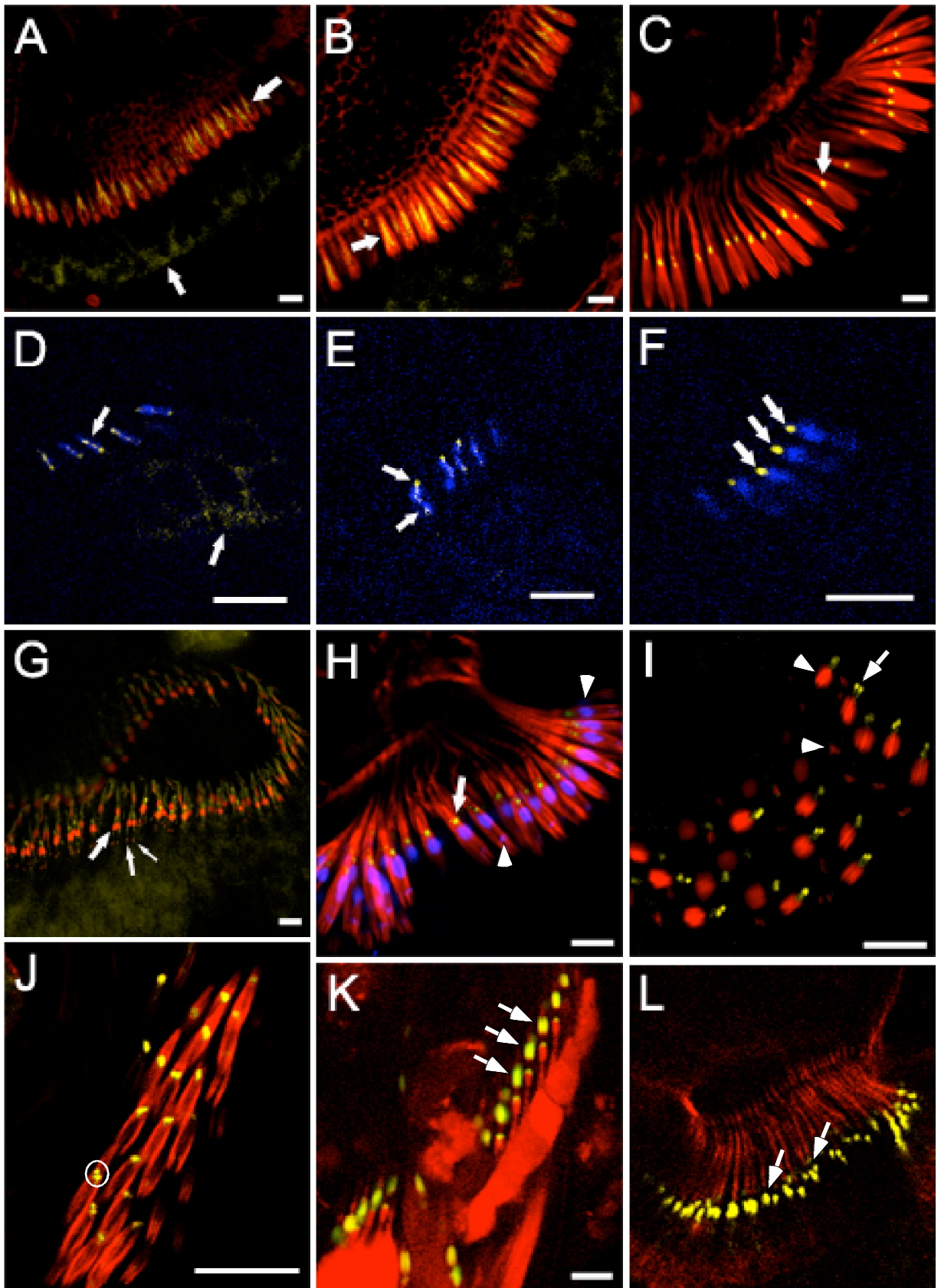


[Figure 3-2] REMPA localizes on ciliary dilations of chordotonal cilia.

The observation of the first instar larvae and embryos under confocal microscopy combined with DIC identifies the localization of REMPA on a ciliary dilation of chordotonal cilia. Scale bar: 8 μm .

(A-C) DIC image (A) shows larval lateral chordotonal neurons ensheathed by scolopale cells and distally connected to cap cells. Inside a scolopale cell, a dendritic cilium is visible (A, arrow). The bulky structure inside the scolopale cells is the ciliary dilation (arrowheads). REMPA labeling points a specific spot (B, arrowheads). REMPA signal was present on a round-shape structure of chordotonal cilia near a cap cell in a merged image (C, arrowheads).

(D-F) The DIC image for embryonic stage 17 illustrates the anatomical structure of chordotonal cilia including cap proteins (arrows), scolopale cells, and ciliary dilation (arrowheads) (D). The triangle shape at the end of cilia is cap cell (arrows) and a small bulky structure near the cap cell is a ciliary dilation (D, arrowheads). Consistently, REMPA (B, REMPA only) is found specifically on ciliary dilation of chordotonal cilia in embryos (F, merged, arrowheads).

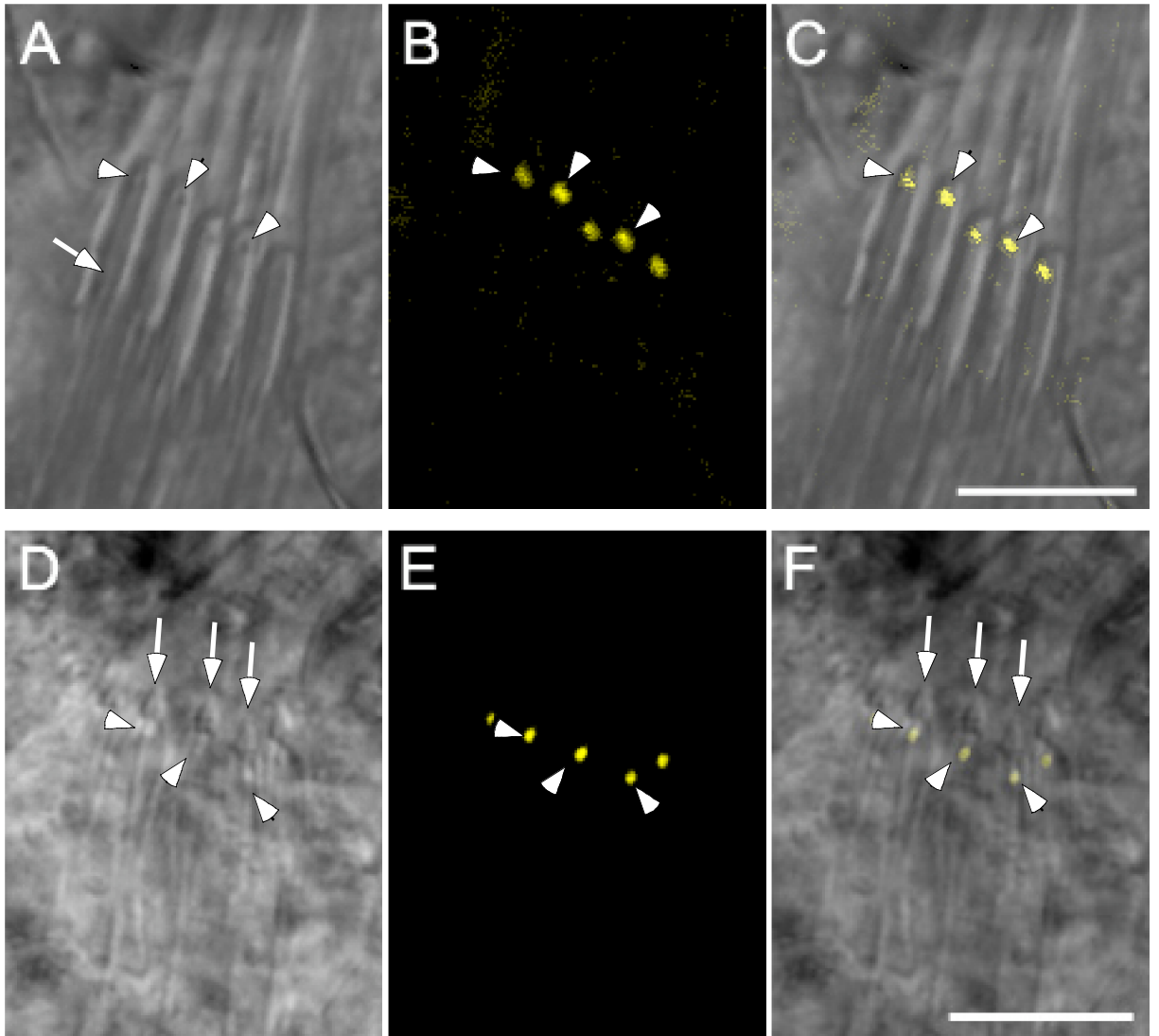


[Figure 3-3] The localization of REMPA and Eys is not affected by the alternation of IAV but by the mutation of IFT components.

Iav, one of TRVP channel subunits contributing to transduce the auditory stimulus in Johnston's organ, does not affect the localization and stability of REMPA. Scale bar: 8 μm .

(A-C) phalloidin staining apparently shows no morphological defect on *iav* scolopale cells and REMPA (arrows) localizes on *iav* ciliary dilations normally as observed in wild type (A). 21A6 also normally labels on both *iav* antennal chordotonal (B) and femoral chordotonal cilia (C, arrowheads). (yellow, REMPA; red, phalloidin; blue, 21A6)

(D and E) femoral chordotonal cilia of *rempA*^{+/-} (D) and *rempA*^{-/-} (E) stained by 21A6.

While Eys is detected on the proximal region to a ciliary dilation in scolopale cells of the wild type (D, arrowheads), it mislocalizes around the ciliary base from near ciliary dilation in *rempA*^{-/-} (E, arrowheads).

(F and G) femoral chordotonal cilia of *osegI*^{+/-} (F) and *osegI*^{-/-} (G) stained by 21A6 and phalloidin. Similarly, Eys-labeling in *osegI* shows mislocalization to the base of cilia in scolopale cells (G, arrowheads), being different from wild type (F, arrowheads). (blue, 21A6; red, phalloidin)

(H and I) 21A6 labeling in antennal chordotonal cilia of *btv*^{+/-} (H) and *btv*^{-/-} (I) stained by phalloidin. Like in other IFT components involved in ciliogenesis, Eys mislocalized to the base of cilia (arrowhead). (yellow, REMPA; blue, 21A6)

(J-L) schematic of 21A6-labeling in mechanosensory mutants. In wild type, Eys locates inside scolopale at the proximal region to a ciliary dilation. Eys is also detected on the base area of cilia (J). The chordotonal cilia of *iav* having a normal morphology do not affect the localization of Eys, suggesting that Eys localization is activity-independent (K).

The 21A6 labeling pattern in *iav* chordotonal cilia is not different from in wild type as shown in (D), (F), and (H). Notably, *rempA*, *oseg1*, and *btv* which all have defects in ciliary configuration show mislocalized Eys in chordotonal cilia. They all mislocalized around the base near the inner segment of cilia in scolopale cells.

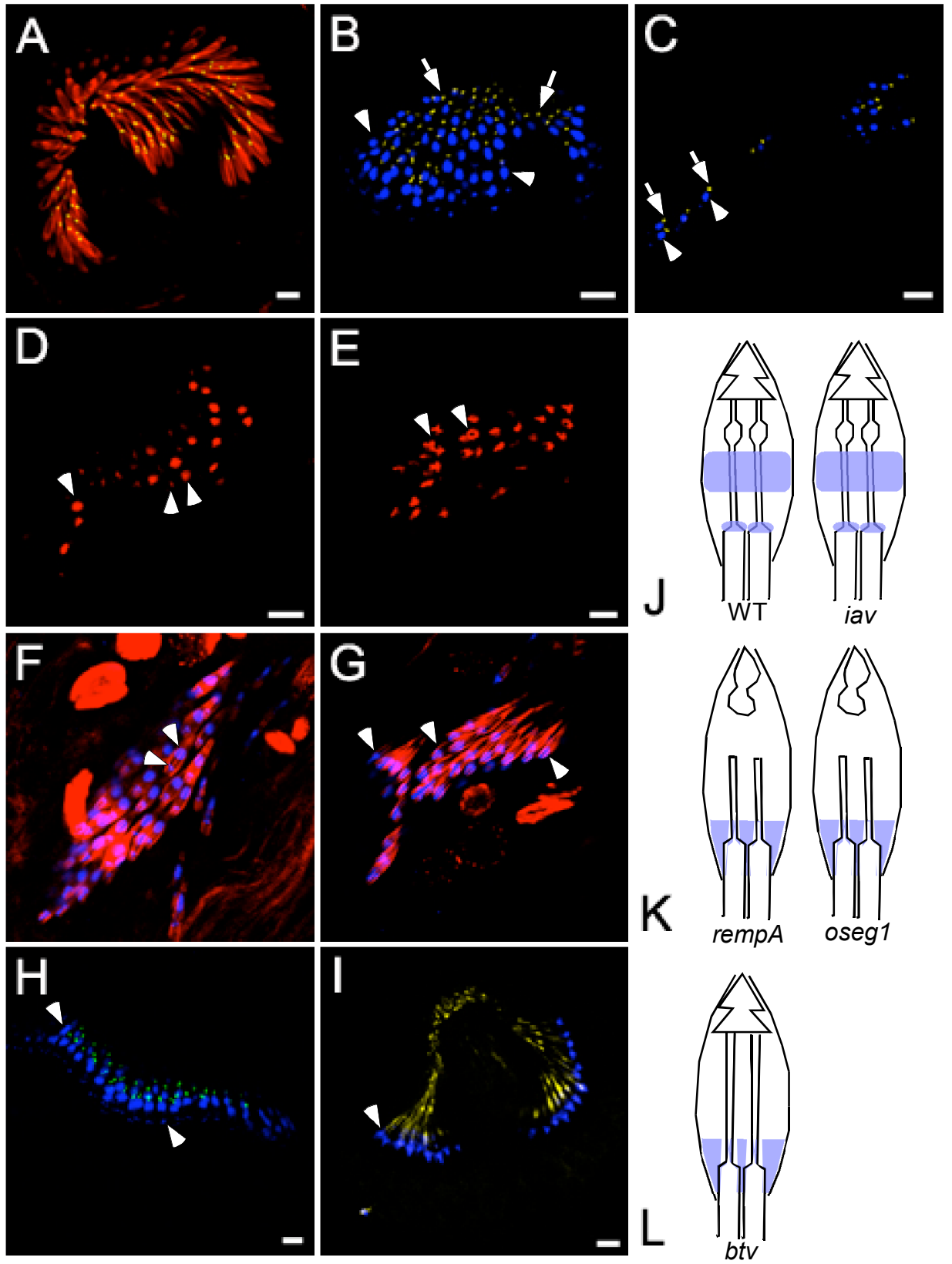


[Figure 3-4] The localization pattern of NOMPB on development.

NOMPB was reported to localize along the cilia. To compare with a REMPA labeling pattern, NOMPB labeling pattern was examined on development of chordotonal cilia. NOMPB also has a differential localization pattern like REMPA though it is not perfectly same. Scale bar: 8 μm .

(A-C) In early stage, NOMPB appears along short cilia (A, arrow), and it concentrates along the cilia as the cilia differentiate (B, arrows). In the late stage, NOMPB is found to amass around a ciliary dilation and is partly localized on the base of cilia (C, arrows). (green, NOMPB; red, 22C10)

(D and E) NOMPB localization was examined using the counterstaining with 21A6, because the 21A6 labeling region on chordotonal cilia had already been determined by double labeling with REMPA. The box in (D) was magnified to (E). NOMPB labels around ciliary dilations and NOMPB locates distal to the area labeled by 21A6 (arrowhead). NOMPB is weakly detected also distally to the ciliary dilation (E, arrow) as well as the base of cilia (D, arrow). (green, NOMPB; red, 21A6)

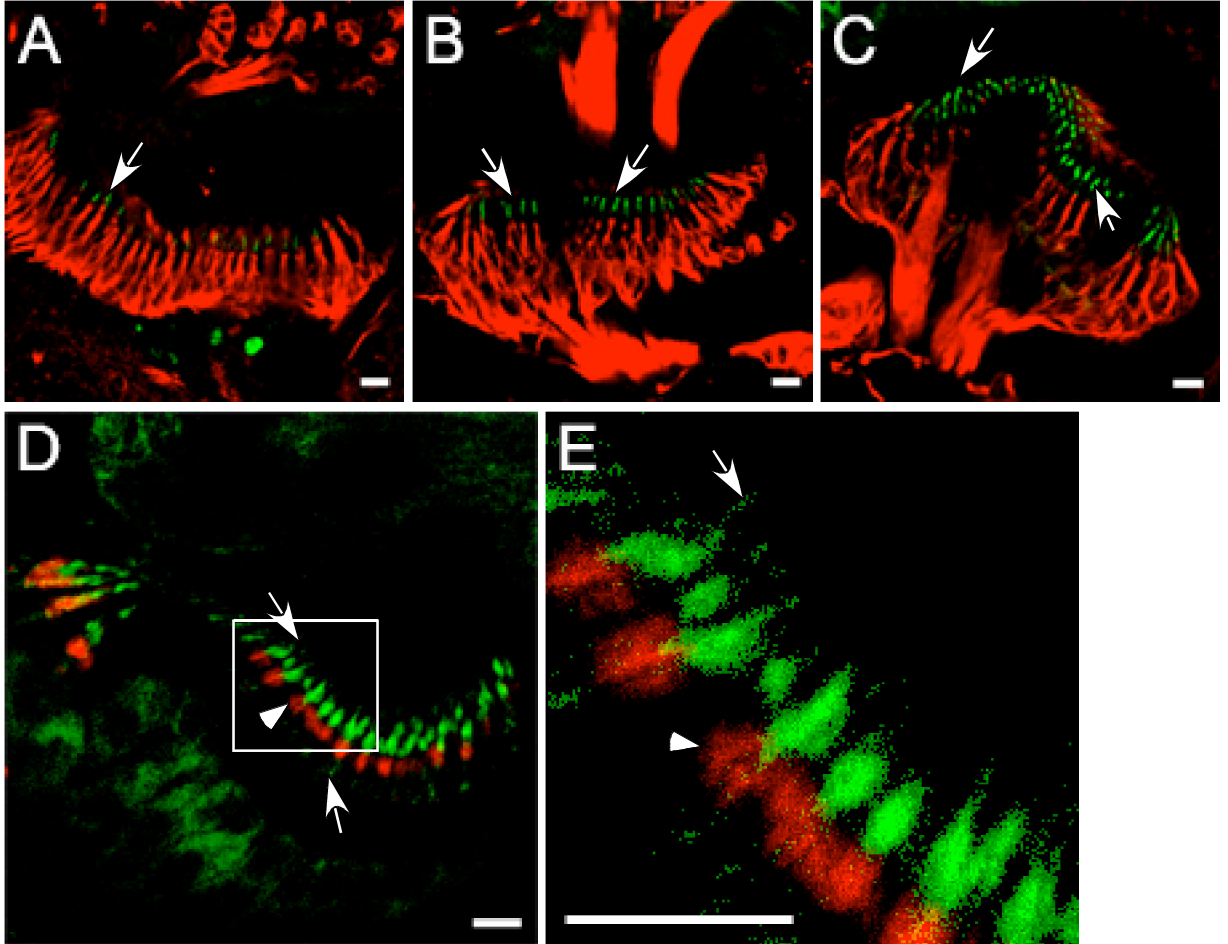


[Figure 3-5] REMPA localizes apart from bristle base in es organs.

REMPA labeling was examined in abdominal bristle organs at late pupal stage by DIC and confocal microscopy. The signal is very weak but distinguished. Scale bar: 8 μ m.

(A-D) DIC images display that REMPA (arrows) is apart from bristle bases, indicating that it does not locate on the most distal region, a tubular body.

(E and F) Confocal microscopy also displays that REMPA (arrows) does not contact a bristle base in a socket. REMPA localization in es cilia appears on a specific spot.

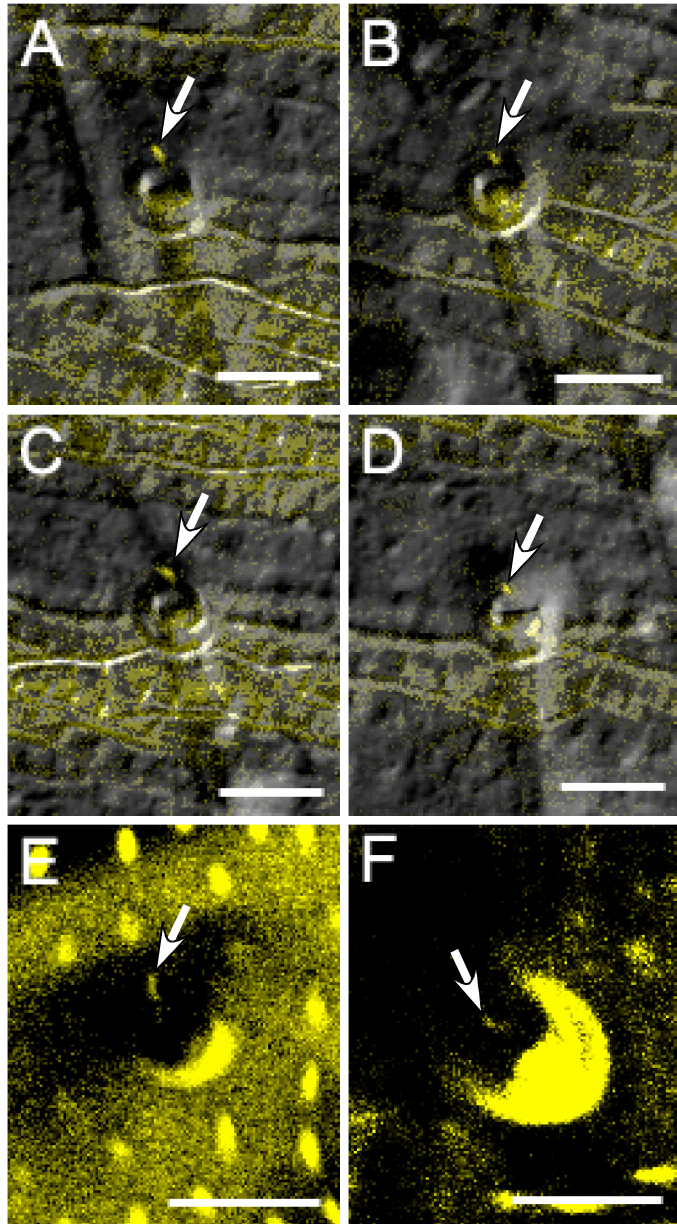


[Figure 3-6] REMPA localizes on a connecting cilium in es organs.

To know where REMPA localizes in abdominal es organs, a pupal abdomen was isolated and stained with antibodies both against NOMPA and against Eys. NOMPA is a component of the dendritic cap which covers a tubular body in es organs. 21A6 is mAb against Eys and found to proximally label next to NOMPA in a previous study. Scale bar: 8 μ m.

(A -F) To determine the detected signal is false positive or not, wild type without *P{REMPA-YFP}* transgene was examined (A and D) by staining with NOMPA. Only NOMPA signal was detected (A and D, arrows). To define REMPA labeling region, es organs were double stained with NOMPA antibody (C and F, red, arrows). (B) and (E) show REMPA only labeling (arrowheads), and (C) and (F) show merged pictures with NOMPA staining respectively (arrows). REMPA (B, C, E, and F, arrowheads) labels a distinct region from a NOMPA-stained dendritic cap contacting a bristle base. (red, NOMPA; yellow or green, REMPA)

(G-J) Abdominal bristle cilia of REMPA transgenic flies are stained with 21A6. (H) and (J) are merged pictures with 21A6 staining from single labeled (G) and (I) respectively (arrows). REMPA labeling is exactly matched with 21A6 staining (arrows), and 21A6 occupancy appears a bit larger than REMPA labeling area.

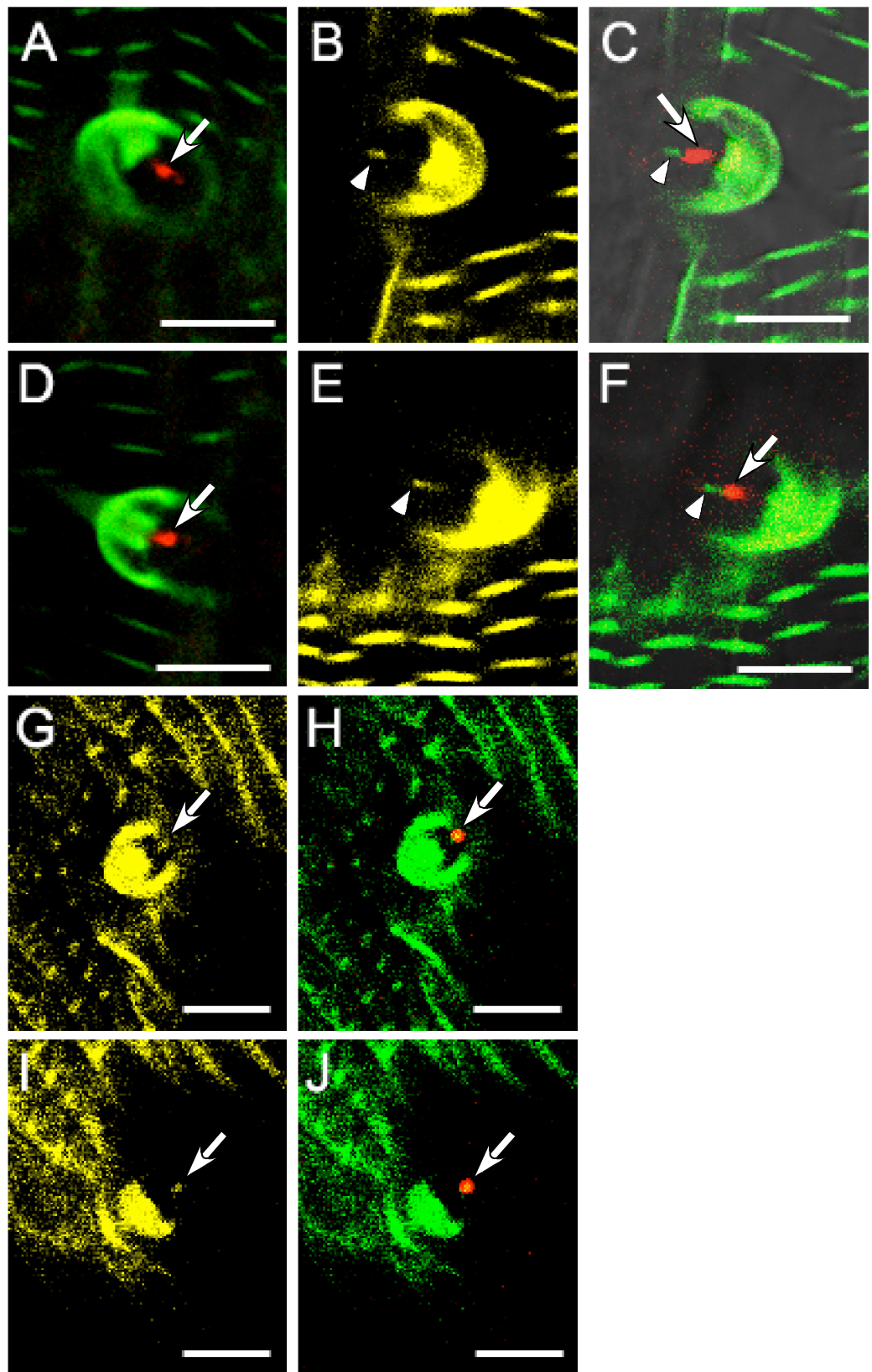


[Figure 3-7] REMPA localizes on the connecting cilium of campaniform sensilla.

Campaniform sensilla have differential morphological shapes of a ciliary outer segment to the level. The most distal level of cilia where a dendritic cap protein is detected has a rod shape, and the proximal level of cilia corresponding to the connecting cilium has a round shape. Thus, the staining pattern could provide a key to define the localization on cilia. Scale bar: 8 μm .

(A and C) the labeling pattern of REMPA displays a round form, representing that REMPA localizes on a connecting cilium. (A) shows REMPA only (arrowhead), and (C) shows double labeling with 21A6 antigen (arrow), which meets an agreement with the overlapped labeling pattern of REMPA and 21A6 discovered in abdominal es cilia in [Figure 3-2G-J]. (yellow, REMPA; red, NOMPA)

(B) The localization of REMPA in campaniform sensilla from a side view presents a gap (arrows) between REMPA labeling spot and the outmost surface, indicating that REMPA labels a connecting cilium not contacting the outmost surface of sensilla.

(D and E) NOMP B, one of anterograde components, is also detected on a connecting cilium in campaniform sensilla by consistently showing a round form of labeling (D, arrowheads). The observation from the side also displays a similar localization pattern to REMPA on a connecting cilium with no contact (arrows) to the most distal surface of cilia.

(F) Different from the REMPA and NOMP B localization of a round shape, NOMPA distinctively displays a rod shape staining, approving that NOMPA localizes on the outmost region of cilia.

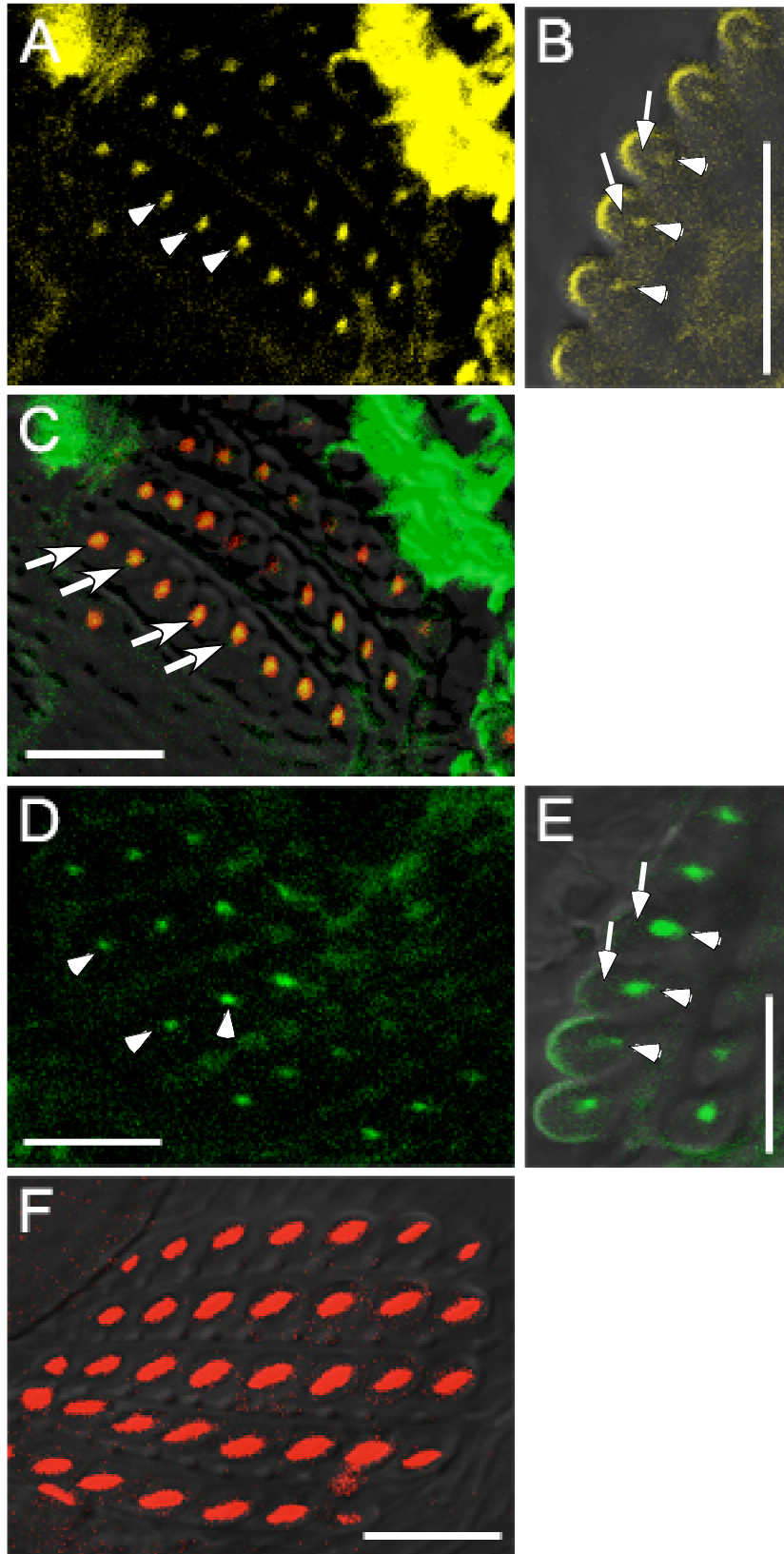


[Figure 3-8] REMPA is not detected in *oseg1* both at early and late stages

IFT-A subcomplex is composed of REMPA/IFT140 and OSEG1/IFT122. To know each protein is required for the formation and stability of the IFT-A complex, REMPA localization was examined in *oseg1* with counterstaining with 22C10 (red) and Alexa-568 conjugated Phalloidin (blue). Scale bar: 8 μ m.

(A and B) REMPA (yellow) labels along the differentiating chordotonal cilia in the wild type (A, arrow), but it is not detected in *oseg1* (B) at the same stage.

(C and D) Consistently, after the chordotonal cilia complete differentiation, REMPA (yellow) was not detected in *oseg1* (D) at a late stage while detected in wild type (C, arrow).

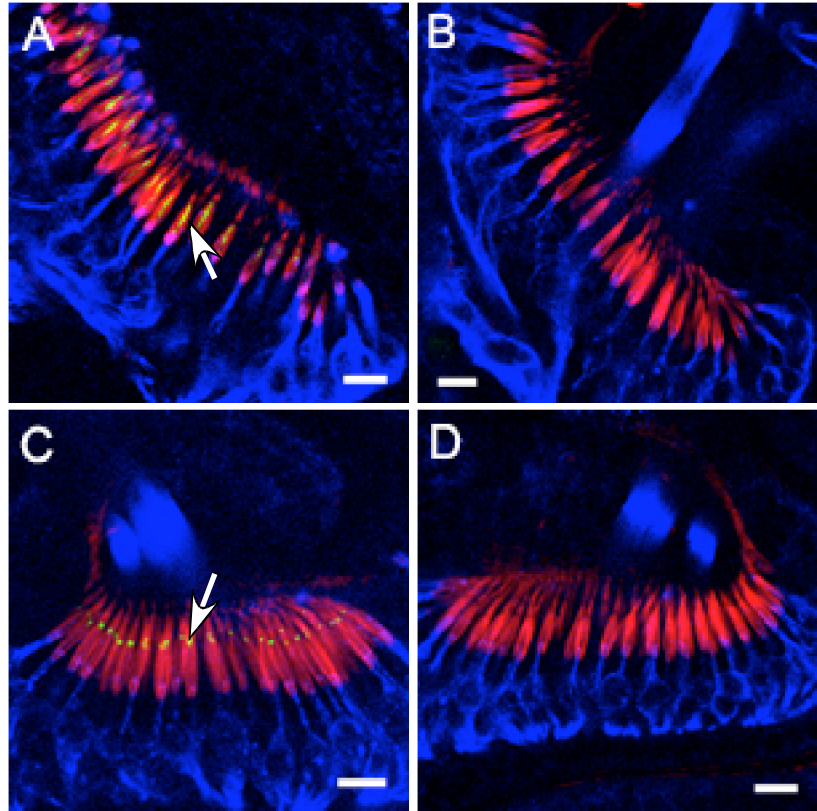


[Figure 3-9] REMPA is delocalized in *b1v* es and chordotonal organs.

(A and B) REMPA labeling (A, arrows) in campaniform sensilla of a *b1v* haltere displays as a rod form as shown in NOMPA staining (Fig 3-3F), but not normal round shape observed in (Fig 3-3A). The side view (B) illustrates that REMPA stretched to the apical surface where NOMPA positions (B, arrows). This is dissimilar from that in wild type background (Fig 3-3B). (yellow, REMPA) Scale bar: 8 μ m.

(C-F) In *b1v* abdominal bristles, the REMPA (arrows) localization pattern is similar to that observed in the campaniform sensilla. (C) and (E) are REMPA only labeled, and (D) and (F) are double labeled with NOMPA. REMPA extended out to the apical surface to contact a bristle base, so they overlapped with NOMPA staining region (arrowheads), which is different from its normal localization which is proximal to NOMPA labeling area. (yellow, REMPA; green, REMPA; red, NOMPA)

(G-J) REMPA delocalizes in *b1v* antennal chordotonal cilia (I and J) compared to in wild type (G and H). It extends out to cuticle beyond the cap protein and accumulates at a tip (I and J, arrowheads). (G) and (I) were double stained to (H) and (J) respectively with phalloidin. Phalloidin staining defines the position labeled by REMPA (G and H) and describes to what extend the REMPA is dispersed in *b1v* chordotonal cilia (I and J). (yellow, REMPA; blue, phalloidin)

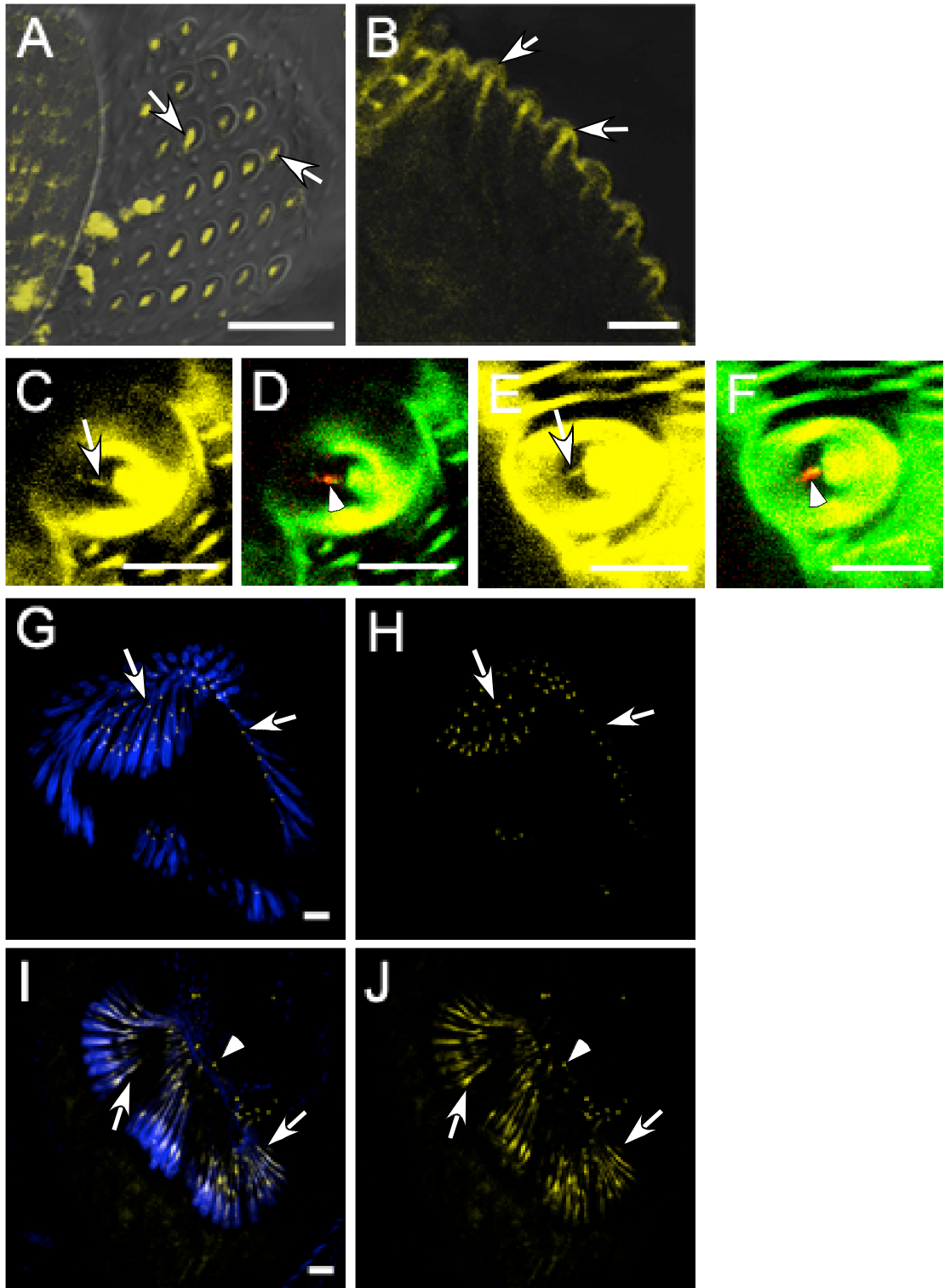


[Figure 3-10] NOMPB is delocalized in *btv* CHO.

NOMPB was examined in *btv* to see whether IFT-B proteins are delocalized like REMPA protein. Samples were double-labeled with Alexa-568 conjugated phalloidin (yellow, REMPA; red, phalloidin). Scale bar: 8 μ m. (green, NOMPB; red, phalloidin)

(A-D) The antennal chordotonal cilia of NOMPBGFP transgenic flies combined with *btv* were examined. The wild type (A) shows a normal localization pattern of NOMPB (arrows) as previously observed in other heterozygous cilia. (C) presents the highly magnified cartoon of NOMPB localization in (A). NOMPB localizes along the cilia with accumulating around a ciliary dilation (A and C, arrows). In contrast, in *btv* (B), NOMPB localizes along the cilia in an irregular pattern showing more dispersed without concentratin around a ciliary dilation (D, arrows). Instead, NOMPB in *btv* shows an accumulation at the apical tip of the cilia near the cuticle (B and D, arrows), more likely observed as REMPA in *btv*.

(E and F) The femoral chordotonal cilia in *btv* show a similar localization pattern of NOMPB as detected in antennal chordotonal cilia. The wild type cilia show a normal labeling pattern of NOMPB (E, arrows), but the *btv* cilia show more irregular and thick accumulation of NOMPB at the tip of cilia (F, arrow).

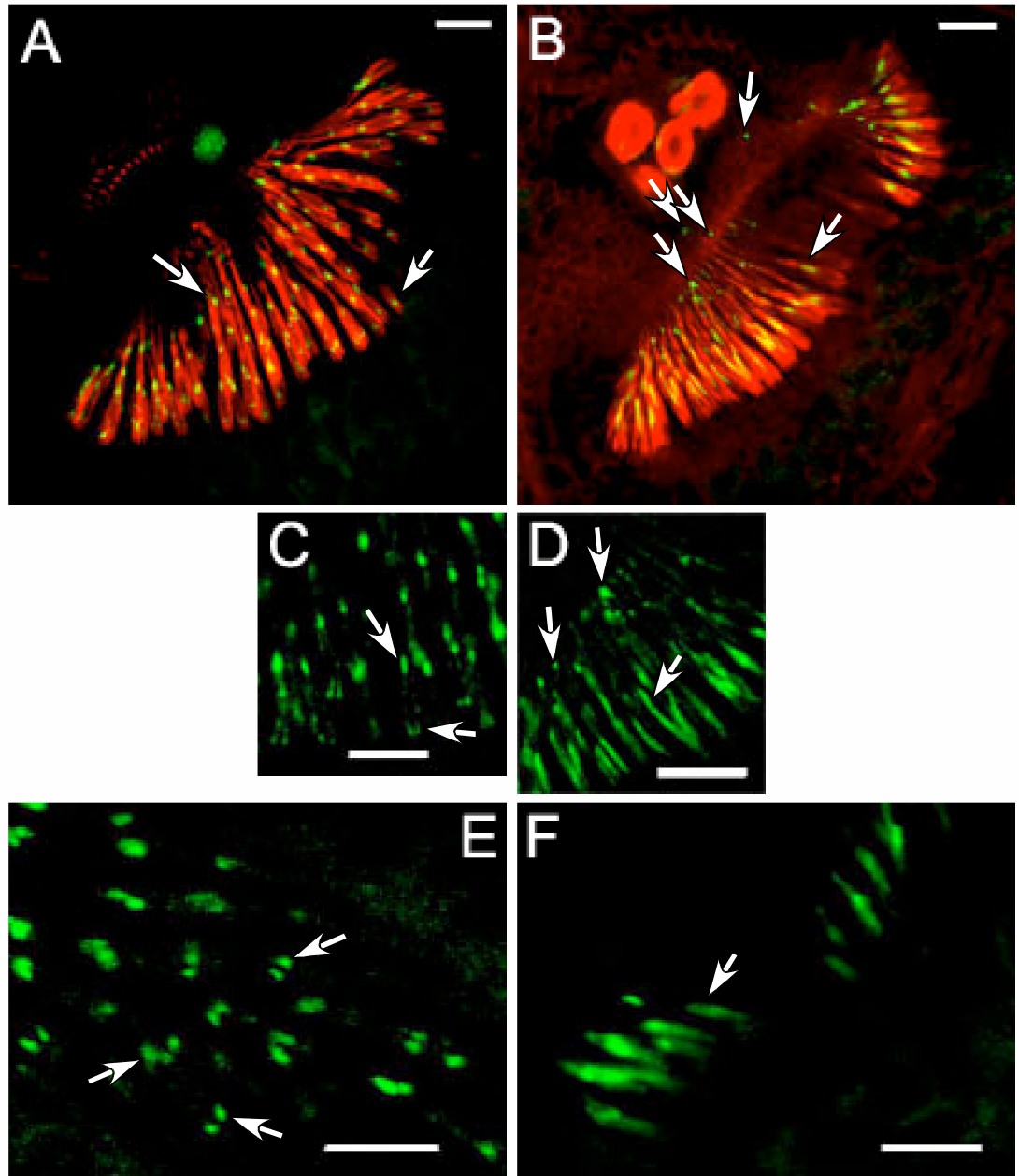


[Figure 3-11] The *b₁* chordotonal cilia are not truncated and the organization of NOMPA in *b₁* looks normal.

To know the *b₁* chordotonal cilia are not truncated, RFP-filled mechanosensory neurons were observed under confocal microscopy and the morphological organization of NOMPA and a dendritic cap protein, was examined in *b₁*. Scale bar: 8 μ m.

(A and B) DIC image illustrates the whole structure of chordotonal organs composed of two cilia innervated in one scolopale cell, and double arrowhead-shaped dendritic cap. Wild type shows ciliary dilations (black arrows) near the dendritic cap which are surrounded by a scolopale cell (A, arrowhead). In *b₁*, a ciliary dilation is missing (B) and cilia surrounded by a scolopale cell (B, arrowhead) were observed. Notably, *b₁* chordotonal cilia are not truncated (B) but look thick (black arrowheads). Double arrowhead shape of a dendritic cap looks normal (B, white arrowhead).

(C and D) *elav*-driven RFP filling doesn't detect shortened cilia in *b₁* (D) compared to wild type (C). 21A6 staining is normal in wild type (C, arrow), but a delocalized pattern is observed in *b₁* antennal chordotonal organs (D, arrows).

(E and F) Femoral chordotonal organs visualized by RFP are indistinguishable between wild type (E) and *b₁* (F). In wild type, ciliary dilations are seen (E, arrows), but not in *b₁* (F, arrows).

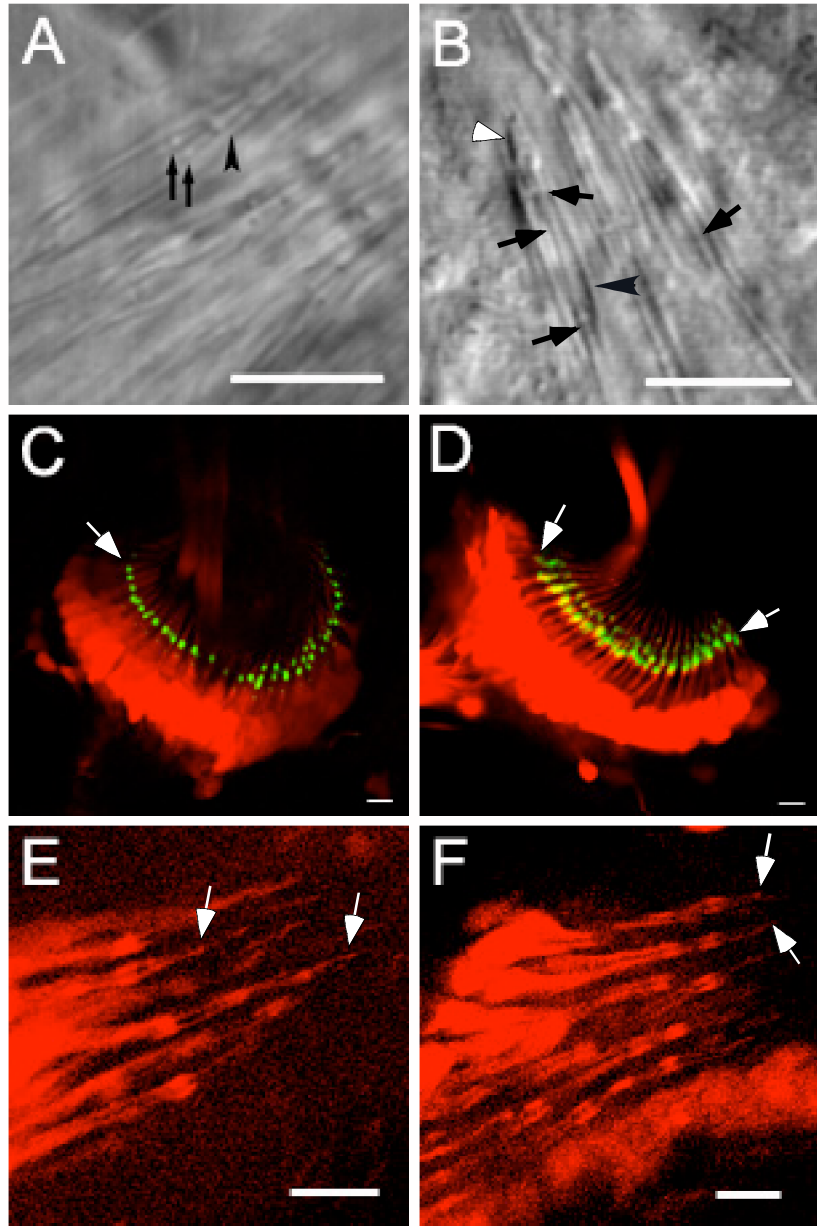


[Figure 3-12] REMPA in *kinesin-2* mutants

While a *kinesin-II* null mutant has missing cilia, a *kinesin-II* hypomorph has the complete length of a cilium and retains the ciliary dilation which apically misplaces. To see where REMPA localizes in the *kinesin-II* null mutant and whether REMPA still localizes on a mislocalized ciliary dilation, REMPA was examined in *kinesin-II* null and hypomorphic mutants. Scale bar: 8 μm .

(A and B) The DIC image in wild type presents the double arrow shaped dendritic caps (A, arrowheads), ciliary dilations (A, arrows), and cilia surrounded by scolopale cells.

The merged picture with REMPA and DIC image displays exactly overlapped localization of REMPA and a ciliary dilation (B, arrows). (yellow, REMPA)

(C and D) The *kinesinII* hypomorph shows slightly narrow and long dendritic caps. In this picture, it hardly detects the ciliary dilation as in wild type. A few bulky structures (C and D, arrows) like a ciliary dilation were found in the dendritic caps (C, arrowheads).

The merged picture with REMPA and DIC image illustrates the REMPA in dendritic caps (D, arrowheads). In some cases, REMPA was detected at the ending tip of the dendritic cap (D, white arrows). (yellow, REMPA)

(E and F) The double staining with phalloidin exhibits the distally mislocalized REMPA around the apical tip of scolopale cells (F, arrows). But, in wild type, REMPA and a ciliary dilation is found near the proximal area of a dendritic cap (E, arrows). (yellow, REMPA; red, phalloidin)

(G and H) (G, arrows) presents the normal localization of REMPA in wild type. In *kinesinII* null mutant where cilia are missing, REMPA was found very faint on the tip of inner segment of ciliated neurons surrounded by very short and round-shaped scolopale cells (H, arrows). (yellow, REMPA; red, phalloidin)

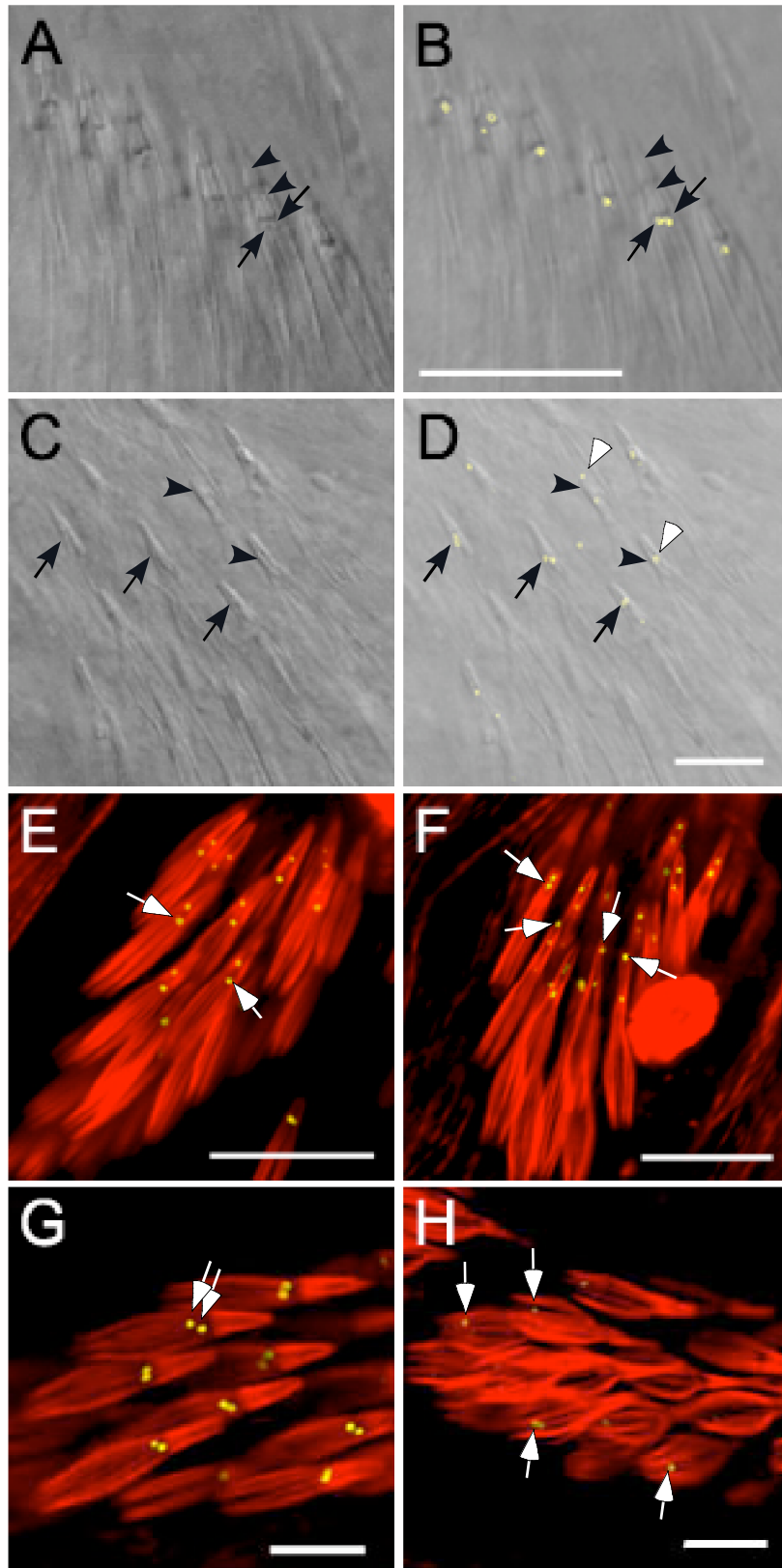


[Figure 3-13] REMPA and NOMPB were not detected in *dyf-1*.

Scale bar: 8 μm .

(A and B) The *elav*-driven RFP expression accentuates the intact outer segment of femoral chordotonal cilia in wild type (A, bracket). In (A), an arrowhead indicates the tip of an inner segment, and an arrow indicates a ciliary dilation. On the contrary, the outer segments of cilia are completely absent in *dyf-1* mutant (B, bracket).

(C and D) DIC images illustrate the overlapped two arrowhead appearance of cap protein (arrowhead), ciliary dilation (arrow), and scolopale cells in wild type (D). In *dyf-1*, ciliary outer segments and ciliary dilation are missing (white arrowheads) and irregular shapes of dendritic cap (black arrowheads) are found while scolopale cell looks intact.

(E and F) REMPA localization in femoral chordotonal cilia counterstained with 21A6 in wild type (E) and *dyf-1* (F). A wild type shows normal localization of REMPA (arrows) and 21A6 (arrowhead). Two yellow foci place distal to 21A6 staining area (E). However, REMPA was not detected in *dyf-1* (F). 21A6 labeling (arrowhead) is also aberrant like in other IFT mutants, validating that Eys might be connected to ciliary morphology in mechanosensory organs.

(G and H) NOMPB localization in femoral chordotonal cilia counterstained with 22C10 in wild type (G) and *dyf-1* (H). NOMPB was normally localized in wild type (G, arrows), but was not detected in *dyf-1* (H, arrows).

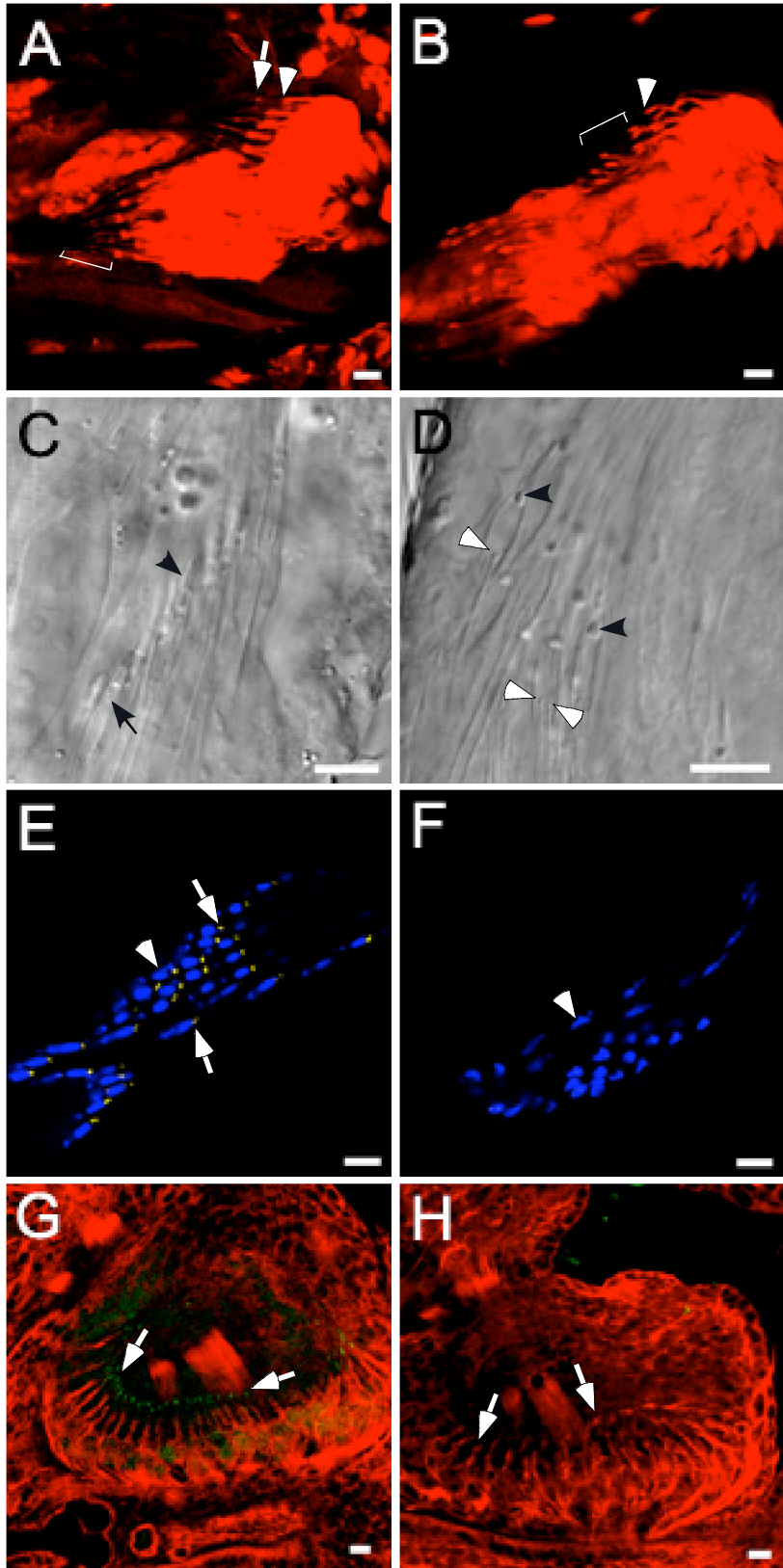


[Figure 3-14] REMPA localization is normal in *BBS8*

Scale bar: 8 μm .

(A and B) The expression of RFP reveals the whole shape of the chordotonal cilia in both wild type (A) and *BBS8* (B). *BBS8* flies apparently maintain full length of the outer segment of cilia (B, bracket) filled with RFP as observed in wild type (A, bracket).

(C and D) Uniform dendritic caps are observed in wild type (C, white arrowhead) and *BBS8* (D, white arrowhead) by DIC microscopy. Ciliary dilations (arrows), ciliary outer segment, and scolopale cells are all normal in both (C) and (D). The ciliary structure of *BBS8* might be normal, based on the findings that dendritic caps are disorganized in mutants retaining shortened cilia.

(E and F) REMPA localization was normal in wild type (E) and *BBS8* (F). REMPA was detected on ciliary dilations in both flies (arrows).

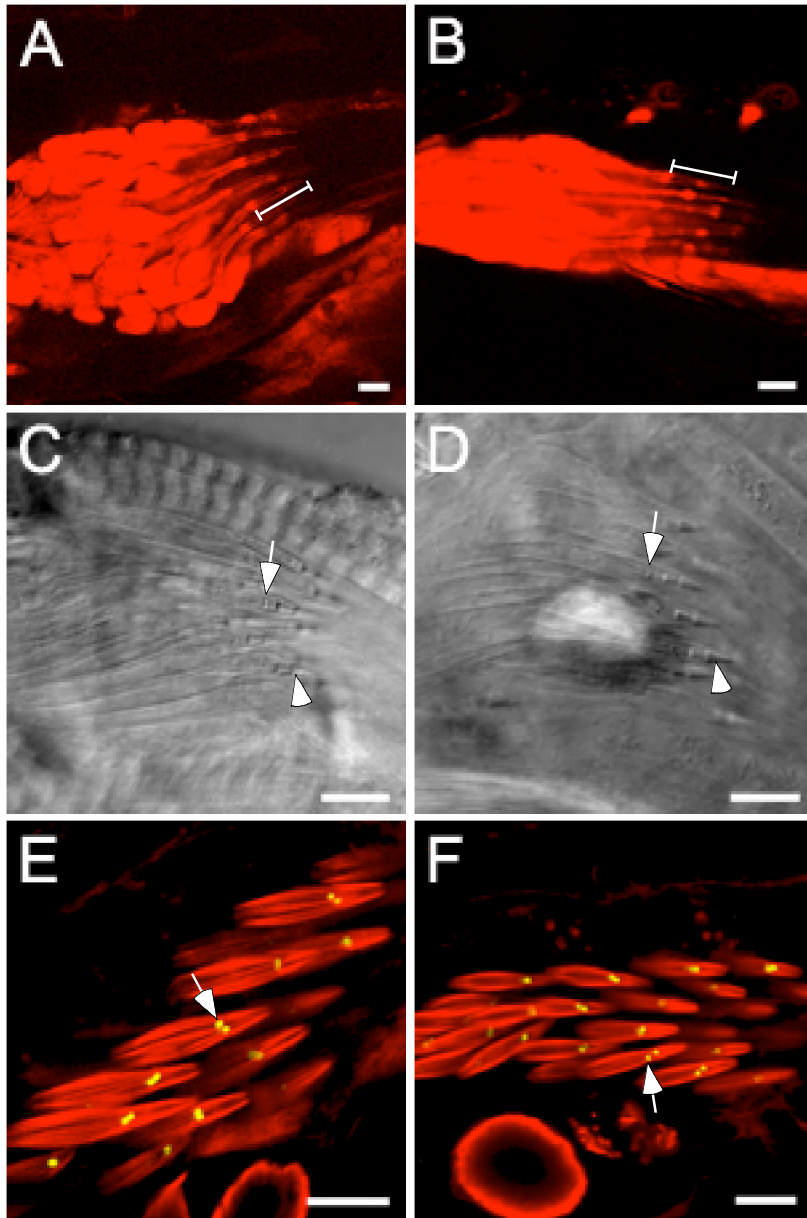
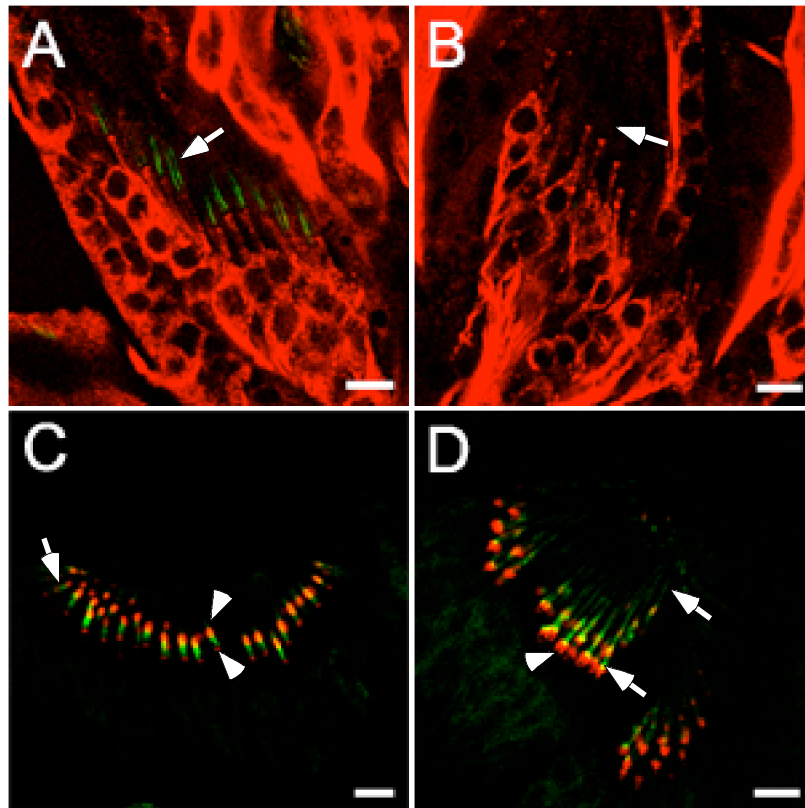


[Figure 3-15] IAV is delocalized in *btv* and absent in *rempA*

The localization of IAV, one of TRPV channel subunits required for the *Drosophila* auditory transduction, was examined in IFT-A mutant cilia. Scale bar: 8 μ m.

(A and B) IAV localizes on the proximal region to ciliary dilation in wild type chordotonal cilia (A, arrow), but was not detected in *rempA* (B, arrow). (green, IAV; red, 22C10)

(C and D) The localization of IAV limited to the proximal region of cilia (arrow) is thoroughly defined by the double labeling with 21A6 which labels the proximal region to the ciliary dilation and around the ciliary base (C, white arrowheads). IAV was leaked into the distal region of a ciliary dilation in *btv* (D, arrows), and 21A6 delocalized to the base part of scolopale cells (D, white arrowhead). (green, IAV; red, 21A6)



Chapter 4 :

Chemosensory defects

in *BBS* mutants

1. Generation of *BBS1* & *BBS8* deletions
2. Chemosensory phenotype
3. Localization of BBS1

BBS (Bardet-Biedl syndrome) is a human genetic disease having symptoms broadly related to ciliary function. The localization of BBS proteins on cilia was discovered in nematode and mammalian cells. To investigate BBS function in fly sensory cilia, I generated BBS deletion mutants both by male recombination and by FRT-FLP recombination. Unexpectedly, BBS mutant flies don't show mechanosensory defects, unlike IFT mutants. They have normal auditory response and wild type ciliary morphology. Also, REMPA localization was normal in BBS mutant chordotonal cilia.

To test for chemosensory defects, I used two behavioral analyses: larval chemotaxis assay and proboscis extension reflex assay, which revealed in a larval chemotaxis defect and severely reduced frequency of PER. BBS1 showed as severe a defect as found in Or83b, an olfactory-null mutant, and BBS3 showed a high sensitivity to a lower concentration of isoamyl acetate. YFP-tagged BBS1 was detected in chemosensory neurons in the labellum at pupal stage and on the basal part of dorsal organ in larvae. A role limited to chemosensory transduction might explain functional differentiation of BBS proteins in cilia compared to the role of IFT molecules, suggesting that each kind of protein might have a differential functional conservation and a phylogenetic adaptation.

Materials and methods

Stocks for deletions

To generate the BBS1 deletion, two stocks carrying dominant markers, *Df(3L)Ly*, *R¹ sens^{Ly-1}/In(3L)P, gm¹* (BL563) and *R¹ D¹ red¹ Sb¹/TM6* (BL1689) were obtained from Bloomington stock center, and the P insertion stock, *EP(3)3144*, from Szeged stock center. *w;TM6B, Tb, Hu, e/TM3, Sb* for isogenization and *w, y/w; sco, cn/ CyO H{P{Δ2-3}}HoP2.1* as a transposase have been kept in the lab stock. Four *BBS1* deletions generated by imprecise excision were a gift from Terry Watnick, MD, a collaborator in Johns Hopkins University and were used to complementation-test BBS1 deletion stocks generated in the lab.

For generating the BBS8 deletion based on FLP-FRT recombination, two P insertion stocks, e02462 and e02898, were obtained from Exelixis. A heatshock-inducible recombinase, *P{ry^{+17.2}=hsFLP}1, w¹¹¹⁸; Adv¹/CyO* (BL6), and a dominant marker stock, *w¹¹¹⁸; wg^{Sp-1}/CyO; sens^{Ly-1}/TM6B, Tb¹* (BL8136) were obtained from Bloomington stock center. The deficiency chromosomes for *BBS1* and *BBS8*, *Df(3L)BSC27/TM6B, Tb¹* (BL6867) and *Df(2L)al/ In(2L)Cy, Cy¹* (BL3548) respectively, were from Bloomington stock center. *BBS3 PiggyBac* insertion, *PBac{PB}CG7735^{c06844}*, was also obtained from Bloomington stock center. Flies were kept on standard medium at 21-25°C.

Stocks for examining sensory defects

To distinguish homozygotes of BBS1 and BBS3 from balanced flies in a pupal stage, I purchased second and third GFP balancer chromosomes from Bloomington stock

center: $y^1 w^*$; $D^* gl^3/TM3$, $P\{w^{+mC}=GAL4-Kr.C\}DC2$, $P\{w^{+mC}=UAS-GFP.S65T\}DC10$, Sb^1 (stock# 5195) and w^* ; $L^2 Pin^1/CyO$, $P\{GAL4-Kr.C\}DC3$, $P\{UAS-GFP.S65T\}DC7$ (stock# 5194). In these stocks, GFP is indirectly driven by *Kruppel* (*Kr*) promoter so that GFP is easily detected from an early stage (embryonic stage 9) to an adult (Casso et al., 2000). This successfully helped to distinguish the homozygous progeny of *BBS* mutants from heterozygotes. I established two lines of $w;BBS1/TM6BTb$ in which I can select homozygous flies by body size and $w;BBS1/TM3$, $P\{w^{+mC}=GAL4-Kr.C\}DC2$, $P\{w^{+mC}=UAS-GFP.S65T\}DC10$, Sb^1 for *BBS1*. I obtained $BBS3/CyO$, $P\{GAL4-Kr.C\}DC3$, $P\{UAS-GFP.S65T\}DC7$ and $BBS8/CyO$, $P\{GAL4-Kr.C\}DC3$, $P\{UAS-GFP.S65T\}DC7$ by genetic crosses. *Or83b* mutant flies for olfactory tests were kindly provided by Dr. Vosshall in Rockefeller University.

Visualization of sensory cilia in BBS mutants

The sensory cilia of *BBS1* and *BBS3* were observed by the expression of membrane bounded GFP using *elav* promoter. *BBS8* mechano and chemosensory cilia were examined by the filling of RFP driven by *elav* promoter. I dissected pupae out in PBT in order to isolate 2nd antennal segments for mechanosensory cilia, and 3rd antennal segments, wings, and legs for chemosensory cilia. Samples were fixed for 20 minutes with 4% formaldehyde followed by washing 3 times with PBT. The embedded samples, in 80% glycerin on a slideglass, were observed using confocal microscopy (Leica, DMIRE2).

Auditory recording

Auditory response of *BBS* mutants to the sound was measured using a tungsten

needle on the second segment of antennae as described in chapter 3.1.

Larval Chemotaxis assay

I examined chemosensory defect of *BBS* mutants using two kinds of chemotaxis assays. First, I modified the larval chemotaxis assay which had been developed by Heimbeck *et al.* The behavior of attraction and avoidance involves a choice. A choice behavior is complicated to analyze because it can be affected by stimulant itself and other factors like central processing. Assuming that larvae preferentially follow an attractable odor, I tested one individual larva at one time to exclude a possible group behavior (Devaud, 2003). Initially, I placed one larva on the center of a petridish covered by 1% agarose gel. Undiluted odorant was introduced on one side and control on the other side of the petridish with the lid of a microtube (Fig. 4-5A). I used 5 day old 3rd instar larvae after washing with 15% sucrose solution and rinsing with water two times. I used *Canton-S* and heterozygous *BBS* flies as a positive control and *Or83b* mutants as a negative control. *Or83b* is required for olfaction, encoding a broadly expressed odorant receptor that dimerizes with other specific odorant receptors (Larsson et al., 2004).

I traced them for a total of 10 min and marked their position at 2.5 minute intervals to score its choice: does it go toward an odorant or away from it? I separate a test petridish into three parts of an odorant, a control, and a neutral region (Fig. 4-5A). I scored tested larvae following the chart (Fig. 4-5B). Time starts to count right after the petridish is covered. According to the movement in the first 2.5 minutes, I give those who move toward the odorant side +2 points. If they stay in the same district, I give them +0 points, and if they move toward control side, I give them a penalty of -2 points. For every subsequent 2.5 minute, if they move toward odorant side from neutral or control sides, I

add +1 point more, and if they move away from odorant side, I subtract a point. If they stay continuously in odorant region, I give them +1 in each time period, and if they stay in the neutral region, I give them 0 point. If they stay in control side continuously, I give them -1 point repeatedly. If they show perfect attraction to an odorant, then they obtain +5 points in total, and if they are indifferent, they have around 0. The total point around -5 indicates repulsion.

The camera recording-based chemosensory behavior

To verify the reliability of the larval chemotaxis test on the round petridish and to reason the scoring for the test, I used a newly developed chemotaxis assay in Dr. Leslie Vosshall's lab in Rockefeller University. They have set up three different larval chemotaxis assays: one is to test the trace for the exponential gradient of an odor, another is to test a taxis for the linear gradient of an odor which is more difficult than the exponential gradient traces, and the other is the test how close and how long larvae stays around the odor. I used three different modes of larval chemotaxis. For exponential gradient analysis composed of 6 different concentrations of an odor, from 0 to 1M. The odor was diluted in paraffin oil to keep the odorant stuck to the inside of the lid of 96 well. The different odors were diluted in dark bottles and introduced to the lid by a multipipette apparatus. Immediately, the lid was placed on top of the other lid which has 3% agarose gel covered on the top of the lid. The larvae was put between the first and the second lowest concentration spot facing the head to the higher concentration direction. For five minutes, the larval tracing is automatically tracked, videotaped and tracked with Ethovision software (Noldus, Wageningen, The Netherlands). The collected data were analyzed by Wilcoxon test ($p < 0.05$).

Proboscis extension reflex (PER) assay

I anesthetized 2-5 day old flies on ice. After immobilizing them on a coverglass using myristic acid of which melting point is 56°C, I introduced a drop of sugar solution from 1×10^{-4} to 1M to the tip of first leg (tarsi). I checked whether the fly extends out the labellum or not. Flies were starved for 14-16 hours before test, and were only humidified. Flies were saturated with water before administrated sugar solution. Each fly was tested only one time and a total of 50 flies were tested at each sugar concentration.

YFP tagged rescue construct

I used The *Drosophila* Gateway™ Vector Collection (Invitrogen, CA) to obtain the YFP tagged BBS1 genomic rescue construct. The rescue construct includes the whole sequence of *msl-3* to rescue both male lethality and *BBS1*. This genomic fragment was amplified by PCR using two pairs of primers: BF (CACCGAATGCATCCAACCTCCAA GC), Pro-R (TAAGGGCCCTGGAAAATTGTATTTCATTATGGAATCT), AF (CCGGTT GCTAAG GACAAGAA), and GR(AGGCGCGCCACCCTTGAAGGCTGC CTCGGA TTGG) bearing *AscI* site on 3' end right after the deleted stop codon of the exon 3 of the BBS1 genome. The first fragment was generated from BF and Pro-R by PCR and the last part was from FF and GR. After the first fragment was inserted into the pENTR™/D-TOPO® vector (Invitrogen, CA), the second fragment of BBS1 rescue gene was inserted into the pENTR by *DraIII* and *AscI*. Because the final rescue construct of pENTR™/D-TOPO® for *BBS1* contains missense mutation on exon 1 and exon 2, I replaced the fragment between *DraIII* and *SallI* with *SD17491*, BBS1 EST clone. This *SD17491* includes the first intron. The obtained pENTR™/D-TOPO® for *BBS1* was

recombined with a pDEST vector containing *venus* coding sequence by LR clonase (LR reaction). The final destination vector containing *BBS1* genome and *venus* was injected into eggs to obtain the transgenic flies as introduced in the previous chapter.

Visualization of YFP tagged BBS1 on ciliated organs

I dissected pupae out in PBT solution to isolate antennal segments and chemosensory organs like a labellum and a maxillary palp. These collected samples were fixed in 4% formaldehyde in PBT for 20 minutes and washed 3 times for 10 minutes each. To distinguish the detail subcellular compartment, I incubated samples with Alexa 568 conjugated phalloidin (1:1000, Molecular Probe, OR) in PBT for 1-2 hours and washed with PBT 3 times for 20minutes. Stained samples were embedded in Vectashield (Vectorlabs, CA) and examined using Confocal Microscopy (Leica, DMIRE2).

4.1. The generation of *BBS1* & *BBS8* deletions

The initial start to be interested in BBS proteins was begun with the mapping of *rempA*. *BBS8* was one of two candidates for *rempA*. Though *rempA* turned out to be IFT140, *BBS8* was a newly identified ciliary protein whose function was almost completely unknown. Since IFT proteins are required for ciliary assembly, I was curious

if BBS proteins are also involved in ciliogenesis and how BBS proteins are involved in *Drosophila* sensory transduction. Therefore, we decided to generate fly BBS mutants. A previous study of BBS gene expression by a promoter fusion assay in *Drosophila* revealed that all BBS genes are expressed in ciliated sensory organs (Avidor-Reiss et al., 2004). Furthermore, well developed genetic manipulation in the fly allows a particular gene to be deleted and the usage of deficiency chromosomes enables us to test the triallelic inheritance.

Six of twelve *BBS* genes in humans are well conserved in *Drosophila* (table 4-1). Figure 4-1 shows a schematic of the domains of six fly *BBS* homologs. They show no similar functional domain to one another because all the *BBS* genes have been identified from the symptoms not based on the protein domain structure. BBS3 has an Arf (ADP ribosylation factor) domain, which is a small GTP binding protein involved in many biological activities including vesicle trafficking (Burd et al., 2004). BBS4 and 8 contain TPR motifs which are also found in some IFT proteins. TPR motifs are known to be related to protein-protein interaction (D'Andrea and Regan, 2003). BBS5 has DM16 motif which is a predicted repeat domain and BBS9 has two coiled-coil domains. Though they possess different combinations of domain structure, they are likely to be involved in the same pathway of a signaling cascade on ciliary function ending up to same consequential failure. Interestingly, BBS 7 is not conserved in *Drosophila*, but present in mosquito, bee, nematode, and vertebrate. Considering BBS proteins might be involved in ciliary function based on the localization pattern of BBS proteins in other organisms (Blacque et al., 2004; Fan et al., 2004; Li et al., 2004), BBS7 may play a role for host-seeking by thermosensation or detecting CO₂ which are all specifically related to the features for survival of mosquito.

To study the BBS proteins in *Drosophila* sensory cilia, I generated fly *BBS* mutants. One of the advantages of *Drosophila* as a model system is that there are a lot of available transposon stocks which allows researchers to readily attempt to generate a targeted deletion by genetic manipulation. If there are transposons in useful positions, this is easily achieved, by either P element-based techniques or recombination with FLP recombinase and FRT-bearing insertions (Parks et al., 2004; Thibault et al., 2004).

P-elements excise imprecisely when transposing via the P transposase. Their excision generates a double-strand break in the chromosome, leaving or sequences from the P elements behind or creating small deletions around the original P element insertion point (Gloor et al., 1991; Kaufman and Rio, 1992). This is repaired either by homologous recombination or by non-homologous end-joining. Non-homologous end-joining occurs possibly by fusion of broken DNA ends, conversion, or duplication, giving a variety of excision products. The use of this approach allows researchers to create local mutations in genes neighboring the original P-element insertion. Deletions with two P element insertions which are flanked by dominant markers is easily detected by different combinations of markers (Preston and Engels, 1996).

PiggyBac is a useful transposon for a precise gene-deletion targeting (Thibault et al., 2004). Exelixis investigators reported that, in the presence of FLP recombinase, many deletions whose end points are precisely defined are produced from the PiggyBack insertion lines containing FRT sites by trans- recombination (Parks et al., 2004). There are 3 types of FRT-bearing transposon according to the location of a 199 bp FRT fragment to the white⁺ transgene: XP and WH types are 5' and RB type is 3' of the white⁺ transgene. PB type piggyback does not contain a FRT site. Depending on each combinatorial pair of XP and PiggyBac insertions, targeted deletion can be detected by

the loss of white⁺ gene or PCR (Parks et al., 2004). I generated two BBS mutants, BBS1 and BBS8, by male recombination based on P-element and FRT-FLP recombination respectively.

BBS1 (CG14825) deletion was generated by male recombination

To approach how BBS1 protein is involved in sensory cilia, I generated *BBS1* mutants by male recombination where the transposase drives the P-element recombination in the absence of meiotic recombination in male testes. Male specific lethal-3 (*msl-3*), the neighbor gene of *BBS1*, has a P element in exon 1, about 200bp away from the putative start codon of *BBS1* (Fig. 4-2A). This leads to male lethality so that *EP(3)3144* produces no male homozygotes. *BBS1* is cytogenetically located on 65E4. The dominant markers which flank the *BBS1* locus at both sides are required to isolate the *BBS1* deleted flies from the final crosses. For example, *Df(3L)Ly, R¹ sens^{Ly-1}/In(3L)P* has one flanking marker, R¹, at 62B8-12 and the other, sens^{Ly-1}, at 70A3-5. When this chromosome is aligned with *EP(3)3144* on *msl-3* under transposase activity, P element excision and recombination occurs. Therefore, the BBS1 deletion was recovered by the combination of white eye color and sens^{Ly-1} phenotype as shown in Figure. 4-2B. In this way, three lines of *BBS1* deletion mutant were isolated from male recombination. These lines fail to complement four lines of *BBS1* deletion mutant generated by imprecise excision from Terry Watnick, MD, a collaborator in Johns Hopkins University and the deficiency chromosome. The gene deletion was confirmed by PCR of genomic DNA. *BBS1* mutant flies are viable and fertile and look normal in behavior, but a male homozygote is lethal as *BBS1* deletion was originated from the P element on *msl-3*.

BBS3 (CG7735) has PiggyBac insertions on exon 4.

The amino acid sequence alignment shows that BBS3 is well conserved (Fig. 4-3B). *PiggyBac* insertion for *BBS3* mutant is available in Bloomington stock center (Fig. 4-3A). BBS3 encodes *ADP ribosylation factor-like (ARL) 6* protein. ARL6 is a member of the RAB-SAR-ARF-ARL family of small GTP binding proteins. The amino acid changes found in BBS3 patients were marked in Figure 4-3B. Three amino acid substitutions were discovered: one is near the P loop; the other two are on 169 and 170. The structural comparison of ARL6 and ARF6 whose amino acid sequences are 43% identical and 62% similar indicates that these three amino acids all locate near GTP-binding site, suggesting that these substitutions might affect the GTP-binding activity, therefore, leading to the pathogenic phenotype of *BBS3* (Fan et al., 2004). A *PiggyBac* insertion in the 4th exon of *BBS3* was verified by Inverse PCR (Fig. 4-3A, 3B, red square) which might lead to a truncated form of protein. Also, the *PiggyBac* insertion in *BBS3* might cause pathogenic phenotype due to the near position to the GTP-binding site. A *BBS3* homozygous mutant is viable and fertile.

BBS8 (CG13691) was generated by FRT-FLP recombination.

To generate *CG13691 (BBS8)* deletion mutants using FRT and FLP system (Parks et al., 2004), I looked up available insertions around *CG13691* (Fig. 4-4A). I found *RB e04262* downstream and *RB e02898* is upstream of *CG13691*. However, this putative deletion also contains *CG13692* encoding a putative ADP ribosylation factor (ARF) GTPase activator. Even though *CG13692* is not determined to be involved in the BBS phenotype, we attempted to obtain a deletion for *CG13691* and *CG13692*, because a deletion of *CG13691* alone could then be obtained by rescuing *CG13692* by

germ line transformation. Also, it would be interesting to test if *CG13692* deletion affects the ciliary function by rescuing *CG13691*. Thus, *CG13691* and *CG13692* deletion mutant was generated by FRT-FLP recombination as described by Parks et al. (Fig. 4-4B) (Parks et al., 2004). I have screened 9 independent lines of deletion mutant out of 200 isolated flies, indicating 4.5% efficiency. I checked a genomic deletion by PCR of progenies from the cross of homozygous deletion mutants as well as the progeny from the deletion and the deficiency chromosome for *CG13691*, *Df(2L)al*. *CG13691* and *CG13692* deletion mutants looks to behave normally, and homozygotes are viable and fertile, implying that neither gene is essential for viability.

4.2. The Chemosensory Phenotype

All IFT and BBS proteins are known to be involved in ciliary function. If BBS function is well conserved, *BBS* mutants should show similar phenotypes in diverse organisms. If BBS proteins are components of IFT particles, *BBS* mutants should show a similar phenotype. However, unlike nematode and mammal where *BBS* mutants show a ciliary failure as well as a disrupted microtubule organization, the fly *BBS* mutants don't seem to exhibit conspicuous uncoordination or defective ciliary structure. Instead, they have a chemosensory specific defect. This implies that BBS function in *Drosophila* might be distinguishable from other organisms. How do BBS proteins contribute to ciliated

sensory neurons in *Drosophila*? Do BBS proteins play different roles in mechanosensory versus chemosensory cilia? To answer these questions, I attempted to define the phenotype of generated *BBS* deletions and a *BBS3* insertion.

BBS1, 3, and 8 mutants have a normal auditory response.

All ciliary mutants leading to mechanosensory defect show abnormal behavior. Mutants involved in ciliary differentiation (IFTs, unc) are severely uncoordinated, while mutants involved in sensory transduction (NAN, IAV) are sedentary. Considering that BBS proteins are known to be associated with ciliary function, and that *Drosophila* mechano- and chemosensory neurons contain ciliated endings, *BBS* mutant flies could have a defect in both mechano- and chemosensory behavior. Moreover, BBS promoters drive expression in ciliated neurons in *Drosophila* (Avidor-Reiss et al., 2004). However, *BBS1*, *BBS3* and *BBS8* mutant flies appear to have normal behavior. They might have a subtle behavioral phenotype unable to be easily detected. To see if *BBS* flies have a reduced sound-evoked response, I measured the extracellular potential change upon auditory stimuli. Consistent with the normal behavior of *BBS1, 3, and 8* mutants, the sound-evoked response in *BBS* mutants was not different from that in wild type (Fig. 4-6A).

It was shown that combinations of three mutations present more severe BBS symptoms in humans (Katsanis et al., 2001a). To examine if BBS phenotype penetrance in *Drosophila* follows triallelic inheritance, I combined one homozygous *BBS* deletion mutant with the heterozygous deficiency chromosome on the other *BBS* loci and tested an auditory response. These flies showed not only the coordinated behavior but also a similar pattern of a sound evoked response to homozygous *BBS* deletion mutants (Fig. 4-

6B). Taken together, *BBS* deletions do not lead to mechanosensory defect, indicating that *BBS* proteins are not required for mechanosensory transduction in *Drosophila*.

BBS1, 3, and 8 mutants have chemosensory defects.

The fact that fly chemosensory transduction also occurs in a ciliary structure implies that chemosensory behavior might be affected by *BBS* mutations. Concomitantly, *BBS1*, *BBS2* and *BBS4* knock-out mice showed anosmia, and *BBS4* deletion does not generally lead to missing cilia in a whole body (Kulaga et al., 2004; Mykytyn et al., 2004; Nishimura et al., 2004). This series of results suggests that *BBS* mutations in flies might selectively lead to a chemosensory defect. To test this hypothesis, I examined *BBS* mutant flies using the larval chemotaxis assay and the proboscis extension reflex assay. For the larval chemotaxis assay, I took two methods. First, I tested larvae with two attractive odorants, propionic acid and 1-butanol. The control was attracted by both odorants, while *Or83b* larvae were indifferent (Fig. 4-7). Heterozygous *BBS1* larvae showed as high a chemotactic score as the control did. A *BBS1* mutant displayed a lower preference for 1-butanol but was not as severely defective as an *Or83b* mutant was. For propionic acid, a *BBS1* mutant did not show a significantly defective response. However, *BBS3* heterozygotes and homozygote showed no distinctive defect to either odorants.

Secondly, to verify the reliability of the larval chemosensory test and the taxis score, I tested each *BBS* mutant larva in the automatic tracking box which has been newly developed in Dr. Vosshall's Lab in Rockefeller University. I tested them with isoamyl acetate, one of the attractants, serially diluted in paraffin oil in terms of three contexts: How a mutant larva responds in the exponential odor gradient, the linear odor gradient, and the single droplet environments. In the exponential gradient where the concentration

of an odor increases exponentially from 0.03M to 1M (0.03M, 0.06M, 0.12M, 0.25M, 0.5M, 1.0M) larva easily follows the odors, but the linear gradient (0M, 0.1M, 0.2M, 0.3M, 0.4M, 0.5M) doesn't allow larvae to track the odor as easily as in the exponential gradient setup. The single droplet assay provides how sensitive and attracted a larva is to the odor by measuring the time that a larva stays in an odor zone and the distance from a larva to an odor source. I found that *BBS1* has similar severity as *Or83b* mutant to the isoamyl acetate from the exponential gradient setup (Fig. 4-8A, D). *BBS3* seems not to have as severe a defect as *BBS1* and *Or83b*, but abnormal traces showed that they have unknown defect to track the odors (Fig. 4-8A, E) in the exponential gradient assay.

To test the sensitivity and attractiveness to each concentration of isoamyl acetate, I put a larva near one droplet of the odor and measured the mean distance from the larva and the odor source and the time the larva stayed in the odor zone. *BBS1* showed similar indifference to the odor as an *Or83b* larva does in all concentrations, except 0.25M (Fig. 4-9A). Though the p value ($p=0.091$) from the comparison with *Or83b* at 1.0M is higher than 0.05, indicating that the response of *BBS1* is similar to that of *Or83b*, it is not clear why it shows a shorter mean distance pattern especially at 0.25M in the graph (Fig. 4-9A).

The attractiveness of *BBS3* to the odor at 0.06M, 0.25M, and 1.0M was significantly different from the profile of *Or83b*. Interestingly, *BBS3* shows higher sensitivity at 0.06M, a low concentration at which the mean distance of wild type is longer (Fig. 4-9B), suggesting that *BBS3* might have a high sensitivity at lower concentration of isoamyl acetate.

To investigate the putative high sensitivity found in the behavior of *BBS3* larvae at lower concentrations, I tested *BBS3* larvae on a steep linear gradient. This gradient is composed of six 0.1M-difference concentrations of the odor (0.0M, 0.1M, 0.2M, 0.3M,

0.4M, and 0.5M), and gives a harder environment for larva to follow the odor. In this setup, both *BBS3* ($p=1.6 \times 10^{-8}$) and wild type ($p=2.5 \times 10^{-11}$) are significantly different from *Or83b^{-/-}*. However, the p value of *BBS3* and wild type was on the borderline ($p=0.0167$) which is as same as the cut-off corrected by Bonferroni correction. This suggests the defective chemotaxis of *BBS3* shouldn't be underestimated though the picture of median (Fig. 4-10A) shows a not-significant difference between the medians of two samples. A bigger group might offer an unambiguous conclusion.

The zonogram summing all the traces shows an intriguing pattern in *BBS3* (Fig. 4-10B and C). Whereas wildtype traces concentrated on to the odor line, *BBS3* traces were dispersed all around the test place. To look at the pattern of traces, *BBS3* seems to be able to reach the highest odor (0.5M), but the pathway to reach the pinnacle is not as robust as found in wildtype, suggesting that *BBS3* might have a high sensitivity to an odor presumably due to the loss of protein function with hybrid or truncated protein. The defective chemotaxis of *BBS1* found in the exponential gradient assay and single droplet assay is consistent with the finding from the first assay performed in the lab. The lack of a defect in *BBS3* from the first assay is seemingly similar to the result from the exponential gradient assay. However, the elaborate setup subsequently discovered the high sensitivity of *BBS3* to a lower odor concentration, which moreover reasons why no defect in *BBS3* was found in the first assay. This also indicates that the different setup targeting different behavioral context is useful to identify unknown behavioral defects.

I tested taste in adult flies by proboscis extension reflex (PER), where touching tarsi on the leg with a drop of sugar solution elicits an extending out of a labellum. This is an all-or-none response, relying little on subjective judgment. *BBS 1*, *BBS3*, and *BBS8*

mutants all ended up with a severely reduced response rate compared to controls and heterozygotes (Fig. 4-11). The control demonstrates about 75-90% frequency to 1M sugar solution, while mutants only displayed about 10-30%. No gender difference was observed. This indicates that *BBS1*, *3*, and *8* mutants have chemosensory defects, suggesting that the function of BBS proteins in *Drosophila* are probably limited to chemosensory transduction.

BBS1, 3, and 8 mutants have normal morphology of sensory cilia

I found that *BBS1*, *3* and *8* mutants have a normal auditory response, but have defective chemosensory behavior. Does this chemosensory phenotype stem from the morphological defect in cilia? To examine the relevance of the phenotypic behavior and a ciliary structure, I generated BBS mutant lines that express GFP or RFP in sensory neurons, using the *elav>Gal4, UAS>CD8::GFP* system and *elav>Gal4, UAS>RFP* (Fig. 4-12). Interestingly, *elav*-driven visualization of ciliary neurons illustrated normal ciliary morphology –neither missing nor short- in mechanosensory and chemosensory organs of *BBS* mutants (Fig. 4-12). In wing margins, chordotonal organs, legs, and third antennal segments, intact cilia were all present. This finding suggests that BBS1 protein is not needed for ciliary assembly. Intriguingly, this is different from findings in other species like nematode, mouse, and human. In nematode, all *BBS* mutants have truncated or absent cilia in sensory neurons (Blacque et al., 2004; Fan et al., 2004; Li et al., 2004). Olfactory layers are disorganized and absent in each BBS1 and BBS4 null mouse (Kulaga et al., 2004).

However, in case of *Drosophila*, the intact ciliary structure is consistent with normal behavior and auditory recordings. The chemosensory defect discovered in *BBS1*,

3, and 8 mutant flies suggests that *BBS* mutants might have impaired chemosensory cilia, but the ciliary morphology through GFP/RFP expression appears normal. Not all cilia in a *BBS4* null mouse were generally affected through out the whole body (Mykytyn et al., 2004). Therefore, BBS proteins might be functionally related to cilia for specific sensory transduction or involved in odorant receptor trafficking to proper locations. However, the observation using GFP expression on sensory neurons has limited resolution to deduce the normal morphology of mutant cilia. To substantiate an integral ciliary structure in chemosensory defective *BBS* flies compared to other organisms, EM analysis remains to be done. Taken together, BBS dysfunction originates from signaling transduction rather than ciliary assembly.

4.3. Localization of BBS1

The fly *BBS* mutants have a chemosensory specific defect and normal ciliary morphology. To know whether BBS proteins specifically localize on chemosensory neurons, I generated YFP tagged *BBS1* rescue flies and examined BBS1 localization in sensory organs.

BBS1 specifically localizes on chemosensory sensilla.

The promoter fusion expression of *BBS* genes were detected in both

mechanosensory (chordotonal and ES organ) and chemosensory (antenna-maxillary organ) organs (Avidor-Reiss et al., 2004), but this contrasts the active behavior and normal auditory response seen in the BBS mutants. Moreover, a virtual picture was not provided in the paper publication. Although the preliminary data indicated no defects in mechanosensory transduction in *BBS1* mutant, it needs to be determined whether the localization of BBS1 related to cilia in the mechanosensory organ can account for no phenotype on the mechanosensory organ. The *YFP*-tagged genomic *BBS1* gene was expressed in chemosensory neurons. It localizes on chemosensory cilia not on mechanosensory cilia (Fig. 4-13A-D). The phalloidin counterstaining illustrates that BBS1 specifically labels the chemosensory cilia. This is consistent with the behavioral and electrophysiological phenotype of BBS1 deletion mutants. It is required to use the specific chemosensory receptor markers in order to examine whether *bbs* genes are differentially localized in the particular chemosensory subset. However, no further observation was made. The BBS1-YFP visualizes the basal region of a dorsal organ not a terminal organ. Compared to the autofluorescence of a wildtype, the YFP signal seems specific (Fig. 4-13E-H). Though it is not determined which subset of the chemosensory cilia the BBS1 localizes on, the clear visualization of YFP signal on a dorsal organ suggests that BBS1 function is involved in chemosensory cilia in a larva. This is on the same line with the result of the larval chemotaxis assay of *BBS1*. However, the examination of the localization of BBS1 on other *BBS* homologs and the localization of other OR proteins in *BBS1* mutants will provide a valuable information to infer how BBS proteins are involved in chemosensory transduction.

[Figure 4-1] Six *Drosophila* *BBS* homologs and Domain structures

(A) Six of twelve *BBS* homologs are conserved in *Drosophila*. Mutant flies that were generated and obtained for the stock center are indicated with *. *BBS3*, *BBS4*, and *BBS8* contain an x-box motif through which gene expression is regulated by RFX transcription factor.

(B) *BBS* fly homologs do not share a common domain structure. *BBS1* does not have a distinctive functional domain similar to other proteins. *BBS3* has an Arf domain. *BBS4* and *BBS8* contain TPR motifs. *BBS5* has a DM16 domain, and *BBS9* has coiled-coil motifs.

A

BBS	flyhomolog	Region	Df	domain	Genome(AA)
BBS1*	CG14825	3L – 65E4	Df(3L)BSC27		2257bp(605) 3 exons
BBS3*	CG7735	2R - 56D6	BL17783	Arf, x-box	775bp(202) 4 exons
BBS4	CG13232	2R – 47D5	Df(2R)ix ⁸⁷ⁱ³	TPR, x-box	3333bp(486) 10 exons
BBS5	CG1126	3R – 82D7	Df(3R)110	DM16 repeat	1376bp(381) 5 exons
BBS8*	CG13691	2L – 21C6	Df(2L)al	TPR, x-box	1839bp(549) 4 exons
BBS9	CG15666	2R-57D12	Df(2R)	Coiled coil	2941bp(789)

B

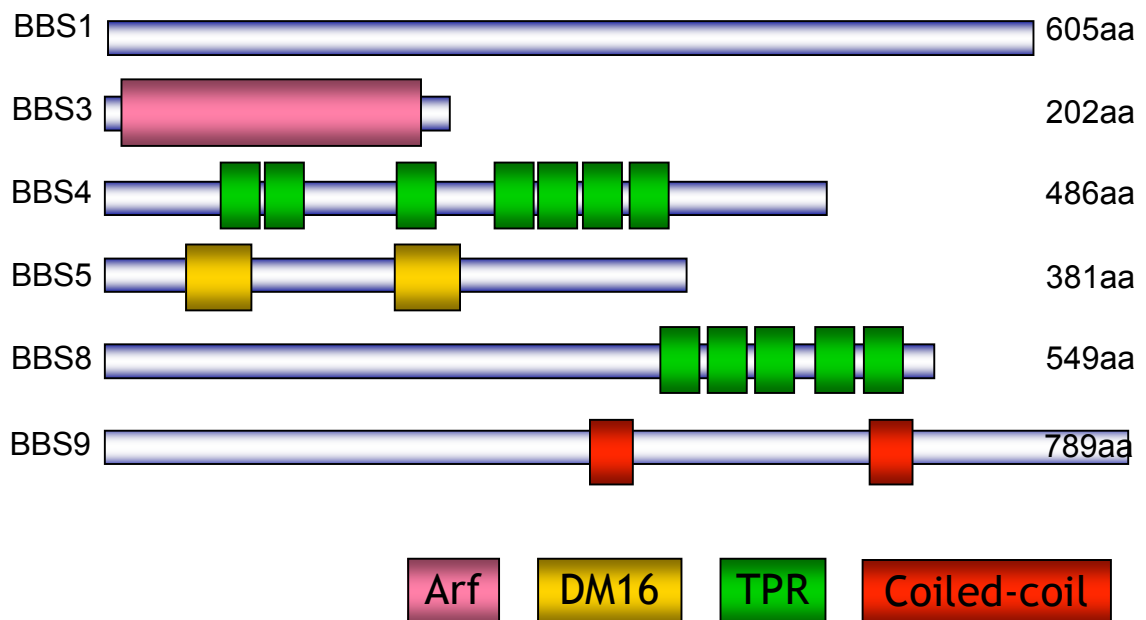


[Figure 4-2] The cytogenetic map and the deletion scheme of BBS1

(A) Cytogenetic map of *BBS1* and dominant markers

BBS1 is located on 65E4, and two dominant markers, R^1 and $sens^{Ly-1}$, are located on 62B8-12 and 70A3-5 respectively. P element nearby *BBS1* is inserted on exon1 of *msl-3*. In the presence of transposase, jumping out of P element produces a nick and recombines with the other strand where two markers reside. *Roughened* (R^1) shows large dark facets on eyes. *Lyra* ($sens^{Ly-1}$) shows a narrow shape of wings whose lateral margins were excised. Therefore, the isolation of Lyra without recombinase after the recombination gives the possible *BBS1* deletion.

(B) The deletion scheme of *BBS1* by male recombination

Males containing dominant markers (R^1 and $sens^{Ly-1}$) and a transposase were isolated by roughened, Lyra, and curly wing phenotype, and crossed with P element insertions (*EP(3)3144*). Curly males showing Roughened and Lyra phenotype without tubby were isolated from this cross where P element recombination theoretically occurs. These males were crossed with balancers to isolate recombined males that only show Lyra not Roughened. After a setup for independent lines, the *BBS1* deletion was confirmed by PCR.

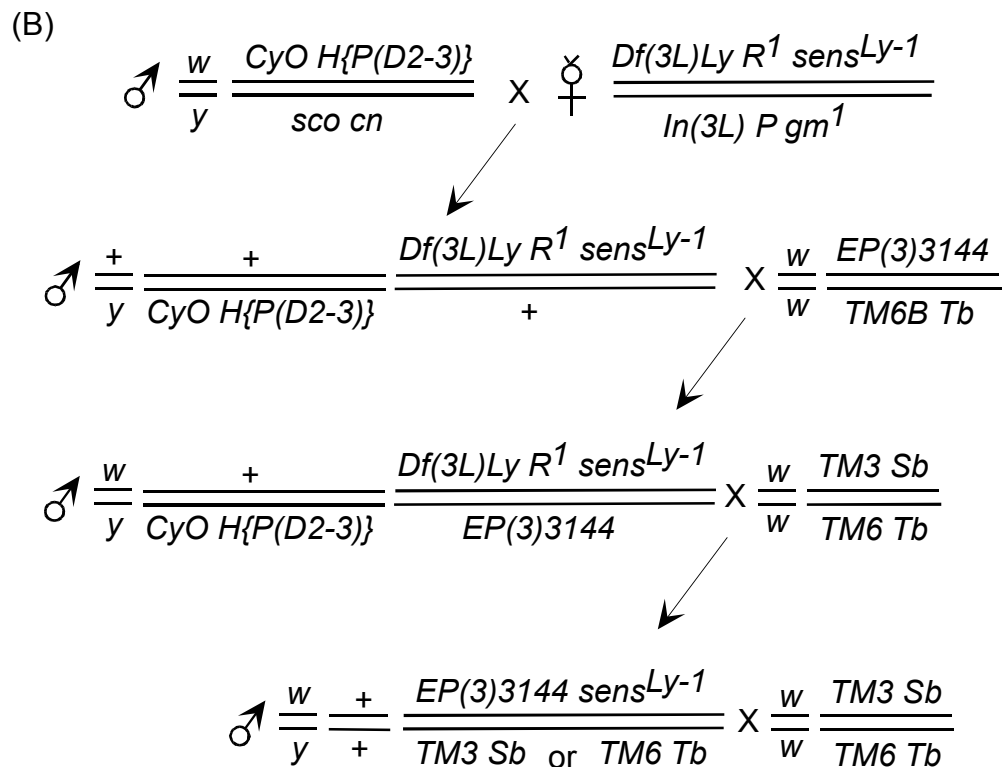
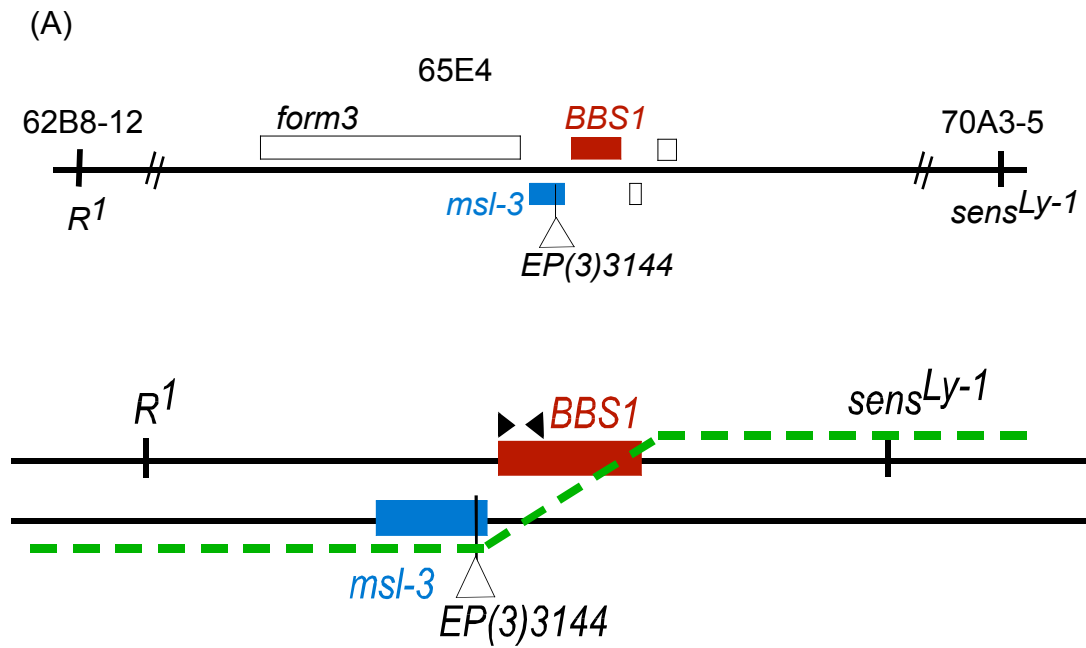


[Figure 4-3] The cytogenetic map and the insertional position of *PBac{PB}CG7735^{c06844}*

(A) The cytogenetic map of *BBS3*

BBS3 encodes a small GTP binding protein, and a fly *BBS3* homolog cytogenetically positions on 56D7. PBac insertion, *{PB}^{c06844}* locates on the coding region of exon 4.

(B) The alignment of *BBS3* homologs

The whole sequence is well conserved. Based on the structural simulation of ARF6, the predicted P loop was indicated by the outline (orange) on GLDNSGKTT. One pathological mutation was discovered in this region from human patients. The Inverse PCR confirmed that the *{PB}^{c06844}* is inserted on serine residue (red rectangle). Though this is not a conserved residue, the mutations in near two residues, G169A and L170W, are found to be involved in human pathology of BBS. These three mutations found in BBS patients all position near the GTP binding site, suggesting that the PiggyBac insertion on the *BBS3* fly homolog might also affect the pathogenic phenotype based on the regional vicinity to the GTP binding site.

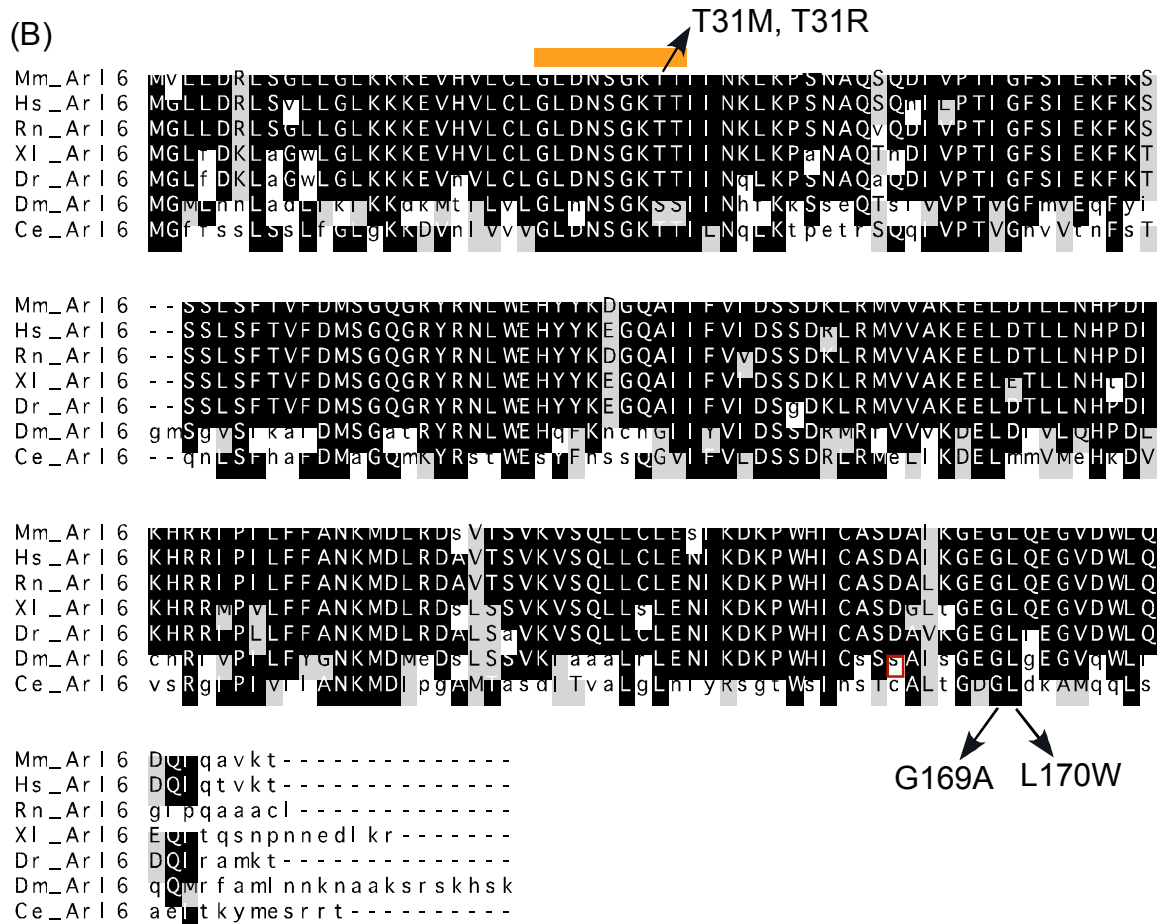
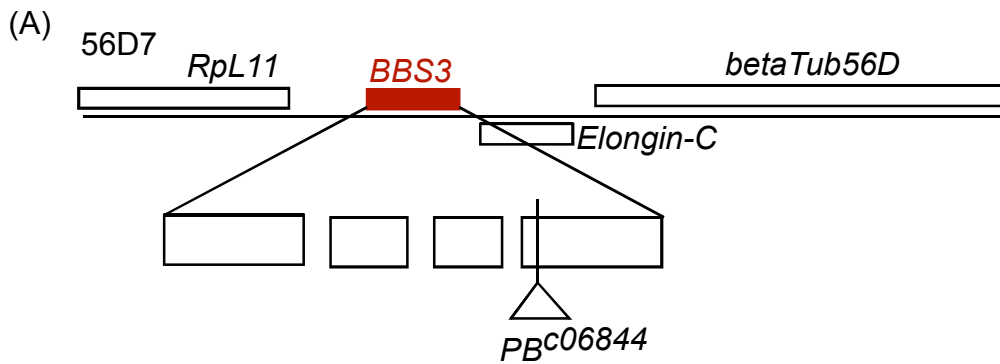


[Figure 4-4] Cytogenetic map and deletion scheme of *BBS8*

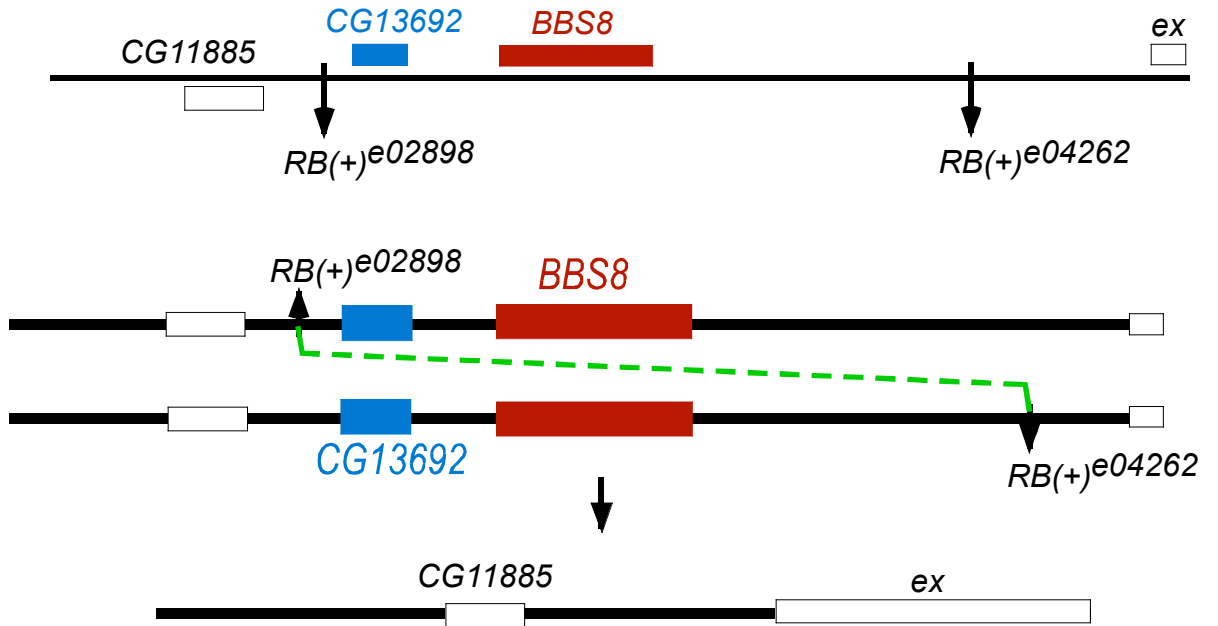
(A) The cytogenetic map of *BBS8* (*CG13691*) and PBac insertions

The 1.84kb long *BBS8* gene is cytogenetically located at 21C2 on the end of the left arm of chromosome two. *CG13692* is located 1.0kp upstream of *CG13691*. Two PBac insertions which are able to lead the deletion of *CG13691* by the FRT-FLP recombination regionally end up with the deletion of both genes, *CG13691* and *CG13692*: *PBac{RB}e02898* places upstream from *CG13692*; *PBac{RB}e04262* on 3.4kb downstream of *CG13691*. *CG13692* encodes putative ADP ribosylation factor (ARF) GTPase activator.

(B) The deletion scheme of *BBS8* by FLP-FRT recombination

The recombination was allowed to occur by the activation of FLP with heat shock for 1 hour at 37°C for 5 consecutive days, two days after two FRT bearing insertions were crossed. Non curly virgin females were isolated and crossed with dominant markers. Each curly male was isolated and crossed with dominant marker females to set up an independent line. I checked genomic deletions by PCR of progenies from the cross of deletion mutants and the deficiency chromosome for *CG13691*, *Df(2L)al*.

A



B

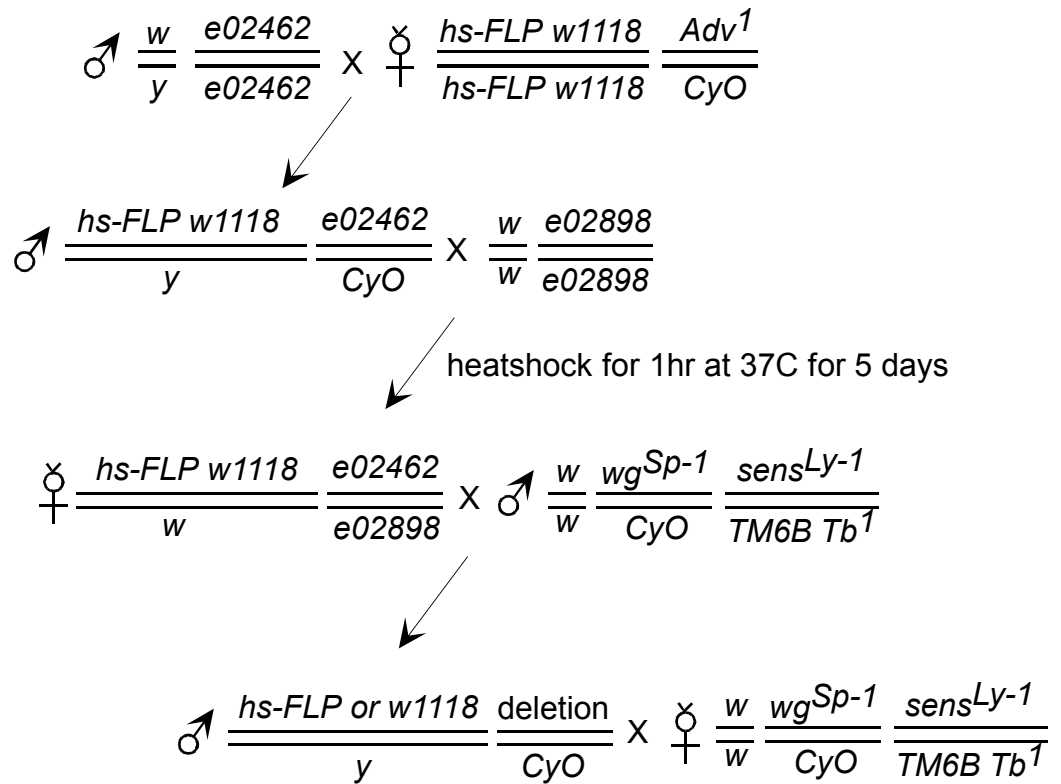


[Figure 4-5] The larval chemotaxis assay developed from Heimbeck (1999) and the scoring method.

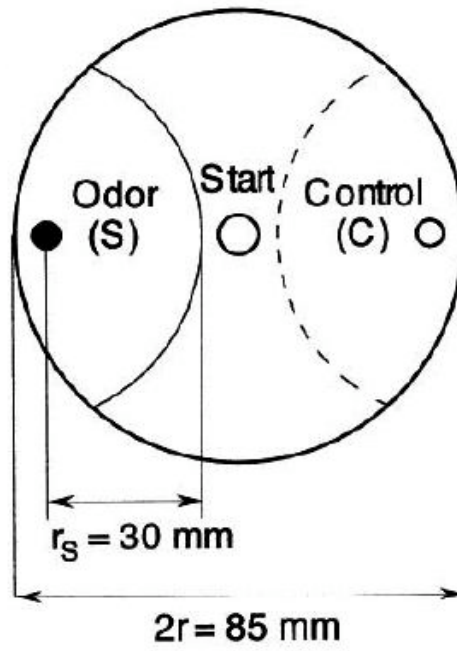
(A) The larval chemotaxis assay developed from Heimbeck (1999)

A round Petri dish covered by 1% agarose gel was separated into three districts: one side is odor, another side control, and the rest part is neutral. 3MM paper soaked with an undiluted odor in the lid of a microtube was placed on the odor side and water on the control side. Larva was placed in the middle facing the perpendicular direction to the odor. The larva was tracked for 10 minutes and checked the positioning place every 2.5 minutes.

(B) Scoring method for larval chemotaxis assay.

Initially I started from 0 point in the neutral region. For the first 2.5 minutes, I gave 2 points reward to those moving toward the odor side and -2 points penalty to those moving toward the control side. If a larva stays on the neutral region, I gave +0 point. In a subsequent movement, I gave +1 point to those moving from the control or neutral region to neutral or the odor side respectively. If they stay in same region, then I give them +1 (in the odor region), +0 (in the neutral region), and -1 (in the control region) point according to the district where they are found to keep staying. If they go backward to the neutral or control side from the odor side, I gave them -1 penalty. If they jump two districts, I gave them +2 or -2 points according to their moving direction. Therefore, the final score a larva wins is up to +5 points for the attraction and down to -5 points for the repulsion. Around +0 points indicates the indifference.

(A)



(B)

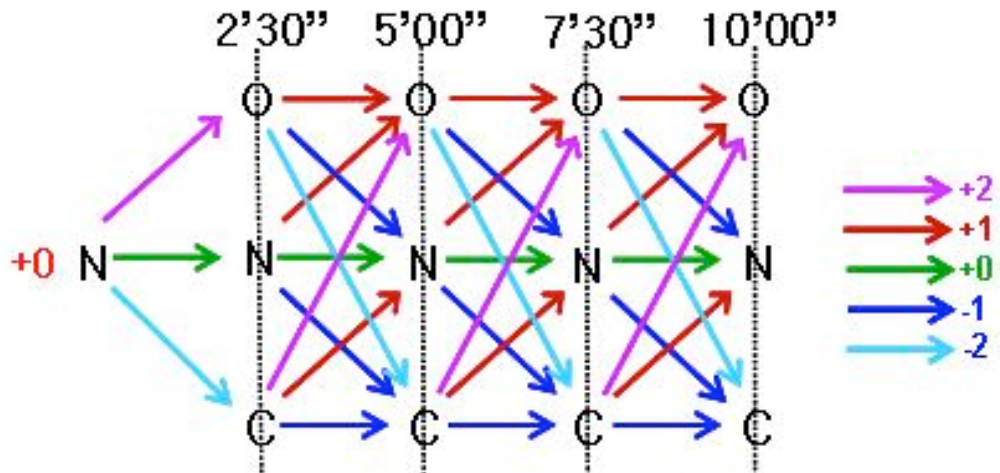


[Figure 4-6] The sound-evoked response of BBS mutants is indistinguishable from that of wild type.

(A) 6-14-1 and 1-5-1 are *BBS1* alleles. *BBS1*^{-/-} and *BBS1*^{-/+} show no different sound-evoked response. *BBS3*^{-/-} and *BBS3*^{-/+} also have normal sound-evoked response.

Consistently, *BBS8*^{-/-} and *BBS8*^{-/+} displays similar auditory response to the pulse stimuli.

(B) To test triallelic inheritance in *Drosophila* BBS mutants, *BBS1*^{-/-} combined with heterozygous *BBS4* deletion shows as similar auditory response as *BBS1*^{-/+} combined with heterozygous *BBS4* deletion.

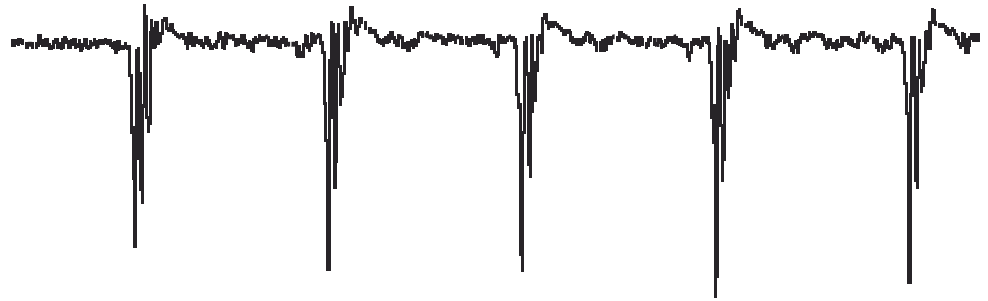
A



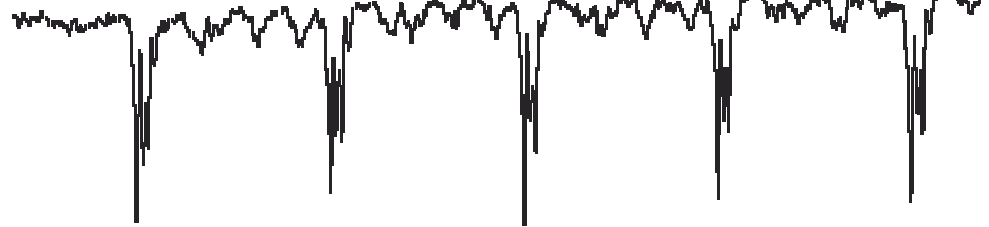
B



BBS1/+;BBS4/+



BBS1;BBS4/+



0.2mV
10msec

[Figure 4-7] Larval chemotaxis assay

To test *BBS1* and *BBS3* larvae for chemotaxis, two odors were used: 1-butanol and propionic acid. For a positive control, *canton-S*, *BBS1/TM3*, and *BBS3/CyO* were used and *Or83b^{-/-}* was used as a negative control. Positive controls show high attractant score, but negative control shows indifference to both odors. *BBS1* shows indifference to 1-butanol, but not significantly different from control to propionic acid. On the other hand, *BBS3* displayed no different response to both odors from positive controls.

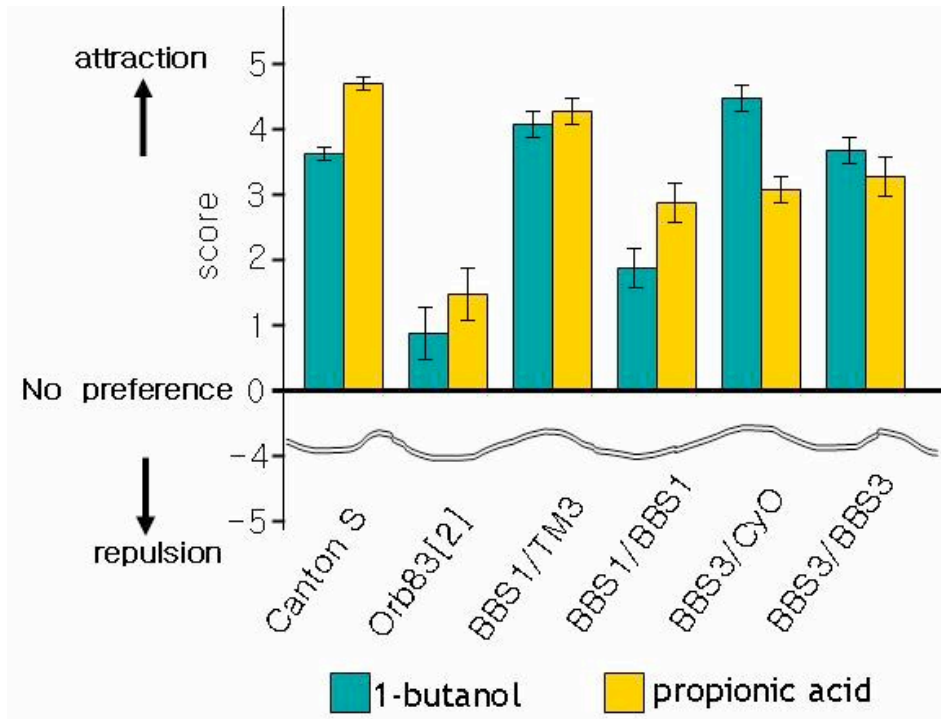


[Figure 4-8] The exponential gradient assay for larval chemotaxis of *BBS1* and *BBS3*

Larval behavior in the exponential gradient of isoamyl acetate was examined. The odor was administrated onto the inside of a 96well cell culture dish lid by diluting in paraffin oil. The larva was placed between the lowest (0.03M) and the second lowest concentration (0.06M) of isoamyl acetate on the 3% agarose gel on the top of a 96well cell culture dish lid (B). All the movement of each larva were tracked and recorded. Data were analyzed by wilcoxon test ($\alpha = 0.05$). N=18-20

(A) The chemotactic score of *BBS1* and *BBS3* shows that *BBS1* is considered not to be significantly different from *Or83b* null mutant ($p=0.72$) but significantly different from wildtype ($p=1.1 \times 10^{-4}$) when it is calculated for the 95% reliability. In contrast, *BBS3* displays difference from *Or83b* ($p=0.0334$), but no difference from wildtype ($p=0.12$). The taxis score of null is significantly different from that of the wildtype ($p=2.8 \times 10^{-6}$). Interestingly, *BBS3* has very wide distribution along the chemotaxis score though its median lies near the wildtype value.

(B) The schematic picture illustrates the outcast for the larval chemotaxis assay. It has 6 different concentrations of isoamyl acetate and indicates the initial position of a larva.

(C-E) Three zonograms present all the traces of larva toward the exponential gradient of isoamyl acetate. Wild type shows the concentrated traces on the string of gradient odors

(C). *BBS1* shows distracted traces (D), while *BBS3* shows comparatively concentrated but a bit wider distribution (E) than wild type.

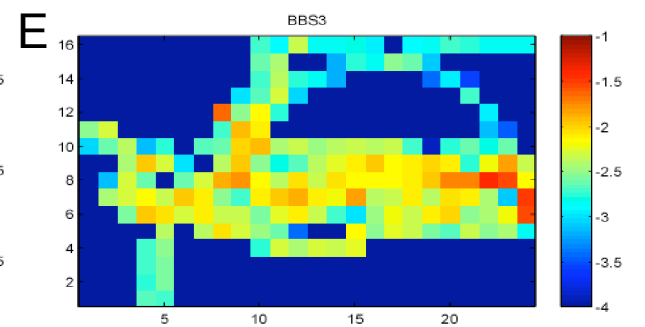
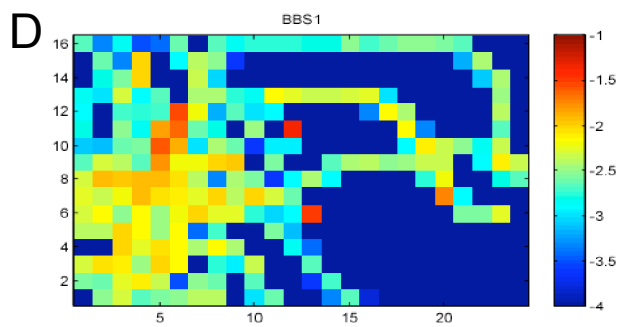
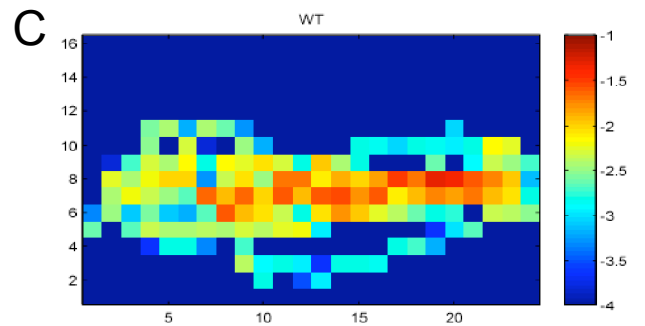
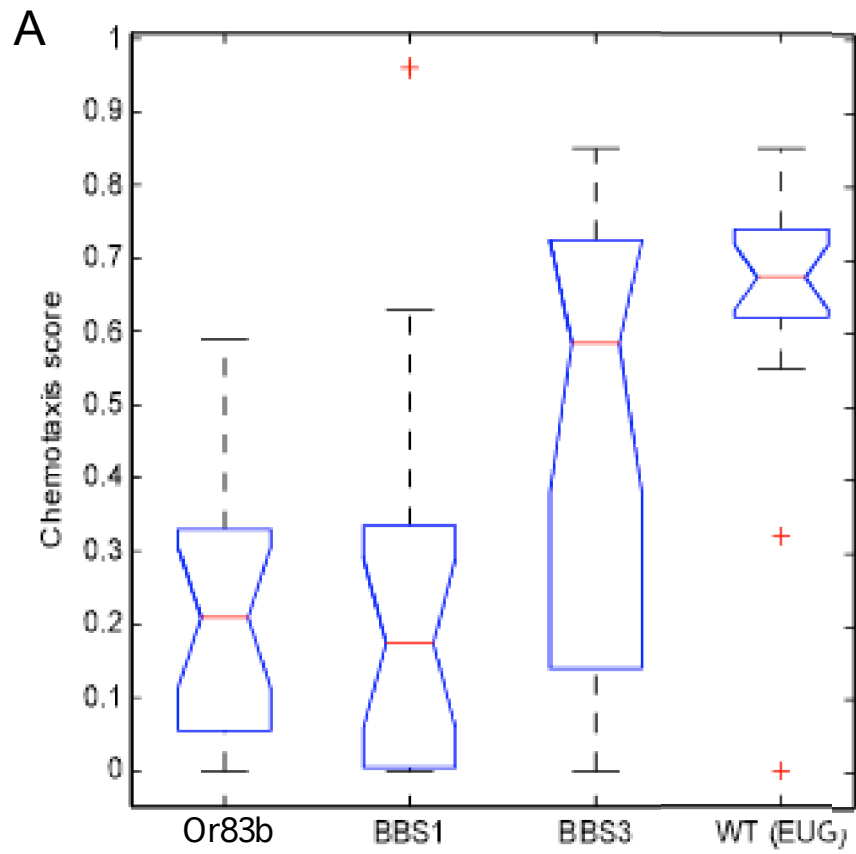
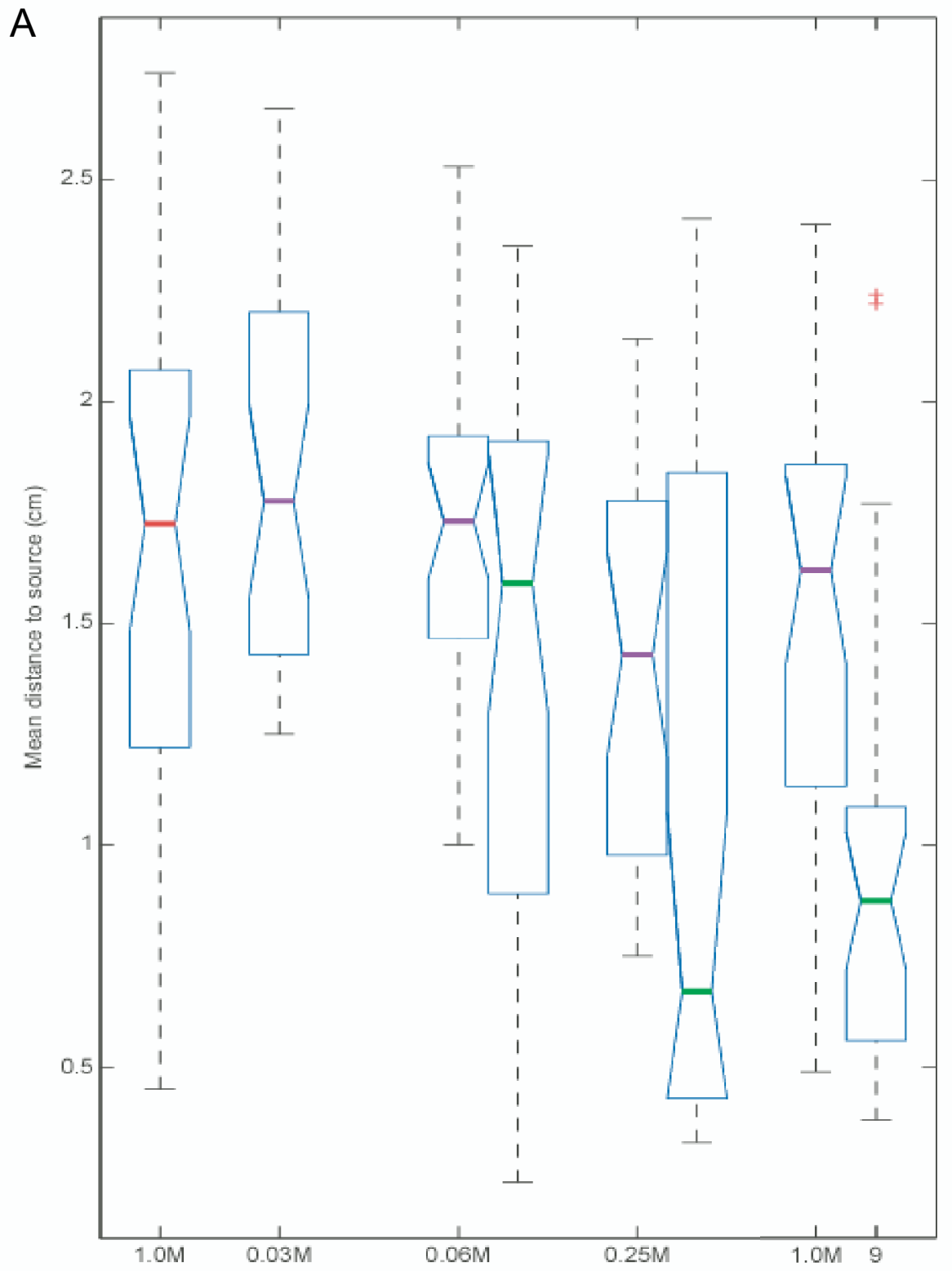


[Figure 4-9] Single droplet assay for *BBS1* and *BBS3*

It shows how far larvae stay around the odor of each concentration. The y-axis of the graph illustrates the mean distance (cm) to source, and the x-axis indicates each concentration of isoamyl acetate. Here 4 different concentrations were tested: 0.03M, 0.06M, 0.25M, and 1.0M. N=28-30.

(A) The longer mean distance indicates repulsion or undetectability. The mean distance of *Or83b* at 1.0M is significantly different from that of wildtype at 1.0M. When the mean distance of *BBS1* at each concentration was compared to the value of *Or83b* at 1.0M, all p values were bigger than 0.05 (0.0784 at 0.03M, 0.68 at 0.06M, 0.091 at 0.25M, and 0.72 at 1.0M), suggesting that the mean distance for *BBS1* is not different from that for *Or83b* in 95% reliability. It is noted that the mean distance of *BBS1* at 0.25M shows a moderate attraction to the odor, but, in this case, the wildtype has a wide distribution and also shows more attracted to odor than at higher concentration. (red, *Or83b*; blue, *BBS1*; green, *w¹¹¹⁸*)

(B) *BBS3* at 0.03M has not different mean distance from *Or83b* at 1.0M (p=1.0). However, *BBS3* shows higher sensitivity than wildtype at moderate concentrations (0.06M and 0.25M), showing a broad distribution. (red, *Or83b*; blue, *BBS3*; green, *w¹¹¹⁸*)



B

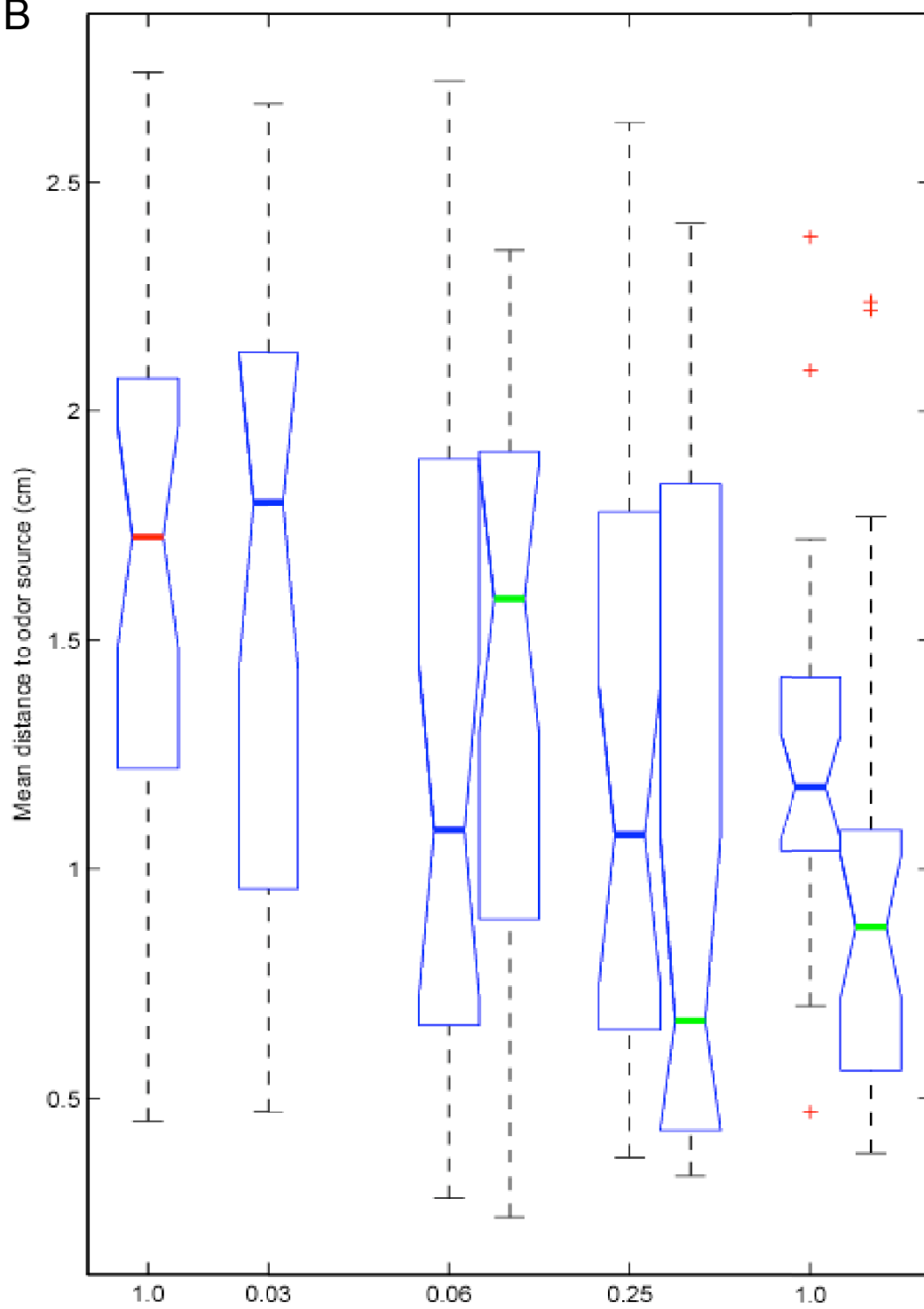


[Figure 4-10] The steep linear gradient assay for BBS3

BBS3 was tested in the steep linear gradient of isoamyl acetate from 0.0M to 0.5M (0.0M, 0.1M, 0.2M, 0.3M, 0.4M, and 0.5M). N=40

(A) The chemotaxis score shows that *BBS3* is significantly different from *Or83b* ($p=1.6 \times 10^{-8}$), but not significantly different from wild type ($p=0.0167$), suggesting that *BBS3* is attracted by isoamyl acetate and is able to detect the odor. However, alpha value threshold ($\alpha=0.0167$) corrected by Bonferroni correction is same as the p value of *BBS3* and wild type, suggesting that *BBS3* chemotax is not as completely normal as wild type. Bonferroni correction is for several independent tests which should be considered for statistical significance. Given alpha value ($\alpha=0.05$) may be appropriate for an individual comparison, but not proper for multiple sets. Therefore, lowered α value ($0.05/N$) is required to eliminate false positive.

(B-C) The zonogram collects the different traces from wild type (B) and *BBS3* (C). Whereas wild type displays the robust movement along the odor spots, *BBS3* shows high variations of traces. *BBS3* looks to reach the highest concentration of odor, but they don't follow the odor gradient line, suggesting that they might be sensitive enough to detect the odor from far distance.

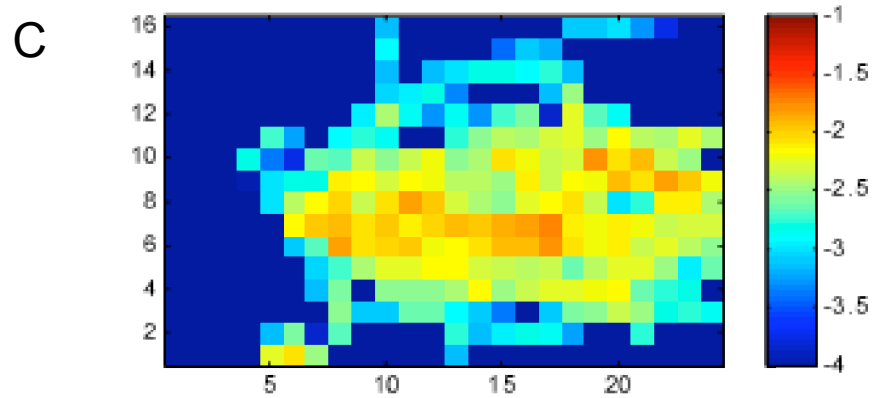
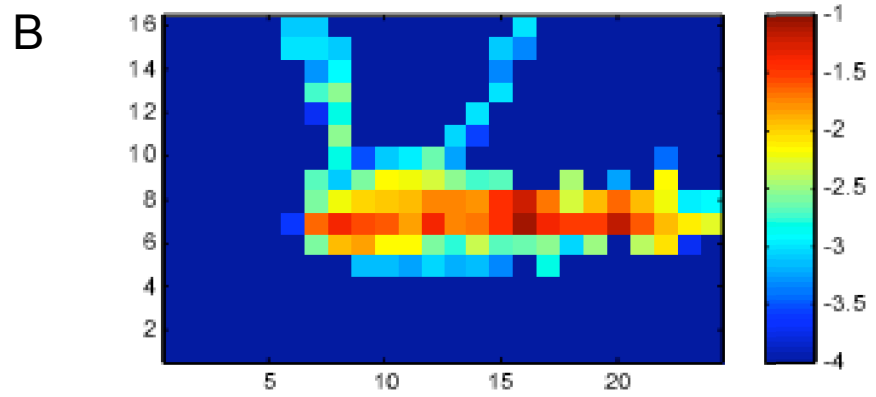
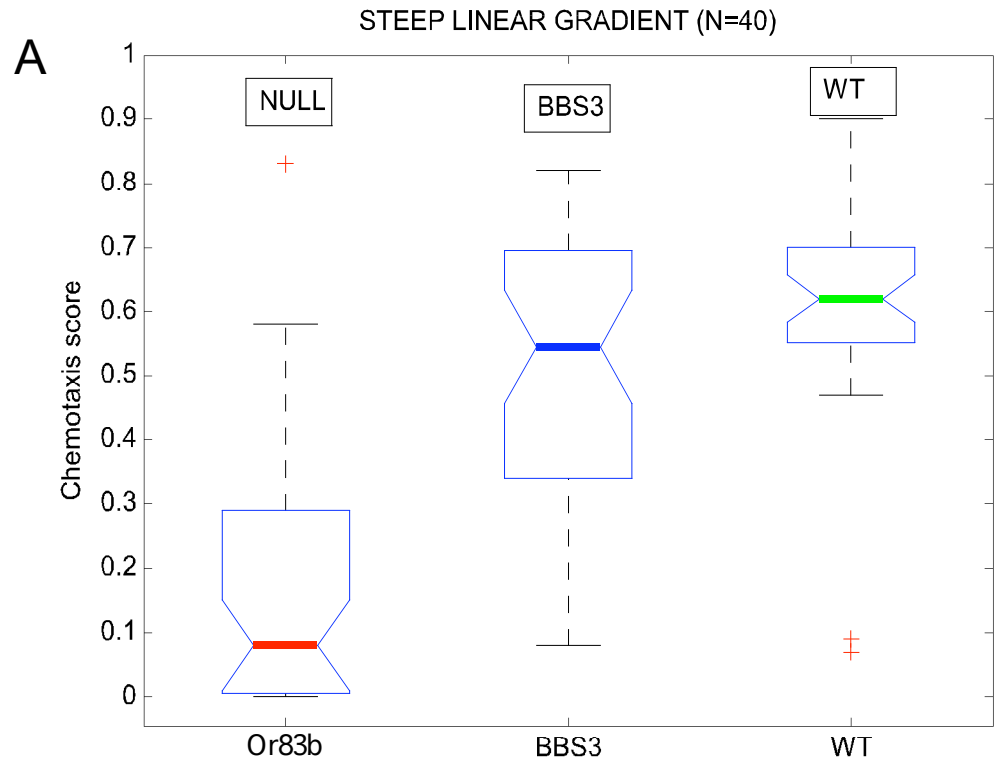


[Figure 4-11] PER test for *BBS* mutants

It shows proboscis extension reflex (PER) frequency of *BBS* mutants to a sugar solution.

Males and females showed no significant difference in PER. Control and *BBS1*

heterozygotes showed dramatically increased PER frequency to 1M sugar, whereas *BBS1*,

BBS3, and *BBS8* mutants exhibit severely lower frequency compared to the control. Line

indicates control or heterozygous and dot line signifies mutant.

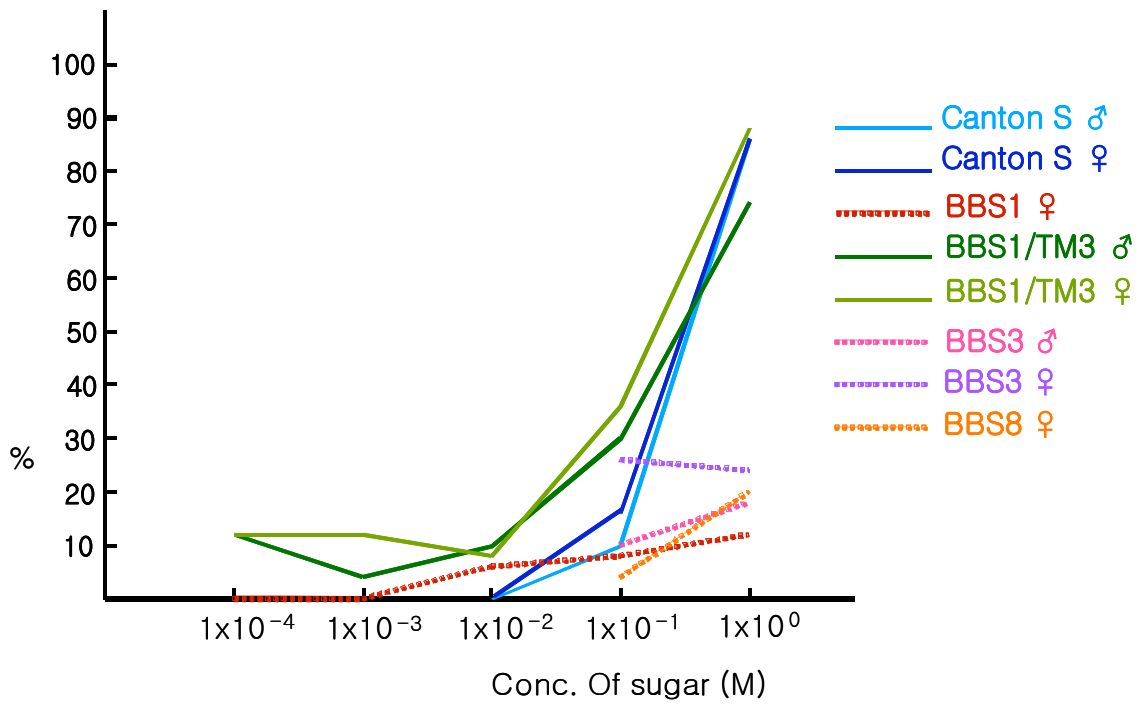


[Figure 4-12] The morphology of chemosensory cilia in BBS mutants

Membrane-bound mCD8::GFP expression in mechanosensory and chemosensory cilia in *BBS1*. First and third columns are *BBS1* heterozygotes, and second and fourth columns are *BBS1* homozygotes. There are cilia in wing margin at adult stage (A and B), and pupa stage (C and D). Cilia still present on legs (E, F) and femoral chordotonal organs (G and H). Second antennal segment (I and J) and third antennal segment (K and L) apparently do not have missing cilia.

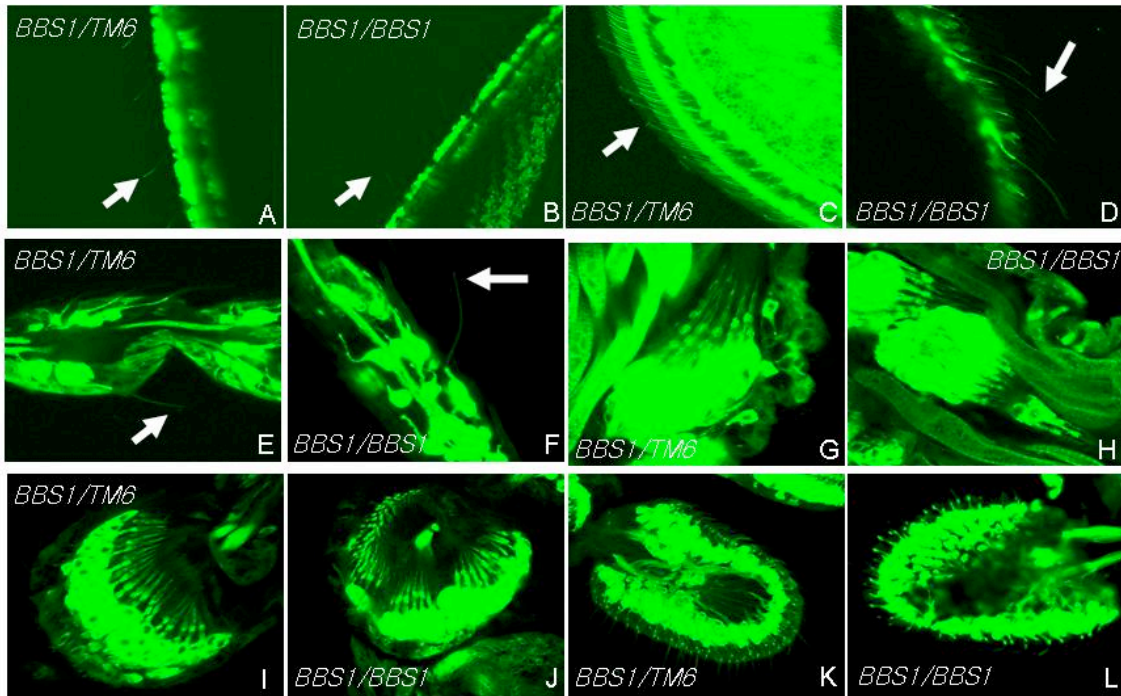
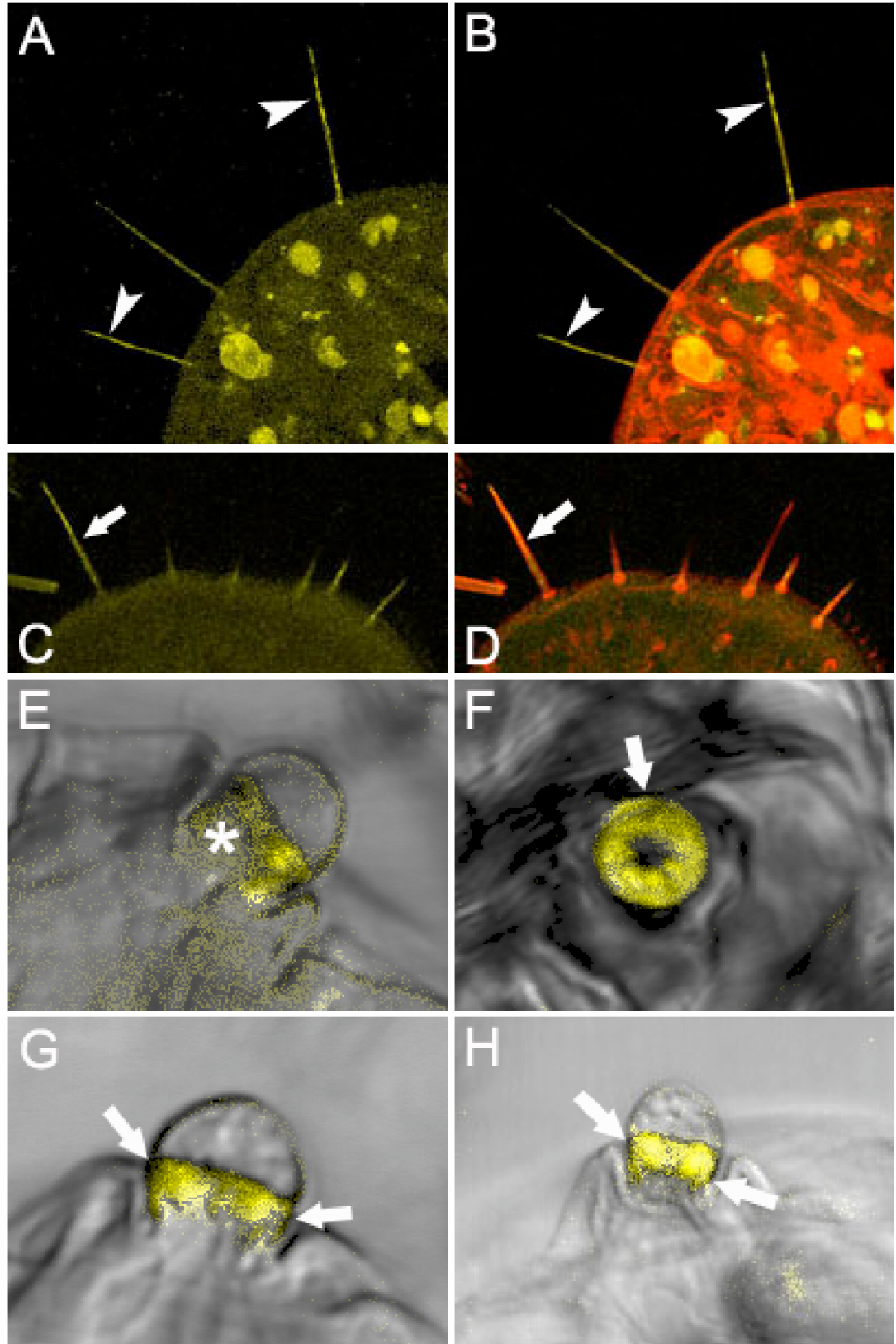


[Figure 4-13] The localization of BBS1 protein on chemosensory ciliated neurons

BBS1 localizes on chemosensory cilia of a labellum and a dorsal organ in a larva.

(A-D) The BBS1 signal was detected in chemosensory cilia of a pupal labellum. To visualize the surrounding structure, Alex568-conjugated phalloidin was used.

(E-H) A larva has two kinds of chemosensory organs: dorsal organ and terminal organ. BBS1 was found in dorsal organ (F-H), especially on the basal part of round shape of a dorsal organ. To confirm that the detected BBS1 signal is not an artifact, control larval chemosensory organs were examined (E). The autofluorescence (E, *) in the control larva was very dim compared to the BBS1 signal.



Chapter 5:

The roles of IFT & BBS proteins in Fly sensory cilia

1. IFT-A in mechanosensory cilia
2. Type I mechanosensory organs
3. BBS proteins in chemosensory cilia
4. A model for IFT-based transport in fly cilia

*IFT proteins are well conserved and are required for ciliary assembly and maintenance. From the analysis of Chlamydomonas and nematode mutants, IFT-A was previously known to be involved in retrograde transport. In this thesis, a special role of IFT-A proteins in mechanosensory cilia is inferred from the specific localization of REMPA on the ciliary dilation. The findings that the IAV ion channel was mislocalized in *btv* mutants and was not detected in *rempA* mutants suggest that the ciliary dilations sort chordotonal-specific transducing molecules to proximal cilia in a dynein-dependent manner. This result, together with their domain composition, also supports the idea that IFT proteins evolved from COP vesicle coat proteins. The different localization of REMPA on the connecting cilium in *es* organs and on the ciliary dilation in *ch* organs proposes that REMPA might have different roles in *es* and *ch* organs. Moreover, the localization of TRPV proteins relative to the ciliary dilation in chordotonal organ highlights the function of the ciliary dilation on chordotonal cilia for mechanosensory transduction. However, what REMPA does on the connecting cilium in *es* organs is not clear.*

BBS proteins couple transport of IFT-A and IFT-B subcomplexes in nematode sensory cilia. However, BBS function does not affect IFT-based ciliogenesis in Drosophila, unlike in C. elegans. Mechanosensory behavior and REMPA localization are normal in fly BBS mutants. Chemosensory defects were discovered by larval chemotaxis assay and PER assay. The BBS1 localization is specific to chemosensory organ. This indicates that BBS function is partly involved in ciliary function but selectively adapted to chemosensory transduction. However, how BBS function is involved in chemosensory function, and which subset of chemosensory cilia is affected, remain to be answered.

1. The role of IFT-A in mechanosensory cilia

IFT proteins have been considered to be involved in ciliary assembly and maintenance (Cole et al., 1998). Though ciliary function is crucial in significant signaling transduction like Hedgehog or PCP, the underlying mechanism how IFT particles are involved in signal transduction are unknown (Huangfu and Anderson, 2005; Huangfu et al., 2003; Park et al., 2006). A recent study on *Chlamydomonas* first demonstrated that IFT is directly associated with the signaling transduction of gamete mating (Wang et al., 2006). It is challenging to investigate a role of IFT proteins other than in ciliary assembly, because IFT is an essential pathway for ciliary build up. Details of how IFT proteins are working and interacting in ciliogenesis are not determined yet. In this regard, findings from REMPA on ciliary dilations suggest several possible roles of IFT-A proteins implicated in ciliary function for mechanosensory transduction.

Johnston's organ containing about 100 scolopidial units is in charge of the response to sound in *Drosophila* (Eberl et al., 2000). Chordotonal organs are found in insects and crustaceans of Arthropoda (Merritt, 1997). A ciliary dilation is a unique structure having paracrystalline inclusion and it is only discovered in chordotonal organs. While IFT-B related mutations lead to missing cilia, mutations in *rempA* and *oseg1* resulted in truncated cilia and disrupted ciliary dilations. *btv* is the mutant having the full length of cilia without a ciliary dilation, which instead is filled with vacuoles (Eberl et al., 2000). These IFT-A related mutants commonly have no sound-evoked response. This electrophysiological defect might be simply explained by shortened cilia which cause a disconnection from a dendritic cap. However, in addition to ultrastructure characteristics of these mutants where ciliary dilations are destroyed, the localization pattern of REMPA

on chordotonal cilia in different mutants provide an interesting insight on a specific role of IFT-A proteins and the ciliary dilation involved in ciliary motility or in mechanosensory transduction. Moreover, leaking of IAV into the distal zone of a ciliary dilation in *btv* suggests a significant function of a ciliary dilation in sorting cargoes. I summarized the localization pattern of REMPA, NOMPB and Eys in different mutant background in Fig 5-1.

REMPA is involved in retrograde transport

The different localization pattern of REMPA during development of mechanosensory cilia strongly suggests that REMPA possibly plays dual roles according to the development of cilia. REMPA labels along the cilia when cilia differentiate, but after which REMPA concentrates on ciliary dilations. During the maturation of chordotonal cilia, REMPA seems to be involved in retrograde transport in *Drosophila* sensory cilia. This is unequivocally supported by the accumulation of NOMPB in IFT-A mutants, *rempA* and *oseg1*. In larval and adult chordotonal organs, NOMPB accumulates on the distal tip of truncated cilia. NOMPB accumulation was found on the tip of inner segment of missing cilia in *kinesin-II* null mutants (Han et al., 2003), while REMPA appeared very faint on the tip of *kinesin-II* null mutant inner segment. This indicates that the stability of IFT-B proteins might not be influenced by dysfunction of retrograde proteins and motors.

In contrast, no REMPA signal in *oseg1*, another IFT-A mutant, at early and late developmental stages was detected, indicating that the interaction within a subcomplex seems required for the protein stability or expression. Therefore, the defect of one IFT-A protein might lead to the disruption of IFT-A subcomplex, consequently resulting in an

impaired ciliogenesis. However, NOMPB is not degraded in *btv* and accumulates at the distal tip of chordotonal cilia. This implies that BTV might partly play a role as a retrograde motor. *btv* cilia are not truncated, unlike *rempA* cilia. Since the consequence of ciliary differentiation is the formation of ciliary dilations, REMPA is required for the ciliary dilation formation, presumably which might be needed for the completion of the full length of cilia including a distal zone of a ciliary dilation in cilia development. In this regard, it is likely to be more important that REMPA is a component of ciliary dilations than that REMPA is involved in retrograde transport.

REMPA is a component of a ciliary dilation

The concentration of REMPA on a ciliary dilation as a result of ciliary differentiation suggests that REMPA is a molecular component of ciliary dilations. With lack of OSEG1, another IFT-A particle, REMPA was not detected in truncated chordotonal cilia. This is distinguished from the accumulated NOMPB on the tip of shortened cilia in *oseg1* and *rempA*, IFT-A mutants which lack a ciliary dilation. Even at the early developmental stage of *oseg1* cilia, REMPA was not detected in the cytoplasm, implying that REMPA and OSEG1 might require each other for either expression or protein stability for the IFT-A complex formation. Interestingly, the lack of a ciliary dilation in *btv* dispersed REMPA along the cilia, accumulating REMPA at the distal end of cilia. Moreover, REMPA was located on the reduced ciliary dilation which distally mislocalized inside a dendritic cap in *kinesin-II* hypomorph.

Conversely, the developmental observation of NOMPB localization discovered that NOMPB clustered around the ciliary dilation after cilia matured not specifically present on the ciliary dilation, unlike REMPA. In *kinesin-II* null mutant, NOMPB was

accumulated on the tip of inner segment of missing cilia, but REMPA was dimly detected. This suggests that IFT-A and IFT-B molecules in *Drosophila* chordotonal cilia behave differently. If REMPA was examined in *nompB* mutant where cilia are missing, REMPA might be detected in a similar pattern to that in *kinesin-II* null mutant. Taken together, these findings suggest that IFT-A proteins compose the ciliary dilation.

Another resilient evidence supporting the idea that REMPA protein is a component of the ciliary dilation is that IFT proteins have a structural similarity with COPI and clathrin vesicle coats (Avidor-Reiss et al., 2004) (Fig. 2-7). The composition of their protein structure are similar in that they have N-terminal WD40 repeats folding into β -propeller and C-terminal TPR motifs folding into α -superhelical structure. These COPI and clathrin vesicle proteins are involved in intracellular trafficking (Kirchhausen, 2000). Indeed, REMPA has 5-6 WD repeat at N-terminus and 7-8 TPR motifs at C-terminus (Fig. 2-7A). Moreover, the contour of a ciliary dilation obtained by EM is very similar to COP vesicles (Gurkan et al., 2006). Interestingly, ultrastructure analysis of ciliary dilations shows a repeat pattern of an electron dense structure which is dependent on the level of section plane. Based on the structural configuration and domain structure similarity between IFT-A proteins and coated vesicles, the function of coated vesicles suggest that the ciliary dilation composed of IFT-A supercomplex might be involved in sorting cargoes, though the mechanism underlying how a ciliary dilation is formed is not determined.

A ciliary dilation might function as a sorting station

What does the ciliary dilation composed of IFT-A supracomplex do on the chordotonal cilia? *btv* mutant is a very useful material to investigate this issue. *btv* is a

mechanosensory mutant, showing no sound-evoked response, like IFT-A mutants (Avidor-Reiss et al., 2004; Eberl et al., 2000). EM analysis (Eberl et al., 2000) and RFP expression (Fig. 3-11) revealed that *btv* retain a full length of a chordotonal cilium but a ciliary dilation is absent. REMPA and NOMP B localization in *btv* chordotonal cilia resulted in a similar pattern, scattering along the cilia with accumulation at the distal tip of cilia. This strongly supports that BTV functions as a retrograde motor and is not related to IFT protein stability.

In particular, a previous finding that TRPV ion channels, which is required in chordotonal cilia to produce sound-evoked potentials and to regulate their active motility, is normally localized proximal to the ciliary dilation suggests that a ciliary dilation might limit the localization of TRPV proteins (Gong et al., 2004). In *btv* where a ciliary dilation is absent, a TRPV subunit, IAV leaks into the distal zone of cilia. This assures the role of a ciliary dilation for the proper position of channel proteins.

Then, does a ciliary dilation play a role as a simple barrier or have a more complex function? If a ciliary dilation serves as a barrier, IAV might localize on the proximal zone to a ciliary dilation in *rempA* cilia. IAV, however, was not detected in *rempA* (Fig. 3-15) as well as in *osegl* (nonpublished data). Moreover, the IAV localization illustrates a proximal cilia as well as a round-shaped bulb on a ciliary dilation in larval chordotonal cilia (Gong et al., 2004). Though this was not detected in adult chordotonal cilia, this difference might be caused by a different developmental stage when the signal was examined. In an early stage right after the ciliary differentiation completes, the IFT complex including cargoes such as transducing molecules stops by a ciliary dilation and the cargo would be resorted into new subcomplex for proper destination. After the proper localization of these molecules, very small amount of

proteins would be replaced by IFT transport, which makes it impossible to detect the amassed localization on the ciliary dilation. This is why IAV was not detected in *remPA* and *oseg1* where a ciliary dilation is disrupted.

Conversely, REMPA localization was not affected by *iav* mutation, indicating that REMPA is activity-independent. The presence of a ciliary dilation might be primarily required for the localization of IAV. These suggest a novel model on the role of ciliary dilation and a transporting mechanism that a ciliary dilation might function as a sorting station where transducing and signaling molecules are resorted for a proper localization.

A ciliary dilation is mostly found near a dendritic cap. And two ciliary dilations innervated in one scolopale cell are observed to position in non-overlapped plane. Though the apically mislocalized ciliary dilation inside a dendritic cap by hypomorphic activity of Kinesin-II protein suggests the possible modulating function of Kinesin-II and BTV on the formation of a ciliary dilation, it is not known how they are involved in the ciliary dilation formation and what signal actually have it to form on that position, which is especially intriguing. In addition, it is still not clear whether a ciliary dilation is directly correlated to mechanosensory transduction than in sorting. Besides, whether a ciliary dilation keeps dynamically changing a position to tune mechanosensory stimuli remains to be answered.

The function of BTV and the ciliary structure for mechanosensory transduction.

In order to document a role of a ciliary dilation, it requires elaborating the role of BTV because *btv* mutant has no ciliary dilation and is instead filled with vacuoles but has a full length of cilia. Why do retrograde IFT-A mutants have short cilia but a *btv*,

retrograde dynein motor mutant, doesn't, despite they are all involved in retrograde transport? The stability of IFT-A proteins are dependent on each other and independent on BTV. This was partly clarified by no detection of REMPA in *oseg1* and delocalized REMPA along the cilia in *btv*. This might currently account for why IFT-A defect results in truncated cilia and dysfunction of BTV leads to a full length of cilia. The dispersed localization pattern of REMPA and NOMP B in *btv* suggests the retrograde motor function of BTV. The lack of retrograde motor might deliver and accumulate the IFT molecules to the far end of cilia tip. However, the possibility suggested by the replacement of ciliary dilation with vacuole cannot be excluded that BTV also plays an important role in ciliary dilations, like stabilizing molecules in ciliary dilations. BTV with IFT-A proteins might constitute a ciliary dilation, being involved in protein sorting. This indicates that transporting mechanism in *Drosophila* mechanosensory cilia might be different from other organisms such as *Chlamydomonas* or nematodes. The intriguing pattern of REMPA and NOMP B localization on different mutant backgrounds provide a new interpretation on the functional structure of the mechanosensory cilia.

How is Eys involved in mechanosensory transduction?

Recently, *eyes shut (eys)* was identified to encode Agrin/Perlecan-related proteoglycan involved in interrhabdomeral space formation which is required for the optical isolation of individual photoreceptor cells during eye development (Husain et al., 2006). 21A6 is a mAb against Eys. The localization of REMPA and Eys in mechanosensory cilia uncovered that only REMPA specifically detects ciliary dilations so far, and 21A6 labels around the ciliary base and, most predominantly, concentrates in the lumen area proximal to ciliary dilations. As a result of localization of Eys in different

mutant backgrounds, *Eys* is likely to be related to ciliary morphology, especially an axonemal structure. In the mutants which have a normal axonemal structure like *iav* and *kinesin-II* hypomorph, *Eys* localization is normal. In IFT-A, IFT-B, and *btv* mutants where axonemal defects are found, *Eys* delocalized to the base of cilia. This suggests that there might be a protein on the corresponding cilia to interact with *Eys*. The chordotonal cilia stained by horseradish peroxidase (HRP), which basically labels the multiple carbohydrate epitopes on neuronal membranes (Jan and Jan, 1982; Sun and Salvaterra, 1995), appears markedly curled to touch a scolopale cell membrane (Husain et al., 2006). Therefore, I hypothesize that, like the function of *Eys* in the epithelium lumen formation and maintenance in eye development, *Eys* presumably plays an important role to keep two or three cilia which are innervated in a scolopale cell isolated individually and separate from a scolopale inner membrane cell in a mechanosensory organ in order to facilitate the ciliary motility. It will be interesting to examine the localization of REMPA, NOMP, and IAV in *eyes* mutant cilia in order to know if the behavior of IFT proteins and channel proteins are affected by *eyes* mutation. Indeed, *eyes* affects auditory response but not severely (personal communication with Dr Kernan), which might be due to abnormal position of mechanosensory cilia inefficiently supported by *Eys* matrix in the scolopale lumen.

2. Type I mechanosensory organs

es and chordotonal organs categorized in type I sensory organ in *Drosophila* share several common features. They all have ciliated neuron surrounded by accessory cells, but it was thought that they might possess different transducing mechanisms due to

the structural difference. Indeed, different transducing components were suggested in two ciliated organs. First identified TRP channel involved in mechanosensory transduction, NompC, has dramatic defect in bristle mechanosensory current but a slight defect in sound evoked response (Walker et al., 2000). TRPV channel subunits, IAV and NAN, are only expressed in chordotonal organs (Gong et al., 2004). Though NOMPC localization in sensory organs has not been defined, the examination of auditory mechanics by measuring the sound-evoked vibration on transducing channel mutants suggests that NOMPC also contributes to chordotonal transduction (Gopfert et al., 2006). The comparison of transducing mechanism is a good way to learn how functionally and evolutionally two sensory organs are related. The addition of protein localization result will potentially flourish the discussion on two ciliated organs which yet have different functional and structural properties. In particular, the restricted localization of REMPA on a ciliary dilation makes it intriguing to compare two ciliated organs in the view of linking the function with structure. Initially we thought that the tubular body in es organs would be a functional equivalent of the ciliary dilation in chordotonal organs because their morphological silhouette of having a bulky structure is similar and the ciliary dilation has been considered to be an modified tubular body (Keil, 1997).

In addition to the bulky appearance of two structures, it is also similar that both a ciliary dilation and a tubular body place close to a dendritic cap through which presumably the mechanical stimuli may be delivered. Thus, the initial speculated position of REMPA in es organs was a tubular body. However, REMPA labeled a ciliary dilation in chordotonal organs and a connecting cilium in es organs. Besides, NOMPB seems to concentrate around a ciliary dilation after ciliary differentiation. In chordotonal organ, NOMPA labels from around the ciliary tip of double microtubules extending to the distal

end near the cuticle. EM showed scolopale rods extending to the cuticle which pattern was also observed by phalloidin staining. In es organ, NOMPA stains the whole surface of a tubular body which physically contacts a bristle base. Based on these structural proteins specifying the compartment of cilia in each organ, we propose an interesting model to explain the functional equivalent of two distinct sensory organs in *Drosophila* (Fig. 5-2).

The connecting cilium of es organs is the equivalent of the ciliary dilation of chordotonal organs, based on REMPA localization. The tubular body in es organs is directly connected to a bristle shaft through a dendritic cap, so that a tubular body might be the counterpart of the area covering ciliary tip to the far distal end connected to the cuticle, because this region is wrapped by NOMPA. This contains unidentified microtubule structure, and is where the stimulation is received from the cuticular stretch. According to this model, the proximal region of cilia where NAN and IAV localize restrictedly must be a featured zone of chordotonal cilia. Comparing to the ciliary structure of nematodes where a cilium is compartmented into middle segment of 9+0 and distal segment of microtubule singlet, we suggest that the distal part of nematode cilia is the functional counterpart of tubular body and long distal region after the ciliary dilation. Middle segment of nematodes functionally corresponds to a connecting cilium and a proximal cilia including ciliary dilation, though the scale would be slightly different. At this point, we can't determine which sensory organ is evolutionarily archaic, but each ciliary structure is morphologically well modified to commit a specific function.

The model for the functional equivalent of es and chordotonal organs that we propose is supported by the result of REMPA and NOMPB localization in *btv*. REMPA and NOMPB dispersed along the cilia in *btv* background, visualizing a distal

compartment of cilia. As described previously, *btv* (Eberl, 1999; Eberl et al., 2000) showed slightly different behavioral phenotype from the *rempA* flies. *btv* flies are sedentary while *rempA* flies are uncoordinated. Consistently, electrophysiological recording discovered that both flies have a defect in auditory response. However, *btv* flies don't have defective mechanoreceptor potential (MRP) in thoracic macrochaete bristles (Eberl et al., 2000), while *rempA* shows severe deficits in MRP (Kernan et al., 1994). This allowed us to speculate that the structural difference of two sensory organs of *Drosophila* would selectively use the different set of proteins for ciliary assembly and sensory transduction. However, the examination of REMPA localization in *btv* es organs exhibited a similar pattern with discovered in *btv* chordotonal organs. REMPA labeling distally extended to the NOMPA labeling region in es organs. This suggests that BTV would function as a retrograde motor in es organs as well.

Then, why does BTV dysfunction result only in dramatic defect of sound-evoked response in chordotonal organs and no obvious defect in es organs? This might be able to be explained by the fact that a ciliary dilation and TRPV channel subunits are only specific to chordotonal organs. If the ciliary dilation serves as a sorting station, signaling transducers are reorganized first in ciliary dilations and come back to locate on proximal cilia. Retrograde motor would be required for this. The malfunction of retrograde motor would generate the pattern of IAV localization similar to REMPA or NOMPB in *btv*. I propose this is why *btv* mutant phenotype doesn't include the proprioceptive defect in es organs, although BTV localizes on both es and chordotonal organs. That is, TRPV channel is specific to chordotonal organs and proper localizations of these molecules require the resorting in ciliary dilations, but es organs don't necessarily have ciliary dilation structure nor transducing apparatus to resort. Although the big damage of

chordotonal organs in *btv* is easily explicated by the different structural characteristics demanding specific molecules, how is no defect in es organs where BTV dysfunction was proved to affect IFT molecules able to be interpreted? Btv function in es organs might be limited to a retrograde function during ciliary differentiation, or the electrophysiological recording might not satisfy the resolution window to detect a subtle defect caused by mutant in *btv*. The identification of BTV localization would help to make up the model. IFT transporting for mechanosensory transduction in chordotonal cilia including ciliary dilations might not be a simple process or an organization.

3. The role of BBS proteins in chemosensory cilia

The evidence of BBS proteins being related to a ciliary function.

All known orthologs of the mammalian Bardet-Biedl syndrome (BBS) proteins are expressed specifically in ciliated sensory neurons in *C. elegans*, raising the possibility that disruption of these proteins will lead to ciliary defects. Several reports on their expressions, localizations and mutants phenotypes strongly suggested that they would be involved in ciliary function. It is proposed that BBS function might be associated with cilia due to the following reasons: First, most of BBS proteins are localized on cilia or the related structure, particularly near the pericentriolar region around the basal body, in *C. elegans* and *D. melanogaster* (Avidor-Reiss et al., 2004; Blacque et al., 2004; Li et al., 2004). In mice, immunostaining reveals the specific localization of BBS on ciliary tissues. Second, the phenotype of BBS animal models attests to the functional possibility of BBS on cilia. For example, BBS1 and BBS4 patients have anosmia, and *BBS1, 4 and 2* null mice displayed olfactory dysfunction; Loss of BBS7 and BBS8 in *C. elegans*

compromises the IFT function and causes the defect in chemotaxis to volatile compounds. In addition, the disruption of *BBS5* in *Chlamydomonas* inhibited flagella formation. Third, the conservation of X-box, the element regulated by *rfx* transcriptional factor, on the promoter region of almost all *BBS* genes in *C. elegans* and *Drosophila* implicates the regulation of expression on cilia (Ansley et al., 2003; Avidor-Reiss et al., 2004; Haycraft et al., 2001; Li et al., 2004), in that it is uniquely expressed on cilia. Most of genes extensively expressed in cilia contain the binding element of RFX. These examples substantiate that the function of BBS will be correlated with cilia. However, it remains unanswered how BBS proteins are implicated in ciliary function and how they cooperate when functioning *in vivo*.

BBS function limited to chemosensory transduction in Drosophila

The function of BBS proteins is obviously distinguished from that of IFT molecules in *Drosophila*. The normal morphology in mechano and chemosensory cilia and normal localization of REMPA on a ciliary dilation in *BBS1* and *BBS8* mutants indicates that BBS proteins are not involved in IFT-based ciliogenesis. It seems eminent that BBS proteins have a ciliary function (Avidor-Reiss et al., 2004). However, a series of evidences obtained from testing *BBS1*, *BBS3*, and *BBS8* mutants presented no mechanosensory function. The triallelic recombination of *BBS1-BBS4* and *BBS1-BBS8* did not produce any defective behavior or impaired auditory response at all. The homozygotic and triallelic recombined flies are not only very coordinated in the context of walking, flying, jumping, and standing but also are viable and fertile. Instead, larval chemotaxis assay and PER test revealed that *BBS* mutants have chemosensory specific defects. *BBS1* protein specifically localizes in chemosensory cilia. These findings

strongly suggest that BBS proteins are involved in chemosensory transduction. It is likely that BBS function is only limited to subset of sensory cilia. This case is also found in BBS 4 null mice where not all cilia are affected in the body (Mykytyn et al., 2004). These proteins might be involved in a specific pathway of chemosensory signaling or in trafficking of olfactory receptors or gustatory receptors.

I found that *BBS1* and *BBS3* mutants show a bit different chemosensory defect pattern. *BBS1* has severe chemosensory defect. The larval behavior of *BBS3* mutants to olfactory stimuli doesn't look different from wild type. But an elaborating experimental setup revealed that BBS mutants have higher sensitivity to lower concentrations of an odor and not perfectly succeed to find the highest odor concentration as wild type. Though I found chemosensory defect of *BBS* mutants and localization of BBS1 on chemosensory organs, it is not known what BBS proteins do in fly chemosensory transduction. BBS3 is small GTP binding protein found to localize in chemosensory cilia in *C. elegans* (Fan et al., 2004). The mutant phenotype was not identified but it transports along the cilia with IFT particles (Fan et al., 2004). The examination on the localization of olfactory receptors or gustatory receptors in *BBS* mutant backgrounds will reveal if BBS proteins are involved in chemosensory receptor trafficking in *Drosophila*. If BBS proteins are not required for ciliogenesis but involved in facilitating IFT function, the test for the location of IFT in *BBS* mutants might not be sufficient to see obvious defect with the loss of BBS. In this case, it might be better to test IFT subcomplex A and B flows in *BBS* mutants using time-lapse spinning-disc microscopy.

4. The IFT-based transporting Model in fly cilia

IFT-based ciliogenesis is independent of BBS function in Drosophila

Assembly of sensory cilia in *Drosophila* is different from in nematodes. This is determined by several evidences. First, BBS proteins are not involved in IFT transport in *Drosophila* sensory cilia. This was supported by the normal ciliary morphology and normal localization of REMPA on ciliary dilations. In nematodes, *BBS* mutations result in truncation of sensory cilia. A mutated BBS8 leads to different velocity of each IFT subcomplex, suggesting that BBS8 might couple two subcomplexes (Ou et al., 2005). This ultimately ends up with accumulated of IFT-B on truncated cilia because IFT-B is connected to OSM-3 motor which solely transports into the distal segment. However, BBS1 and BBS8 deletions and BBS3 insertion do not lead to any defect related to ciliary morphology and to localization of IFT molecules in *Drosophila*. Rather, BBS function in *Drosophila* appears to be limited to chemosensory transduction, in contrast to nematodes where BBS proteins directly involved in IFT transporting and its facilitation. However, How BBS proteins contribute to chemosensory transduction is not determined.

Secondly, the different morphology of *dyf-1* cilia suggests that DYF-1 function might be distinct between *Drosophila* and nematodes. Nematode *dyf-1* mutant has truncated cilia, showing similar defect to *osm-3* mutant (Snow et al., 2004). *Osm-3* mutant loses distal segment which is dependent on OSM-3 (Snow et al., 2004). This result concluded that DYF-1 is an activator or a connector for OSM-3 and IFT-B complex. However, fly *dyf-1* mutants are missing cilia, and NOMP-B and REMPA were not detected in this mutant background. Missing cilia is a feature of IFT-B mechanosensory mutants. Because I didn't examine the REMPA localization in *nompB*, it is not able to be determined whether IFT-B affects the IFT-A complex stability or if IFT-B particles within IFT-B complex are required for one another for stability like IFT-

A. Interestingly, DYF-1 has two properties for IFT-A and IFT-B subparticles, as missing cilia is the feature of IFT-B proteins, and no detected REMPA signal was observed in *osegl* mutant. Taken together, these findings suggest that DYF-1 might be a component of IFT-B complex in *Drosophila* or function as a connector IFT-A and IFT-B subcomplexes. One interesting question is whether *Drosophila* uses other anterograde motor such as *osm-3*, like nematodes. *Drosophila* has *osm-3* homolog on 4th chromosome.

Thirdly, IFT-A function and localization on chordotonal cilia is unique in *Drosophila*. IFT-A particles are not simply involved in retrograde transport. They are elements of ciliary dilations with BTV. Compared to nematodes where IFT and BBS are all involved in IFT-based transporting (Fan et al., 2004; Ou et al., 2005; Snow et al., 2004), the ciliary dilation is a critical structure for channel subunit trafficking and localization. The characteristic structure requires specifically modified function of proteins and transporting mechanism.

A ciliary dilation is a core for IFT transport in chordotonal cilia

As previously described, a ciliary dilation is the key structure permitting the special transporting mechanism in chordotonal cilia of *Drosophila*. IFT-based transport is deeply related to the presence of a ciliary dilation. Based on the novel model (Fig. 5-3), a ciliary dilation is formed as a result of differentiation of cilia. This is composed of IFT-A particles and BTV. Previously, I have already explained the most of detailed about the behavior of molecules related to channel subunits or IFT particles in respect to a role of ciliary dilations according to this model. After a ciliary dilation is formed, the turnover of IFT-A particles might be very slow. The inducible transgene, UAS-REMPA tagged by YFP, will be able to show the turnover rate after ciliary dilations are formed in a wild

type background. How cargoes such as TRPV channel subunits are transported into the ciliary dilation by IFT complex is not known though I discovered ciliary dilations are required. Also, a sorting mechanism in ciliary dilations remained to be determined. How Kinesin-II and BTV motor are involved in this regulation is another interesting issue. Probably a lot of proteins are going to be implicated in this procedure and this mechanism will be very delicate and complicated. More molecules structurally and physiologically involved in mechanosensory transduction should be identified and characterized. Important hints could come from the molecules which are already identified in coated vesicles.

In conclusion, my thesis work found two ciliary proteins, IFT and BBS, are functionally distinct. It highlights that IFT mechanism and function in *Drosophila* chordotonal cilia which is different from conventional role of IFT proteins found in *Chlamydomonas* (Rosenbaum and Witman, 2002). I identified *rempA* encodes IFT140, one of IFT-A components and showed a ciliary dilation is composed of IFT-A proteins. Based on the findings, I propose that a ciliary dilation is a sorting station which partitions chordotonal cilia into two functionally distinct compartments, providing a basis for a novel mechanism of IFT-based transporting in *Drosophila* chordotonal cilia. Besides, BBS function is limited to chemosensory transduction in *Drosophila*.

[Figure 5-1] The summary of protein localization in mutants

In wild type chordotonal cilia, REMPA localizes specifically on the ciliary dilation. NOMPB localizes along the cilia, mostly concentrating around the ciliary dilation. REMPA localization was not altered in *iav* mutant. The localization of REMPA on the ciliary dilation is confirmed by the examination on *kinesin-II* hypomorph where REMPA was detected on the ciliary dilation whose location is shifted into dendritic caps. BBS proteins do not affect the REMPA localization. REMPA was not detected in *oseg1* mutant. NOMPB accumulates on the tip of truncated cilia in *oseg1* and *rempA*. REMPA and NOMPB were not detected in *dylf-1* and dispersed along the cilia in *btv*. IAV normally localizes on the proximal cilia in wild type, but in *rempA*, IAV was not detected. IAV was leaked into distal cilia in *btv*. Eys seems to be related to ciliary morphology. In mutants having the normal ciliary morphology, Eys have normal localization pattern as wild type.

Summary of protein localization in mutants

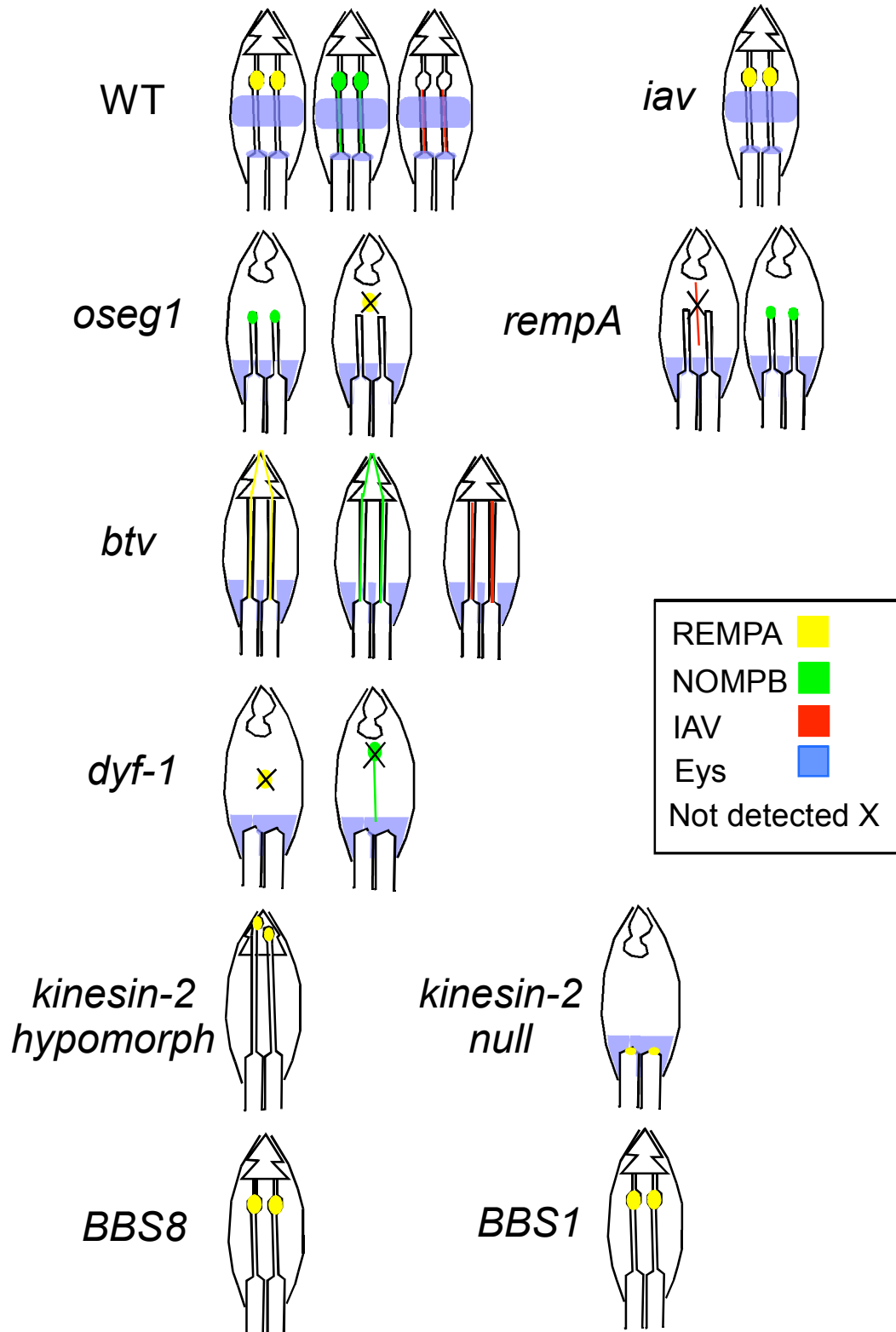
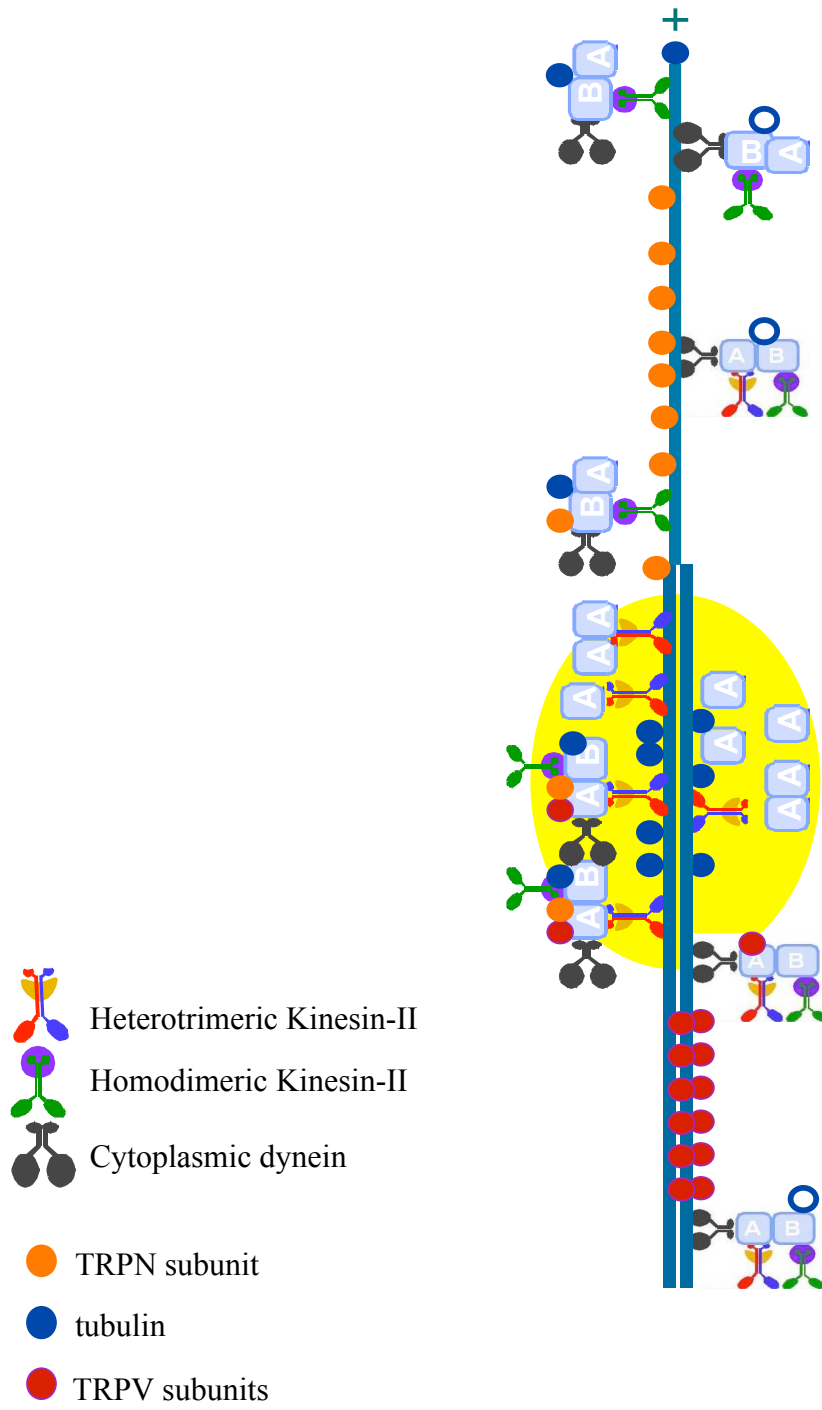


[Figure 5-2] The functional relationship between ES and CHO

Schematic shows the localization pattern of proteins identified in the structure of ES organ and chordotonal organ. Two chordotonal neurons are innervated in one scolopale cell. NOMPA surrounds the tubular body in ES organs and wraps the distal part of cilia near ciliary dilation in chordotonal organs. Eyes is found around a connecting cilium in ES organs, and found in lumen and on the base of cilia in a scolopale cell. IAV localizes specifically on the proximal to ciliary dilations in chordotonal organs. REMPA localizes on a connecting cilium in ES organs and ciliary dilations in chordotonal organs. The region covered by NOMPA in ES organs is equivalent to ciliary distal region in chordotonal organ. When a connecting cilium is considered to be correspondent to the region including ciliary dilations and the proximal cilia where IAV is found in chordotonal organs, this region in chordotonal organs is structurally and functionally modified for chordotonal role. It is interesting to know where NOMPC protein localizes, but it is not known yet.

[Figure 5-3] The IFT-based transporting mechanism in chordotonal cilia

A ciliary dilation is a sorting station where cargoes including TRPV channel subunits and signaling molecules are reorganized to target the proper destination. For example, IAV is transported to a ciliary dilation first and localizes back to proximal cilia by BTV. It is not clear if IFT-A and IFT-B molecules are always coupled. It is not known whether homodimeric Kinesin-II is used in sensory cilia in *Drosophila*.



Bibliography

- Adams, M. D., Celniker, S. E., Holt, R. A., Evans, C. A., Gocayne, J. D., Amanatides, P. G., Scherer, S. E., Li, P. W., Hoskins, R. A., Galle, R. F., *et al.* (2000). The genome sequence of *Drosophila melanogaster*. *Science* *287*, 2185–2195.
- Andersen, K. L., Echwald, S. M., Larsen, L. H., Hamid, Y. H., Glumer, C., Jorgensen, T., Borch-Johnsen, K., Andersen, T., Sorensen, T. I., Hansen, T., and Pedersen, O. (2005). Variation of the McKusick–Kaufman Gene and Studies of Relationships with Common Forms of Obesity. *J Clin Endocrinol Metab* *90*, 225–230.
- Ansley, S. J., Badano, J. L., Blacque, O. E., Hill, J., Hoskins, B. E., Leitch, C. C., Kim, J. C., Ross, A. J., Eichers, E. R., Teslovich, T. M., *et al.* (2003). Basal body dysfunction is a likely cause of pleiotropic Bardet–Biedl syndrome. *Nature* *425*, 628–633.
- Avidor–Reiss, T., Maer, A. M., Koundakjian, E., Polyanovsky, A., Keil, T., Subramaniam, S., and Zuker, C. S. (2004). Decoding cilia function: defining specialized genes required for compartmentalized cilia biogenesis. *Cell* *117*, 527–539.
- Badano, J. L., Ansley, S. J., Leitch, C. C., Lewis, R. A., Lupski, J. R., and Katsanis, N. (2003a). Identification of a novel Bardet–Biedl syndrome protein, BBS7, that shares structural features with BBS1 and BBS2. *Am J Hum Genet* *72*, 650–658.
- Badano, J. L., and Katsanis, N. (2002). Beyond Mendel: an evolving view of human genetic disease transmission. *Nat Rev Genet* *3*, 779–789.
- Badano, J. L., Kim, J. C., Hoskins, B. E., Lewis, R. A., Ansley, S. J., Cutler, D. J., Castellan, C., Beales, P. L., Leroux, M. R., and Katsanis, N. (2003b). Heterozygous mutations in BBS1, BBS2 and BBS6 have a potential epistatic effect on Bardet–Biedl patients with two mutations at a second BBS locus. *Hum Mol Genet* *12*, 1651–1659.
- Badano, J. L., Leitch, C. C., Ansley, S. J., May–Simera, H., Lawson, S., Lewis, R. A., Beales, P. L., Dietz, H. C., Fisher, S., and Katsanis, N. (2006). Dissection of epistasis in oligogenic Bardet–Biedl syndrome. *Nature* *439*, 326–330.
- Baker, J. D., Adhikarakunnathu, S., and Kernan, M. J. (2004). Mechanosensory–defective, male–sterile *unc* mutants identify a novel basal body protein required for ciliogenesis in *Drosophila*. *Development* *131*, 3411–3422.
- Baker, S. A., Freeman, K., Luby–Phelps, K., Pazour, G. J., and Besharse, J. C. (2003). IFT20 links kinesin II with a mammalian intraflagellar transport complex that is conserved in motile flagella and sensory cilia. *J Biol Chem* *278*, 34211–34218.
- Beales, P. L., Badano, J. L., Ross, A. J., Ansley, S. J., Hoskins, B. E., Kirsten, B., Mein, C. A., Froguel, P., Scambler, P. J., Lewis, R. A., *et al.* (2003). Genetic interaction of BBS1 mutations with alleles at other BBS loci can result in non–Mendelian Bardet–Biedl syndrome. *Am J Hum Genet* *72*, 1187–1199.

- Beales, P. L., Elcioglu, N., Woolf, A. S., Parker, D., and Flinter, F. A. (1999). New criteria for improved diagnosis of Bardet-Biedl syndrome: results of a population survey. *J Med Genet* *36*, 437-446.
- Bisgrove, B. W., and Yost, H. J. (2006). The roles of cilia in developmental disorders and disease. *Development* *133*, 4131-4143.
- Blacque, O. E., Li, C., Inglis, P. N., Esmail, M. A., Ou, G., Mah, A. K., Baillie, D. L., Scholey, J. M., and Leroux, M. R. (2006). The WD repeat-containing protein IFTA-1 is required for retrograde intraflagellar transport. *Mol Biol Cell* *17*, 5053-5062.
- Blacque, O. E., Perens, E. A., Boroevich, K. A., Inglis, P. N., Li, C., Warner, A., Khattra, J., Holt, R. A., Ou, G., Mah, A. K., *et al.* (2005). Functional genomics of the cilium, a sensory organelle. *Curr Biol* *15*, 935-941.
- Blacque, O. E., Reardon, M. J., Li, C., McCarthy, J., Mahjoub, M. R., Ansley, S. J., Badano, J. L., Mah, A. K., Beales, P. L., Davidson, W. S., *et al.* (2004). Loss of *C. elegans* BBS-7 and BBS-8 protein function results in cilia defects and compromised intraflagellar transport. *Genes Dev* *18*, 1630-1642.
- Bodmer, R., Carretto, R., and Jan, Y. N. (1989). Neurogenesis of the peripheral nervous system in *Drosophila* embryos: DNA replication patterns and cell lineages. *Neuron* *3*, 21-32.
- Boletta, A., and Germino, G. G. (2003). Role of polycystins in renal tubulogenesis. *Trends Cell Biol* *13*, 484-492.
- Burd, C. G., Strohlic, T. I., and Gangi Setty, S. R. (2004). Arf-like GTPases: not so Arf-like after all. *Trends Cell Biol* *14*, 687-694.
- Burn, R. A. (1950). Deafness and the Laurence-Moon-Biedl syndrome. *Br J Ophthalmol* *34*, 65-88.
- Caldwell, J. C., and Eberl, D. F. (2002). Towards a molecular understanding of *Drosophila* hearing. *J Neurobiol* *53*, 172-189.
- Carlson, J. R. (1996). Olfaction in *Drosophila*: from odor to behavior. *Trends Genet* *12*, 175-180.
- Carlson, S. D., Hilgers, S. L., and Juang, J. L. (1997). First developmental signs of the scolopale (glial) cell and neuron comprising the chordotonal organ in the *Drosophila* embryo. *Glia* *19*, 269-274.
- Carroll, K., Gomez, C., and Shapiro, L. (2004). Tubby proteins: the plot thickens. *Nat Rev Mol Cell Biol* *5*, 55-63.
- Casso, D., Ramirez-Weber, F., and Kornberg, T. B. (2000). GFP-tagged balancer chromosomes for *Drosophila melanogaster*. *Mech Dev* *91*, 451-454.
- Chao, A. T., Dierick, H. A., Addy, T. M., and Bejsovec, A. (2003). Mutations in eukaryotic

release factors 1 and 3 act as general nonsense suppressors in *Drosophila*. *Genetics* *165*, 601–612.

Chiang, A. P., Beck, J. S., Yen, H. J., Tayeh, M. K., Scheetz, T. E., Swiderski, R. E., Nishimura, D. Y., Braun, T. A., Kim, K. Y., Huang, J., *et al.* (2006). Homozygosity mapping with SNP arrays identifies TRIM32, an E3 ubiquitin ligase, as a Bardet–Biedl syndrome gene (BBS11). *Proc Natl Acad Sci U S A* *103*, 6287–6292.

Chiang, A. P., Nishimura, D., Searby, C., Elbedour, K., Carmi, R., Ferguson, A. L., Secrist, J., Braun, T., Casavant, T., Stone, E. M., and Sheffield, V. C. (2004). Comparative genomic analysis identifies an ADP–ribosylation factor–like gene as the cause of Bardet–Biedl syndrome (BBS3). *Am J Hum Genet* *75*, 475–484.

Chung, Y. D., Zhu, J., Han, Y., and Kernan, M. J. (2001). *nompA* encodes a PNS–specific, ZP domain protein required to connect mechanosensory dendrites to sensory structures. *Neuron* *29*, 415–428.

Clyne, P. J., Warr, C. G., and Carlson, J. R. (2000). Candidate taste receptors in *Drosophila*. *Science* *287*, 1830–1834.

Clyne, P. J., Warr, C. G., Freeman, M. R., Lessing, D., Kim, J., and Carlson, J. R. (1999). A novel family of divergent seven–transmembrane proteins: candidate odorant receptors in *Drosophila*. *Neuron* *22*, 327–338.

Cole, D. G. (2003). The intraflagellar transport machinery of *Chlamydomonas reinhardtii*. *Traffic* *4*, 435–442.

Cole, D. G., Chinn, S. W., Wedaman, K. P., Hall, K., Vuong, T., and Scholey, J. M. (1993). Novel heterotrimeric kinesin–related protein purified from sea urchin eggs. *Nature* *366*, 268–270.

Cole, D. G., Diener, D. R., Himelblau, A. L., Beech, P. L., Fuster, J. C., and Rosenbaum, J. L. (1998). *Chlamydomonas* kinesin–II–dependent intraflagellar transport (IFT): IFT particles contain proteins required for ciliary assembly in *Caenorhabditis elegans* sensory neurons. *J Cell Biol* *141*, 993–1008.

Corbit, K. C., Aanstad, P., Singla, V., Norman, A. R., Stainier, D. Y., and Reiter, J. F. (2005). Vertebrate Smoothed functions at the primary cilium. *Nature* *437*, 1018–1021.

D'Andrea, L. D., and Regan, L. (2003). TPR proteins: the versatile helix. *Trends Biochem Sci* *28*, 655–662.

Das, A. K., Cohen, P. W., and Barford, D. (1998). The structure of the tetratricopeptide repeats of protein phosphatase 5: implications for TPR–mediated protein–protein interactions. *Embo J* *17*, 1192–1199.

Davenport, J. R., and Yoder, B. K. (2005). An incredible decade for the primary cilium: a look at a once–forgotten organelle. *Am J Physiol Renal Physiol* *289*, F1159–1169.

de Bruyne, M., Clyne, P. J., and Carlson, J. R. (1999). Odor coding in a model olfactory organ: the *Drosophila* maxillary palp. *J Neurosci* *19*, 4520–4532.

de Cuevas, M., Tao, T., and Goldstein, L. S. (1992). Evidence that the stalk of *Drosophila* kinesin heavy chain is an alpha-helical coiled coil. *J Cell Biol* *116*, 957–965.

Deane, J. A., Cole, D. G., Seeley, E. S., Diener, D. R., and Rosenbaum, J. L. (2001). Localization of intraflagellar transport protein IFT52 identifies basal body transitional fibers as the docking site for IFT particles. *Curr Biol* *11*, 1586–1590.

Devaud, J. M. (2003). Experimental studies of adult *Drosophila* chemosensory behaviour. *Behav Processes* *64*, 177–196.

dIlorio, P. J., Moss, J. B., Sbrogna, J. L., Karlstrom, R. O., and Moss, L. G. (2002). Sonic hedgehog is required early in pancreatic islet development. *Dev Biol* *244*, 75–84.

Dubruille, R., Laurencon, A., Vandaele, C., Shishido, E., Coulon-Bublex, M., Swoboda, P., Couble, P., Kernan, M., and Durand, B. (2002). *Drosophila* regulatory factor X is necessary for ciliated sensory neuron differentiation. *Development* *129*, 5487–5498.

Dunipace, L., Meister, S., McNealy, C., and Amrein, H. (2001). Spatially restricted expression of candidate taste receptors in the *Drosophila* gustatory system. *Curr Biol* *11*, 822–835.

Eberl, D. F. (1999). Feeling the vibes: chordotonal mechanisms in insect hearing. *Curr Opin Neurobiol* *9*, 389–393.

Eberl, D. F., Hardy, R. W., and Kernan, M. J. (2000). Genetically similar transduction mechanisms for touch and hearing in *Drosophila*. *J Neurosci* *20*, 5981–5988.

Edeling, M. A., Smith, C., and Owen, D. (2006). Life of a clathrin coat: insights from clathrin and AP structures. *Nat Rev Mol Cell Biol* *7*, 32–44.

Efimenko, E., Bubb, K., Mak, H. Y., Holzman, T., Leroux, M. R., Ruvkun, G., Thomas, J. H., and Swoboda, P. (2005). Analysis of *xbx* genes in *C. elegans*. *Development* *132*, 1923–1934.

Eley, L., Yates, L. M., and Goodship, J. A. (2005). Cilia and disease. *Curr Opin Genet Dev* *15*, 308–314.

Elkins, T., Zinn, K., McAllister, L., Hoffmann, F. M., and Goodman, C. S. (1990). Genetic analysis of a *Drosophila* neural cell adhesion molecule: interaction of fasciclin I and Abelson tyrosine kinase mutations. *Cell* *60*, 565–575.

Fan, Y., Esmail, M. A., Ansley, S. J., Blacque, O. E., Boroevich, K., Ross, A. J., Moore, S. J., Badano, J. L., May-Simera, H., Compton, D. S., *et al.* (2004). Mutations in a member of the Ras superfamily of small GTP-binding proteins causes Bardet-Biedl syndrome. *Nat Genet* *36*, 989–993.

Farag, T. I., and Teebi, A. S. (1989). High incidence of Bardet Biedl syndrome among the

Bedouin. *Clin Genet* 36, 463–464.

Ferrante, M. I., Zullo, A., Barra, A., Bimonte, S., Messaddeq, N., Studer, M., Dolle, P., and Franco, B. (2006). Oral–facial–digital type I protein is required for primary cilia formation and left–right axis specification. *Nat Genet* 38, 112–117.

Fischer, E., Legue, E., Doyen, A., Nato, F., Nicolas, J. F., Torres, V., Yaniv, M., and Pontoglio, M. (2006). Defective planar cell polarity in polycystic kidney disease. *Nat Genet* 38, 21–23.

Forti, E., Aksanov, O., and Birk, R. Z. (2007). Temporal expression pattern of Bardet–Biedl syndrome genes in adipogenesis. *Int J Biochem Cell Biol* 39, 1055–1062.

Fujiwara, M., Ishihara, T., and Katsura, I. (1999). A novel WD40 protein, CHE-2, acts cell–autonomously in the formation of *C. elegans* sensory cilia. *Development* 126, 4839–4848.

Gervais, F. G., Singaraja, R., Xanthoudakis, S., Gutekunst, C. A., Leavitt, B. R., Metzler, M., Hackam, A. S., Tam, J., Vaillancourt, J. P., Houtzager, V., *et al.* (2002). Recruitment and activation of caspase–8 by the Huntingtin–interacting protein Hip–1 and a novel partner Hippi. *Nat Cell Biol* 4, 95–105.

Gibbons, B. H., Asai, D. J., Tang, W. J., Hays, T. S., and Gibbons, I. R. (1994). Phylogeny and expression of axonemal and cytoplasmic dynein genes in sea urchins. *Mol Biol Cell* 5, 57–70.

Gloor, G. B., Nassif, N. A., Johnson–Schlitz, D. M., Preston, C. R., and Engels, W. R. (1991). Targeted gene replacement in *Drosophila* via P element–induced gap repair. *Science* 253, 1110–1117.

Gong, Z., Son, W., Chung, Y. D., Kim, J., Shin, D. W., McClung, C. A., Lee, Y., Lee, H. W., Chang, D. J., Kaang, B. K., *et al.* (2004). Two interdependent TRPV channel subunits, inactive and Nanchung, mediate hearing in *Drosophila*. *J Neurosci* 24, 9059–9066.

Gopfert, M. C., Albert, J. T., Nadrowski, B., and Kamikouchi, A. (2006). Specification of auditory sensitivity by *Drosophila* TRP channels. *Nat Neurosci* 9, 999–1000.

Grace, C., Beales, P., Summerbell, C., Jebb, S. A., Wright, A., Parker, D., and Kopelman, P. (2003). Energy metabolism in Bardet–Biedl syndrome. *Int J Obes Relat Metab Disord* 27, 1319–1324.

Gurkan, C., Stagg, S. M., Lapointe, P., and Balch, W. E. (2006). The COPII cage: unifying principles of vesicle coat assembly. *Nat Rev Mol Cell Biol* 7, 727–738.

Han, Y. G., Kwok, B. H., and Kernan, M. J. (2003). Intraflagellar transport is required in *Drosophila* to differentiate sensory cilia but not sperm. *Curr Biol* 13, 1679–1686.

Hartenstein, V., and Posakony, J. W. (1989). Development of adult sensilla on the wing and notum of *Drosophila melanogaster*. *Development* 107, 389–405.

Haycraft, C. J., Schafer, J. C., Zhang, Q., Taulman, P. D., and Yoder, B. K. (2003). Identification of CHE-13, a novel intraflagellar transport protein required for cilia formation. *Exp Cell Res* 284, 251–263.

Haycraft, C. J., Swoboda, P., Taulman, P. D., Thomas, J. H., and Yoder, B. K. (2001). The *C. elegans* homolog of the murine cystic kidney disease gene Tg737 functions in a ciliogenic pathway and is disrupted in *osm-5* mutant worms. *Development* 128, 1493–1505.

Hearn, T., Renforth, G. L., Spalluto, C., Hanley, N. A., Piper, K., Brickwood, S., White, C., Connolly, V., Taylor, J. F., Russell-Eggitt, I., *et al.* (2002). Mutation of ALMS1, a large gene with a tandem repeat encoding 47 amino acids, causes Alstrom syndrome. *Nat Genet* 31, 79–83.

Hekmat-Scafe, D. S., Steinbrecht, R. A., and Carlson, J. R. (1997). Coexpression of two odorant-binding protein homologs in *Drosophila*: implications for olfactory coding. *J Neurosci* 17, 1616–1624.

Hirokawa, N., Pfister, K. K., Yorifuji, H., Wagner, M. C., Brady, S. T., and Bloom, G. S. (1989). Submolecular domains of bovine brain kinesin identified by electron microscopy and monoclonal antibody decoration. *Cell* 56, 867–878.

Holme, R. H., and Steel, K. P. (2002). Stereocilia defects in *waltzer* (*Cdh23*), *shaker1* (*Myo7a*) and double *waltzer/shaker1* mutant mice. *Hear Res* 169, 13–23.

Hou, Y., Pazour, G. J., and Witman, G. B. (2004). A dynein light intermediate chain, D1bLIC, is required for retrograde intraflagellar transport. *Mol Biol Cell* 15, 4382–4394.

Huang, B., Rifkin, M. R., and Luck, D. J. (1977). Temperature-sensitive mutations affecting flagellar assembly and function in *Chlamydomonas reinhardtii*. *J Cell Biol* 72, 67–85.

Huangfu, D., and Anderson, K. V. (2005). Cilia and Hedgehog responsiveness in the mouse. *Proc Natl Acad Sci U S A* 102, 11325–11330.

Huangfu, D., Liu, A., Rakeman, A. S., Murcia, N. S., Niswander, L., and Anderson, K. V. (2003). Hedgehog signalling in the mouse requires intraflagellar transport proteins. *Nature* 426, 83–87.

Husain, N., Pellikka, M., Hong, H., Klimentova, T., Choe, K. M., Clandinin, T. R., and Tepass, U. (2006). The agrin/perlecan-related protein eyes shut is essential for epithelial lumen formation in the *Drosophila* retina. *Dev Cell* 11, 483–493.

Ibanez-Tallon, I., Heintz, N., and Omran, H. (2003). To beat or not to beat: roles of cilia in development and disease. *Hum Mol Genet* 12 *Spec No 1*, R27–35.

Jan, L. Y., and Jan, Y. N. (1982). Antibodies to horseradish peroxidase as specific neuronal markers in *Drosophila* and in grasshopper embryos. *Proc Natl Acad Sci U S A*

79, 2700–2704.

Jekely, G., and Arendt, D. (2006). Evolution of intraflagellar transport from coated vesicles and autogenous origin of the eukaryotic cilium. *Bioessays* 28, 191–198.

Karcher, R. L., Deacon, S. W., and Gelfand, V. I. (2002). Motor–cargo interactions: the key to transport specificity. *Trends Cell Biol* 12, 21–27.

Katsanis, N., Ansley, S. J., Badano, J. L., Eichers, E. R., Lewis, R. A., Hoskins, B. E., Scambler, P. J., Davidson, W. S., Beales, P. L., and Lupski, J. R. (2001a). Triallelic inheritance in Bardet–Biedl syndrome, a Mendelian recessive disorder. *Science* 293, 2256–2259.

Katsanis, N., Lupski, J. R., and Beales, P. L. (2001b). Exploring the molecular basis of Bardet–Biedl syndrome. *Hum Mol Genet* 10, 2293–2299.

Kaufman, P. D., and Rio, D. C. (1992). P element transposition in vitro proceeds by a cut–and–paste mechanism and uses GTP as a cofactor. *Cell* 69, 27–39.

Keil, T. A. (1997). Functional morphology of insect mechanoreceptors. *Microsc Res Tech* 39, 506–531.

Keller, L. C., Romijn, E. P., Zamora, I., Yates, J. R., 3rd, and Marshall, W. F. (2005). Proteomic analysis of isolated chlamydomonas centrioles reveals orthologs of ciliary–disease genes. *Curr Biol* 15, 1090–1098.

Kernan, M., Cowan, D., and Zuker, C. (1994). Genetic dissection of mechanosensory transduction: mechanoreception–defective mutations of *Drosophila*. *Neuron* 12, 1195–1206.

Kim, J., Chung, Y. D., Park, D. Y., Choi, S., Shin, D. W., Soh, H., Lee, H. W., Son, W., Yim, J., Park, C. S., *et al.* (2003). A TRPV family ion channel required for hearing in *Drosophila*. *Nature* 424, 81–84.

Kim, J. C., Badano, J. L., Sibold, S., Esmail, M. A., Hill, J., Hoskins, B. E., Leitch, C. C., Venner, K., Ansley, S. J., Ross, A. J., *et al.* (2004). The Bardet–Biedl protein BBS4 targets cargo to the pericentriolar region and is required for microtubule anchoring and cell cycle progression. *Nat Genet* 36, 462–470.

Kim, J. C., Ou, Y. Y., Badano, J. L., Esmail, M. A., Leitch, C. C., Fiedrich, E., Beales, P. L., Archibald, J. M., Katsanis, N., Rattner, J. B., and Leroux, M. R. (2005). MKKS/BBS6, a divergent chaperonin–like protein linked to the obesity disorder Bardet–Biedl syndrome, is a novel centrosomal component required for cytokinesis. *J Cell Sci* 118, 1007–1020.

Kirchhausen, T. (2000). Three ways to make a vesicle. *Nat Rev Mol Cell Biol* 1, 187–198.

Klein, D., and Ammann, F. (1969). The syndrome of Laurence–Moon–Bardet–Biedl and allied diseases in Switzerland. Clinical, genetic and epidemiological studies. *J Neurol Sci* 9, 479–513.

- Kozminski, K. G., Beech, P. L., and Rosenbaum, J. L. (1995). The *Chlamydomonas* kinesin-like protein FLA10 is involved in motility associated with the flagellar membrane. *J Cell Biol* *131*, 1517–1527.
- Kozminski, K. G., Johnson, K. A., Forscher, P., and Rosenbaum, J. L. (1993). A motility in the eukaryotic flagellum unrelated to flagellar beating. *Proc Natl Acad Sci U S A* *90*, 5519–5523.
- Kulaga, H. M., Leitch, C. C., Eichers, E. R., Badano, J. L., Lesemann, A., Hoskins, B. E., Lupski, J. R., Beales, P. L., Reed, R. R., and Katsanis, N. (2004). Loss of BBS proteins causes anosmia in humans and defects in olfactory cilia structure and function in the mouse. *Nat Genet* *36*, 994–998.
- Larsson, M. C., Domingos, A. I., Jones, W. D., Chiappe, M. E., Amrein, H., and Vosshall, L. B. (2004). Or83b encodes a broadly expressed odorant receptor essential for *Drosophila* olfaction. *Neuron* *43*, 703–714.
- Li, J. B., Gerdes, J. M., Haycraft, C. J., Fan, Y., Teslovich, T. M., May-Simera, H., Li, H., Blacque, O. E., Li, L., Leitch, C. C., *et al.* (2004). Comparative genomics identifies a flagellar and basal body proteome that includes the BBS5 human disease gene. *Cell* *117*, 541–552.
- Li, X., Staszewski, L., Xu, H., Durick, K., Zoller, M., and Adler, E. (2002). Human receptors for sweet and umami taste. *Proc Natl Acad Sci U S A* *99*, 4692–4696.
- Lindemann, B. (1996). Taste reception. *Physiol Rev* *76*, 718–766.
- Liu, A., Wang, B., and Niswander, L. A. (2005). Mouse intraflagellar transport proteins regulate both the activator and repressor functions of Gli transcription factors. *Development* *132*, 3103–3111.
- Lupski, J. R., de Oca-Luna, R. M., Slaugenhaupt, S., Pentao, L., Guzzetta, V., Trask, B. J., Saucedo-Cardenas, O., Barker, D. F., Killian, J. M., Garcia, C. A., and *et al.* (1991). DNA duplication associated with Charcot-Marie-Tooth disease type 1A. *Cell* *66*, 219–232.
- Malnic, B., Hirono, J., Sato, T., and Buck, L. B. (1999). Combinatorial receptor codes for odors. *Cell* *96*, 713–723.
- Marszalek, J. R., Liu, X., Roberts, E. A., Chui, D., Marth, J. D., Williams, D. S., and Goldstein, L. S. (2000). Genetic evidence for selective transport of opsin and arrestin by kinesin-II in mammalian photoreceptors. *Cell* *102*, 175–187.
- May, S. R., Ashique, A. M., Karlen, M., Wang, B., Shen, Y., Zarbali, K., Reiter, J., Ericson, J., and Peterson, A. S. (2005). Loss of the retrograde motor for IFT disrupts localization of Smo to cilia and prevents the expression of both activator and repressor functions of Gli. *Dev Biol* *287*, 378–389.
- McGrath, J., Somlo, S., Makova, S., Tian, X., and Brueckner, M. (2003). Two populations

of node monocilia initiate left-right asymmetry in the mouse. *Cell* *114*, 61–73.

Merritt, D. J. (1997). Transformation of external sensilla to chordotonal sensilla in the cut mutant of *Drosophila* assessed by single-cell marking in the embryo and larva. *Microsc Res Tech* *39*, 492–505.

Merz, A. J., So, M., and Sheetz, M. P. (2000). Pilus retraction powers bacterial twitching motility. *Nature* *407*, 98–102.

Mochizuki, T., Saijoh, Y., Tsuchiya, K., Shirayoshi, Y., Takai, S., Taya, C., Yonekawa, H., Yamada, K., Nihei, H., Nakatsuji, N., *et al.* (1998). Cloning of *inv*, a gene that controls left/right asymmetry and kidney development. *Nature* *395*, 177–181.

Montmayeur, J. P., and Matsunami, H. (2002). Receptors for bitter and sweet taste. *Curr Opin Neurobiol* *12*, 366–371.

Moore, J. D., and Endow, S. A. (1996). Kinesin proteins: a phylum of motors for microtubule-based motility. *Bioessays* *18*, 207–219.

Morgan, D., Turnpenny, L., Goodship, J., Dai, W., Majumder, K., Matthews, L., Gardner, A., Schuster, G., Vien, L., Harrison, W., *et al.* (1998). *Inversin*, a novel gene in the vertebrate left-right axis pathway, is partially deleted in the *inv* mouse. *Nat Genet* *20*, 149–156.

Morris, R. L., and Scholey, J. M. (1997). Heterotrimeric kinesin-II is required for the assembly of motile 9+2 ciliary axonemes on sea urchin embryos. *J Cell Biol* *138*, 1009–1022.

Murcia, N. S., Richards, W. G., Yoder, B. K., Mucenski, M. L., Dunlap, J. R., and Woychik, R. P. (2000). The Oak Ridge Polycystic Kidney (*orp*k) disease gene is required for left-right axis determination. *Development* *127*, 2347–2355.

Mykytyn, K., Braun, T., Carmi, R., Haider, N. B., Searby, C. C., Shastri, M., Beck, G., Wright, A. F., Iannaccone, A., Elbedour, K., *et al.* (2001). Identification of the gene that, when mutated, causes the human obesity syndrome BBS4. *Nat Genet* *28*, 188–191.

Mykytyn, K., Mullins, R. F., Andrews, M., Chiang, A. P., Swiderski, R. E., Yang, B., Braun, T., Casavant, T., Stone, E. M., and Sheffield, V. C. (2004). Bardet-Biedl syndrome type 4 (BBS4)-null mice implicate *Bbs4* in flagella formation but not global cilia assembly. *Proc Natl Acad Sci U S A* *101*, 8664–8669.

Mykytyn, K., Nishimura, D. Y., Searby, C. C., Beck, G., Bugge, K., Haines, H. L., Cornier, A. S., Cox, G. F., Fulton, A. B., Carmi, R., *et al.* (2003). Evaluation of complex inheritance involving the most common Bardet-Biedl syndrome locus (BBS1). *Am J Hum Genet* *72*, 429–437.

Mykytyn, K., Nishimura, D. Y., Searby, C. C., Shastri, M., Yen, H. J., Beck, J. S., Braun, T., Streb, L. M., Cornier, A. S., Cox, G. F., *et al.* (2002). Identification of the gene (BBS1) most commonly involved in Bardet-Biedl syndrome, a complex human obesity syndrome.

Nat Genet 31, 435–438.

Nadeau, J. H. (2001). Modifier genes in mice and humans. *Nat Rev Genet* 2, 165–174.

Nauli, S. M., Alenghat, F. J., Luo, Y., Williams, E., Vassilev, P., Li, X., Elia, A. E., Lu, W., Brown, E. M., Quinn, S. J., *et al.* (2003). Polycystins 1 and 2 mediate mechanosensation in the primary cilium of kidney cells. *Nat Genet* 33, 129–137.

Nelson, G., Chandrashekar, J., Hoon, M. A., Feng, L., Zhao, G., Ryba, N. J., and Zuker, C. S. (2002). An amino-acid taste receptor. *Nature* 416, 199–202.

Nelson, G., Hoon, M. A., Chandrashekar, J., Zhang, Y., Ryba, N. J., and Zuker, C. S. (2001). Mammalian sweet taste receptors. *Cell* 106, 381–390.

Nishimura, D. Y., Fath, M., Mullins, R. F., Searby, C., Andrews, M., Davis, R., Andorf, J. L., Mykytyn, K., Swiderski, R. E., Yang, B., *et al.* (2004). *Bbs2*-null mice have neurosensory deficits, a defect in social dominance, and retinopathy associated with mislocalization of rhodopsin. *Proc Natl Acad Sci U S A* 101, 16588–16593.

Nishimura, D. Y., Searby, C. C., Carmi, R., Elbedour, K., Van Maldergem, L., Fulton, A. B., Lam, B. L., Powell, B. R., Swiderski, R. E., Bugge, K. E., *et al.* (2001). Positional cloning of a novel gene on chromosome 16q causing Bardet-Biedl syndrome (BBS2). *Hum Mol Genet* 10, 865–874.

Nishimura, D. Y., Swiderski, R. E., Searby, C. C., Berg, E. M., Ferguson, A. L., Hennekam, R., Merin, S., Weleber, R. G., Biesecker, L. G., Stone, E. M., and Sheffield, V. C. (2005). Comparative genomics and gene expression analysis identifies BBS9, a new Bardet-Biedl syndrome gene. *Am J Hum Genet* 77, 1021–1033.

Nonaka, S., Shiratori, H., Saijoh, Y., and Hamada, H. (2002). Determination of left-right patterning of the mouse embryo by artificial nodal flow. *Nature* 418, 96–99.

Nonaka, S., Tanaka, Y., Okada, Y., Takeda, S., Harada, A., Kanai, Y., Kido, M., and Hirokawa, N. (1998). Randomization of left-right asymmetry due to loss of nodal cilia generating leftward flow of extraembryonic fluid in mice lacking KIF3B motor protein. *Cell* 95, 829–837.

Okada, Y., Takeda, S., Tanaka, Y., Belmonte, J. C., and Hirokawa, N. (2005). Mechanism of nodal flow: a conserved symmetry breaking event in left-right axis determination. *Cell* 121, 633–644.

Olbrich, H., Fliegau, M., Hoefele, J., Kispert, A., Otto, E., Volz, A., Wolf, M. T., Sasmaz, G., Trauer, U., Reinhardt, R., *et al.* (2003). Mutations in a novel gene, NPHP3, cause adolescent nephronophthisis, tapeto-retinal degeneration and hepatic fibrosis. *Nat Genet* 34, 455–459.

Olbrich, H., Haffner, K., Kispert, A., Volkel, A., Volz, A., Sasmaz, G., Reinhardt, R., Hennig, S., Lehrach, H., Konietzko, N., *et al.* (2002). Mutations in DNAH5 cause primary

ciliary dyskinesia and randomization of left-right asymmetry. *Nat Genet* *30*, 143–144.

Ostrowski, L. E., Blackburn, K., Radde, K. M., Moyer, M. B., Schlatzer, D. M., Moseley, A., and Boucher, R. C. (2002). A proteomic analysis of human cilia: identification of novel components. *Mol Cell Proteomics* *1*, 451–465.

Otto, E., Hoefele, J., Ruf, R., Mueller, A. M., Hiller, K. S., Wolf, M. T., Schuermann, M. J., Becker, A., Birkenhager, R., Sudbrak, R., *et al.* (2002). A gene mutated in nephronophthisis and retinitis pigmentosa encodes a novel protein, nephroretinin, conserved in evolution. *Am J Hum Genet* *71*, 1161–1167.

Otto, E. A., Schermer, B., Obara, T., O'Toole, J. F., Hiller, K. S., Mueller, A. M., Ruf, R. G., Hoefele, J., Beekmann, F., Landau, D., *et al.* (2003). Mutations in INVS encoding inversin cause nephronophthisis type 2, linking renal cystic disease to the function of primary cilia and left-right axis determination. *Nat Genet* *34*, 413–420.

Ou, G., Blacque, O. E., Snow, J. J., Leroux, M. R., and Scholey, J. M. (2005). Functional coordination of intraflagellar transport motors. *Nature* *436*, 583–587.

Park, S. K., Shanbhag, S. R., Wang, Q., Hasan, G., Steinbrecht, R. A., and Pikielny, C. W. (2000). Expression patterns of two putative odorant-binding proteins in the olfactory organs of *Drosophila melanogaster* have different implications for their functions. *Cell Tissue Res* *300*, 181–192.

Park, T. J., Haigo, S. L., and Wallingford, J. B. (2006). Ciliogenesis defects in embryos lacking inturned or fuzzy function are associated with failure of planar cell polarity and Hedgehog signaling. *Nat Genet* *38*, 303–311.

Parks, A. L., Cook, K. R., Belvin, M., Dompe, N. A., Fawcett, R., Huppert, K., Tan, L. R., Winter, C. G., Bogart, K. P., Deal, J. E., *et al.* (2004). Systematic generation of high-resolution deletion coverage of the *Drosophila melanogaster* genome. *Nat Genet* *36*, 288–292.

Pazour, G. J. (2004). Comparative genomics: prediction of the ciliary and basal body proteome. *Curr Biol* *14*, R575–577.

Pazour, G. J., Baker, S. A., Deane, J. A., Cole, D. G., Dickert, B. L., Rosenbaum, J. L., Witman, G. B., and Besharse, J. C. (2002). The intraflagellar transport protein, IFT88, is essential for vertebrate photoreceptor assembly and maintenance. *J Cell Biol* *157*, 103–113.

Pazour, G. J., Dickert, B. L., Vucica, Y., Seeley, E. S., Rosenbaum, J. L., Witman, G. B., and Cole, D. G. (2000). *Chlamydomonas* IFT88 and its mouse homologue, polycystic kidney disease gene *tg737*, are required for assembly of cilia and flagella. *J Cell Biol* *151*, 709–718.

Pazour, G. J., Dickert, B. L., and Witman, G. B. (1999). The DHC1b (DHC2) isoform of

cytoplasmic dynein is required for flagellar assembly. *J Cell Biol* *144*, 473–481.

Pazour, G. J., and Rosenbaum, J. L. (2002). Intraflagellar transport and cilia-dependent diseases. *Trends Cell Biol* *12*, 551–555.

Pazour, G. J., Wilkerson, C. G., and Witman, G. B. (1998). A dynein light chain is essential for the retrograde particle movement of intraflagellar transport (IFT). *J Cell Biol* *141*, 979–992.

Perkins, L. A., Hedgecock, E. M., Thomson, J. N., and Culotti, J. G. (1986). Mutant sensory cilia in the nematode *Caenorhabditis elegans*. *Dev Biol* *117*, 456–487.

Pesavento, P. A., Stewart, R. J., and Goldstein, L. S. (1994). Characterization of the KLP68D kinesin-like protein in *Drosophila*: possible roles in axonal transport. *J Cell Biol* *127*, 1041–1048.

Piperno, G., and Mead, K. (1997). Transport of a novel complex in the cytoplasmic matrix of *Chlamydomonas* flagella. *Proc Natl Acad Sci U S A* *94*, 4457–4462.

Porter, M. E., Bower, R., Knott, J. A., Byrd, P., and Dentler, W. (1999). Cytoplasmic dynein heavy chain 1b is required for flagellar assembly in *Chlamydomonas*. *Mol Biol Cell* *10*, 693–712.

Praetorius, H. A., and Spring, K. R. (2001). Bending the MDCK cell primary cilium increases intracellular calcium. *J Membr Biol* *184*, 71–79.

Praetorius, H. A., and Spring, K. R. (2003). Removal of the MDCK cell primary cilium abolishes flow sensing. *J Membr Biol* *191*, 69–76.

Preston, C. R., and Engels, W. R. (1996). P-element-induced male recombination and gene conversion in *Drosophila*. *Genetics* *144*, 1611–1622.

Qin, H., Rosenbaum, J. L., and Barr, M. M. (2001). An autosomal recessive polycystic kidney disease gene homolog is involved in intraflagellar transport in *C. elegans* ciliated sensory neurons. *Curr Biol* *11*, 457–461.

Qin, H., Wang, Z., Diener, D., and Rosenbaum, J. (2007). Intraflagellar transport protein 27 is a small G protein involved in cell-cycle control. *Curr Biol* *17*, 193–202.

Riesgo-Escovar, J. R., Woodard, C., and Carlson, J. R. (1994). Olfactory physiology in the *Drosophila* maxillary palp requires the visual system gene *rdgB*. *J Comp Physiol [A]* *175*, 687–693.

Rosenbaum, J. L., and Witman, G. B. (2002). Intraflagellar transport. *Nat Rev Mol Cell Biol* *3*, 813–825.

Ross, A. J., May-Simera, H., Eichers, E. R., Kai, M., Hill, J., Jagger, D. J., Leitch, C. C., Chapple, J. P., Munro, P. M., Fisher, S., *et al.* (2005). Disruption of Bardet-Biedl syndrome ciliary proteins perturbs planar cell polarity in vertebrates. *Nat Genet* *37*, 1135–1140.

Rubin, G. M., and Spradling, A. C. (1982). Genetic transformation of *Drosophila* with transposable element vectors. *Science* *218*, 348–353.

Sanzen, T., Harada, K., Yasoshima, M., Kawamura, Y., Ishibashi, M., and Nakanuma, Y. (2001). Polycystic kidney rat is a novel animal model of Caroli's disease associated with congenital hepatic fibrosis. *Am J Pathol* *158*, 1605–1612.

Sarmah, B., Latimer, A. J., Appel, B., and Wenthe, S. R. (2005). Inositol polyphosphates regulate zebrafish left–right asymmetry. *Dev Cell* *9*, 133–145.

Sarpal, R., Todi, S. V., Sivan–Loukianova, E., Shirolkar, S., Subramanian, N., Raff, E. C., Erickson, J. W., Ray, K., and Eberl, D. F. (2003). *Drosophila* KAP interacts with the kinesin II motor subunit KLP64D to assemble chordotonal sensory cilia, but not sperm tails. *Curr Biol* *13*, 1687–1696.

Scholey, J. M. (1996). Kinesin–II, a membrane traffic motor in axons, axonemes, and spindles. *J Cell Biol* *133*, 1–4.

Scott, K., Brady, R., Jr., Cravchik, A., Morozov, P., Rzhetsky, A., Zuker, C., and Axel, R. (2001). A chemosensory gene family encoding candidate gustatory and olfactory receptors in *Drosophila*. *Cell* *104*, 661–673.

Shakir, M. A., Fukushige, T., Yasuda, H., Miwa, J., and Siddiqui, S. S. (1993). *C. elegans* *osm-3* gene mediating osmotic avoidance behaviour encodes a kinesin–like protein. *Neuroreport* *4*, 891–894.

Signor, D., Wedaman, K. P., Orozco, J. T., Dwyer, N. D., Bargmann, C. I., Rose, L. S., and Scholey, J. M. (1999). Role of a class DHC1b dynein in retrograde transport of IFT motors and IFT raft particles along cilia, but not dendrites, in chemosensory neurons of living *Caenorhabditis elegans*. *J Cell Biol* *147*, 519–530.

Simons, M., Gloy, J., Ganner, A., Bullerkotte, A., Bashkurov, M., Kronig, C., Schermer, B., Benzing, T., Cabello, O. A., Jenny, A., *et al.* (2005). Inversin, the gene product mutated in nephronophthisis type II, functions as a molecular switch between Wnt signaling pathways. *Nat Genet* *37*, 537–543.

Slavotinek, A. M., Stone, E. M., Mykytyn, K., Heckenlively, J. R., Green, J. S., Heon, E., Musarella, M. A., Parfrey, P. S., Sheffield, V. C., and Biesecker, L. G. (2000). Mutations in MKKS cause Bardet–Biedl syndrome. *Nat Genet* *26*, 15–16.

Smith, T. F., Gaitatzes, C., Saxena, K., and Neer, E. J. (1999). The WD repeat: a common architecture for diverse functions. *Trends Biochem Sci* *24*, 181–185.

Snow, J. J., Ou, G., Gunnarson, A. L., Walker, M. R., Zhou, H. M., Brust–Mascher, I., and Scholey, J. M. (2004). Two anterograde intraflagellar transport motors cooperate to build sensory cilia on *C. elegans* neurons. *Nat Cell Biol* *6*, 1109–1113.

Stocker, R. F. (1994). The organization of the chemosensory system in *Drosophila*

melanogaster: a review. *Cell Tissue Res* 275, 3–26.

Stocker, R. F., Lienhard, M. C., Borst, A., and Fischbach, K. F. (1990). Neuronal architecture of the antennal lobe in *Drosophila melanogaster*. *Cell Tissue Res* 262, 9–34.

Stoetzel, C., Laurier, V., Davis, E. E., Muller, J., Rix, S., Badano, J. L., Leitch, C. C., Salem, N., Chouery, E., Corbani, S., *et al.* (2006). BBS10 encodes a vertebrate-specific chaperonin-like protein and is a major BBS locus. *Nat Genet* 38, 521–524.

Stoetzel, C., Muller, J., Laurier, V., Davis, E. E., Zaghoul, N. A., Vicaire, S., Jacquelin, C., Plewniak, F., Leitch, C. C., Sarda, P., *et al.* (2007). Identification of a novel BBS gene (BBS12) highlights the major role of a vertebrate-specific branch of chaperonin-related proteins in Bardet-Biedl syndrome. *Am J Hum Genet* 80, 1–11.

Sun, B., and Salvaterra, P. M. (1995). Two *Drosophila* nervous system antigens, Nervana 1 and 2, are homologous to the beta subunit of Na⁺,K⁺-ATPase. *Proc Natl Acad Sci U S A* 92, 5396–5400.

Tabish, M., Siddiqui, Z. K., Nishikawa, K., and Siddiqui, S. S. (1995). Exclusive expression of *C. elegans* *osm-3* kinesin gene in chemosensory neurons open to the external environment. *J Mol Biol* 247, 377–389.

Tanaka, Y., Okada, Y., and Hirokawa, N. (2005). FGF-induced vesicular release of Sonic hedgehog and retinoic acid in leftward nodal flow is critical for left-right determination. *Nature* 435, 172–177.

Thibault, S. T., Singer, M. A., Miyazaki, W. Y., Milash, B., Dompe, N. A., Singh, C. M., Buchholz, R., Demsky, M., Fawcett, R., Francis-Lang, H. L., *et al.* (2004). A complementary transposon tool kit for *Drosophila melanogaster* using P and piggyBac. *Nat Genet* 36, 283–287.

Troemel, E. R., Chou, J. H., Dwyer, N. D., Colbert, H. A., and Bargmann, C. I. (1995). Divergent seven transmembrane receptors are candidate chemosensory receptors in *C. elegans*. *Cell* 83, 207–218.

Troemel, E. R., Kimmel, B. E., and Bargmann, C. I. (1997). Reprogramming chemotaxis responses: sensory neurons define olfactory preferences in *C. elegans*. *Cell* 91, 161–169.

Vosshall, L. B. (2000). Olfaction in *Drosophila*. *Curr Opin Neurobiol* 10, 498–503.

Vosshall, L. B., Amrein, H., Morozov, P. S., Rzhetsky, A., and Axel, R. (1999). A spatial map of olfactory receptor expression in the *Drosophila* antenna. *Cell* 96, 725–736.

Vosshall, L. B., Wong, A. M., and Axel, R. (2000). An olfactory sensory map in the fly brain. *Cell* 102, 147–159.

Walker, R. G., Willingham, A. T., and Zuker, C. S. (2000). A *Drosophila* mechanosensory transduction channel. *Science* 287, 2229–2234.

Wang, Q., Pan, J., and Snell, W. J. (2006). Intraflagellar transport particles participate

directly in cilium-generated signaling in *Chlamydomonas*. *Cell* 125, 549–562.

Wick, M. J., Ann, D. K., and Loh, H. H. (1995). Molecular cloning of a novel protein regulated by opioid treatment of NG108–15 cells. *Brain Res Mol Brain Res* 32, 171–175.

Wicks, S. R., de Vries, C. J., van Luenen, H. G., and Plasterk, R. H. (2000). CHE-3, a cytosolic dynein heavy chain, is required for sensory cilia structure and function in *Caenorhabditis elegans*. *Dev Biol* 221, 295–307.

Yamazaki, H., Nakata, T., Okada, Y., and Hirokawa, N. (1995). KIF3A/B: a heterodimeric kinesin superfamily protein that works as a microtubule plus end-directed motor for membrane organelle transport. *J Cell Biol* 130, 1387–1399.

Yamazaki, H., Nakata, T., Okada, Y., and Hirokawa, N. (1996). Cloning and characterization of KAP3: a novel kinesin superfamily-associated protein of KIF3A/3B. *Proc Natl Acad Sci U S A* 93, 8443–8448.

Ybe, J. A., Brodsky, F. M., Hofmann, K., Lin, K., Liu, S. H., Chen, L., Earnest, T. N., Fletterick, R. J., and Hwang, P. K. (1999). Clathrin self-assembly is mediated by a tandemly repeated superhelix. *Nature* 399, 371–375.

Yoder, B. K., Hou, X., and Guay-Woodford, L. M. (2002). The polycystic kidney disease proteins, polycystin-1, polycystin-2, polaris, and cystin, are co-localized in renal cilia. *J Am Soc Nephrol* 13, 2508–2516.

Zhang, Q., Davenport, J. R., Croyle, M. J., Haycraft, C. J., and Yoder, B. K. (2005). Disruption of IFT results in both exocrine and endocrine abnormalities in the pancreas of Tg737(orpk) mutant mice. *Lab Invest* 85, 45–64.

Zito, I., Downes, S. M., Patel, R. J., Cheetham, M. E., Ebenezer, N. D., Jenkins, S. A., Bhattacharya, S. S., Webster, A. R., Holder, G. E., Bird, A. C., *et al.* (2003). RPGR mutation associated with retinitis pigmentosa, impaired hearing, and sinorespiratory infections. *J Med Genet* 40, 609–615.